APPLICATION OF C_3F_7CN/CO_2 GAS MIXTURES FOR RETRO-FILLING SF_6-DESIGNED GAS INSULATED EQUIPMENT RATED AT TRANSMISSION VOLTAGES

A thesis submitted to the University of Manchester for the degree of

Doctor of Philosophy

in the Faculty of Science and Engineering

2020

LOIZOS LOIZOU

Department of Electrical and Electronic Engineering

Blank Page

Contents

Word Count: 47,667

Blank Page

List of Figures

Blank Page

List of Tables

List of Abbreviations

SF_6	Sulphur hexafluoride
C_3F_7CN	Heptafluoro-iso-butyronitrile
CO_2	Carbon dioxide
N_2	Nitrogen
GWP	Global Warming Potential
GIL	Gas Insulated Line
GIB	Gas Insulated Busbar
GIS	Gas Insulated Switchgear
AIS	Air Insulated Substation
AC	Alternative Current
DC	Direct Current
SI	Switching Impulse
LI	Lightning Impulse
PD	Partial Discharge
PDIV	Partial Discharge Inception Voltage
PDEV	Partial Discharge Extinction Voltage
PRPD	Phase-Resolved Partial Discharge
POC	Protrusion on Conductor
POE	Protrusion on Enclosure
UHF	Ultra-High Frequency
HV	High Voltage
U_{50}	50% breakdown voltage
f	Field utilisation factor
α	Ionisation coefficient
η	Attachment coefficient
FEA	Finite Element Analysis
V-t	Voltage-time
E_{max}	Maximum electric field
$(E/p)_{crit}$	Critical electric field
$(E_b/p)_{max}$	Pressure-reduced breakdown field strength

Blank Page

Abstract

The most significant drivers behind climate change are the greenhouse gases mainly caused by human activities. Environmental agreements, such as the Kyoto Protocol and the F-gas legislation, have been put in place to control the emission of greenhouse gases. Sulphur hexafluoride (SF_6), the most potent man-made greenhouse gas in existence, is widely used in the power industry as a dielectric medium in gas insulated equipment. Hence, the power industry has been looking for replacements to phase out the use of SF_6 in the power equipment. This thesis investigates the possibility of replacing SF_6 in existing gas insulated lines (GILs) and busbars (GIBs) within the power network with the more environmentally friendly C_3F_7CN/CO_2 gas mixtures.

Two types of electrical characterisations were carried out in this study, namely breakdown voltage and partial discharge (PD) tests. Coaxial and hemispherical rod-plane electrode configurations, with electric fields as found in practical GIL/GIB equipment, were used for AC and lightning impulse (LI) breakdown tests. For the PD tests under AC voltage, needles were attached to the high voltage and grounded electrode of plane-plane and hemispherical rod-plane configurations to mimic protrusion defects that can occur in practical GIL/GIB equipment. SF_6 was tested as a benchmark and compared to the performance of C_3F_7CN/CO_2 gas mixtures. Finally, a full-scale, 420/550 kV rated GIB demonstrator, filled with SF_6 first and then with the 20% C_3F_7CN / 80% CO_2 gas mixture, was subjected to type tests of various voltage waveforms in accordance to IEC standards.

The results showed that the 20% C_3F_7CN / 80% CO_2 gas mixture has comparable LI and AC breakdown performance to SF_6 under quasi-uniform fields. However, as the fields become more non-uniform, the 20% C_3F_7CN / 80% CO_2 gas mixture has lower LI breakdown voltages than SF_6 especially under positive polarity. The PD tests showed that the 20% C_3F_7CN / 80% CO_2 gas mixture has a poorer performance than SF_6 under highly divergent fields but can exceed the inception and extinction values of SF_6 when more uniform fields are used. The type tests using the full scale GIB demonstrator showed that the 20% C_3F_7CN / 80% CO_2 gas mixture has passed all the required voltage levels as SF_6. This could lead to at least 190 t of SF_6 being replaced with the 20% C_3F_7CN / 80% CO_2 gas mixture in the UK power network, where a reduced GWP can result to the CO_2 equivalent emissions being decreased by 95% of the current annual leakages. The findings in this thesis are an encouraging step towards a technically viable SF_6-free retro-fill solution for existing GIL/GIB installed for the 400 kV transmission network in the UK.

Blank Page

Declaration

No portion of the work referred to in the thesis has been submitted in support of an application for another degree or qualification of this or any other university or other institute of learning.

Blank Page

Copyright Statement

Blank Page

Acknowledgment

I would like to start one of the most important sections in my thesis by expressing my sincere gratitude to my supervisors, Dr Tony Chen and Dr Qiang Liu, for all the support and assistance given throughout the years. Both brilliant individuals who have accepted me as a young engineer and with their guidance allowed me to develop into an experienced researcher. Special thanks to Prof. Ian Cotton who has also provided valuable advices about the project throughout the years.

I would also like to thank all the industrial partners who have supported this project over the years, both financially and with their technical input, and more specifically: Mark Waldron and Dr Gordon Wilson from National Grid and Mark Gledhill, Reyad Abdulqader, Rainer Kurz and John Owens from 3M.

I am also grateful to Dr Richard Gardner, Dr Vidyadhar Peesapati and Dr Christos Zachariades who helped me a lot during my experimental work and for having lots of fruitful conversations with them that helped me throughout my testing period. I would also like to take this opportunity to thank people from HVPD Ltd and more specifically Andreas Kokkotis, Roberto Fernandez Bautista and Dr Malcom Seltzer-Grant for being very helpful and providing the equipment used for all the Partial Discharge experiments in this thesis.

My PhD would not be as enjoyable as it was without the people that were around me all these years. I would like to thank all my office and Ferranti Building friends at The University of Manchester and more specifically Dr Shanika Matharage, Dr ShengJi Tee, James Hill, Zong Wen Yan, Shen Shuhang and Dr Ibrahim Iddrissu for all the entertaining talks we had whilst working late on our projects. Having people to discuss about your problems and motivate each other can really keep you going! Last but not least, none of this would have been possible without the amazing company I had when returning back to my flat after the long and tiring days spent at the university. Shout out to the best flatmates and friends one could have over the course of a very stressful and difficult PhD project. These are Alexandros Mannari, Vasileios Tsormpatzoudis, Camran Ahmed and Antonis Efthymiou. I appreciate all their help and support throughout the years.

I would also like to use a new page for the most important people in my life. These people did not only support me throughout my PhD project but have always been there for me providing infinite love and care.

Words are not enough to express my gratitude to my parents, Pantelis and Andri Loizou, who have always been by my side and supported my education and choices in life. I would also like to thank my sister, Angela Loizou, and her son who always supported me. All my family members have taught me three very important things in life: be humble, appreciate what you have and always ask for more but never be greedy.

Finally, I cannot begin to express my thanks to my partner, Malvina Nicolaou, for her selfless love and understanding. She has been my rock, my greatest supporter and the person who could always lift me up when I was down and motivate me to keep going through difficult times.

Chapter 1 Introduction

1.1 Background

Growing reliance on operating appliances, electronics as well as electric vehicles has rapidly increased the demand for electrical energy in modern society over the past few years. Electricity is delivered through transmission and distribution networks, which vary in voltage levels, in order to minimise transmission losses and ensure safe supply to the consumer. Transformers are used to provide an efficient, reliable and cost-effective method of supplying electricity to industrial and residential consumers by changing these voltage levels. However, transformers rely on other assets used in substations to protect the network from overload and short circuit faults (such as lightning strikes and switching operations) through current interruption processes. These assets, known as switchgear, are used to ensure long term service reliability and operational safety of electricity networks [1]. In the early 20^{th} century, switchgear predominantly used air and oil as their insulation and arc-quenching mediums. Since 1960s, sulphur hexafluoride (SF_6) was preferred to those media, especially for high voltage applications [1], [2].

SF_6 is a colourless, odourless, non-flammable and chemically inert gas which has been used in gas insulated equipment for decades owing to its exceptional dielectric insulation and arc quenching capabilities. Applications of SF_6 include gas insulated switchgear (GIS), lines (GILs) and busbars (GIBs). Despite the many benefits of SF_6, it has one major drawback: a global warming potential (GWP) of 23,500 times greater than CO_2 [3]. The long atmospheric lifetime of 3,200 years and the high radiative forcing efficiency are two crucial factors that categorise SF_6 as a significant contributor to greenhouse gas emissions. The power industry is the main user of SF_6 responsible for the annual use of approximately 10,000 tons, accounting for 80% of the global SF_6 inventory [4].

The SF_6 concentration in the atmosphere has risen over 20% from 2010 to 2015 [4] and is predicted to continue growing at a similar rate until 2025 [5], resulting in an increasing awareness of the need to find an environmentally friendly replacement gas for SF_6. An

existing strategy proposed by the equipment manufacturers for the power industry is to upgrade and replace SF_6-filled equipment in the network with new state-of-the-art equipment specifically designed for suitable SF_6 alternatives [4], [6]. While this is intended to reduce overall SF_6 emissions, it is costly and replacing all existing SF_6-filled assets worldwide with new-builds is time consuming. An alternative approach is to investigate the feasibility of retro-filling existing SF_6-filled equipment with alternative gases, which is the aim of this PhD study.

There is a general consensus that any alternative candidate should have a considerably lower GWP than SF_6. However, the gas should also satisfy a strict list of requirements such as high dielectric strength, good arc-quenching capability (for GIS), low boiling point as well as being chemically inert, non-toxic and non-flammable. $(CF_3)_2$-CF-CN or C_3F_7CN, also commercially known as Novec^{TM} 4710 Insulating Gas, is an emerging candidate which is used in combination with a carrier gas (CO_2, N_2 or dry air) due to its relatively high boiling point. A key advantage of C_3F_7CN is the shorter atmospheric lifetime of 30 years while SF_6 can remain in the atmosphere for nearly 3,200 years before decomposing, resulting in a comparatively higher accumulative environmental impact. C_3F_7CN has a GWP of 2,090 which is almost a tenth of the GWP of SF_6 [7]. While the GWP of pure C_3F_7CN is still relatively high, the GWP of 4% C_3F_7CN mixtures can achieve up to 98% reduction in comparison to SF_6 [6], [8].

Early dielectric studies on C_3F_7CN have shown encouraging results about its insulation capabilities compared to SF_6 [4], [9]. AC breakdown tests performed under relatively uniform fields (parallel disk electrodes) have shown that by increasing the C_3F_7CN concentration in a gas mixture with CO_2, N_2 or dry air the insulation performance can be improved significantly [9]. C_3F_7CN/CO_2 mixtures were found to outperform the corresponding C_3F_7CN/N_2 and C_3F_7CN/dry air mixtures and a 20% C_3F_7CN mixture was found to achieve a slightly better breakdown performance than SF_6 [9]. However, it is important to fully characterise the dielectric behaviour of C_3F_7CN/CO_2 gas mixtures under different experimental conditions before it can be proposed as a retro-fill solution for SF_6-insulated high voltage equipment.

1.2 Research Objectives

The aim of this PhD thesis is to investigate the possibility of using C_3F_7CN/CO_2 gas mixtures, and more specifically 20% C_3F_7CN / 80% CO_2, as a potential retro-fill solution for existing SF_6-filled GILs and GIBs in the UK power network. Benchmark tests will be conducted using SF_6 for a comparative study to determine a suitable C_3F_7CN mixture. Breakdown, partial discharge tests at reduced scale and BS EN/IEC type tests at full scale will be conducted under different test conditions e.g. pressure, voltage waveform, impulse polarity etc. This thesis will mainly cover the following research objectives:

(i) Comparison of the breakdown characteristics of SF_6 and C_3F_7CN mixtures under quasi-uniform and weakly quasi-uniform fields

GIL/GIB are mainly coaxial cylindrical shaped equipment which result in weakly non-uniform electric fields. This specific type of geometry is used to characterise the performance of the gas candidates under representative field uniformity as found in practical equipment. Lightning impulse (LI) and AC breakdown tests with various experimental conditions are conducted in this study.

(ii) Comparison of the partial discharge characteristics of SF_6 and a pre-determined C_3F_7CN mixture in divergent and highly divergent fields

Engineering imperfections in GILs and GIBs, such as small protrusions and floating particles, can disrupt the field uniformity of the equipment and introduce regions with extreme electric field enhancements. These electric field disruptions lead to partial discharges (PDs). Therefore, it is important to understand the PD behaviour of C_3F_7CN gas mixtures compared to SF_6 in the presence of defects which can affect their performance in full-scale GIL/GIB equipment. PD behaviour is characterised in terms of partial discharge inception voltage (PDIV) and extinction voltage (PDEV). PDs can be initiated using needles with varying lengths to change the field uniformity from divergent to highly divergent electric fields. Phase resolved partial discharge (PRPD) patterns are also used to analyse the difference in PD behaviour between SF_6 and the pre-determined C_3F_7CN/CO_2 mixture.

(iii) Comparison of type test results for SF_6 and a pre-determined C_3F_7CN gas mixture using a full-scale 420/550 kV GIB demonstrator

A SF_6-alternative insulation material, such as C_3F_7CN or its mixture, cannot be proposed as a potential solution unless it is type tested on practical GIL/GIB equipment. The investigation focuses on whether a pre-determined C_3F_7CN gas mixture can replace SF_6 in existing GIB assets in the UK network through type tests on a purposely build GIB demonstrator. This can establish a level of confidence that the gas mixture could be retro-filled in SF_6-designed GIBs in UK substations in terms of insulation design.

1.3 Major Contributions

The major contributions of this thesis are given as follows:

(i) LI and AC breakdown characteristics of the 16/84% and 20/80% C_3F_7CN/CO_2 concentration gas mixtures under weakly non-uniform electric fields were obtained. Using quasi-uniform electric fields, the 20% C_3F_7CN / 80% CO_2 gas mixture has comparable LI and AC breakdown performance to SF_6. As fields become more non-uniform than quasi-uniform (described as weakly quasi-uniform in this thesis), SF_6 has significantly higher positive LI breakdown voltages than the 20% C_3F_7CN / 80% CO_2 gas mixture, while the negative LI breakdown voltages are comparable for both gases. Breakdown results have essentially shown that the 20% C_3F_7CN / 80% CO_2 gas mixture can have equivalent performance to SF_6 in GIL/GIB representative field uniformities.

(ii) PD characteristic comparisons of SF_6 and the 20% C_3F_7CN / 80% CO_2 gas mixture under divergent and highly divergent electric fields were obtained using different needle lengths and electrode configurations. Using a hemispherical rod-plane or plane-plane electrode configuration and a needle-to-plane gap distance of 10 mm, SF_6 demonstrates higher PDIV/EV values than the 20% C_3F_7CN / 80% CO_2 gas mixture for a needle length of 15 mm but with a shorter needle length of 5 mm both gases behave similarly. PRPD patterns have shown a different behaviour for the two gases where the PD activities for the 20% C_3F_7CN / 80% CO_2 gas mixture go through a 3-stage transition phase on the AC waveform. PD results have provided a level of confidence that the 20% C_3F_7CN / 80% CO_2 gas mixture

could suppress PD activity as successfully as SF_6 when protrusions up to 5 mm exist within the GIL/GIB equipment.

(iii) Type tests on a full-scale 420/550 kV GIB demonstrator used in the UK transmission network were conducted according to the BS EN/IEC 62271-204 standard, using the 20% C_3F_7CN / 80% CO_2 mixture as a retro-fill solution. The results show that the gas mixture passes all the required standard (using 15 switching and lightning impulse shots per polarity according to the standard) and non-standard (30 switching and lightning impulse shots per polarity) type tests at the specified voltage levels like SF_6. Moreover, these outcomes have shown that the 20% C_3F_7CN / 80% CO_2 gas mixture could start to be used in pilot applications within substations in England since the type tests have established a technical confidence that this mixture can be used in full-scale equipment.

(iv) Study on the reduction of carbon emissions by retro-filling SF_6-designed equipment with the 20% C_3F_7CN / 80% CO_2 gas mixture and the evaluation of the possibility of using the specific solution due to its limitation of having a high boiling point of -10°C was carried out. This study shows that using the C_3F_7CN/CO_2 gas mixture as a retro-fill solution can reduce the equivalent CO_2 emissions by 95% and that this gas mixture can be effective in several National Grid substations in England since the mean daily minimum temperature recorded in the past 20 years was -3.4°C, which is higher than the boiling temperature of the gas mixture.

1.4 Thesis Outline

The structure of the chapters presented in this thesis are as follows:

Chapter 1 Introduction

This chapter provides an overview on the background and motivation of the PhD study and also presents an outline for the thesis content.

Chapter 2 Literature Review

This chapter briefly introduces the use of SF_6 in gas insulated equipment and the advantages of using it over air insulated equipment. It also describes the environmental concerns of SF_6 that resulted in SF_6-alternatives being considered in the power industry. A review of previously investigated SF_6-alternatives is given, where C_3F_7CN/CO_2 gas mixtures emerge as the most technically viable candidate for retro-fill applications in high voltage equipment. Finally, the chapter gives an overview of the already existing research on C_3F_7CN gas.

Chapter 3 Experimental Setup and Gas Handling Procedures

This chapter presents the experimental setups and gas handling procedures used for the tests in this thesis. An overview of the pressure vessel and electrode configuration design and development is given. The gas handling setup, such as gas carts and analysers, and gas handling procedures, including vacuum, filling, mixing and recovery are illustrated in order to demonstrate the gas treatment reliability for the electrical tests of this thesis.

Chapter 4 Breakdown Characteristics of SF_6 Gas and C_3F_7CN/CO_2 Gas Mixtures

This chapter reports the LI and AC breakdown strengths of C_3F_7CN/CO_2 gas mixtures in comparison to SF_6 in weakly non-uniform fields. The up-and-down method is used to determine the 50% LI breakdown voltage, U_{50}, under different experimental conditions such as pressure, field uniformity, impulse polarity, gap distance and C_3F_7CN concentration in the gas mixture. The progressive stress procedure is used to acquire the average AC breakdown voltage of SF_6 and the 20% C_3F_7CN / 80% CO_2 gas mixture in coaxial configurations. Additional parameters such as the V-t characteristics and the pressure-reduced breakdown field strength, $(E_b/p)_{max}$, are analysed using data acquired from experiments which allow further comparison between SF_6 and the C_3F_7CN/CO_2 mixtures.

Chapter 5 Partial Discharge Characteristics of SF_6 Gas and 20% C_3F_7CN / 80% CO_2 Gas Mixture

This chapter investigates the PD characteristics of SF_6 and 20% C_3F_7CN / 80% CO_2 gas mixture using external Ultra-High Frequency (UHF) sensors. Hemispherical rod-plane and

plane-plane electrode configurations with needle protrusion are used to model defects as found in practical GIL/GIB equipment. Different field uniformities are achieved using a variable needle length; specifically, 5 mm and 15 mm. PDIV and PDEV are determined for both gases. PRPD patterns and UHF captured signals are used to compare the behaviour of SF_6 and 20% C_3F_7CN / 80% CO_2 gas mixture in different PD fault configurations.

Chapter 6 Retro-fill Investigation of a GIB Demonstrator Rated for Transmission Voltages

This chapter gives an overview on the performance of the 20% C_3F_7CN / 80% CO_2 gas mixture in a full-scale 420/550 kV GIB demonstrator. The SF_6-designed GIB demonstrator retro-filled with the 20% C_3F_7CN / 80% CO_2 gas mixture is type tested for both 420 kV and 550 kV voltage ratings. Material compatibility tests are also performed on the O-ring material by placing the EPDM elastomer used in existing GIL/GIB equipment in an oven operating at 105°C for more than 3 months. Finally, the impact of a retro-fill solution for the UK transmission network using the 20% C_3F_7CN / 80% CO_2 mixture is given where the equivalent CO_2 emissions can reduce up to 95% compared to SF_6.

Chapter 7 Conclusion and Future Work

This chapter provides the main conclusions drawn from the work in this thesis and suggests possible future work that can be done in order to further investigate the possibility of replacing SF_6 in high voltage equipment with C_3F_7CN mixtures.

Blank Page

Chapter 2 Literature Review

2.1 Introduction

The power industry mainly uses SF_6 as an insulation and arc-quenching medium in high voltage switchgear used in gas insulated substations. Insulation applications involve the use of SF_6 in busbars while for arc-quenching applications SF_6 is used in circuit breakers (CB). Less common applications of SF_6 as an insulating medium is in GIL which provide an alternative transmission method to overhead lines and underground cables [1]. SF_6 gas insulated substations offer numerous advantages over air insulated substations (AIS), the most important one being the compactness and reduced footprint [10], [11]. Similarly, GIL filled with SF_6 offer several advantages for high power transmission capacity such as low transmission losses [12], [13]. However, SF_6 has a high environmental impact which is a huge concern when it leaks into the atmosphere.

Environmental agreements, such as the Kyoto Protocol and the F-gas legislation, aim to control the use and emissions of fluorinated gases (F-gases) such as hydrofluorocarbons (HFCs), perfluorocarbons (PFCs) and SF_6 [14], [15]. This has led to a growing urgency to identify gas candidates with a significantly lower GWP than SF_6. However, universally replacing SF_6 in power equipment is proven to be a challenging task as no alternative gas can yet be adopted as a one-for-one replacement. Different families of gases have been studied such as perfluorocarbons [16], fluoroketones [17] and natural occuring gases [18]. All of these were found to have drawbacks which do not allow a simple retro-fill replacement in existing SF_6-containing equipment. Out of the long list of proposed SF_6 alternatives, C_3F_7CN [7] used with a carrier gas appears to be the most technically viable alternative for high voltage equipment.

This chapter provides a review of: (i) technology where SF_6 is used as an insulation and arc-quenching medium (ii) purpose of gas insulated equipment and the benefits of using SF_6 as insulation instead of other media (iii) properties of SF_6 that have led to SF_6-alternatives being investigated as potential retro-fill solutions for high voltage equipment (iv) previously

investigated gas replacements for SF_6 which show that C_3F_7CN is the most technically viable candidate for high voltage applications and (v) summary of the research findings and gaps on C_3F_7CN and its mixtures.

2.2 Main Features and Benefits of Gas Insulated Substations

2.2.1 Gas Insulated Substations Technology

Substations exist in the power network to ensure operational reliability and safe delivery of electric power from generation to the residential and industrial consumers. A substation, as shown in Figure 2-1, mainly consists of transformers, switchgear and arresters. Switchgear are necessary in substations to perform voltage switching and current breaking processes [2] in order to protect the network from transient overvoltages due to lightning strikes on network assets or switching transient voltages due to equipment being connected or disconnected from the power system.

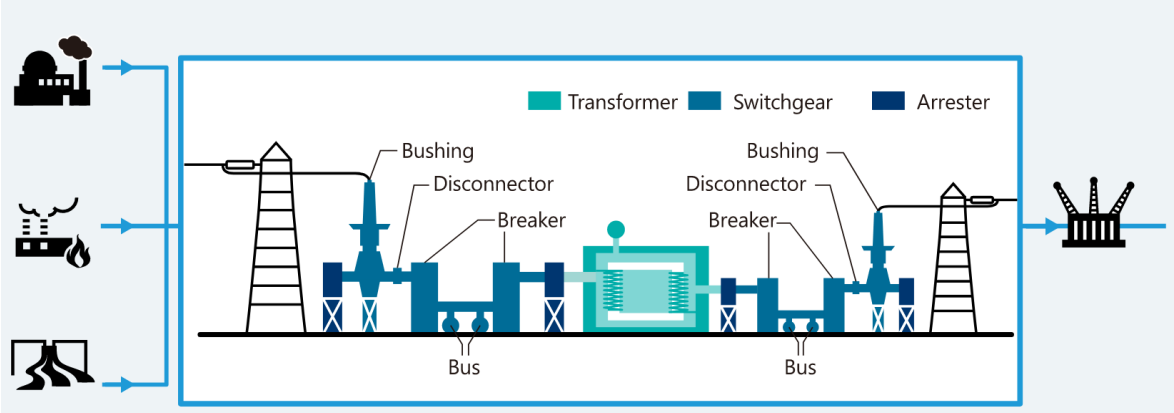

Figure 2-1. Structure of a substation mainly consisting of transformers, switchgear and arresters [19].

The first generation of switchgear used to blast air into the arc to extinguish it. The second generation used oil-immersed electrical contacts for cooling and arc-quenching applications. However, due to the flammable nature of mineral oil, SF_6 was then preferred as a dielectric medium for switchgear because of its inert and non-flammable nature [2]. The main historical development steps of GIS are shown in Table 2-1 [20]. From the first generation of GIS developed in the 1960s, the leading manufacturers have now developed the sixth-generation equipment. Until recently, more than 50,000 bays in over 5,000 high voltage

substations of 52 kV and above were reported to be installed globally across different voltage levels [2], [20].

Table 2-1. GIS steps of development since the 1960s [2], [20].

Year	Description
1960	Start of fundamental studies in R&D for SF_6 technology
1964	Delivery of the first SF_6 circuit breaker
1968	Delivery of first 110 kV GIS
1976	Delivery of first 550 kV GIS
1983	Delivery of the world's largest GIS, at the time, for Itaipu, Brazil
1984	Delivery of the world's highest current GIS, at the time, to Bowmaville, Canada (8000 A, 100 kA)
1986	Delivery of first 800 kV GIS
1996	Introduction of the smallest 123 kV GIS at the time
1997	Introduction of intelligent bay control, monitoring and diagnostics
1999	Introduction of the smallest 145 kV and 245 kV GIS at the time
2000	Introduction of new compact and hybrid solutions Mixed Technology Switchgear (MTS)

Figure 2-1 shows that GIS incorporates four main modular components: bushing, circuit breaker, disconnector and busbar. Bushings are usually gas insulated and their purpose is to connect GIS to other components in a substation such as overhead lines and transformers [11]. Circuit breakers act as interruption devices that can protect the power system by extinguishing the arc during a fault. A circuit breaker contains of two metal contacts that are physically connected to each other and they start to separate as soon as the circuit breaker detects a fault. An arc is established through a nozzle by the metal contact separation where high pressure SF_6 is blasted into it, draws the energy away and eventually extinguishes the arc [21]. Disconnectors are usually placed on either side of the circuit breaker and they are mainly used to provide additional isolation with an open gap. They are used to interrupt small capacitive currents during off-load maintenance operations when the circuit is not active [11], [21]. Lastly, busbars are used as connectors between the aforementioned modules and they come into different configurations such as elbows, tees, or angles. Busbars are essentially a coaxial configuration made of a central conductor and an external enclosure which are both usually made of aluminium. Support insulators, usually made of epoxy resin, are used to hold the conductor in the middle. Both disconnectors and busbars use SF_6 as an insulation medium [11], [21].

2.2.2 Advantages over AIS

GIS using SF_6 as their insulating and arc-quenching medium are generally preferred over AIS due to several advantages listed as follows:

- Reduced dimensional footprint compared to AIS. They are more compact due to the superior dielectric strength of SF_6 in relation to air. GIS only needs around 10-20% of the footprint for an AIS at equivalent voltage level. This allows substations to be built close to densely populated areas or in city centres [2], [11], [21].
- Protection from external environmental conditions such as salty and humid air as well as atmospheric pollution and dust. High voltage components in AIS can be affected by these environmental conditions as they are in open air, but GIS provides gas tightness with the enclosure which protects the live parts. As they are protected from extreme environmental conditions, GIS assets installed since 1968 are still operating with no major issues which indicates high reliability and long-life expectancy of this equipment [2], [11], [21].
- Safe working environment for personnel since the design of GIS ensures that the high voltage components are secured by the grounded enclosure [2], [11], [21].
- Corrosion and earthquake protection since the external enclosure of the GIS uses aluminium alloys to protect the high voltage parts. The metallic structure of the GIS also provides a very good seismic withstand capability [2], [11].
- Factory pre-assembly and tests before being commissioned in substations. The compact size of GIS allows the manufacturers to fabricate and ship the entire bay assembled prior to commissioning, which allows easier installation, reduces the on-site works, associated costs and increases equipment reliability [2], [11], [21].

2.3 Main Features and Benefits of GIL

2.3.1 GIL Technology

GIL is a less common but still an important application of using SF_6 as an insulating medium. GIL is defined as a transmission system without any switching devices, like circuit breakers

and disconnectors, of which its sole purpose is to transmit large amounts of electric power [22]. This type of equipment has the capability of transmitting power in the range of 1000-5000 MVA [12], [21]. Based on GIS technology, GILs were developed in parallel to offer an alternative method to overhead lines and underground cables for transmitting high power capacity over long distance. Table 2-2 shows the development of GIL over the years [22].

Table 2-2. GIL historical development since the 1960s [22].

Year	Description	Country
1960	Start of fundamental studies in R&D for SF_6 technology	USA
1968	Delivery of first GIL	USA / Europe
1974	Delivery of 420 kV GIL	Germany
1976	Delivery of first directly buried GIL	USA
1985	Delivery of 550 kV / 8000 A GIL	Canada
2001	Delivery of first gas mixture GIL	Switzerland

Until 2010, more than 200 km of GIL were operating in more than 200 projects globally [12], [22]. The reported worldwide usage of GIL in terms of length is shown in Table 2-3. Table 2-3 also shows that the main usage of GIL is for 420 and 550 kV voltage rating.

Table 2-3. Cumulative global GIL length installed until 2010 [12].

Rated Voltage, U_r (kV)	GIL Length (km)
1200	1
800	3
550	90
420	110
362	15
242/300	33
72/145/172	38

GIL can be installed above the ground, in open trenches, tunnels or directly buried into the soil [22]. Directly buried GIL is considered the most time saving and economical installation method. Figure 2-2 illustrates an example of a GIL structure [23]. The high voltage conductor is located at the centre of an earthed enclosure and the space in between them is filled with insulating gas. SF_6 was used as the insulation gas for the 1st generation GIL. The 2nd generation GIL replaced pure SF_6 with a gas mixture which mainly consisted nitrogen (N_2) and a small amount of SF_6 in order to reduce the costs of production [12], [13], [24],

[25]. The conductor is usually made of aluminium. The enclosure is made of aluminium alloy which is designed to withstand high operating pressures as well as large mechanical weight when the GIL is directly buried under the soil [12], [13]. Particle traps, built along the length of the line, are used to capture free moving particles in order to reduce the probability of a flashover [22]. The conductor is supported and kept in place by the insulating spacers which are usually made of a mixture of epoxy resin and a filler material such as silicium (fine sand) or aluminium oxide (AlO_3). A filler material's main task is to provide additional mechanical strength when combined with epoxy resin [12]. There are two main types of insulators: open type, where gas flow is allowed between the compartments, and cone or disk type insulators where one compartment is gas tight and isolated from another [22]. Unlike GIS, insulators in GIL are fully enclosed inside the enclosure instead of coupled on the enclosure flanges [22]. Figure 2-2 shows an example of an open insulating spacer.

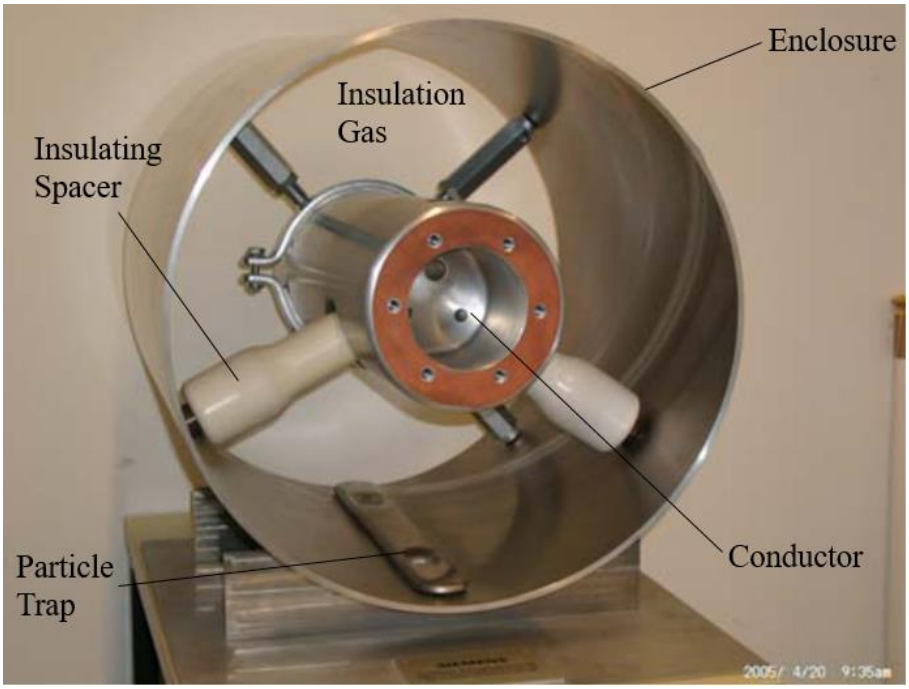

Figure 2-2. GIL internal structure [23].

2.3.2 Advantages of GIL

Benefits of GIL are closely related to the ones provided by GIS. GIL offer several advantages for high electric power transmission and have as follows [12], [13], [22], [24], [26]:

- High power carrying capability and low transmission losses: GIL provide an ideal supplement or alternative transmission method to overhead lines due to their high-power carrying capability. GIL can carry up to 3000 MVA per system at 550 kV rated voltage which allows it to be connected directly to overhead lines without any power reductions. They also have the benefit of being capable to use the same protection and control systems to overhead lines [12]. The large cross-sectional area of their conductor provides low resistive losses. This is important since, for high current transmission systems, the resistive losses can be significantly large [12], [13].
- Increased safety levels for personnel: The high voltage part of the GIL is securely placed within the grounded enclosure which minimizes the risk of external impact to the personnel under internal failure or normal operation [12]. Additionally, GIL are built of aluminium, epoxy resin and insulating gases which are incombustible materials that minimize the probability of a fire hazard [13].
- High reliability and long-life expectancy: GIL do not consist of any active moving parts, such as circuit breakers and switches, which means that there is no need for breaking operations. As it is mainly a passive system, GIL world-wide have been operating for more than 50 years now with no major failures [12]. Short repair times combined with low need for maintenance also makes GIL very reliable transmission systems [26].
- Resistance to thermal and electric ageing: Dielectric gases are non-ageing which contributes to the long operational lifetime of GIL. The maximum operational electric field strength and temperature in GIL are much lower than the values required to start the electric or thermal ageing of the gas [12].
- No external electromagnetic fields: Electromagnetic field regulations exist worldwide, with the limitation values varying in different countries, to protect the public from being exposed to harmful amounts of magnetic fields. The high voltage conductor combined with the grounded enclosure of the GIL form an inductive loop. A reverse current of the same size to the conductor but with 180° phase shift is induced in the grounded enclosure which causes two magnetic fields to be superimposed and cancel each other out [13]. The coupling factor between the two magnetic fields is 95% which means that only 5% can escape the enclosure of the GIL. This is almost negligible compared to other transmission systems such as overhead lines and underground cables [12].

2.4 Insulation Gases for High Voltage Equipment

2.4.1 Electrical Breakdown in Gases

In the absence of electric or magnetic fields, gas molecules move randomly and acquire velocities ranging from zero to infinity. Due to their random movement, molecules collide with each other which can potentially generate charge carriers [21], [27]. The generation of charge carriers from neutral molecules is known as the ionisation process [27]. Ionisation in a gas, and thus generation of charge carriers, can be enhanced through various processes such as ultra-violet radiation, cosmic rays, electric field application etc. However, with the application of a voltage between electrodes, field-assisted ionisation processes prevail the rest and form the deciding factors which lead to an electrical breakdown [27].

2.4.1.1 Generation of Charged Particles

When a voltage is applied on a pair of electrodes which are separated by an insulating gas, conduction current will flow if there are charge carriers present in the gas [21]. Even though a gas is an almost perfect insulator, some charged carriers are always present and can be in the form of [21]:

1. Electrons (negative charge): e^-
2. Positive ions (neutral atom missing an electron): $A^+ = A - e^-$
3. Negative ions (neutral atom with an excess electron): $A^- = A + e^-$

The above charged particles can be generated through various field assisted ionisation procedures which are summarised in Figure 2-3. The charge carriers mainly responsible for the development of an electrical breakdown in a gas are the light and fast-moving free electrons which can cause significant ionisation. In contrast, heavy and slow-moving ions are considered relatively stationary and unable to accumulate enough energy to cause ionisation, thus having reduced effect on the breakdown development process [28].

When an electric field is generated, the main source of free electrons in the gas comes through primary processes in the gas medium such as ionisation of neutral molecules by

collision or from detachment of negative ions. Secondary ionisation processes can also affect the number of free electrons in the gas and this includes the release of electrons from the cathode. Deionisation processes, such as electron attachment, can also affect the electrical breakdown development in the gas by reducing the number of free electrons and therefore inhibiting the discharge growth [21].

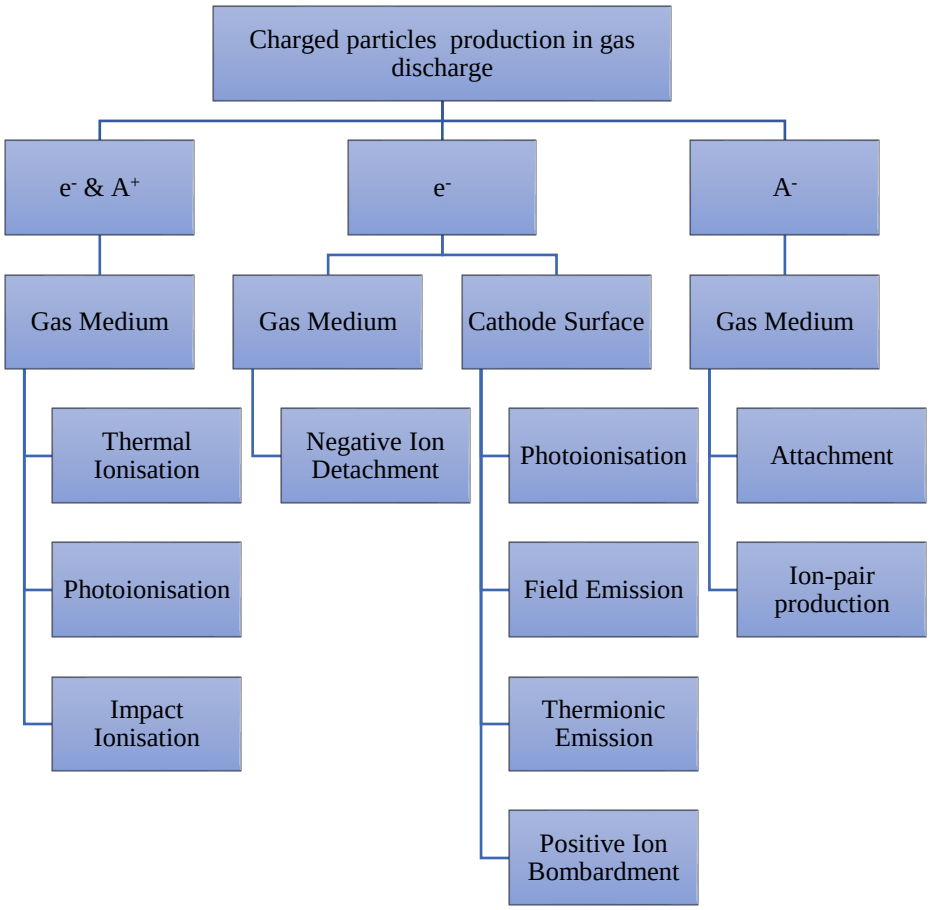

Figure 2-3. Main processes that result to charged particles in a gas discharge development [21].

A brief description of the ionisation and deionisation processes in a gas is given below as described in [21], [27].

Ionisation by Collision (Impact Ionisation)

With an electric field applied to a pair of electrodes, free electrons existing in the gap gain energy and travel towards the anode. On their way to the anode, electrons go through collisions with neutral gas molecules. If the energy acquired by the electron is less than the

ionisation energy of the molecule, an elastic collision will result where the molecule will be excited and go to a higher energy level but not release an electron. However, if the energy of the electron is more than the ionisation energy of the molecule, an inelastic collision will occur where ionisation will take place and a positive ion-electron pair will be created as shown in equation (2-1).

$$A + e^- = A^+ + e^- + e^- \tag{2-1}$$

The positive ion will be attracted to the cathode while the two electrons will gain energy on their way to the anode ionising further molecules [21], [27].

Photoionisation

Excited molecules are unstable, and they will either absorb more energy to become ionised or they will return back to their original stable state radiating the excess energy in the form of a photon. The photoionisation process is shown in equation (2-2):

$$\begin{aligned} A^* &= A + hf_p \\ B + hf_p &= B^+ + e^- \end{aligned} \tag{2-2}$$

Where A^* represents the excited state of molecule A and hf_p is the photon energy which is more than the ionisation energy of molecule B. Molecule B could already be excited from another collision and with the addition of another photon it could lead to ionisation. External sources such as cosmic rays could also excite or ionise molecules with radiation of energy [21], [27].

Thermal Ionisation

Thermal ionisation can also generate charged particles. A rise in the overall temperature of the gas will provide increased kinetic energy to the particles. As the particles move faster, the collisions between the molecules might enhance which will eventually result in increased impact ionisation in the gas. Thermal energy (W_t) can cause ionisation itself as shown in equation (2-3) [21], [27]:

$$A + W_t = A^+ + + e^- \quad (2\text{-}3)$$

Electron Detachment

Electron detachment is another source of electrons. This process is when an electron might detach itself from a negative ion forming a neutral molecule and a free electron as shown in equation (2-4).

$$A^- = A + e^- \quad (2\text{-}4)$$

Even though the number of electrons does not increase in this case, this process could still be considered as ionisation. This is because when electrons are released free, they can move much faster than the slow-moving negative ions. Therefore, light-mass electrons can have a much higher ionisation impact than the heavy-mass negative ion because of their capability of acquiring greater kinetic energy [21], [27].

Cathode Ionisation Processes

The cathode electrode can also provide a supply of charged particles. In the absence of an electric field, charged particles are bound to the cathode through electrostatic forces in the lattice. However, when a minimum specified energy is exceeded (known as work function), electrons can break free and this value is heavily dependent on the material of the electrode [21], [27]. The source of energy required to exceed the work function can come from the following:

- Positive Ion or Excited Molecule Bombardment: If the energy from the impact of a positive ion on the cathode is equal to or more than twice the cathode work function then an electron is released. This will result to at least two electrons being released since one will be used to neutralise the positive ion and the remaining one will be ejected into the gas medium. Electrons can also be ejected into the gas medium when excited molecules strike the cathode [21], [27].
- Photoemission: If the energy of a photon that comes in contact with the cathode is more than the work function then an electron can be emitted from the cathode [21], [27].

- Thermionic Emission: An increase in the electrode temperature can result to electrons being released from the surface of the cathode due to violent thermal lattice vibrations which are a result of increased kinetic energy [21], [27].
- Field Emission: A high electrostatic field surpassing the binding forces that keep the electrons inside the electrode could extract electrons from the cathode surface. This process intensifies with the presence of electrode protrusions and microdefects [21], [27].

Deionisation Processes

Deionisation is defined as the process where charged particles in the gas reduces, especially electrons. Deionisation procedures are in many cases desirable since they inhibit the avalanche growth which leads to an electrical breakdown [21], [27]. Two main deionisation processes are:

- Recombination: Positive and negative ions recombine to form a neutral atom [21], [27].
- Electron Attachment: Atoms from electronegative gases, such as SF_6, have the ability to attach themselves to free electrons and form heavy negative ions which, as described before, are unable to accumulate enough energy to cause ionisation thus inhibiting the electron avalanche development [21], [27].

2.4.1.2 Gas Breakdown Development

As described above, the first step to the gas discharge development is the initiation of free electrons in the gas volume through various ionisation processes. The progression from ionisation to completely bridging the insulation gap with a breakdown development process is shown in Figure 2-4 [21].

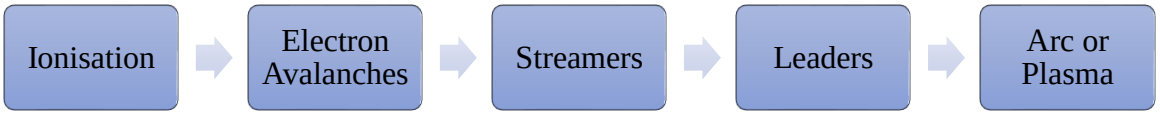

Figure 2-4. Possible discharge processes in gaseous insulation [21].

As shown in Figure 2-4, gas breakdown develops in several steps that are briefly described below:

1. Ionisation: With the application of an electric field, several ionisation processes take place in the gas medium to initiate free electrons which accelerate towards the anode [21], [27], [28].
2. Electron Avalanches: The rate of ionisation is described by the ionisation coefficient (α) which is defined as the number of ionising collisions made by an electron per unit distance as it travels in the direction of the applied electric field. When an electronegative gas is considered, the attachment process is also present in the breakdown development mechanism. The rate of attachment is described by the attachment coefficient (η) which is defined as the number of attachments per electron per unit distance. Both processes depend on the applied electric field, E, and pressure, p. $(E/p)_{crit}$ of a gas represents its critical electric field (which for SF_6 is 89 kV/cm) where α and η are in equilibrium ($\alpha = \eta$). If the electric field applied to the gas is greater than $(E/p)_{crit}$ [$E > (E/p)_{crit}$] then ionisation will be higher than attachment ($\alpha > \eta$) which will lead to the formation of electron avalanches. In contrast, if the applied field is less than the critical field [$E < (E/p)_{crit}$] then attachment is greater than ionisation ($\alpha < \eta$) which leads to the formation of negative ions that inhibit the electron avalanche development [21], [27], [28].
3. Streamers: As ionisation intensifies and electron avalanches develop, a cloud of less mobile positive ions is created in the insulating gap. Therefore, a space charge opposing the applied field is developed between the negatively charged electrons and the positively charged ions. With the progress of time, the electrons will be absorbed by the anode leaving the accumulation of positive ions behind. As a side process, excitation of molecules also occurs from elastic collisions which leads to the emission of photons. Some of these photons are absorbed by the gas molecules leading to further electrons being released in the gas at different distances from the main avalanche. At some point, the space charge electric field will be in the same order of magnitude as the original applied field, and the distortion of electric field will lead to additional, second-generation avalanches to be developed. As auxiliary avalanches are formed and the process keeps repeating, additional generation avalanches will be created which will cause the branching of the main avalanche to several ones. These positive ion branches, or channels, are called streamers and it describes the way an electron avalanche develops from anode to cathode to eventually lead to a breakdown [21], [27], [28].
4. Leaders: Under some experimental conditions, such as high pressures, there is a high probability of some streamer branches to develop into leaders. As the streamer branches grow closer to the cathode, ionisation intensity in some of the branches is more than the

rest. As a result of the higher energy exchange in those specific branches, between the energetic electrons and neutral molecules, the ohmic loss of energy increases which results to significant heating in the specific branch. The temperature of the gas at that region increases which expands the gas and reduces the density of the molecules. As a result of the reduced density, ionisation becomes more efficient and the branch develops to a highly ionised, high-temperature, arc-like channel with is also highly conductive. This channel is defined as leader and it usually the precursor of an electrical breakdown which is also known as arc or plasma [28].

Gas breakdown mechanisms generally follow the above structure, but they can vary with field uniformity. At uniform fields, the electric stress is similar everywhere hence the ionisation and deionisation parameters are constant. At non-uniform fields, there are regions of enhanced electric field and therefore the ionisation patterns can vary within the gap. More details about different breakdown mechanisms can be found in [21], [27], [28].

2.4.2 SF_6 Insulation

SF_6 has been used as an insulant in gas insulated equipment since the 1960s. Its non-toxic, non-flammable and chemically stable nature are key properties which make it ideal for gas handling and insulation purposes [21]. Out of all the properties, the most important one is its high electronegativity. This is defined as the ability of the fluorine atoms to capture free electrons flowing within the gas and form heavy negative ions, which inhibits the development of an electron avalanche process. This attribute makes it a far better insulating gas than non-attaching gases such as air and CO_2. The dielectric strength of SF_6 is about 2.5 to 3 times higher than air and CO_2 [28], [29]. Figure 2-5 shows the difference in AC breakdown voltage for SF_6, air and transformer oil using a sphere-plane electrode configuration with a constant gap distance of 12.5 mm.

As shown in the figure, SF_6 has a significantly higher breakdown voltage than air throughout the pressure range tested. Transformer oil has the highest breakdown strength at low pressures but when SF_6 exceeds 3 bar it has a better breakdown voltage than the other two insulating mediums shown in the figure.

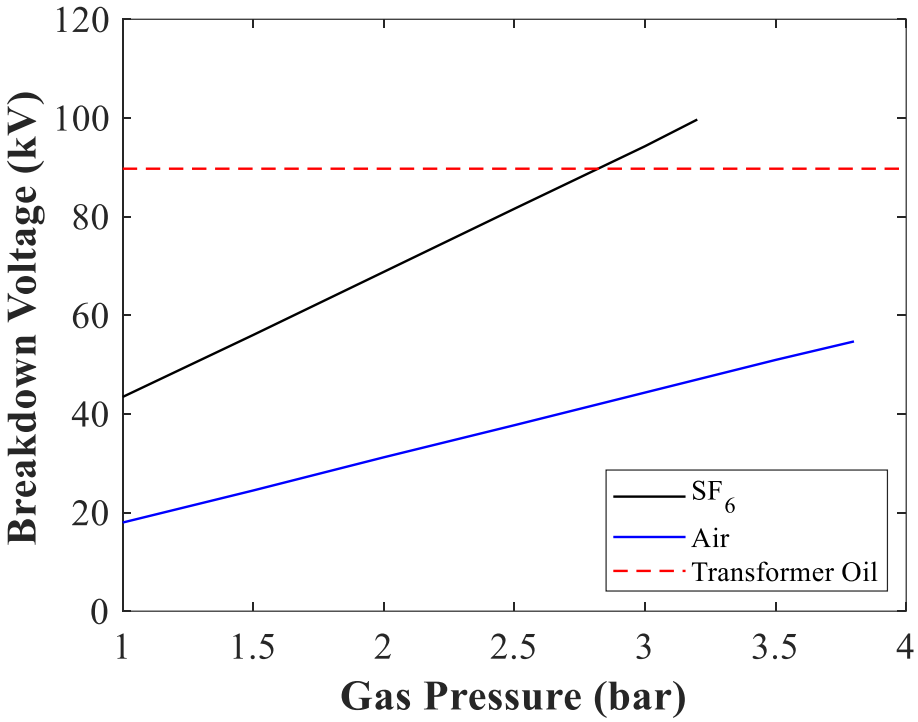

Figure 2-5. Breakdown strength of SF_6, air and transformer oil as a function of pressure using a sphere-plane electrode configuration with a gap distance of 12.5 mm [29].

2.4.3 Environmental Concerns of SF_6

Even though SF_6 is an ideal gas for insulation and arc-quenching purposes, its high environmental impact is a huge concern when it leaks into the atmosphere. Environmental agreements such as the Kyoto Protocol (1997) [30] or the recent EU F-gas regulation (2015) [14], [15] aim to reduce the emissions of the top six greenhouse gases, namely: carbon dioxide (CO_2), methane (CH_4), nitrous oxide (N_2O), hydrofluorocarbons (HFCs), perfluorocarbons (PFCs) and sulphur hexafluoride (SF_6).

According to [3], GWP is defined as "the total energy added to the climate system by a component in question relative to that added by CO_2.". The global warming potential can be given by two values: Absolute Global Warming Potential (AGWP) or the relative Global Warming Potential (GWP). AGWP is given by the integration of the radiative forcing efficiency for a specific time horizon, which is usually a 20- or 100-year period as shown in Figure 2-6. Radiative forcing efficiency is the ability of a gas to absorb sunlight energy and radiate it back which is the main attribute of greenhouse gases. The blue hatched area in Figure 2-6 shows the integrated radiative forcing efficiency from a pulse of CO_2 while the

green and red represent example gases with 1.5- and 13-years lifetimes respectively. GWP is considered as a dimensionless value since it is represented by the ratio of the AGWP of the gas under investigation, in this case SF_6, and the reference gas (CO_2) [3]. CO_2 has been used as the reference gas as it is the most common pollutant in the atmosphere.

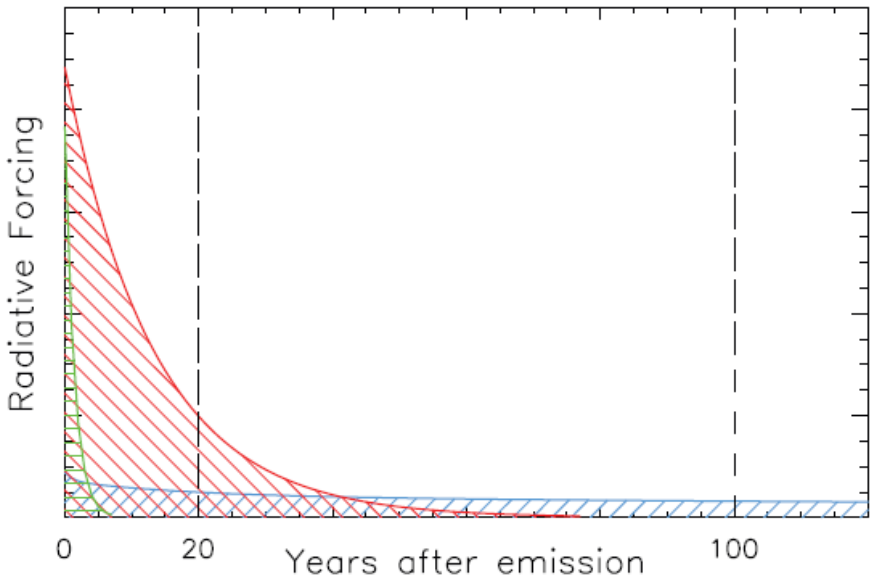

Figure 2-6. Radiative forcing as a function of years after emission and the integrated curves for CO_2 (blue) and example gases with 1.5 (green) and 13 years (red) lifetimes [3].

Despite the very small contribution of SF_6, compared to the rest of the greenhouse gases, its effect is significant because of its extremely high GWP value. More specifically, 1 kg of SF_6 released into the atmosphere is equivalent to approximately 23.5 tons of CO_2 emissions. The comparison of environmental properties between CO_2 and SF_6 is given in Table 2-4.

Table 2-4. GWP and AGWP for 20 and 100-year horizons for CO_2 and SF_6 [3].

Chemical Formula	Lifetime (Years)	Radiative Efficiency (W m^{-2} ppb^{-1})	AGWP 20-year (W m^{-2} yr kg^{-1})	GWP 20-year	AGWP 100-year (W m^{-2} yr kg^{-1})	GWP 100-year
CO_2	-	1.37e-5	2.49e-14	1	9.17e-14	1
SF_6	3,200	0.57	4.37e-10	17,500	2.16e-09	23,500

Due to its long atmospheric lifetime of 3,200 years, emissions of SF_6 accumulate in the atmosphere and therefore its environmental damage increases over time. As shown in Figure 2-7, this has resulted in a steady increase of its global mean concentration in the atmosphere

over the years [4]. Figure 2-7 also shows that from 2010-2015 only, the SF_6 concentration in the atmosphere has increased by more than 20%. In addition, actual SF_6 emissions from developed countries have been found to be at least twice than the reported values [3].

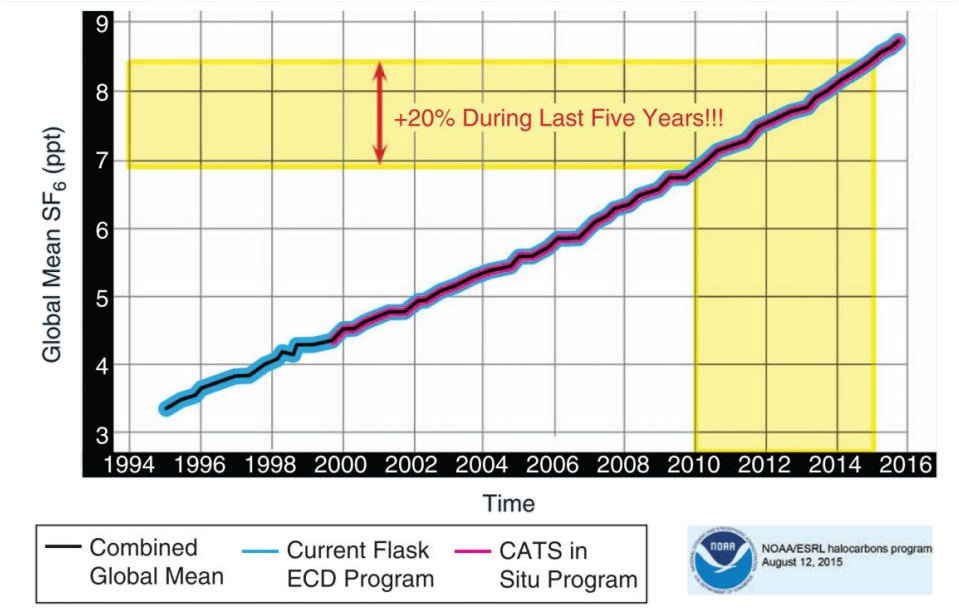

Figure 2-7. Global mean SF_6 concentration increase in the atmosphere from 2010 to 2015 [4].

2.4.4 SF_6 Alternatives for Insulation Applications

The concerns for the environmental impact of SF_6 to the atmosphere have caused its restriction in several applications. However, SF_6 is still widely used in the power industry as there is no readily available one-for-one replacement candidate. As the power industry is the main user of SF_6, responsible for 80% of the total usage worldwide [4], the initiative to replace SF_6 in high voltage equipment applications has been growing over the past few years. An ideal SF_6 replacement gas should satisfy a strict list of requirements, which include [4]:

- High dielectric strength
- Good arc-quenching capability
- Low boiling point
- High thermal and chemical stability
- Compatibility and no corrosion to the equipment materials
- Non-flammable and non-toxic
- Low environmental impact

Depending on the application of the insulating gas, the requirements for a SF_6-alternative can vary. For example, for a gas that is going to be used for passive components, the good arc-quenching capability requirement can be excluded. A review of the most important requirements for the applications of this thesis is given in Section 2.4.6. In the literature, a significant number of gases that were previously examined as potential replacements to SF_6. Families of gases such as perfluorocarbons, fluoroketones and natural gases were investigated where each of them had their own unique advantages as well as disadvantages. A review of the most popular gases studied for SF_6 replacement is given below.

2.4.4.1 Perfluorocarbons (PFCs)

Fluorine, the same chemical element that exists in SF_6, is known to have a highly electronegative nature. Perfluorocarbons (PFCs), which are compounds that only contain carbon and fluorine atoms, have been found to offer a dielectric strength equal to or even greater than SF_6 [18]. Table 2-5 gives an overview of the main properties for PFCs that were studied as SF_6 replacements. As shown in the table, C_4F_8 is the gas with the highest dielectric strength. However, its high boiling point limits its potential for being used as a pure gas and it has to be mixed with a buffer gas [16]. Regarding rest of the PFCs shown in the table, their boiling points are satisfactory, but their dielectric strength is relatively low when compared to SF_6 (less than 1 pu). Nevertheless, the main disadvantage of PFCs, which makes them unsuitable for being used as SF_6-alternatives, is their GWP which lies within the range of 6,000 to 12,000. Despite this GWP being an approximately 50% reduction from SF_6, their environmental impact is still considerably high, and they are also placed amongst the most potent greenhouse gases [16], [18], [31], [32].

Table 2-5. PFCs dielectric strength, GWP and boiling point [16], [18], [31], [32].

Chemical Formula	Dielectric Strength Relative to SF_6 (pu) [16], [18], [31], [32]	GWP 100-year [3]	Boiling Point (°C) [16], [18], [31]
C_4F_8	1.25	9,540	-6.0
C_3F_8	0.88	8,900	-36.7
C_2F_6	0.78	11,100	-78.1
C_3F_6	0.92-1.00	9,200	-29.6
CF_4	0.40	6,630	-128.0

2.4.4.2 Fluoroketones (FKs)

Fluoroketones (FKs), shown in Table 2-6, combine an extremely low GWP with a dielectric strength that can exceed SF_6. However, C_4F_8O has an extremely toxic profile which poses a threat to the personnel handling it and is therefore unsuitable for being considered as a potential SF_6-alternative [18], [32]. $C_5F_{10}O$ and $C_6F_{12}O$ are both safe to use as they are substantially non-toxic in their pure state. However, $C_5F_{10}O$ and $C_6F_{12}O$ have the drawback of having a considerably higher boiling point. At atmospheric pressure, $C_5F_{10}O$ and $C_6F_{12}O$ condense into liquids at temperatures below 26.9°C [33] and 49°C [18], [32] respectively. At room temperature (≈20°C), $C_5F_{10}O$ and $C_6F_{12}O$ cannot be used at a pressure higher than 0.8 bar (abs) and 0.3 bar (abs) respectively [18], [32]. For this reason, the two candidates need to be used as a binary mixture with a carrier gas such as CO_2, N_2 or dry air. However, due to their extremely low saturation vapor pressure, it is difficult to find suitable mix ratios for $C_5F_{10}O$ and $C_6F_{12}O$ gases that can combine the electrical and operational properties to replace SF_6 in high voltage equipment used at pressures up to 6 bar (abs). Gas mixtures of $C_5F_{10}O$, also commonly known as Novec^{TM} 5110 Insulating Gas, with dry air and CO_2 have been investigated as potential SF_6-alternatives for medium voltage applications, where the filling pressure can go down to 1.3 bar (abs) [17], [32].

Table 2-6. FKs dielectric strength, GWP and boiling point [18], [32]–[34].

Chemical Formula	Dielectric Strength Relative to SF_6 (pu) [18], [34]	GWP 100-year [18], [32], [34]	Boiling Point (°C) [18], [32]–[34]
C_4F_8O	-	< 1	0
$C_5F_{10}O$	2.10	< 1	26.9
$C_6F_{12}O$	2.70	< 1	49.0

2.4.4.3 Hydrofluoroolefins (HFOs)

Hydrofluoroolefins are compounds composed of hydrogen, fluorine and carbon atoms. As they have a partially fluorinated nature, their dielectric strength can be compared to SF_6 and at the same time combine a low GWP of less than 10 [18], [32]. However, HFO-1234yf has an extremely flammable nature and is therefore unfitting for replacing SF_6. HFO-1234ze and HFO-1336mzz-Z come with the disadvantages of low dielectric strength and high boiling

point respectively [18]. The most important downside for this group of gases, however, is that a flashover can lead to carbon dust creation on the solid insulators. This carbon dust layer is conductive and can potentially result to a failure of the equipment [18], [32].

Table 2-7. HFOs dielectric strength, GWP and boiling point [18].

Chemical Formula	Dielectric Strength Relative to SF_6 (pu)	GWP 100-year	Boiling Point (°C)
HFO-1234ze	0.85	6	-19.4
HFO-1234yf	-	4	-29.4
HFO-1336mzz-Z	2.20	9	33.4

2.4.4.4 Trifluoroiodomethane (CF_3I)

Investigations on CF_3I are still ongoing [35]–[39] in order to study its potential of replacing SF_6 gas in electrical applications. When pure, CF_3I combines a dielectric strength of 1.2 times the one of SF_6 with a negligible GWP of less than 1 [38]. It has multiple similar properties to SF_6 such as being colourless, non-flammable and highly electronegative as well as having a negligible ozone depleting potential. However, three main disadvantages make it hard to use in high voltage applications: (i) slightly toxic which classifies it as mutagenic and category three health and safety risk [18], [32], [38] (ii) weak C-I chemical bond resulting in iodine deposits that can affect its insulation performance [18], [35], [39] and (iii) only 1.2 times higher dielectric strength than SF_6, making it difficult to lower the boiling point even more (using it as a mixture with a buffer gas such as CO_2 or N_2) whilst maintaining equal dielectric strength to SF_6.

2.4.4.5 Natural Gases

Naturally occurring gases, such as N_2, CO_2 or dry air, already exist in the atmosphere and therefore do not damage the environment [18], [32]. Their main weakness is their low dielectric strength in comparison to SF_6 due to their weakly or non-attaching properties. As shown in Table 2-8, CO_2, N_2 and dry air have a dielectric strength of about a third of SF_6 [18], [28]. Therefore, an operating pressure of three times the one used for SF_6 would be necessary in order to achieve the same insulation level. This will not allow a direct SF_6 replacement to occur, but instead the dimensions, the materials and mechanical structure of

the equipment will need to change to support the increased operating pressure. All of these changes can be time-consuming but also lead to additional re-structure costs in order to use these gases for high voltage applications which have to be considered [18], [32].

Table 2-8. Natural gases dielectric strength, GWP and boiling point [18], [28].

Chemical Formula	Dielectric Strength Relative to SF_6 (pu) [18], [28]	GWP 100-year [18], [28]	Boiling Point (°C)
N_2	0.33	0	-78.5
CO_2	0.30	1	-195.8
Dry Air	0.30	-	-

2.4.5 C_3F_7CN as a Potential SF_6-Alternative

2.4.5.1 Physical Properties

$(CF_3)_2$-CF-CN or C_3F_7CN, also commonly known as Novec^{TM} 4710 Insulating Gas, shares several similar properties to SF_6. The physical properties for both gases are shown in Table 2-9 [7], [40]. Both gases are odourless, colourless and non-flammable. C_3F_7CN has higher molecular weight, boiling point and gas density than SF_6. None of the gases causes any amount of degradation to the ozone layer and this is specified by the ozone depletion potential (ODP) of zero. C_3F_7CN has a GWP of about a tenth of SF_6. The key difference between the two gases lies in the atmospheric lifetime where C_3F_7CN can decompose within 30 years while SF_6 has an accumulative environmental impact over time.

Table 2-9. Comparison of properties between C_3F_7CN and SF_6 [7], [40].

Property (at 25°C)	C_3F_7CN	SF_6
Molecular Weight (g/mol)	195	146
Boiling Point (°C)	-4.7	-63.8
Vapour Pressure (bar)	2.52	21.49
Gas Density at 1 bar (kg/m^3)	7.9	5.9
Atmospheric Lifetime (years)	30	3,200
Ozone Depletion Potential (ODP)	0	0
GWP 100-year	2,090	23,500

2.4.5.2 Insulation Characteristics

Figure 2-8 illustrates the comparison of pure C_3F_7CN and SF_6 in terms of AC breakdown voltage for relatively uniform fields using a parallel disk electrode configuration [7], [9].

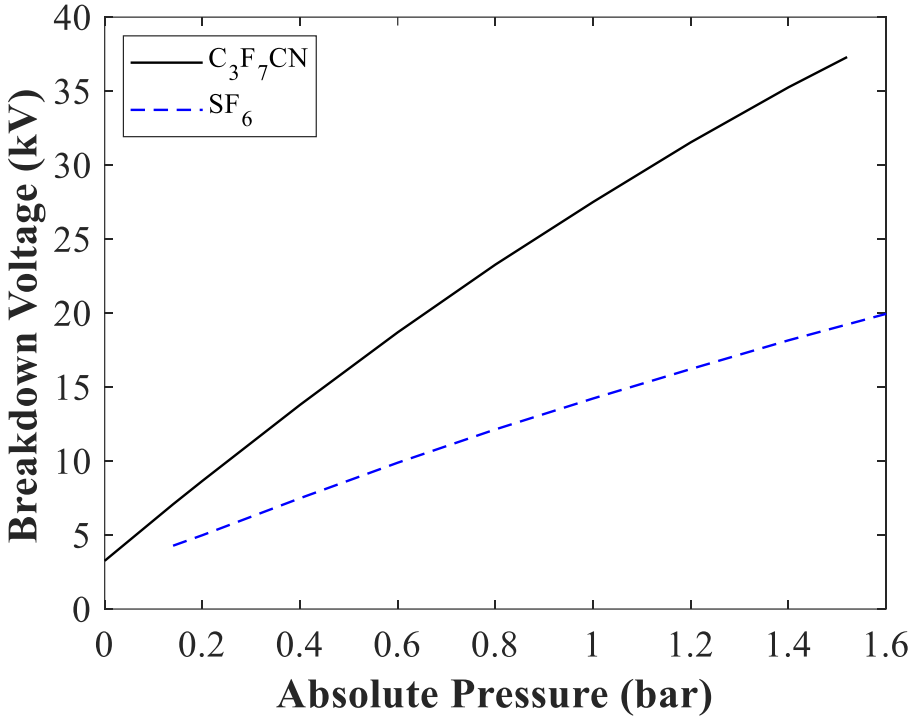

Figure 2-8. AC breakdown voltage comparison between C_3F_7CN and SF_6 for parallel disk electrodes (relatively uniform field) with a gap distance of 2.5 mm [7], [9].

It can be seen from the figure that C_3F_7CN has almost double the breakdown voltage of SF_6 for a pressure range up to 1.6 bar (abs). The breakdown voltage of SF_6 and C_3F_7CN is very similar at low pressures but their difference increases with pressure. It is unlikely, however, for C_3F_7CN to be used in its pure form for GIB and GIL since its high boiling point limits its applications for high operating pressures (up to 5 bar absolute) [7], [9].

2.4.5.3 Saturation Vapour Pressure

The major difference between the two gases is in terms of boiling point and saturation vapour pressure. C_3F_7CN has a boiling point which makes it liquefy at temperatures below -4.7°C in comparison to SF_6 of which the boiling point is -63.8°C. Figure 2-9 displays the difference of the two gases regarding their saturation vapour pressure at room temperature (≈25°C) [7], [9]. At this temperature, C_3F_7CN can only be used up to 2.52 bar (abs) without liquefying

while SF_6 can be used up to approximately 21.49 bar (abs). As mentioned before, this drawback limits its use as a pure gas. However, this restraint can be bypassed by using C_3F_7CN in lower concentrations as part of a mixture with CO_2, N_2 or dry air which reduces the boiling point while keeping a comparable dielectric strength to SF_6.

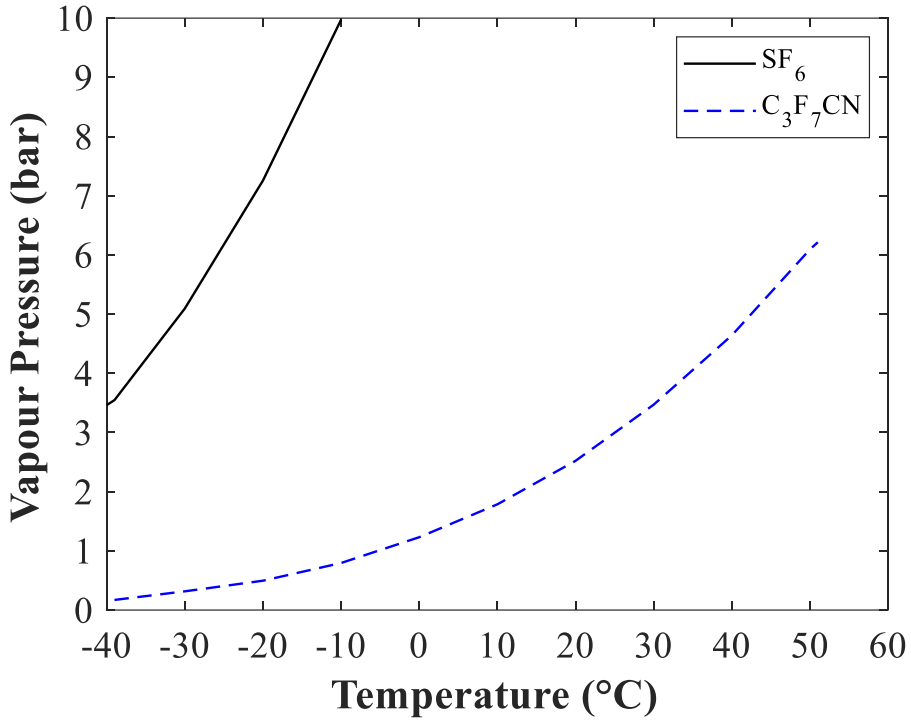

Figure 2-9. Vapour pressure curve as a function of temperature comparing C_3F_7CN and SF_6 [7], [9].

2.4.6 Selection of a Technically Viable Gas Candidate for High Voltage Insulation Applications

Section 2.4.4 has described a considerable number of gases that were previously investigated and proposed as potential replacements to SF_6. This section summarises all the gases studied so far and adopts a simple selection method which is based on four main criteria shown in Figure 2-10.

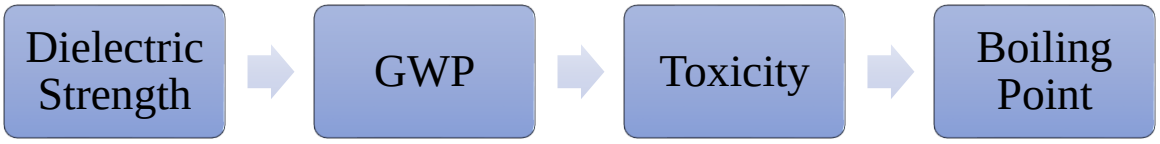

Figure 2-10. Important SF_6-replacement criteria for high voltage insulation applications.

The criteria shown in Figure 2-10 are considered the most important for replacing SF_6 in high voltage insulation applications such as GIB and GIL. Figure 2-11 graphically summarises the assessment process to narrow down an appropriate gas candidate from a wide range of potential SF_6 alternatives [16]–[18], [32], [41]. From this process, even pure C_3F_7CN is filtered out and judged as an unsuitable SF_6-alternative. However, C_3F_7CN/CO_2 gas mixtures have emerged as a gas medium that can be considered technically viable for the retro-fill research investigation carried out in this thesis.

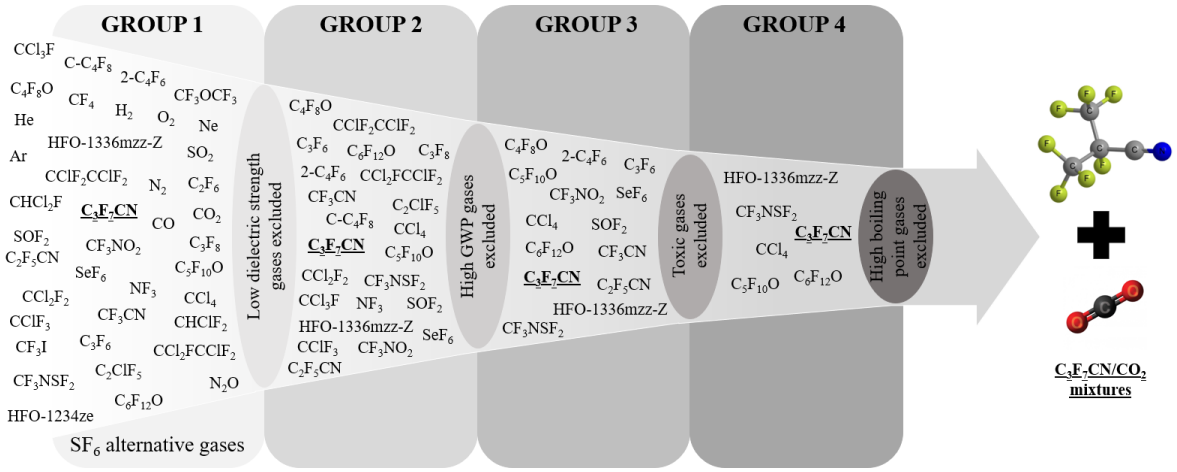

Figure 2-11. Elimination of SF_6 alternatives for high voltage insulation applications based on data from [16]–[18], [32], [41].

Group 1 illustrates a wide selection of potential SF_6 alternatives studied to date [16]–[18], [32], [41]. Group 2 excludes the gases that have low dielectric strength relative to SF_6. Naturally occurring gases are an example of this elimination since they possess dielectric strength of about a third of SF_6 [18], [32]. This would inherently require a higher operating pressure or an increased internal electrical clearance, which not only goes against the efforts to reduce equipment footprint but would also lead to additional complexities in replacing existing SF_6-designed equipment. Group 3 eliminates the undesirable gases that have a relatively high GWP in the range of 4,000 to 12,000. An example being the perfluorocarbon gases which have demonstrated that they can reach or even exceed the dielectric strength of SF_6 because of the presence of multiple fluorine atoms in their molecular structure. However, due to their extremely long atmospheric lifetime (> 2600 years), these gases are also categorised as greenhouse gases [18]. High toxicity gases are eliminated in Group 4 since any alternative to SF_6 gas should not pose a risk to the personnel handling it [42]. Finally, gases with an extremely high boiling point are eliminated in the last stage after Group 4

because they can only be used at low pressures under room temperature (25°C) to prevent liquefaction. Therefore, they are not suitable for high voltage equipment where higher pressures of over 4 bar (abs) are used. The fluoroketone gases family is an example of this group of gases [18], [32]. Following this process of elimination, C_3F_7CN/CO_2 gas mixtures have been selected as potential candidates for further investigation.

2.5 C_3F_7CN/CO_2 as a Gas Mixture

2.5.1 Environmental Impact and Toxicity

Figure 2-11 illustrates that no pure gas, neither C_3F_7CN, was able to combine all four key properties: high dielectric strength, low GWP, low toxicity and low boiling point. Taking all the candidates in Figure 2-11 into consideration, C_3F_7CN used with a carrier gas appears to be the most technically viable alternative. In its pure form, it has a significantly lower environmental impact compared to SF_6 since it has an atmospheric lifetime of 100 times shorter (30 years) and a GWP of about a tenth (2,090) that of SF_6. The overall GWP will reduce further when C_3F_7CN is used as mixtures. In [6], [8], 4%, 6% and 10% C_3F_7CN concentrations were reported to have a reduced GWP of 327, 462 and 690 respectively.

According to the classification, labelling and packaging (CLP) regulation 1272/2008, with a 4-hour LC_{50} (lethal concentration at 50% mortality) between 10,000 to 15,000 [43], C_3F_7CN is classified as a practically non-toxic gas. LC_{50} is defined as the concentration of a gas/gas mixture required in air, with a single exposure of a few hours (usually 4-hour), to lead to the death of 50% of albino rats (male and female) that are under investigation in a time period of at least 14 days [44]. The LC_{50} of a gas/gas mixture is calculated using equation (2-5):

$$LC_{50} = \frac{1}{\sum_i \frac{C_i}{LC_{50}}} \tag{2-5}$$

Where C_i is the mole fraction of the ith toxic component present in the gas mixture and LC_{50i} is the lethal concentration of the ith toxic component [LC_{50} < 5,000 (by volume)]. In BS ISO 10298:2010 [44], the assessment of the gas mixtures toxicity is made according to the parts

per million (ppm) by volume value of LC_{50}. Figures 2-12 and 2-13 show the toxicity and inhalation toxicity values respectively that assess how harmful a gas mixture is.

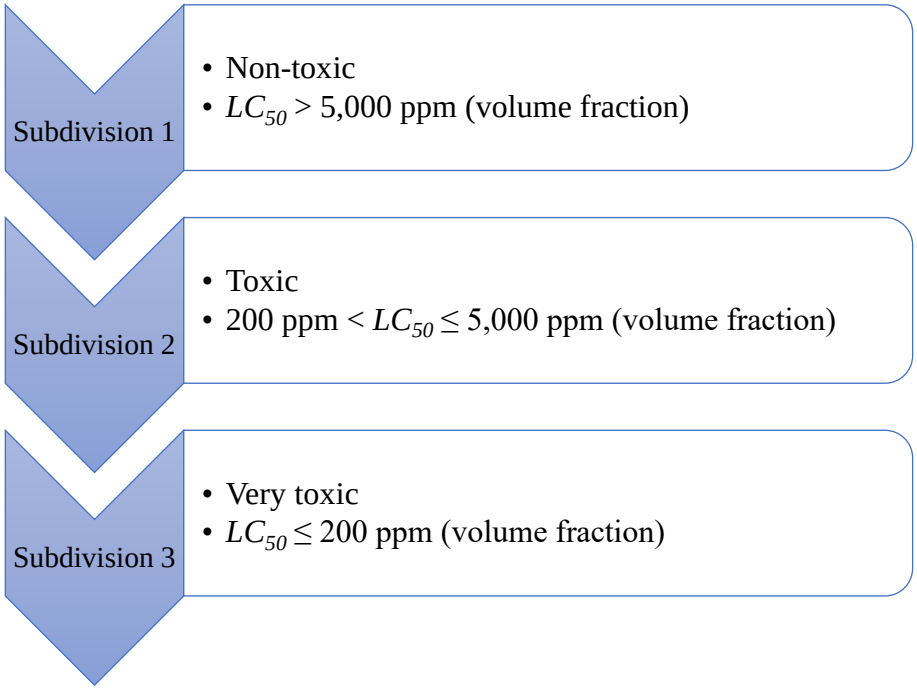

Figure 2-12. Toxicity subdivisions of gas mixtures from non-toxic (subdivision 1) to very toxic (subdivision 3) for 1-hour exposure LC_{50} values [44] .

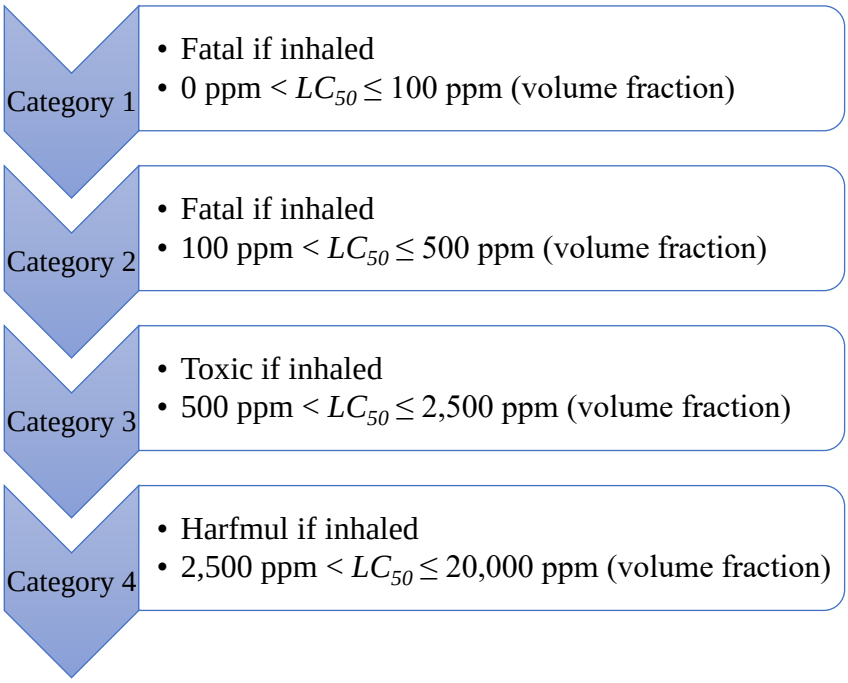

Figure 2-13. Toxicity inhalation categories from fatal (category 1) to harmful (category 4) for 4-hour exposure LC_{50} values[44].

Similar to the GWP, the overall toxicity reduces when C_3F_7CN is used as part of a mixture with CO_2, which indicate that an acceptable personnel safety margin can be achieved in typical gas release scenarios within substations [6], [45]. The LC_{50} values of pure C_3F_7CN and low concentration C_3F_7CN/CO_2 mixtures are shown in Table 2-10.

Table 2-10. LC_{50} 4-hour exposure values for pure C_3F_7CN and C_3F_7CN/CO_2 mixtures [6], [43].

Gas / Gas Mixture	LC_{50} (ppm)	
C_3F_7CN	$10{,}000 < LC_{50} < 15{,}000$	
	Males	Females
4% C_3F_7CN / 96% CO_2	160,000	212,000
10% C_3F_7CN / 90% CO_2	100,000	95,500

2.5.2 Dielectric Strength

As mentioned before, C_3F_7CN is a highly electronegative gas which implies that the more concentration used in a mixture, the higher the dielectric strength of the overall gas mixture. Since the aim of this research is retro-filling SF_6-designed equipment, one must first determine a mixture ratio that has a comparable dielectric performance to SF_6. For the electrode configuration used in Figure 2-8, it was reported that a mixture of 20% C_3F_7CN and 80% CO_2 exhibits comparable dielectric performance to SF_6 and higher than 20% C_3F_7CN mixtures with N_2 or dry air [9]. The breakdown performance of the 20% C_3F_7CN gas mixtures is shown in Figure 2-14.

As shown, CO_2 demonstrates the most favourable dielectric properties for it to be used as a carrier gas with a slight advantage in breakdown voltage. Another advantage of CO_2 over other buffer gases is that in [46] it is reported that it has a superior arc-quenching capability than N_2. There is a clear difference in arc-quenching capabilities between the two gases as CO_2 was found to have an arcing time of approximately 15 μs while for N_2 it was about 220 μs. Despite the 20% C_3F_7CN and 80% CO_2 gas mixture showing potential for replacing SF_6, it must be further experimentally validated using a representative test configuration, like a coaxial geometry, prior to proposing it as a retro-fill solution for GIB and GIL of transmission voltage level applications.

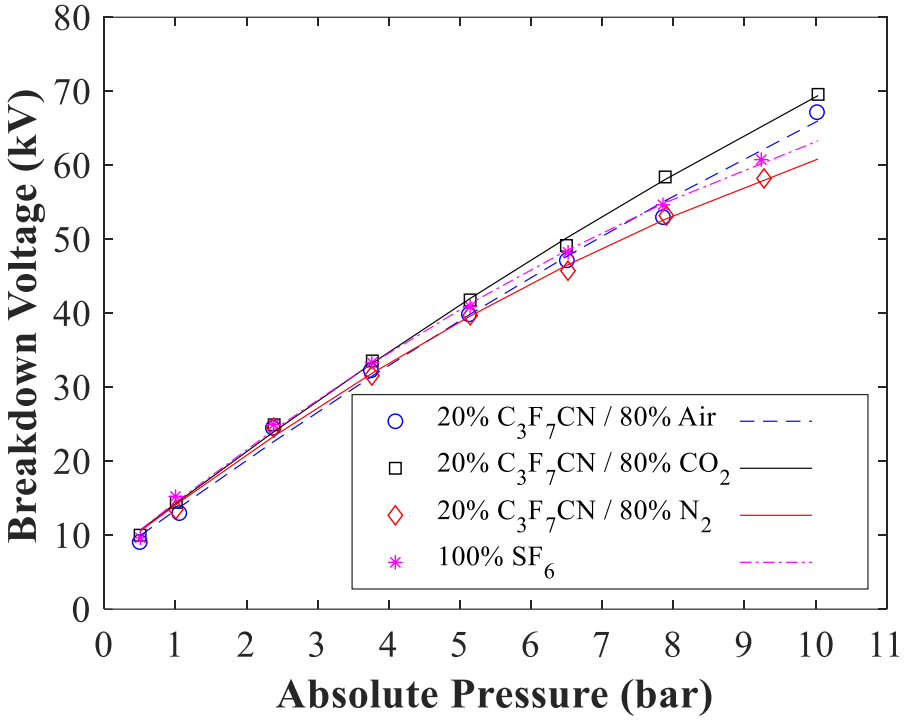

Figure 2-14. AC breakdown voltage comparison between 20% C_3F_7CN gas mixtures and SF_6 for parallel disk electrodes (relatively uniform field) with a gap distance of 2.5 mm [7], [9].

2.5.3 Boiling Point

The key downside of C_3F_7CN compared to SF_6 is the higher boiling point of -4.7°C. The boiling point of C_3F_7CN reduces considerably when used in low concentrations as part of a binary mixture with CO_2. The boiling point as a function of C_3F_7CN concentration for different pressures is plotted in Figure 2-15. The values in this figure were calculated using the Peng-Robinson Equation of State method [47] adapted for C_3F_7CN mixtures and were provided by 3M which is the main manufacturer of the gas.

As shown in the figure, boiling point increases with pressure and C_3F_7CN concentration. Using 20% C_3F_7CN concentration in a gas mixture, which exhibits comparable dielectric strength to SF_6, can reduce the boiling point down to -42°C (at 1 bar absolute) which is a significant decrease from its pure form.

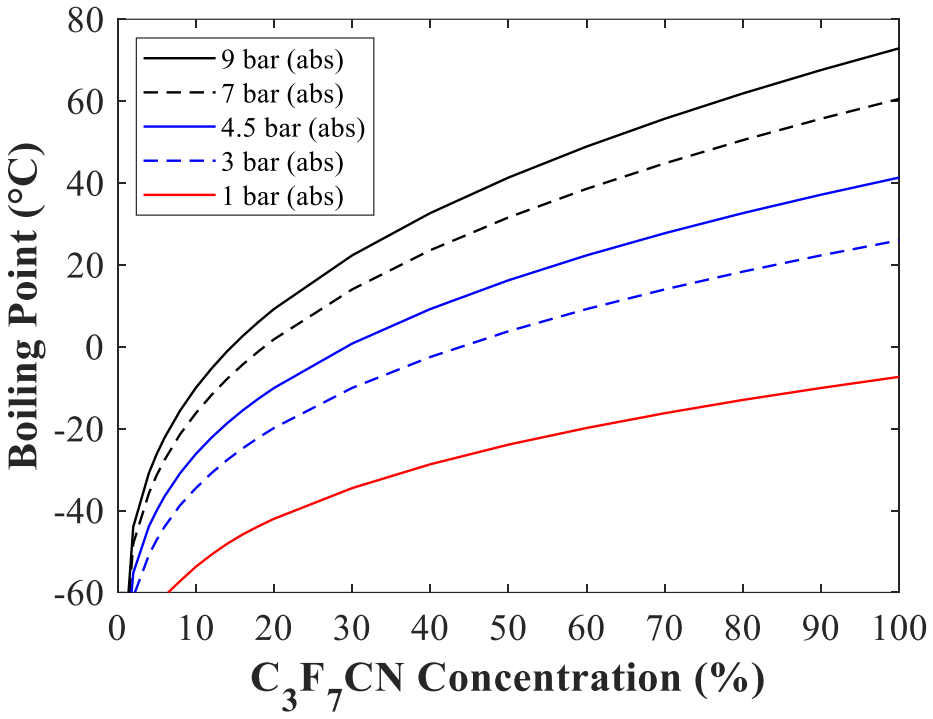

Figure 2-15. Boiling point as a function of C_3F_7CN concentration for a C_3F_7CN/CO_2 gas mixture calculated using the Peng-Robinson Equation of State method.

2.6 Experimental Investigations on C_3F_7CN Gas and its Mixtures

Investigating the possibility of replacing SF_6 in high voltage equipment with C_3F_7CN mixtures involves the process of fully examining the gas behaviour and especially its electrical characteristics. In the literature, the electrical characteristics have been covered by breakdown and PD tests. Both types of tests can be affected by multiple parameters such as pressure, field uniformity, gap distance, buffer gas, voltage waveform shape and polarity [48]. The selection of AC or DC voltage for breakdown or PD tests heavily depends on the nature of the equipment that is under evaluation (e.g. whether HVAC or HVDC GIL applications are investigated). For breakdown voltage studies, insulation materials are also subjected to external and internal overvoltages in the form of LI and SI voltage waveforms respectively. As switching overvoltages in power systems only become important for the voltages of 245 kV and above, LI breakdown tests are more widely used for characterisation as they have more impact on the insulation failure for equipment below 245 kV [27]. This section is to critically review the work done on C_3F_7CN and its mixtures from previous

studies and identify the gaps in research that need to be completed in order to suggest a potential retro-fill solution.

2.6.1 Effect of Buffer Gas, Mixing Ratio and Pressure on Breakdown Voltage

Figure 2-14 has shown that from the results in [9], the buffer gas as well as the mixing ratio makes a difference to the breakdown voltage of the C_3F_7CN gas mixture. Using CO_2 as a buffer gas has shown a better dielectric performance than using N_2 and dry air and a concentration of 20% C_3F_7CN has shown a comparable dielectric strength to SF_6.

Figures 2-16 and 2-17 show the results from [49] on the effect of buffer gas and mixing ratio on the AC breakdown field strength. The breakdown field strength shown in the two figures was acquired using a uniform field with a plane-plane electrode configuration and is illustrated as a function of C_3F_7CN content for different pressures. Regardless of the buffer gas used with C_3F_7CN, the breakdown field strength increases with the C_3F_7CN content.

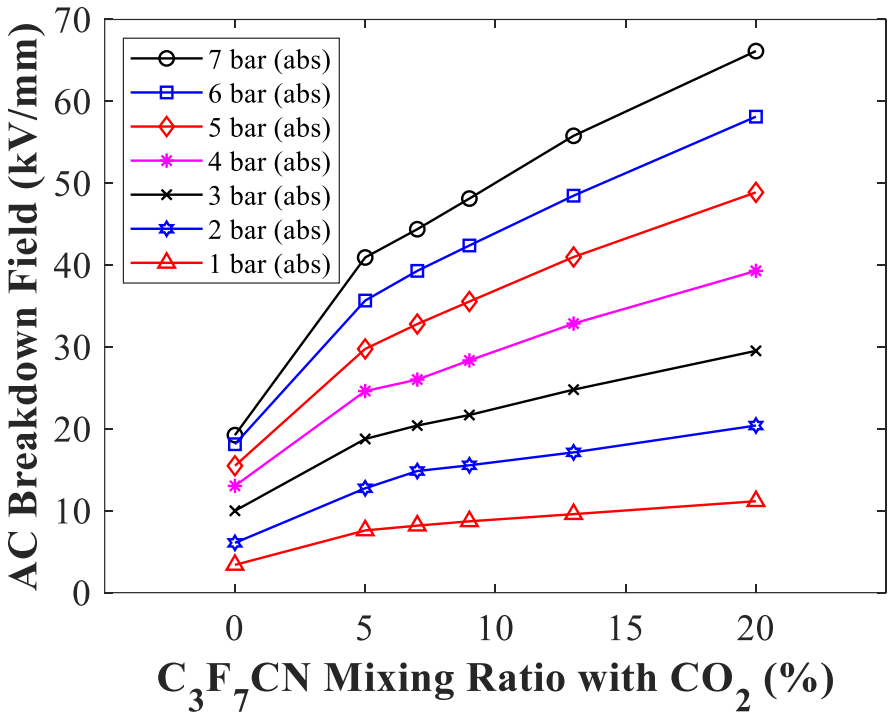

Figure 2-16. AC breakdown field strength as a function of C_3F_7CN mixing ratio with CO_2 as a buffer gas using a plane-plane electrode configuration with a gap distance of 2.5 mm [49].

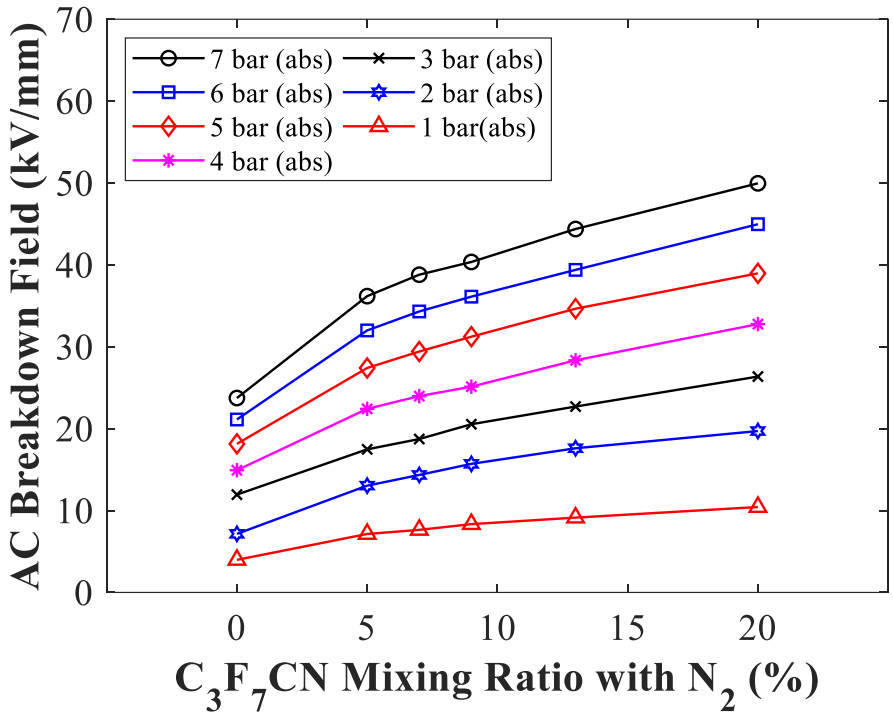

Figure 2-17. AC breakdown field strength as a function of C_3F_7CN mixing ratio with N_2 as a buffer gas using a plane-plane electrode configuration with a gap distance of 2.5 mm [49].

Pure N_2 and CO_2 exhibit a comparable insulation performance as shown in the results presented in Figures 2-16 and 2-17. However, when adding the same percentage of C_3F_7CN in the two buffer gases, the C_3F_7CN/CO_2 mixtures have a better insulation performance than C_3F_7CN/N_2 which validates the results in [9]. As reported in [49], this is attributed to the synergistic effect of the mixtures where the synergy between C_3F_7CN and CO_2 gases is stronger than the C_3F_7CN and N_2 gases which in turn leads to a higher breakdown voltage.

As CO_2 has shown better insulation capabilities than N_2, in mixtures combined with C_3F_7CN, several studies were solely using the former one as the buffer gas. Additional studies using uniform and quasi-uniform electric fields [4], [50] confirmed that an amount of 18-20% C_3F_7CN combined with CO_2 gas can reach a dielectric strength equivalent to SF_6. Figure 2-18 shows the effect of pressure and mixing ratio on the AC breakdown voltage of C_3F_7CN gas mixtures in comparison to SF_6. The breakdown voltages in this figure were acquired with a quasi-uniform field using a sphere-sphere electrode configuration with a gap distance of 2 mm. As shown in the figure, there is a linear correlation between the pressure and the breakdown voltage up to 4 bar (abs) for all the gases illustrated.

The breakdown voltage can increase with pressure since the mean free path (average distance between two successive impact collisions) of the gas molecules is reduced. However, when the pressure exceeds 4 bar (abs), a saturation trend is noticeable which can occur at higher pressures. The non-linear pressure relationship with breakdown voltage has been generally observed in gaseous dielectrics [51], [52]. The breakdown voltage of gaseous insulation mediums tends to saturate at higher pressures, which could be attributed to the increased gas density at higher pressures. There will come a point where density will not make as much of a difference to the ionisation (α) and attachment (η) processes as it did at lower pressures, and this might eventually cause the curve saturation. Similar saturation trend was observed at higher C_3F_7CN concentrations in a gas mixture shown in Figures 2-16 and 2-17. For low C_3F_7CN content mixtures, it is noticeable that the breakdown voltage increased significantly with a small addition of C_3F_7CN to test with pure CO_2 or N_2, which are weakly and non-attaching gases respectively. However, as the C_3F_7CN mixing ratio increases there will come a point like with pressure, where the increased volume of C_3F_7CN in the mixture will not make as much difference to the ionisation or attachment process as it did at lower concentration mixtures [50].

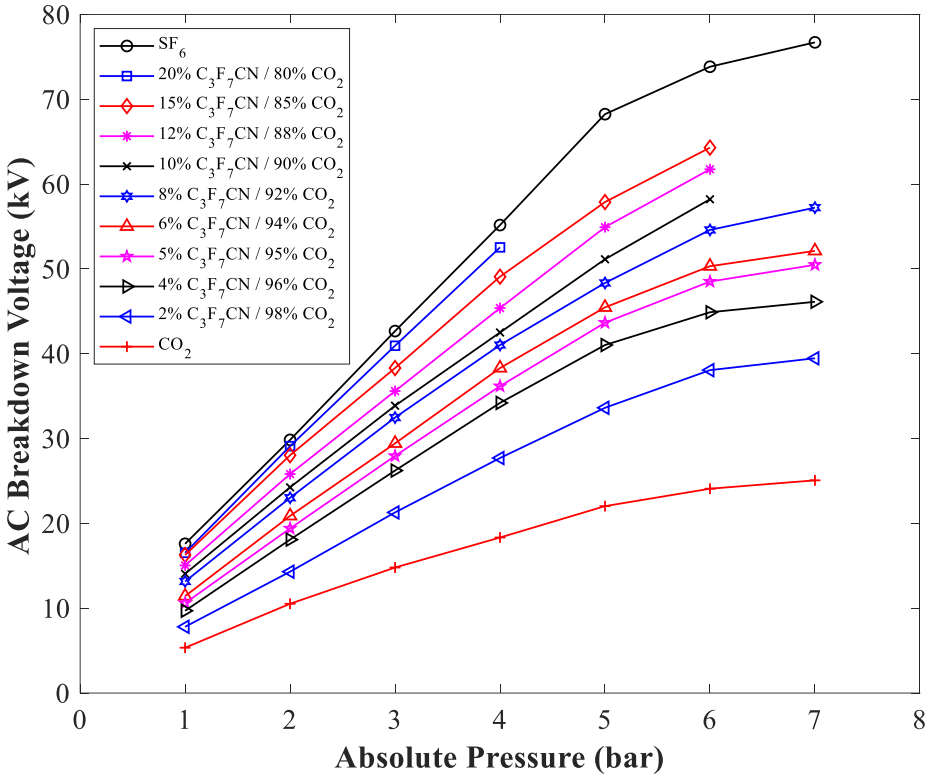

Figure 2-18. AC breakdown voltage as a function of absolute pressure (bar) for C_3F_7CN/CO_2 gas mixtures and SF_6 using a sphere-sphere electrode configuration and a gap distance of 2 mm [50].

2.6.2 Effect of Field Uniformity and Gap Distance on Breakdown Voltage

Dielectric gases can be exposed to different electric field stresses within the power equipment which can ultimately affect their insulation performance. A dielectric medium can have its strongest insulation performance when exposed to uniform fields. However, perfectly uniform fields are hard to achieve in practical equipment and regions of non-uniform fields can weaken the performance of the dielectric medium. GILs and GIBs are usually represented by weakly non-uniform electric fields. However, the existence of triple junctions, protrusions on conductor/enclosure or metallic particles introduce electric field enhancements which expose the insulation gas to extremely non-uniform electric fields [27], [53]. Design parameters of electrode configurations, such as geometry and gap spacing, can alter the electric field from uniform to extremely non-uniform fields in order to test the gas when subjected to different field uniformities. Figure 2-19 illustrates the electrode configurations used in [54] to evaluate the performance of C_3F_7CN/CO_2 mixtures in comparison to SF_6 for different field uniformities. Usually, uniform electric fields are represented by plane-plane configurations and divergent fields use point-plane configurations as shown in Figures 2-19(a) and (b) respectively.

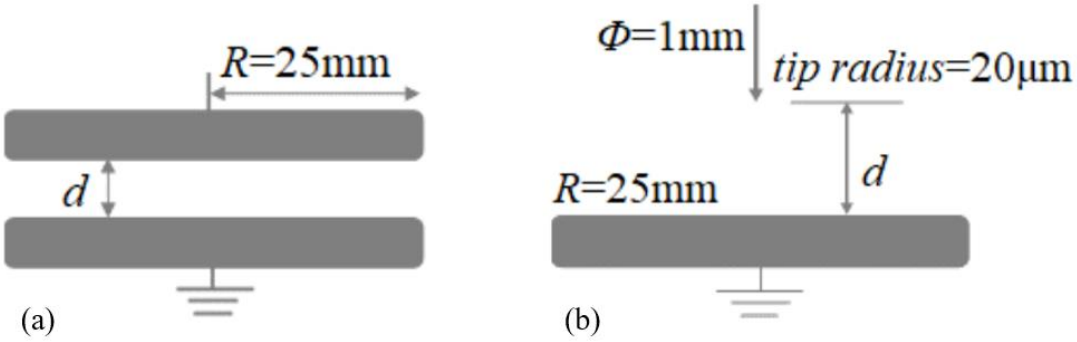

Figure 2-19. (a) Plane-plane and (b) point-plane electrode configurations [54].

The electric field between the high voltage and the ground electrodes can be characterised by the level of field uniformity which is represented by the Schwaiger [53] or field utilisation factor (*f*). An ideal uniform electric field distribution is represented by *f*=1. The generic equation for calculating the field utilisation factor, regardless of electrode shape, is shown below:

$$f = \frac{E_{mean}}{E_{max}} \tag{2-6}$$

Results in [54] have shown that the breakdown voltage behaviour of C_3F_7CN/CO_2 gas mixtures in comparison to SF_6 can change under different field uniformities. Figure 2-20 plots the results for a relatively uniform electric field. The AC breakdown voltages illustrated in this figure were acquired using the plane-plane electrode configuration shown in Figure 2-19(a) with a fixed gap separation of 10 mm. As shown in the figure, under uniform fields, the mixture with 15% C_3F_7CN concentration has a dielectric strength almost equal to SF_6. The breakdown voltage of the 20% C_3F_7CN / 80% CO_2 gas mixture is higher than SF_6, especially at higher pressures. At low pressures, less than 0.4 bar (abs), the breakdown voltage is similar for all the gases shown in Figure 2-20.

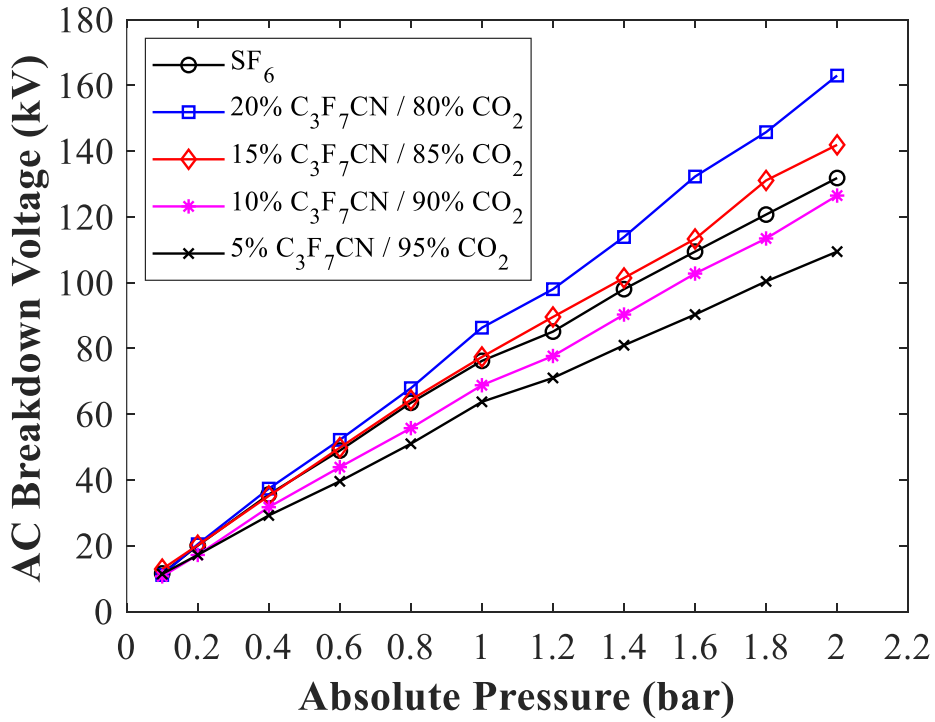

Figure 2-20. AC breakdown voltage comparison between SF_6 and C_3F_7CN/CO_2 mixtures as a function of pressure for a plane-plane electrode configuration with a gap distance of 10 mm [54].

Figure 2-21 illustrates the AC breakdown voltages acquired using the point-plane configuration shown in Figure 2-17(b), with a gap distance of 20 mm, which represents a divergent field [54]. As shown in the figure, SF_6 has a superior breakdown voltage compared to the C_3F_7CN/CO_2 gas mixtures, especially at high pressures. This means that C_3F_7CN/CO_2 mixtures could be more sensitive to corona initiation and non-uniform electric fields, but

this needs further investigation in order to be confirmed. As shown in Figures 2-20 and 2-21, field uniformity can have a significant impact on the dielectric strength of C_3F_7CN/CO_2 mixtures since they have shown a greater responsiveness to the change of electric field than SF_6. SF_6 behaves similarly under plane-plane and point-plane electrode configurations, which means that it might be less affected by defects in the equipment. On the contrary, C_3F_7CN/CO_2 mixtures look more influenced by electric field enhancement and this means that special care has to be taken into consideration when designing new GIS equipment which are adjusted for alternative gases [54].

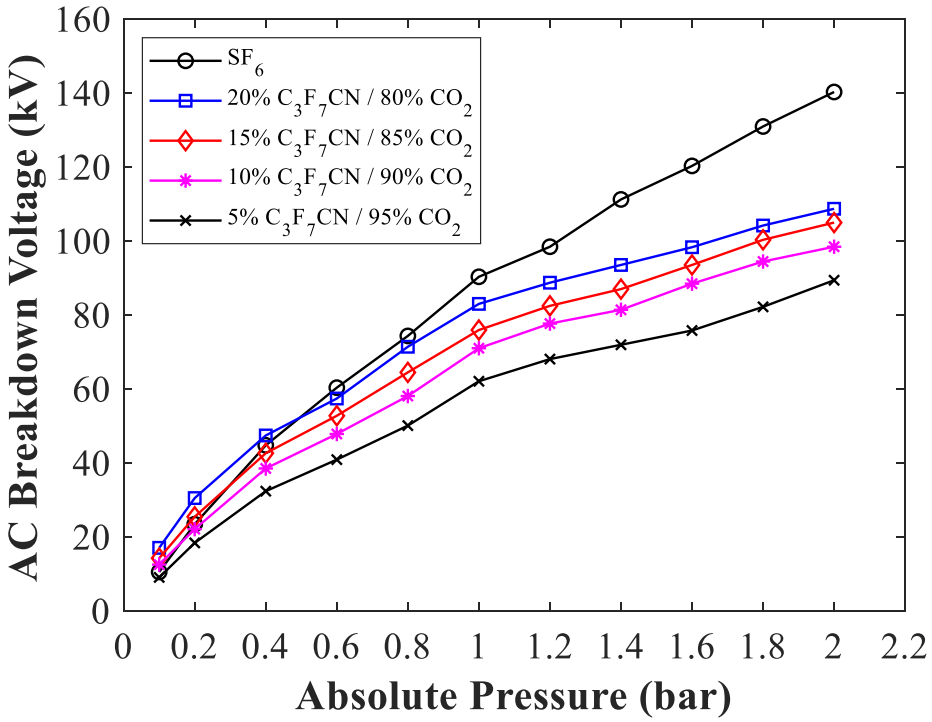

Figure 2-21. AC breakdown voltage comparison between SF_6 and C_3F_7CN/CO_2 mixtures as a function of pressure for a point-plane electrode configuration with a gap distance of 20 mm [54].

Figure 2-22 shows the influence of gap distance on the breakdown voltage of SF_6 and several C_3F_7CN/CO_2 gas mixtures [55]. The AC breakdown characteristics shown in the figure were tested using a sphere-sphere electrode configuration under atmospheric pressure with a varying gap distance. As shown in the figure, the rate of change in breakdown voltage with gap distance is relatively linear and consistent for all the tested gases up to the gap of 20 mm. SF_6 and the 20% C_3F_7CN / 80% CO_2 gas mixture demonstrate a comparable dielectric strength, while the mixtures with less C_3F_7CN concentration have shown a lower breakdown voltage [55].

As shown in Figure 2-22, results reported in [55] are in a good agreement with the investigations in [54] on the effect of gap distance made in plane-plane and sphere-plane configurations. Results in [54] have shown that, under plane-plane and sphere-plane electrode configurations, the mixture with 20% C_3F_7CN concentration has a dielectric strength equal to or greater than SF_6. This shows that under uniform and quasi-uniform electric fields the 20% C_3F_7CN / 80% CO_2 gas mixture has comparable electrical performance to SF_6. Under divergent electric fields with a point-plane electrode configuration, it was found that the breakdown voltage of SF_6 was similar to various C_3F_7CN/CO_2 mixtures for gaps less than 14 mm [54]. However, as the gap separation increased, the breakdown performance of SF_6 was consistently better than the C_3F_7CN mixtures. This shows that the effect of gap distance on breakdown voltage is heavily dependent on the electrode configuration being used.

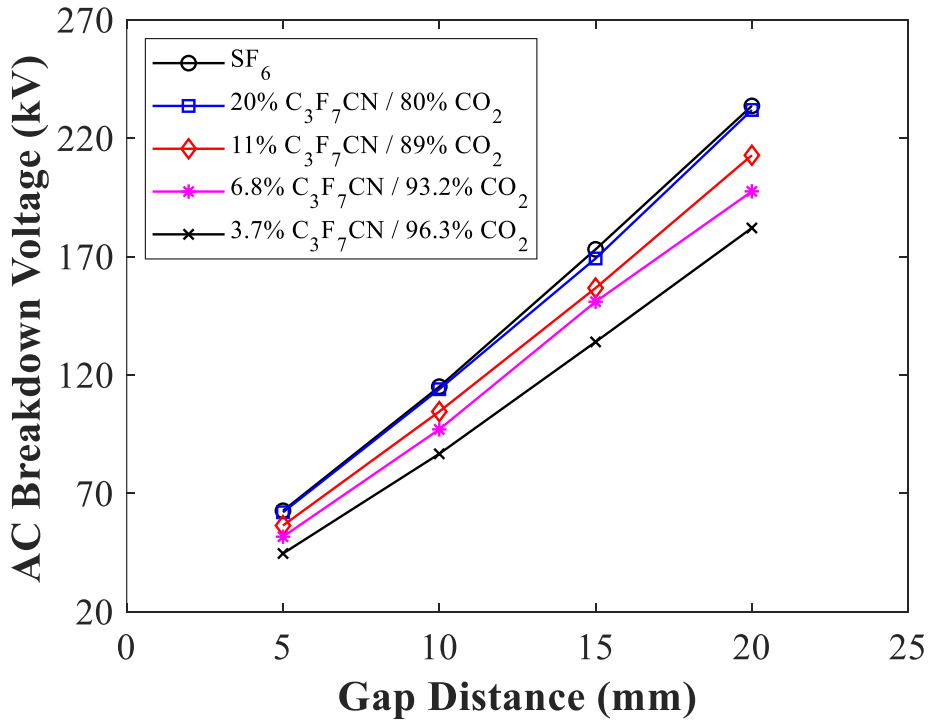

Figure 2-22. AC breakdown voltage comparison between SF_6 and C_3F_7CN/CO_2 mixtures as a function of gap distance for a sphere-sphere electrode configuration at atmospheric pressure (1 bar absolute) [55].

2.6.3 Influence of Polarity on LI and DC Breakdown Voltage

Polarity in voltage waveforms such as LI and direct current (DC) can significantly affect the breakdown characteristics of a gas insulating medium depending on the electrode configuration and thereby the field uniformity tested. Figure 2-23 illustrates results from

[56] for the DC breakdown field strength as a function of absolute pressure for a relatively uniform electric field using a plane-plane electrode configuration and a gap of 3 mm. As shown in the figure, C_3F_7CN/CO_2 mixtures have a negligible polarity difference under uniform fields which is a similar behaviour to what has been previously found with SF_6 [51]. Since the plane-plane configuration is an identical field, small difference in the polarity influence is anticipated since a perfectly uniform field cannot be achieved in practice.

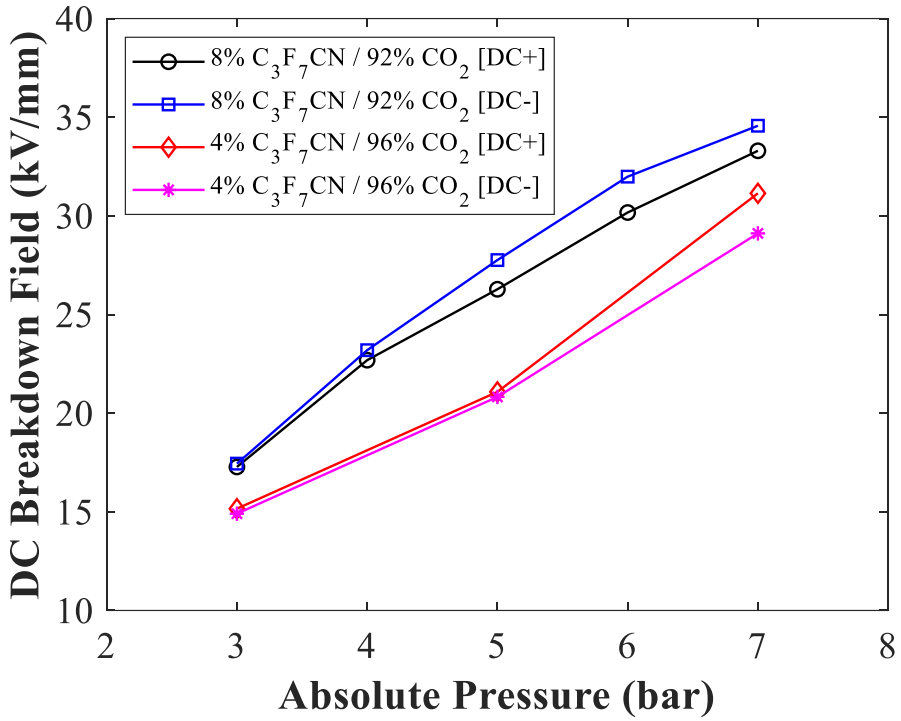

Figure 2-23. DC breakdown strength of C_3F_7CN/CO_2 mixtures as a function of absolute pressure for a plane-plane electrode configuration and a gap distance of 3 mm [56].

However, the polarity can significantly influence the breakdown voltage of a gas medium under non-uniform electric fields [55], [57]–[59]. Figure 2-24 portrays the 50% LI breakdown voltage for a rod-plane electrode configuration as a function of gap distance for C_3F_7CN/CO_2 mixtures and SF_6 [55]. It can be seen that SF_6 and the C_3F_7CN/CO_2 gas mixtures behave similarly under different polarities of a divergent electric field. For the tested gases, the negative breakdown voltages are significantly higher than the positive ones. The breakdown voltage difference between positive and negative breakdown becomes more evident as the gap distance increases. At 5 mm gap distance, both SF_6 and the C_3F_7CN/CO_2 mixture at 10.4 bar show little difference in breakdown voltage because of the polarity change. The polarity influence on the breakdown voltage of divergent electric fields can be explained through the breakdown mechanism shown in Figures 2-25 and 2-26.

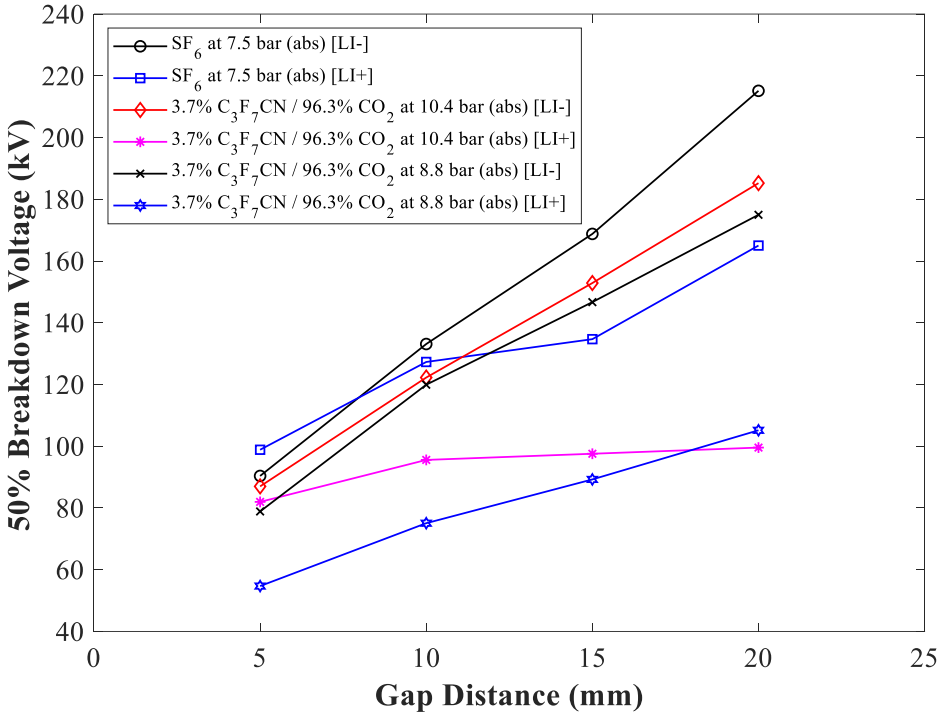

Figure 2-24. 50% LI breakdown voltage of C_3F_7CN/CO_2 mixtures and SF_6 as a function of gap distance for a rod-plane electrode configuration [55].

In the case of a positive point-plane electrode configuration, electrons accelerate from the low field towards the high field region, which is around the high voltage positive electrode, as shown in Figure 2-25(a). As this is the area of high electric field, this is also where most of the ionisation through electron collision process takes place. Due to their higher mobility, electrons are readily drawn and get absorbed by the anode leaving a cloud of positive space charge behind. The space charge disrupts the applied electric field by reducing the field at anode while increasing in the remaining gap. The electric field distribution plot in Figure 2-25(b), shows that for low values of x (close to the high voltage electrode) the electric field reduces from the original while in higher x values (remainder gap distance) the electric field increases. The applied electric field and the distorted electric field are represented by the dotted and solid line in Figure 2-25(b) respectively. As this process develops with time, the positive space charge essentially extends the high voltage electrode closer to the grounded electrode and the region of intense ionisation due to electron collision is moving further into the gap. At some point, the field strength at the tip of the space charge may be high enough for initialising a cathode-directed streamer and eventually bridge the gap which will lead to a complete breakdown [27].

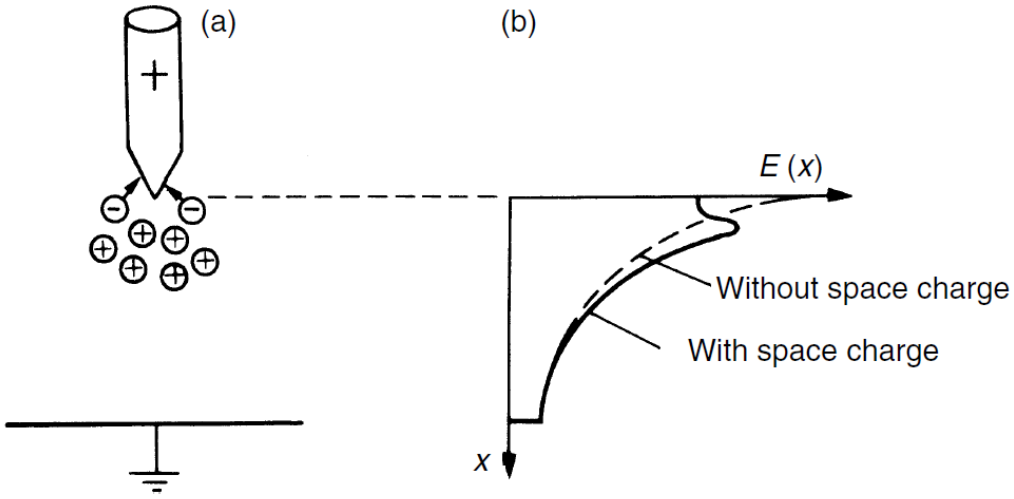

Figure 2-25. (a) Space charge build-up in positive point-plane gap (b) field distortion by space charge [27].

For a negative point-plane electrode configuration, as shown in Figure 2-26(a), electrons are repelled from the high field to the low field region. As electrons slowdown in the low field region, given an electronegative gas is used, they become attached to gas molecules forming heavy negative ions. This leaves a positive space charge behind in the vicinity of the high voltage negative electrode which enhances the field at that area. However, the formation of negative ions drastically reduces the ionisation process further into the gap and also forms an opposite polarity space charge electric field in the middle of the gap which constrains the streamer formation. The reverse space charge electric field can be shown in Figure 2-26(b) where the space charge field drops below the applied field [27].

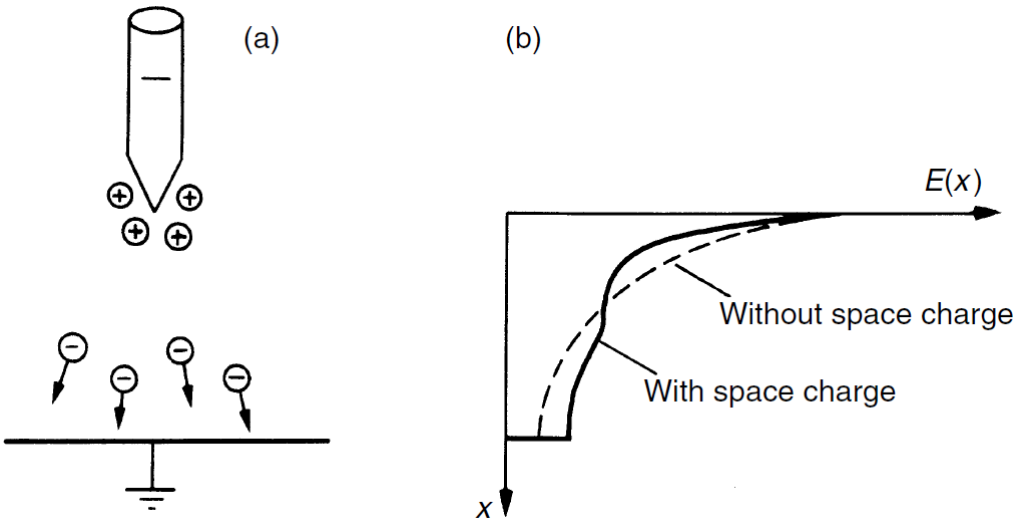

Figure 2-26. (a) Space charge build-up in negative point-plane gap (b) field distortion by space charge [27].

The low electric field due to space charge distortion can slow down and terminate the ionisation process, since eventually the original applied electric field will sweep any space charge that has occurred from this progression. The opposing space electric field and negative ion formation both delay the ionisation process. A higher voltage is required that will exert a higher applied electric field and cause sufficient ionisation to completely bridge the insulation gap and cause a breakdown. For this reason, the breakdown voltage under negative polarity in divergent electric fields is usually higher than the positive [27]. This section shows that polarity in voltage waveforms such as LI and DC can make a significant difference to the breakdown voltage depending on the field uniformity being used [55]–[57], [60].

2.6.4 Effect of Surface Roughness on Breakdown Voltage

The quality of electrode surface finish can significantly impact the breakdown strength of gaseous dielectrics [28], [53], [61], [62]. This is due to the existence of microscopic surface protrusions on rougher surfaces that can lead to a localised electric field enhancement which will result to a stronger ionisation process. Therefore, increased surface roughness can usually reduce the breakdown voltage of a gaseous dielectric. However, the reduction of the breakdown voltage with surface roughness also depends on the sensitivity of different gas mediums to the microscopic protrusions. Different gases react differently with surface roughness variations and it is important to study these characteristics for SF_6-alternatives.

In [63], [64], the effect of surface roughness on the breakdown field strength of C_3F_7CN/CO_2 gas mixtures was investigated. In this study, they have found that the 10% C_3F_7CN / 90% CO_2 gas mixture is less sensitive to increased surface roughness than SF_6. The same conclusion was found for a mixture of 6% C_3F_7CN / 94% CO_2 in [65]. Despite the gas mixtures having lower breakdown field strength than SF_6, it was shown that they have a higher critical point where surface roughness heavily affects their breakdown voltage. Through calculation, they have estimated that mixtures with less than 3% C_3F_7CN concentration should be more sensitive to rougher surfaces than SF_6. For gas mixtures with 3-20% C_3F_7CN concentrations, they have calculated that they will have a critical electrode surface profile similar to SF_6 and they should have comparable surface roughness characteristics [64].

2.6.5 Effect of Epoxy Insulator on Breakdown Voltage

Gas insulation performance in GIBs and GILs can be affected by the presence of support insulators made of epoxy materials. The point where the enclosure aluminium, insulation gas and support insulator interact lead to the existence of triple junctions which form inevitable microscopic irregularities. A poorly designed insulator can introduce the possibility of a surface flashover and reduce the voltage withstand of a gas in GIB and GIL equipment [53].

In [66], the effect of a solid epoxy insulator on the AC breakdown voltage was investigated for SF_6 and C_3F_7CN/CO_2 gas mixtures of different concentrations and pressures. Two Rogowski profiled plane electrodes and epoxy insulators of 15 mm diameter were fabricated to different lengths for the investigation. The authors of this study studied the difference in breakdown voltage with and without an insulating spacer, as well as the effect of an epoxy insulator on the breakdown performance of C_3F_7CN/CO_2 mixtures in comparison to SF_6.

Figure 2-27 [66] illustrates the comparison of breakdown voltages with and without an insulator in between the two plane electrodes. As shown in the figure, both gases react similarly in the presence of an epoxy insulator between the high voltage and the grounded electrode. The results demonstrate that the formation of triple junctions by using a cubic block in-between two electrodes can considerably reduce the breakdown voltage.

Figure 2-28 [66] shows the comparison of insulator surface flashover characteristics for different mixtures of C_3F_7CN/CO_2 gas in comparison to SF_6. The results showed similar correlation of surface flashover voltage with pressure for SF_6 and C_3F_7CN/CO_2 mixtures: relatively linear at lower pressures but saturate with increasing pressure. As shown in Figure 2-28, the flashover voltage of CO_2 gas seems to be unaffected from pressure change with no clear saturation trend observed. Figure 2-28 also shows that a C_3F_7CN concentration saturation is noticeable. When the concentration was increased from 13 to 17% C_3F_7CN, there was only a slight improvement in the surface flashover voltage of the gas mixture and was significantly lower than SF_6. This finding contradicts results reported in other studies [9], [54] that for relatively uniform fields the dielectric strength of 15-20% C_3F_7CN content

mixtures can be equivalent to SF_6. Therefore, it can be concluded that the triple junction effect has more impact on C_3F_7CN/CO_2 gas mixtures than SF_6.

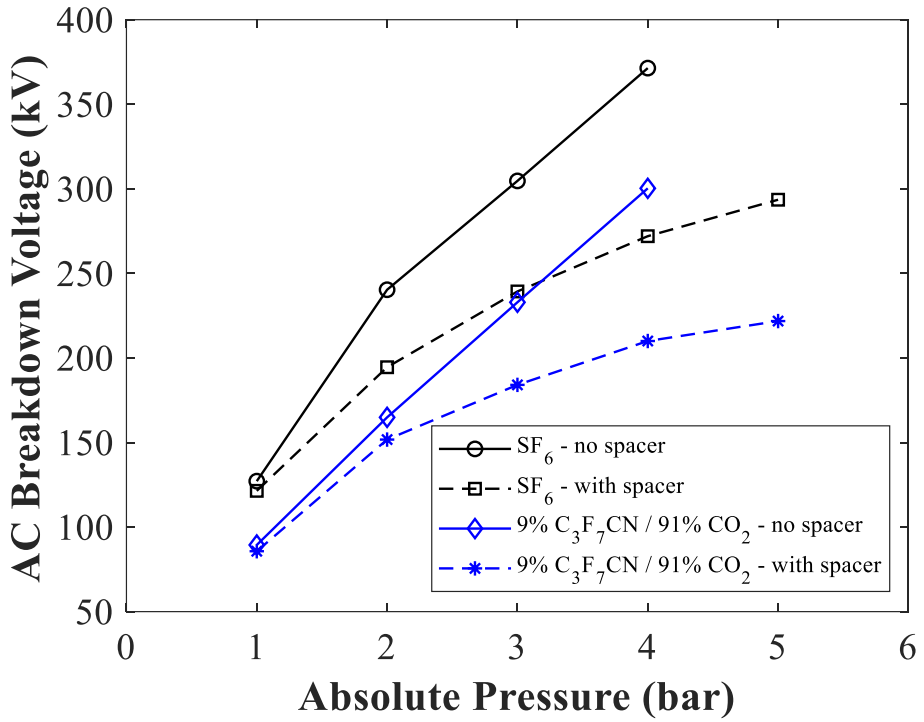

Figure 2-27. Surface flashover voltage and gap breakdown voltage as a function of pressure for 9% C_3F_7CN / 91% CO_2 gas mixture and SF_6 [66].

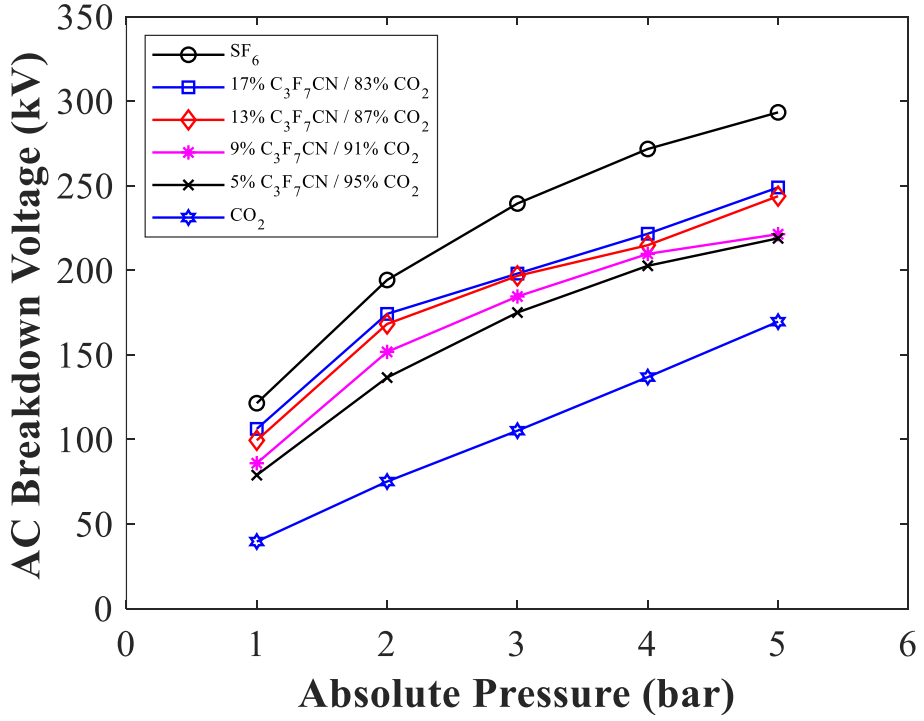

Figure 2-28. Surface flashover voltage as a function of pressure for C_3F_7CN/CO_2 gas mixtures and SF_6 [66].

2.6.6 Partial Discharge Characteristics

2.6.6.1 Partial Discharge Fundamentals

PD is defined as a partial breakdown of insulation over a distance that is usually less than a millimetre. PDs are a result of extreme electric field enhancements at locations where engineering defects, such as conductor/enclosure protrusions, are present (a more detailed description on the types of defects that can result to PDs in GIL/GIB will be given in Chapter 3). The existence of defects will create a local flow of charge carriers, namely ions and electrons, which in turn will result to discharges at that region [27], [28].

The discharges result to physical, chemical and electrical effects which can be used to detect the presence of PDs in an equipment. Acoustic methods can be used to spot PDs since discharges can be followed by the rapid expansion of the ionised gas channel where an acoustic pressure wave is produced. Light output and chemical by-products detection can be used to reveal PDs since discharges will emit light due to the excitation of molecules and also create dissociation of the gas leading to by-products. Lastly, two electrical approaches can be used to detect PDs in gas insulated equipment [27], [28]:

1. Conventional method: Using a test circuit which follows the guidance of BS EN/IEC 60270:2001 [67], a coupling capacitor can be connected in parallel to the PD source and the charge flowing though the capacitor is measured using a quadrupole and a detector. The way the conventional method operates is that after the occurrence of PDs at the defect, the resulting current pulses at some point die away, and the PD source appears as a lumped capacitor with a depleted charge to the test circuit. From there, a replacement charge flows from the coupling capacitor to the PD source which is measured by the detector. Usually, a shielded room is necessary for the conventional method to reduce the external noise which makes it inconvenient for on-site PD detection [28].
2. UHF Method: PD current pulses have a rise time of less than a nanosecond and therefore can radiate electromagnetic waves with frequencies in the GHz region. UHF sensors can be used to capture these waves and display them on a spectrum analyser. The UHF method can offer some advantages over the conventional method for on-site PD detection such as high sensitivity and the ability to locate the PD defects within the

equipment using time of flight measurements. The UHF method will be described in Chapter 5 in more detail [28].

PD characteristics of a dielectric medium in a lab environment are usually defined by their PDIV and PDEV values. According to BS EN/IEC 60270:2001 [67], PDIV is defined as the voltage where repetitive PDs are measured in the test object. In contrast, PDEV is defined as the voltage where repetitive PDs cease to occur in the test object. PDIV and PDEV characteristics are usually used to compare the PD performance of different dielectric materials. PRPD patterns are also used for PD experiments to visualise the repetition rate and amplitude of PD pulses with respect to the phase of the applied voltage. PRPD patterns are helpful for interpreting the PD data and are also being used for condition monitoring and diagnostic techniques for identifying the nature of the PD fault within an equipment [27], [28], [67].

2.6.6.2 C_3F_7CN Mixtures Partial Discharge Studies

Similar to breakdown voltage, PD characteristics can be influenced by different experimental conditions such as pressure, C_3F_7CN mixing ratio and protrusion location (high voltage or grounded electrodes). Currently, few studies have investigated the parameters that can affect the PD characteristics of C_3F_7CN mixtures [54], [68]–[70].

In [54], [68], the effect of C_3F_7CN concentration on the PDIV was investigated for the pressure range of 0.2-1.3 bar and compared to SF_6. The protrusion used for the results in Figure 2-29 was a needle on the ground electrode of a plane-plane configuration. The needle has a height of 2 mm and a tip radius of 20 μm. As shown in Figure 2-29, the results in this study have found that a mixture of 20% C_3F_7CN and 80% CO_2 exhibits similar PD characteristics to SF_6.

All mixtures have comparable PDIV at low pressures, < 0.6 bar and the difference between the 20% C_3F_7CN / 80% CO_2 and SF_6 widens at higher pressures. It was also observed that at higher voltages SF_6 had more discharge activities at a low magnitude (< 40 pC). In contrast, the 20% C_3F_7CN / 80% CO_2 had fewer discharges but at a higher magnitude (> 40

pC). For C_3F_7CN/CO_2 gas mixtures, an increase in C_3F_7CN content results in suppressed PD activities in turn less discharges to be recorded [54], [68].

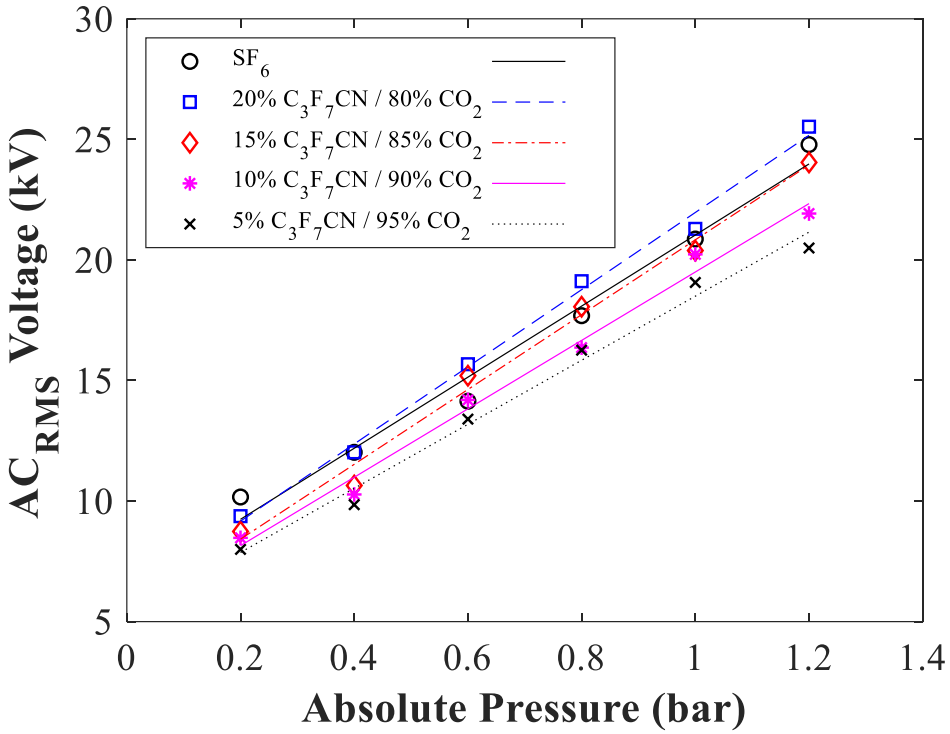

Figure 2-29. PDIV as a function of pressure for C_3F_7CN/CO_2 gas mixtures and SF_6 for a plane-plane electrode configuration with a needle protrusion on the ground plane with a height of 2 mm and a tip radius of 20 μm [54], [68].

In [70], the PD characteristics of g^3 and SF_6 were investigated and compared for two different faults: protrusion on conductor (POC) and protrusion on enclosure (POE). The name g^3 stands for "green gas for grid" and it corresponds to gas mixtures combining 4-10% C_3F_7CN with CO_2 as the buffer gas [6], [8], [15], [23], [32], [71]. The POC and POE arrangements were both made with the same needle of 10 μm tip radius which was placed on the high voltage and ground electrode respectively. Figure 2-30 compares the PDIV of both electrode configurations for both g^3 and SF_6 up to 5 bar (abs). As shown in the figure, the PDIV characteristics increase almost linearly with pressure. For the POC configuration, the PDIV of g^3 was about 76-81% that of SF_6 whereas for the POE configuration it was about 78-84%. PDIV under the POE configuration was in general lower than POC for both gases shown in Figure 2-30.

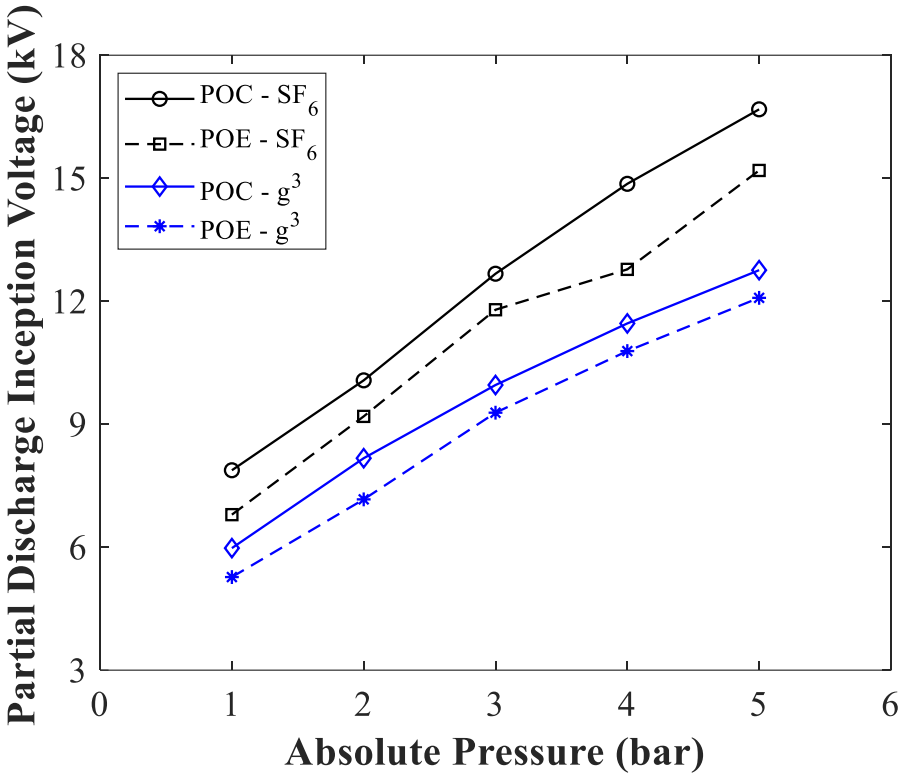

Figure 2-30. PDIV as a function of pressure for g^3 and SF_6 for POC and POE electrode configurations with a needle of a tip radius of 10 μm [70].

The electrical performance of SF_6 and C_3F_7CN mixtures for both breakdown and PD tests can be influenced by numerous factors. However, as seen in the experimental investigations carried out so far, C_3F_7CN mixtures do not always behave the same way as SF_6 with the change in experimental conditions. C_3F_7CN gas mixtures have an additional complexity compared to SF_6, which is the combination of two different gases without intermolecular interference between them. This can lead to a different behaviour than SF_6 which is a strong electronegative gas used alone. It is, therefore, important to fully characterise the mixtures and identify the differences in their performance compared to SF_6. A comprehensive PD and breakdown characterisation of a suitable C_3F_7CN mixture may eventually lead to a complete replacement of SF_6 in the power industry.

2.7 By-products Analysis of C_3F_7CN/CO_2 Gas Mixtures

In [72], a study was carried out to examine the decomposition by-products of C_3F_7CN/CO_2 gas mixtures under breakdown and PD experiments. The analysis of the gas mixtures was conducted using the gas chromatography-mass spectrometry (GC-MS) technique. A brass

point-plate electrode configuration was used to carry out the AC breakdown and PD experiments. For the breakdown tests, 200 breakdowns were carried out with a time interval of 3 minutes in between each application. For the PD experiments, a 72-hour partial discharge experiment was conducted. The gas mixture ratio used was 13.3% C_3F_7CN and 86.7% CO_2 at a pressure of 3 bar (abs) with a purity level of 99.3% and 99.98% for C_3F_7CN and CO_2 gases respectively.

Figure 2-31 shows the GC-MS analysis of the gas mixture before any breakdown or PD experiments took place. As expected, the GC-MS analysis showed the two main components of the gas mixture were CO_2 and C_3F_7CN (or C_4F_7N). Another component, namely C_3HF_7, was found in the analysis but it was specified that it was due to a tiny amount of impurity in the C_3F_7CN gas synthesis.

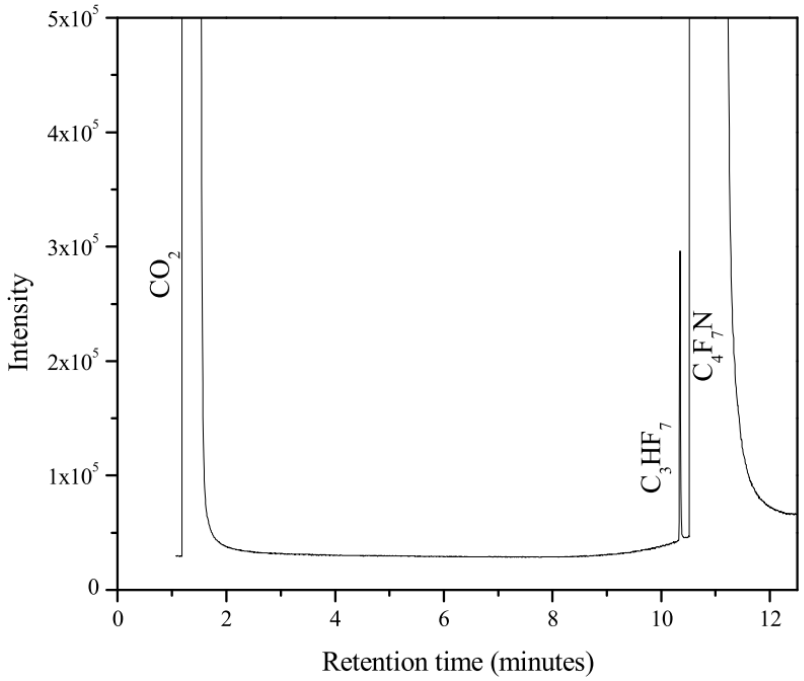

Figure 2-31. GC-MS analysis of C_3F_7CN/CO_2 gas mixture before experiments [72].

Figure 2-32 shows the gas mixture composition after 200 AC breakdowns. The composition by-products found were specifically: CO, CF_4, C_2F_6, C_3F_8, C_3F_6, C_2F_4, C_4F_6, $C_4F_{10}O$, C_2F_3CN, C_2F_5CN, CF_3CN, C_2N_2 and HCN [72]. The breakdown voltage after 200 breakdowns was found to be 97.8% of the initial breakdown voltage which could be because of the C_3F_7CN content reduction. Figure 2-33 illustrates the GC-MS analysis of the decomposed C_3F_7CN/CO_2 gas mixture after the PD experiment. As shown in the figure, the

by-products produced after the PD experiments were: CO, CF_4, C_3F_8, CF_3CN, C_3F_6, $C_4F_{10}O$, C_2F_5CN, C_2N_2, HCN and C_2F_3CN. This agrees with previous report in [73], where by-products were analysed for a 4% C_3F_7CN / 96% CO_2 gas mixture after PD experiments.

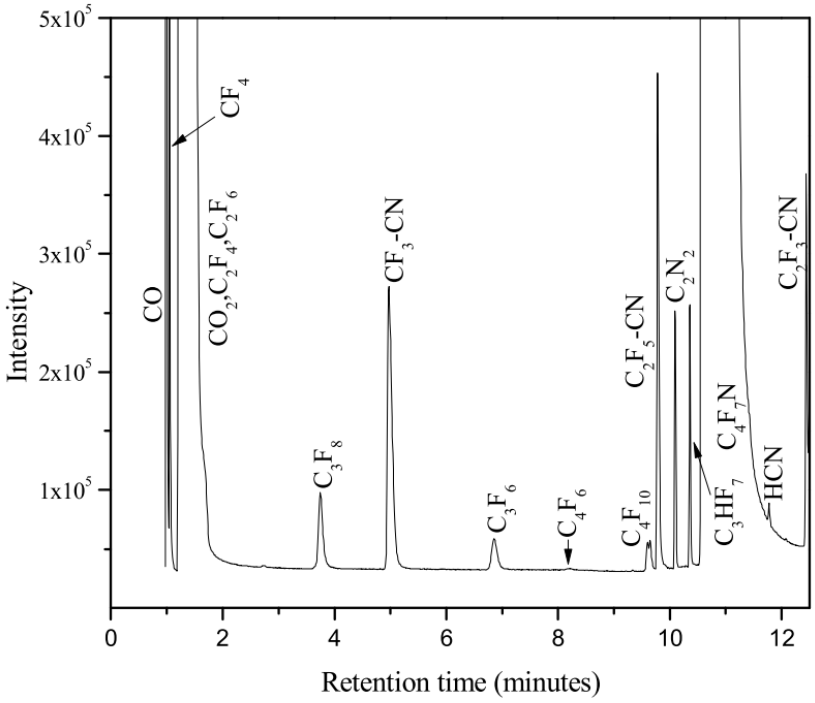

Figure 2-32. GC-MS analysis of C_3F_7CN/CO_2 gas mixture and its decomposition by-products after 200 breakdowns [72].

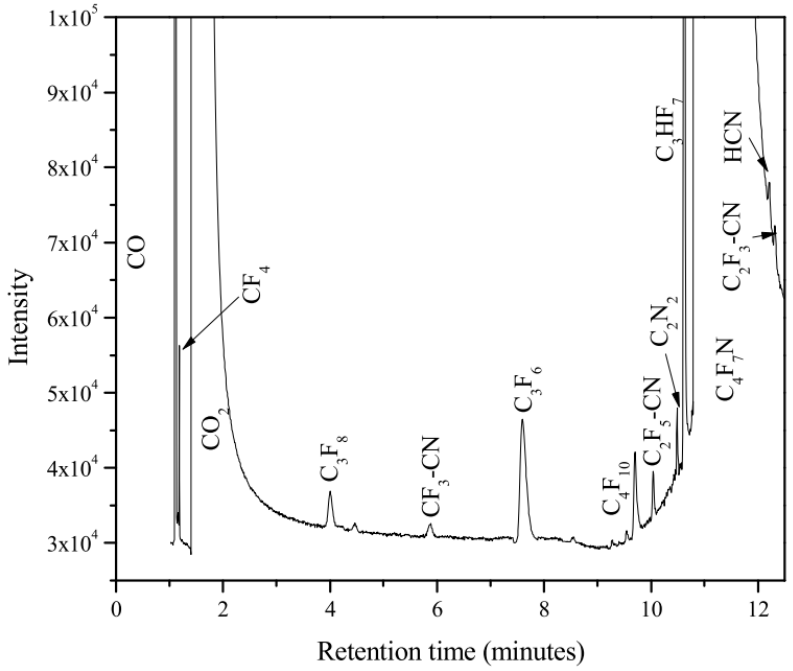

Figure 2-33. GC-MS analysis of C_3F_7CN/CO_2 gas mixture and its decomposition by-products after a 72-hour partial discharge experiment [72].

In general, the number of by-products under breakdown experiments were found to be more than under PD experiments. The largest concentration and most toxic by-product for both experiments was CO with approximately 550 and 200 ppm for breakdown and PD tests respectively. For breakdown experiments the concentration of CF_4 was found to be significantly high as well with roughly 600 ppm [72].

The decomposition by-products of g^3 used in arc-quenching experiments were studied in [8], [74]. The by-products found in [8] are shown in Table 2-11. As shown in the table, the concentration of all the resulting compounds was a very small percentage in the range of 1-100 ppmv. The main degradation product was again found to be CO. These results agree to what has been observed before in [74], where the gas mixture was circulated through a tube furnace at high temperatures and its thermal decomposition was found to begin at approximately 650°C. The gas mixture was fully decomposed at temperatures of 880°C and above which resulted in significant concentration of CO and lower amounts of COF_2, CF_3CN, C_2F_5CN and C_2F_6.

Table 2-11. By-products analysis of arced g^3 [8].

Compounds		Concentration (%)	Concentration (ppm)
CO_2 (carbon dioxide)	g^3	93.5	935,018
C_3F_7CN (heptafluoroisobutyronitrile)		4.06	40,600
CO (carbon monoxide)	by-products	2.4	24,000
CF_2=CFCN (perfluoroacrylonitrile)		0.013	130
CN-CN (ethandinitride)		0.0065	65
CF_3-CF_2-CN (pentafluoropropionitrile)		0.006	60
CF_3-CN (trifluoroacetonitrile)		0.0058	58
$(CH_3)_2SiF_2$		0.0052	52
COF_2 (carbonyl fluoride) + C_3F_8 (octafluoropropane)		0.0014	14
$(CF_3)_2CHCN$ (hexafluoroisobutyronitrile)		0.00019	1.9
$(CF_3)_2C=CF_2$ (perfluoroisobutene)		0.00013	1.3

The acute toxicity level of g^3 after being exposed to arc-quenching experiments was found to be 64,000 ppm. This is roughly 3 times above the upper toxicity level of 20,000 ppm and is therefore not classified in a hazard class according to CLP regulations. However, the same

precautions taken with arced SF_6 is also recommended for C_3F_7CN/CO_2 gas mixtures in order to ensure safety during gas handling procedures [8].

2.8 Summary

This chapter has provided an overview of gas insulated equipment and applications of SF_6. The benefits and environmental concerns of SF_6 as well as the motivation behind the research of investigating for SF_6-alternative gases has been described. A summary was shown on the work done by previous studies on SF_6-replacement candidates and the characteristics of each gas category were analysed. From this summary, C_3F_7CN/CO_2 gas mixtures were judged to be the most technical viable candidate for replacing SF_6. Finally, a literature review was carried out on existing investigations that already exist on C_3F_7CN/CO_2 gas mixtures, which identified important research gaps required for replacing SF_6 in the power industry. The research gaps are listed as follows:

- Experimental investigations to establish the breakdown characteristics performance of C_3F_7CN/CO_2 gas mixtures in comparison to SF_6 using coaxial prototypes with similar field uniformity as found in practical GIL/GIB equipment. These can take place under LI and AC voltage waveforms.
- Detailed studies on the PD characteristics of C_3F_7CN/CO_2 gas mixtures in comparison to SF_6 for different experimental conditions. Parameters such as needle length, pressure, electrode configurations as well as location of defect can be varied in order to fully understand how the alternative gas might react to equipment defects if it eventually replaces SF_6.
- Retro-fill investigation of C_3F_7CN/CO_2 gas mixtures in full-scale GIL/GIB equipment. Despite the breakdown and PD characteristics providing useful information on the behaviour of alternative materials, new gas mixtures must be type tested in actual full-scale GIL/GIB equipment before being proposed as feasible SF_6-replacements. This can essentially provide knowledge of how the new gas mixture will perform when subjected to real life transient overvoltages occurring in the network.

Addressing the research gaps aforementioned would provide key knowledge required for retro-filling SF_6-designed GIL/GIB equipment with an environmentally friendly gas candidate.

Blank Page

Chapter 3 Development of Experimental Setup and Gas Handling Procedures

3.1 Introduction

This chapter provides an overview of (i) the pressure vessel and electrode configuration development and (ii) gas handling setup and procedures adopted for the experimental work conducted in this thesis. A detailed description is given from the design and simulation stage to the fabrication phase of the pressure vessel and test electrodes. Finally, the gas handling setup and procedures used are described in detail.

3.2 Pressure Vessel

3.2.1 Design Development

Figure 3-1 shows the initial designs of the desired pressure vessel with dimensions provided in mm. The pressure vessel has a height and a diameter of 447 and 435 mm respectively, resulting in a volume of approximately 0.066 m^3 or 66 litres. The wall thickness of the pressure vessel circumference is 6 mm. Two viewing windows with an inner diameter of 209.3 mm are included at the opposite sides of the pressure vessel. The viewing windows were designed to be access points for the user to change electrode configurations.

A secondary 25 mm bushing flange is used to attach onto a SF_6-designed bushing. The bottom of the pressure vessel has a flange port with a mechanical actuator to adjust electrode gap distances and it can also be blanked off when the actuator is not being used. O-rings are used in various groove compartments of the vessel where two or more parts are connected but not welded together, which are vulnerable to gas leakage if elastic materials are not used at the point of connection. The bottom flange has inlets fabricated to enable the connection of a pressure gauge and various gas fittings.

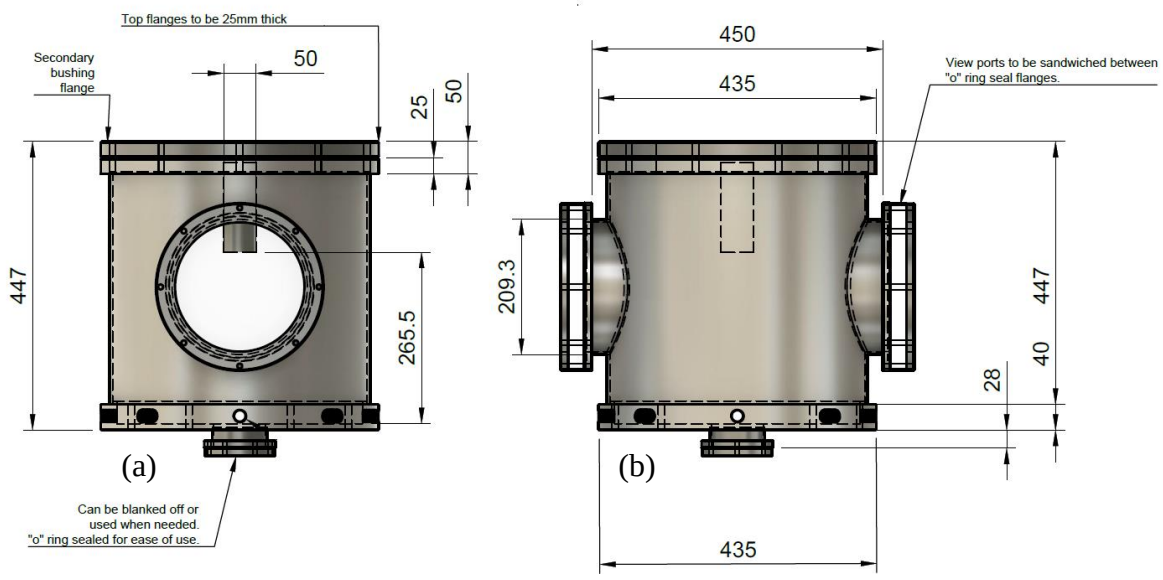

Figure 3-1. Drawings of pressure vessel with dimensions (a) front view and (b) side view.

Figure 3-2 shows the design of the 170-kV rated SF_6-designed bushing that was combined with the pressure vessel shown in Figure 3-1. The bushing has a weight of 77.6 kg, a total height of 1,917 mm and a creepage distance of 5,565 mm. It also has an internal diameter of 200 mm. This leads to a volume of approximately 0.048 m^3 or 48 litres. The bushing conductor is made of aluminium and has a diameter of 60 mm.

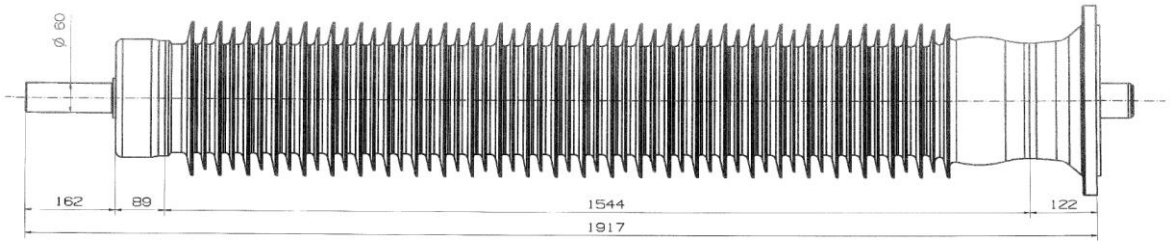

Figure 3-2. 170-kV rated SF_6 bushing design [75].

Table 3-1 shows additional technical data for the bushing shown in Figure 3-2. The manufacturer of the bushing, namely Lapp Insulators, carried out all the necessary tests to ensure that the bushing supplied was fully functioning. The bushing was type tested, while filled with SF_6 at 4.5 bar (abs), in accordance to IEC 60137:2008 to determine the voltages levels it can withstand. It has the capability to be used up to 325 kV and 750 kV of AC and LI voltages respectively as shown in Table 3-1.

Table 3-1. 170-kV rated SF_6 bushing technical data [75].

Technical Data	
Rated Voltage	170 kV
Rated Current	3150 A (50-60 Hz)
Rated Power Frequency Withstand Voltage at 4.5 bar (abs)	325 kV
Rated Lightning Impulse Withstand Voltage at 4.5 bar (abs)	750 kV
Maximum Operating Pressure at 20°C (abs)	8.7 bar

3.2.2 Fabrication and Assembly of Pressure Vessel

Figure 3-3 shows the fabricated stainless-steel pressure vessel assembled with the SF_6 bushing, which gives a total volume of about 114 litres. The vessel was hydrostatically pressure tested up to 20 bar (abs) and vacuum leak checked down to 5 x 10^{-7} mbar. The viewing windows are made of transparent Perspex® cell cast acrylic material which is sandwiched between O-ring sealed flanges. A mechanical linear actuator was fitted at the bottom of the vessel to allow gap adjustment of 1.5 mm per revolution and maximum movement of 100 mm under pressure. The pressure vessel rests on a jacking mechanism stand which provides the capability of lifting or lowering the whole assembly in case the actuator needs to be removed from the bottom flange port.

(a) (b)

Figure 3-3. (a) Pressure vessel assembled with the 170-kV rated bushing (b) pressure vessel main section.

The couplings fitted at the bottom flange of the pressure vessel for vacuum, gas filling and extraction are shown in Figure 3-4. To avoid cross contamination of hoses with different gases, every test gas used in this thesis had its corresponding fitting. Figure 3-4(a) illustrates a DILO DN20 coupling with a silver covering cap which was used solely for CO_2 filling, Figure 3-4(b) shows a smaller size DILO DN8 coupling used for SF_6 filling, recovery and air evacuation whereas Figure 3-4(c) shows a green DILO DN20 alternative gas coupling which was used for pure C_3F_7CN and C_3F_7CN/CO_2 gas mixtures filling, recovery and air evacuation. Vacuum procedures can be performed using both Figure 3-4(b) and Figure 3-4(c) depending on the gas cart being used.

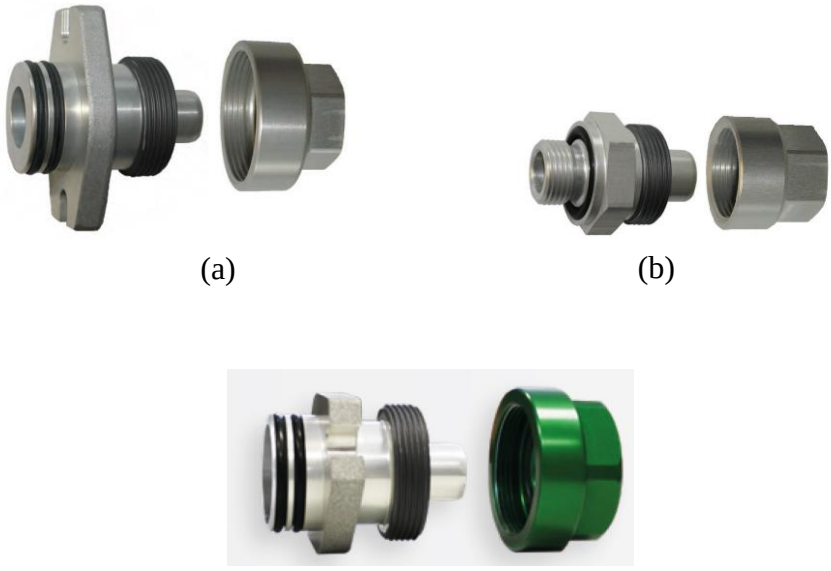

(a) (b)

(c)

Figure 3-4. Gas filling, recovery and evacuation of air couplings (a) DN20 CO_2 coupling (b) DN8 SF_6 coupling (c) DN20 C_3F_7CN and C_3F_7CN/CO_2 gas mixtures coupling.

Figures 3-5(a) and 3-5(b) show the pressure relief valve and gauge used on the pressure vessel respectively. The relief valve located at the bottom of the pressure vessel was pre-set at 8 bar (abs) for safety reasons. If this set pressure is exceeded, the relief valve will be triggered and provide a passage for the excess gas to escape the vessel. Figure 3-5(b) shows the multipurpose pressure gauge used in the pressure vessel. The WIKA pressure gauge shows the values in MPa, psi and bar, ranging from a pressure of 0 bar (abs), which designates vacuum state, up to a maximum pressure of 10 bar (abs).

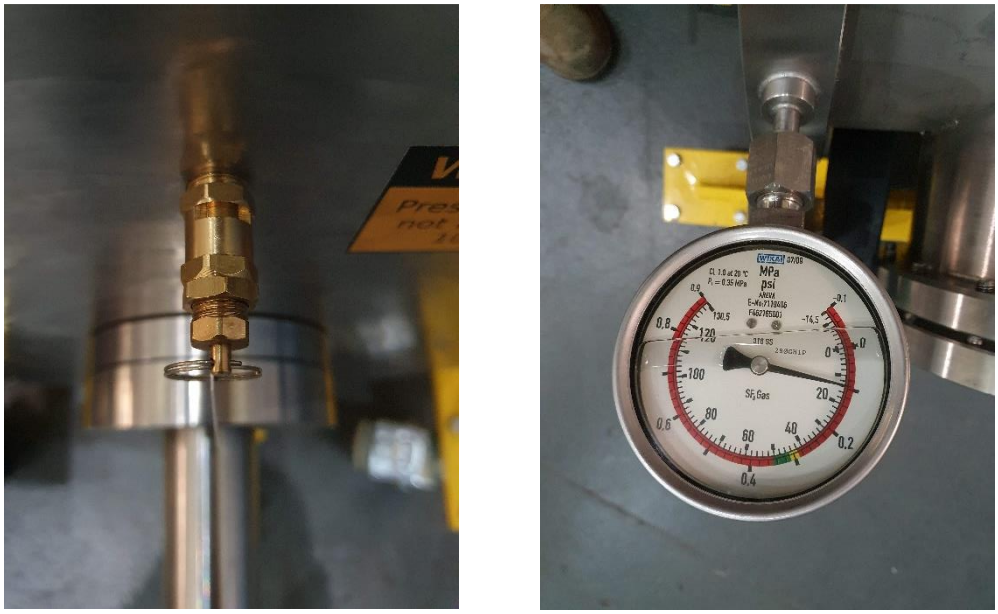

(a) (b)

Figure 3-5. (a) Pressure relief valve set at 8 bar (abs) and (b) WIKA pressure gauge.

3.3 Electrode Development

3.3.1 Reduced-scale Coaxial Prototype – Quasi Uniform Fields

Assembling an industrial-scale demonstrator is costly and time-consuming. For this reason, using a full-scale test rig would not be practical for the optimisation of C_3F_7CN gas mixtures through breakdown tests. A reduced-scale coaxial prototype was developed and fabricated to experimentally determine the breakdown characteristics of the pre-selected C_3F_7CN/CO_2 mixtures with the SF_6 test data used as the reference. The geometrical design of the prototype is scaled down based on the dimensions of a 420/550 kV full-scale GIB demonstrator.

3.3.1.1 Conductor and Enclosure Dimensions for the Reduced-scale Prototype

Figure 3-6 illustrates the internal structure of the 420/550 kV GIB demonstrator, which is essentially a coaxial cylindrical geometry that the reduced-scale prototype was derived. The design is based on a trade-off between field uniformity and the gap spacing (g) between the high voltage conductor and grounded enclosure which is determined by two parameters: conductor radius (R_a) and inner enclosure radius (R_b).

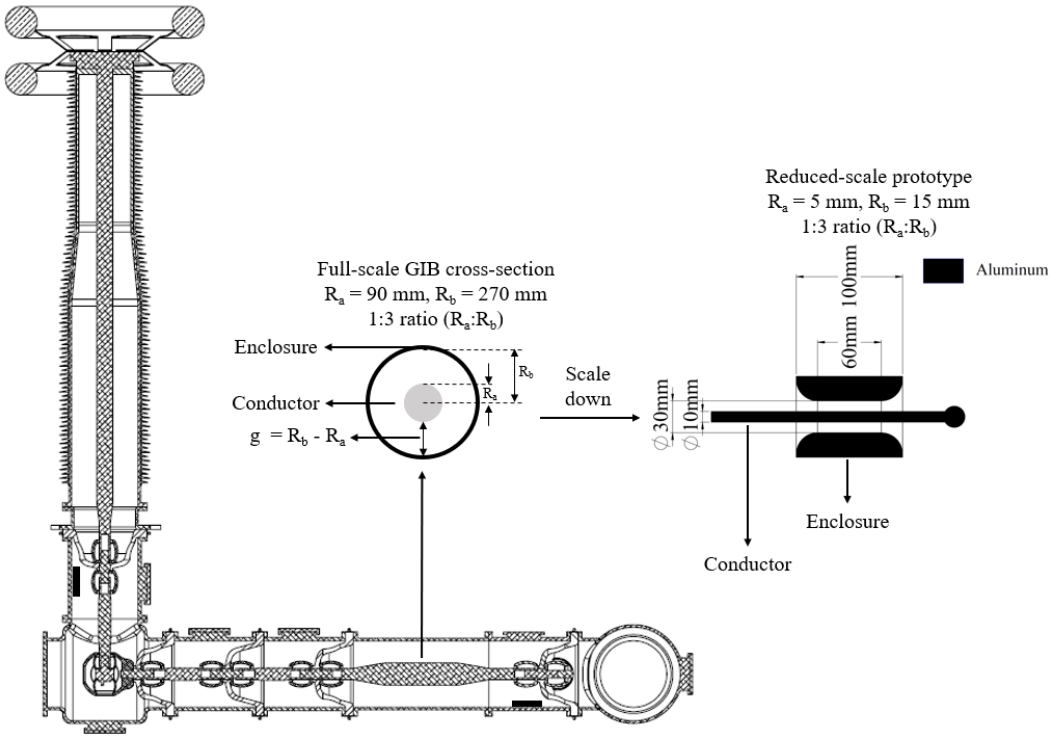

Figure 3-6. Development of reduced-scale coaxial configuration based on a 420/550 kV GIB demonstrator.

An optimal ratio that represents the lowest field intensity applied on the gas insulation can be derived from equation (3-1), which gives the maximum electric field, E_{max} for a given voltage, U in coaxial configurations [53], [27]:

$$E_{max} = \frac{U}{R_a \cdot \ln\left(\frac{R_b}{R_a}\right)} \ (kV/mm) \tag{3-1}$$

In the case of breakdown voltage (U_b), the maximum electric field equals the breakdown field strength (E_b). Therefore, $E_{max} = E_b$ and (3-1) can be re-written with U_b as the subject:

$$U_b = E_b \cdot R_a \cdot \ln\left(\frac{R_b}{R_a}\right) (kV) \tag{3-2}$$

Then, by differentiating (3-2) with respect to R_a, while treating E_b and R_b as constants, maximum U_b is given when:

$$\ln\left(\frac{R_b}{R_a}\right) = 1 \ where \ \left(\frac{R_b}{R_a}\right)_{optimal} = e \approx 2.72 \tag{3-3}$$

Figure 3-6 shows the cross-sectional view of the busbar in the demonstrator, where the ratio of R_b/R_a is equal to 3 and close to the optimal ratio. As shown in the figure, the coaxial prototype was developed to have the same inner enclosure to conductor ratio to attain the same field uniformity. The field utilisation factor equation (3-4) was used to quantify the field uniformity of both setups:

$$f_{coaxial} = \frac{R_a \cdot \ln\left(\frac{R_b}{R_a}\right)}{R_b - R_a} \tag{3-4}$$

Table 3-2 shows that, by keeping the same geometric ratio, the developed coaxial prototype is expected to replicate the quasi-uniform electric field as found in the GIB demonstrator by having the same field utilisation factor.

Table 3-2. Comparison of parameters for the full-scale GIB demonstrator and the reduced-scale prototype.

Parameter	Full-scale GIB demonstrator	Reduced-scale prototype
Conductor Radius (mm) [R_a]	90	5
Inner Enclosure Radius (mm) [R_b]	270	15
Field Utilisation Factor, f	0.549	0.549

Figure 3-7 compares the electric field distribution of the GIB demonstrator and prototype simulated using COMSOL Multiphysics 5.5. As shown in the figure, using a fixed input voltage of 1 kV, E_{max} of the full-scale is roughly 18 times smaller than the reduced-scale prototype which is due to larger equipment dimensions. Note that the E_{max} value can also be calculated using equation (3-1).

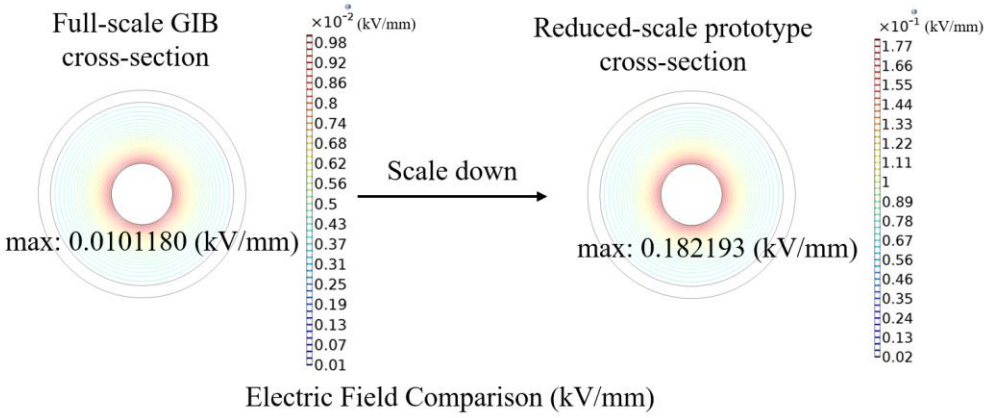

Figure 3-7. Electric field comparison of full-scale and reduced-scale prototype straight sections (kV/mm).

3.3.1.2 Design and Development of Reduced-scale Prototype

Following the dimensioning of the conductor and inner enclosure radius, the internal space-constrained dimensions of the pressure vessel, such as height and diameter, had to be taken into consideration for the design of the reduced-scale prototype. This was through finite element analysis (FEA) simulations and using COMSOL Multiphysics 5.5 software.

It is important for the coaxial breakdowns to occur within the central region of the inner conductor so that the results are not affected by high field intensification at the edges of the enclosure. As a result, the clearance from the grounded pressure vessel, the conductor termination, the support insulator structure and size as well as the rim edge of the coaxial enclosure are factors that must be considered. Therefore, E_{max} location has to be verified through a trial and error simulation process prior to developing a suitable design. The flowchart in Figure 3-8 shows the process of developing the final coaxial design that was used for experiments.

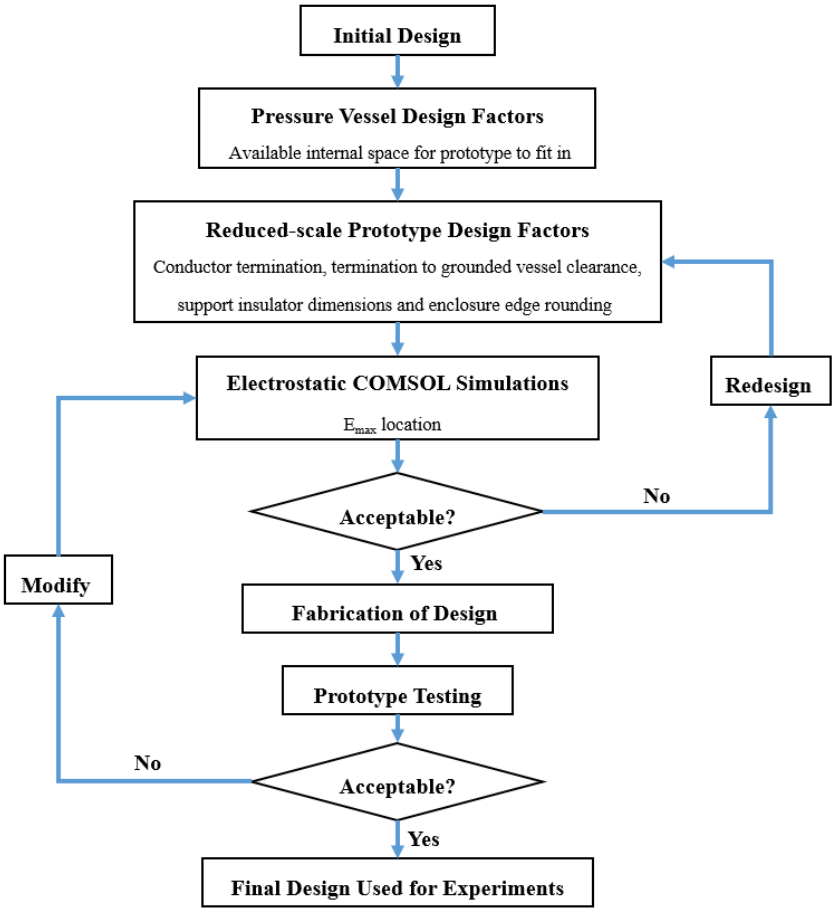

Figure 3-8. Reduced-scale prototype design, development and fabrication process.

The process of developing the reduced-scaled coaxial prototype started by introducing an initial design based on the geometric ratio. After determining the conductor and enclosure diameters, the prototype dimensions were adjusted to the available internal space of the pressure vessel. The geometric design was adjusted to ensure that E_{max} was at the desired location through FEA simulations. The prototype was fabricated and preliminary tested to validate that the design is fully functioning prior to starting the breakdown experiments.

3.3.1.3 Prototype Design, Simulation, Development and Fabrication

Finite Element Analysis (FEA) Method

FEA is a numerical method for solving complex mathematical problems such as a continuous object with infinite degrees of freedom. The purpose of FEA modelling is to subdivide the model into a large number of discrete sized elements and limit the infinite degrees of freedom to finite. The behaviour of these elements is defined by several parameters in the physics study. An example being in electrostatics model, the voltage potential and dielectric permittivity need to be defined. These elements are usually in triangular or quadrilateral shape depending on the model design and number of dimensions. As the model is divided into a large number of simple geometries, the solution to every single element can be approximated by a linear or quadratic function. A Galerkin matrix is assembled for every element and all the individual matrices are then added together into a single matrix, which is used to solve the complex model [76]. COMSOL Multiphysics (Version 5.5) software was used to perform FEA modelling in this thesis and the steps are listed as follows:

- *Geometry Design* – design or import a geometry into the software.
- *Boundary Conditions* – define the materials that are going to be used in the model and their properties. The physics conditions also have to be specified.
- *Meshing and Refinement* – divide the model into a large number of discrete elements and ensure that the final solution is independent of the meshing size.
- *Solution and Visualisation* – extract the data and present the results in tables and figures.

Geometrical Structure

The geometrical structure of a model can either be imported from a CAD software, such as Solidworks, or can be drawn directly in COMSOL. For this study a 2D axisymmetric model was used because the design of a coaxial model is symmetrical in shape and can be solved revolving around a rotation axis. This offers the advantage of reduced computational time since a 3D design requires much higher processor capability. Figure 3-9(a) shows the dimensions of the enclosure, conductor and support insulators used for keeping the conductor centred within the pressure vessel. Figure 3-9(b) shows the design of the reduced-scale prototype attached to the high voltage conductor of the bushing. The insulating gas separates the grounded enclosure from the high voltage conductor and support insulators. The bottom flange of the grounded pressure vessel was included at the lower end of the model to simulate the electric field distribution from the sphere termination of the conductor to the grounded pressure vessel.

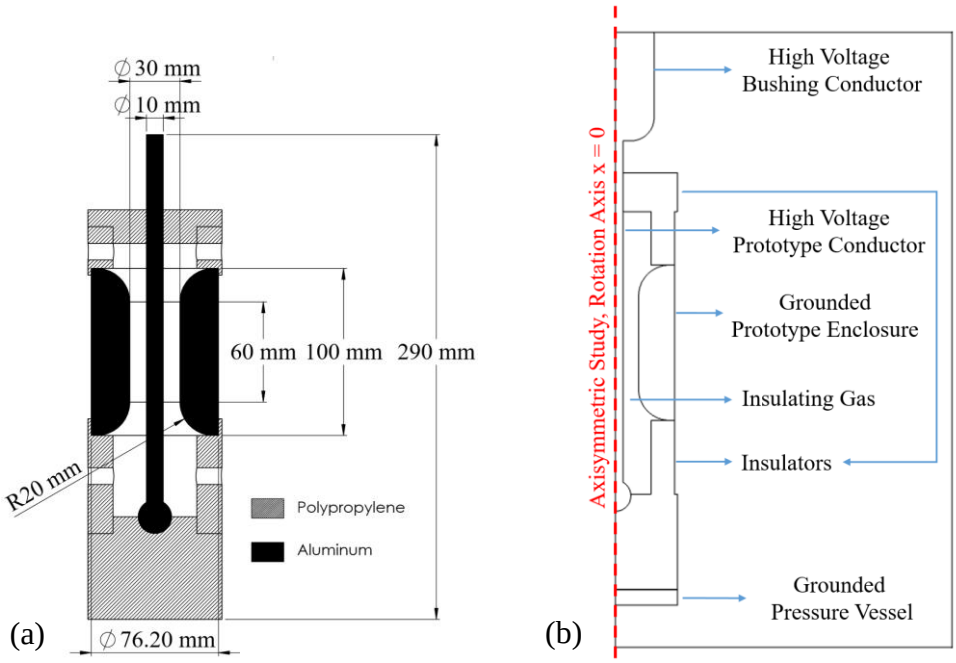

Figure 3-9. (a) Dimensions of the initial reduced-scale prototype (b) COMSOL model geometry structure.

Boundary Conditions

The electrostatics module was used to simulate the electric field distribution. Material properties and the electrostatic boundary conditions need to be defined for this study. The

relative permittivity (ε_r) is an important parameter for the simulation and the permittivity values used are shown in Table 3-3 [77]. Domains labelled as insulators in Figure 3-9(b) were assigned as polypropylene with ε_r of 2.2. Aluminium was used for all the metallic components with ε_r of 1, since metals are conductive materials and will not affect the electric field simulation. Finally, SF_6 was used for the insulating gas surrounding the prototype and ε_r for all gases, including C_3F_7CN, can be treated as unity.

Table 3-3. Relative permittivity values for the components used in the FEA model [77].

Materials	Relative Permittivity, ε_r	Components
Polypropylene	2.2	Insulators
SF_6	1	Insulating Gas
Aluminium	1	Conductor, Enclosure and Vessel

Figure 3-10(a) shows the ground boundary conditions for the enclosure and the pressure vessel, whereas Figure 3-10(b) shows the high voltage boundary conditions for the bushing and prototype conductors. COMSOL pre-assigns 0 V to the grounded boundary condition while the high voltage electric potential was set as 1 kV for all the simulations.

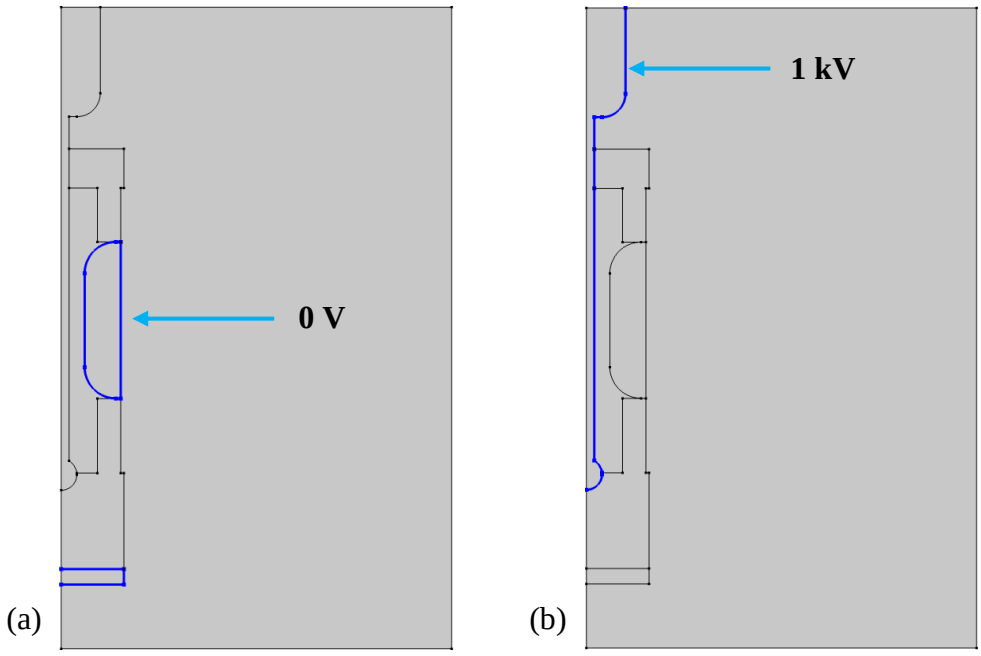

Figure 3-10. Boundary conditions for (a) ground and (b) high voltage electrodes for the reduced-scale prototype.

Geometry Meshing

Geometry meshing is the most significant factor for achieving a reliable accuracy for the results of the FEA model [78]. COMSOL introduces a number of built-in physics controlled meshes which helps the user to divide the model into smaller elements. The built-in parameter has a range from ‘extremely coarse’ to ‘extremely fine’ and the selection depends on the geometrical complexity and the computational capacity of the central processor unit (CPU) being used.

Figure 3-11 shows the meshing of the initial model of the reduced-scale prototype. By default, COMSOL introduces more refined elements in narrow regions while wider regions include larger elements [79]. For the specific model, triangular meshing was used and as shown in the figure at narrow regions, such as the conductor termination and the enclosure-insulator junction, a higher number of smaller elements was used.

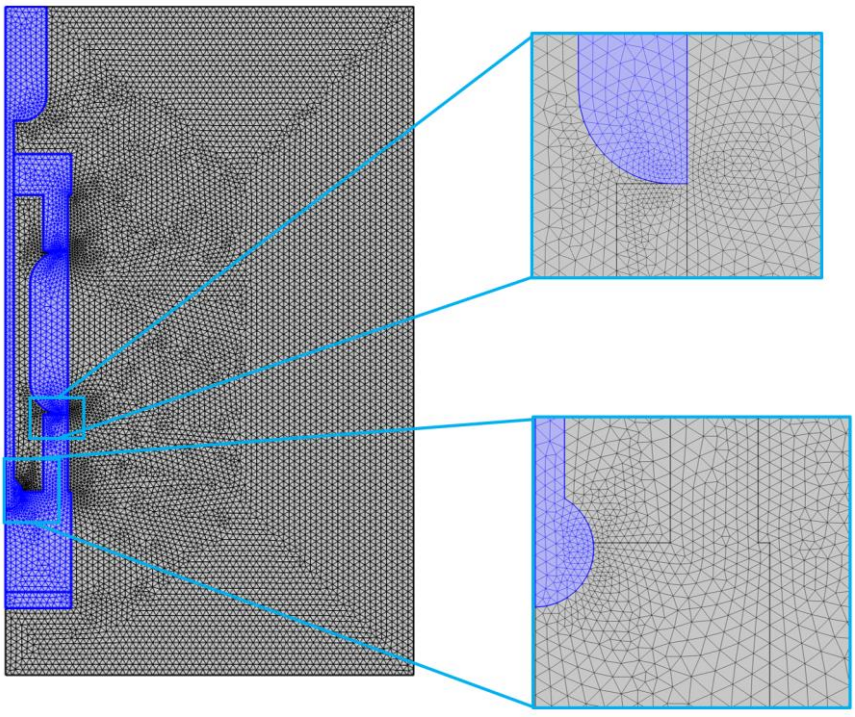

Figure 3-11. Finite element meshing for the reduced-scale prototype.

Finer meshes will more accurately represent the geometry of a model but also require higher computational resources and longer simulation time [78]. Since the accuracy of the solution is directly related to the meshing of the model, it is important to make sure that at some point

the simulation results are mesh independent. This can be done through a process called "mesh refinement" which essentially involves resolving the model with increasingly finer mesh up to the point that the accuracy of the solution provided does not significantly change with the number of elements added [80]. Reaching this point essentially means that the error of the solution is minimised, and the model converges towards the true value. Figure 3-12 illustrates the mesh refinement process carried out on the reduced-scale prototype. The meshing applied on the model starts with the COMSOL built-in coarse mesh all the way to extremely fine. The curve shows the E_{max} variation with increasing number of elements using finer meshes. For this model, the extremely fine built-in mesh was further edited to make sure the solution reached a stable value. As seen in Figure 3-12, the solution reaches a stable point at around 0.181 kV/mm whereby increasing the number of elements makes no significant difference to the value.

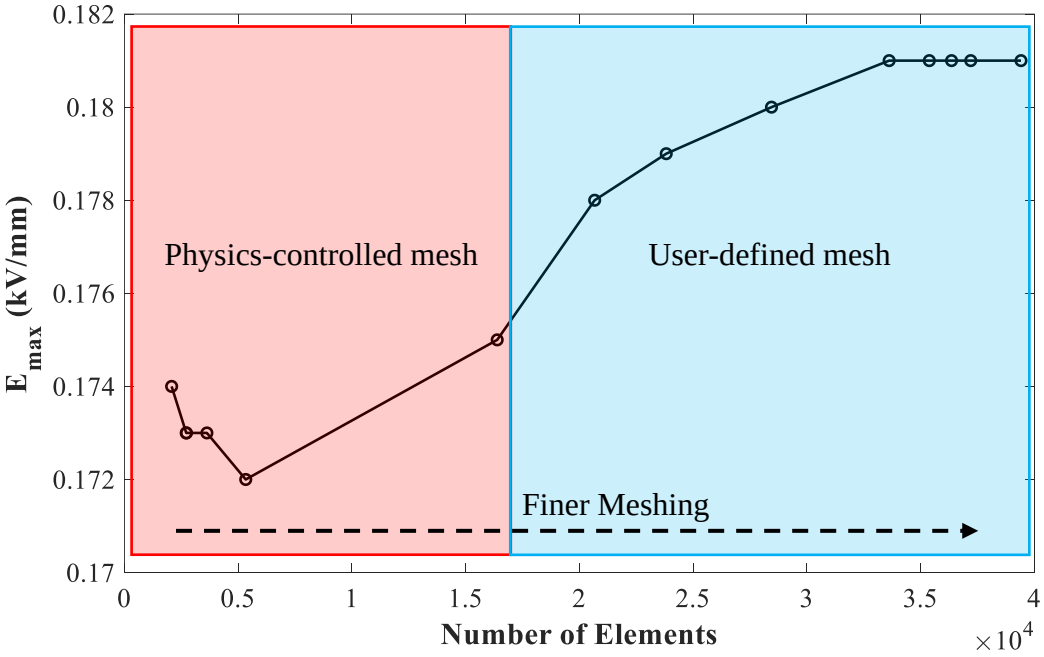

Figure 3-12. E_{max} as a function of number of elements used in the reduced-scale prototype FEA modelling as part of the mesh refinement process.

Another way to inspect the quality of meshing for the FEA model in COMSOL is through the minimum element quality parameter [81]. This is a parameter that is given by COMSOL every time a meshing has been assigned to a model. COMSOL defines the ideal and best possible quality mesh for a model to have a minimum element quality of 1. In contrast, a minimum element quality of 0 represents degenerated elements which will provide an inaccurate solution to the mathematical problem. COMSOL also defines that a minimum

element quality of more than 0.1 is sufficient to give an accurate solution. The closer the minimum element quality statistic is to unity the better the accuracy of the solution provided. For this model, following the mesh refinement process, a minimum element quality of 0.55 was achieved which indicates that the solution to the simulation gives an accurate value. It is important to note that mesh refinement process and minimum element quality inspections were carried out on all COMSOL models in this thesis in order to ensure the quality of all the simulations is adequate.

Simulation Results and E_{max} Location

Figure 3-13 shows the E_{max} in the central region of the conductor using a constant voltage of 1 kV. The conductor tip is terminated with a large spherical electrode, with a diameter twice the one of the conductor, to minimize the high field region. A sufficient clearance of more than double the gap distance between the conductor and the inner enclosure is kept from the bottom of the pressure vessel. These precautions are to ensure that a breakdown will not take place from the end tip of the conductor to the grounded test cell. The enclosure edges were also chamfered to avoid any breakdown occurrence along the edge of the enclosure. In summary, by introducing smoother edges to the design, such as sphere conductor termination or rounding the enclosure edges, there is a more uniform field at the critical design regions which ensures that coaxial breakdowns occur at the location of interest.

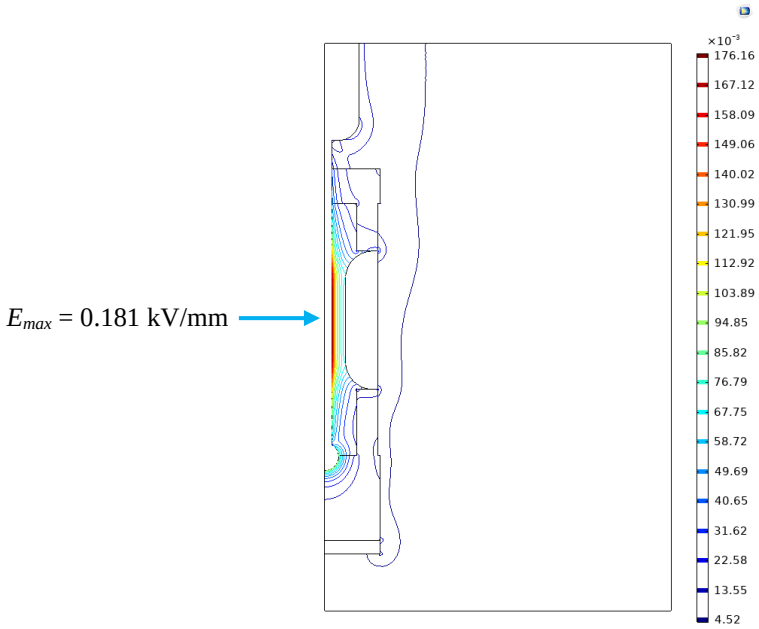

Figure 3-13. Reduced-scale prototype E_{max} (kV/mm) location for 1 kV applied voltage.

Breakdown Testing and Flashover Evidence

Figure 3-14(a) shows the coaxial electrode fully assembled while Figure 3-14(b) illustrates its individual parts. The coaxial electrodes and insulators are made of aluminium and polypropylene respectively. The support structure was used to represent a similar function as the conical insulators whilst keeping the conductor centred, as found in practical equipment. Electrodes were polished to a mirror finish with a mean surface roughness of 0.6 μm.

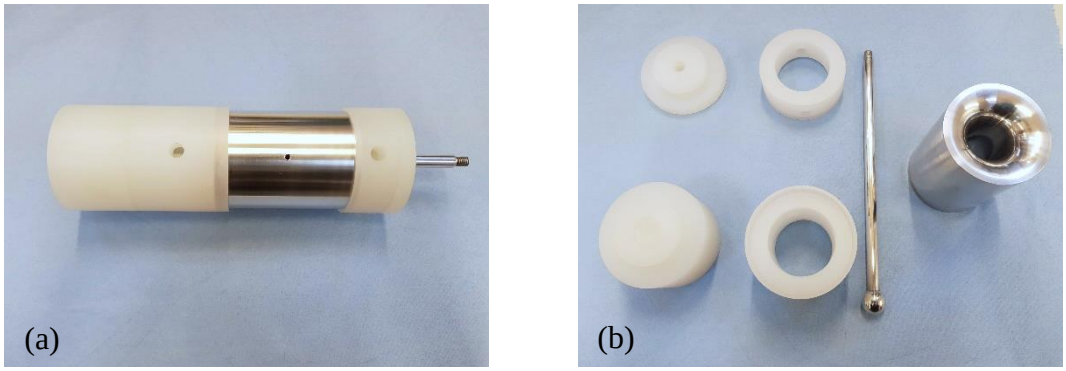

Figure 3-14. Fabricated reduced-scale coaxial prototype (a) fully assembled and (b) disassembled into individual components.

The fabricated reduced-scale prototype was tested under LI breakdown for both polarities. Following the first few breakdowns, the voltage value noticeably decreased with further breakdowns. After inspection, it was found that breakdowns may be result of surface flashover along the polypropylene insulator as shown in Figure 3-15. Despite E_{max} being at the desired location in FEA simulations, COMSOL does not take into consideration the surface discharge development process.

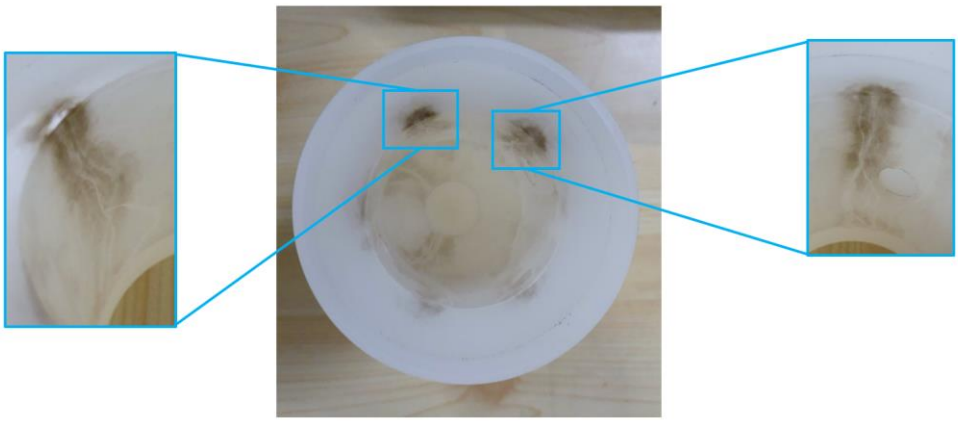

Figure 3-15. Surface flashover on the polypropylene insulator.

As shown in Figure 3-16, the surface flashover took place from the sphere termination to the edge of the enclosure. The reduced-scale prototype had to be modified for the final design in order to ensure that breakdowns occur at the desired central location of the conductor as shown in Figure 3-13.

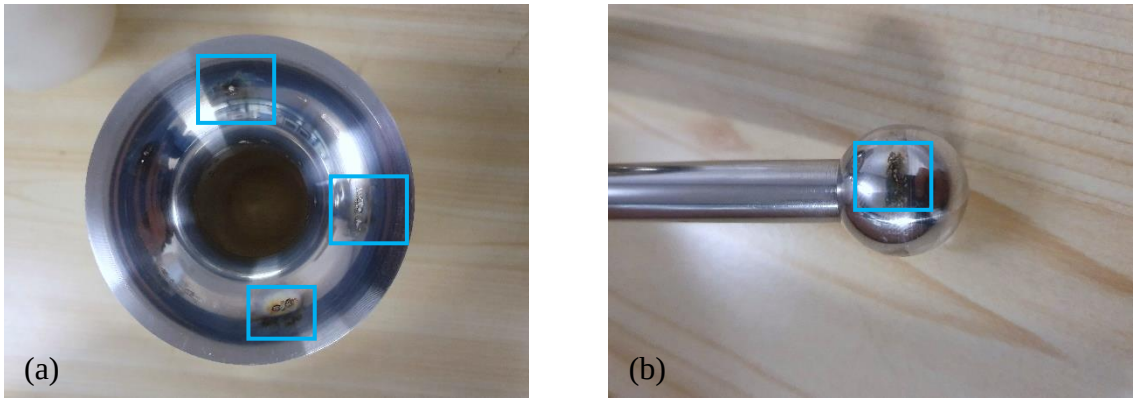

Figure 3-16. Breakdown voltage location for the initial reduced-scale prototype design on the (a) enclosure and (b) conductor sphere termination.

3.3.1.4 Finalised Prototype Design

Figure 3-17(a) shows the final design with a modification made to increase the clearances from the conductor to the enclosure edges. The top insulators were elongated to extend the creepage distance. The bottom insulator was modified so that the sphere termination is not in contact with the polypropylene insulators. Figure 3-17(b) shows the new FEA model for the final prototype design. As before, E_{max} location is at the desired region but with longer creepage distance. This would ensure that the coaxial breakdowns are independent of the edge effect so that the measured results are statistically independent.

Figure 3-18(a) shows the disassembled components including coaxial electrode and insulators. Figure 3-18(b) demonstrates that the breakdowns took place at the desired location meaning the prototype could be used for the breakdown tests of this thesis.

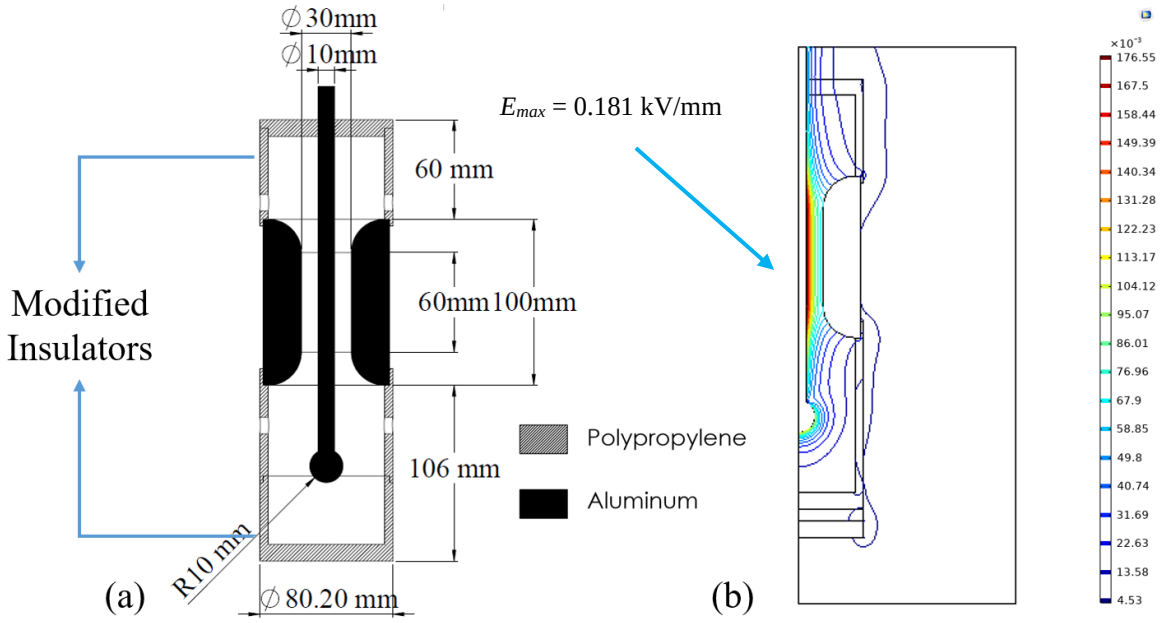

Figure 3-17. Reduced-scaled prototype final design (a) dimensions and materials and (b) electric field distribution simulation and E_{max} location (kV/mm) for 1 kV applied voltage.

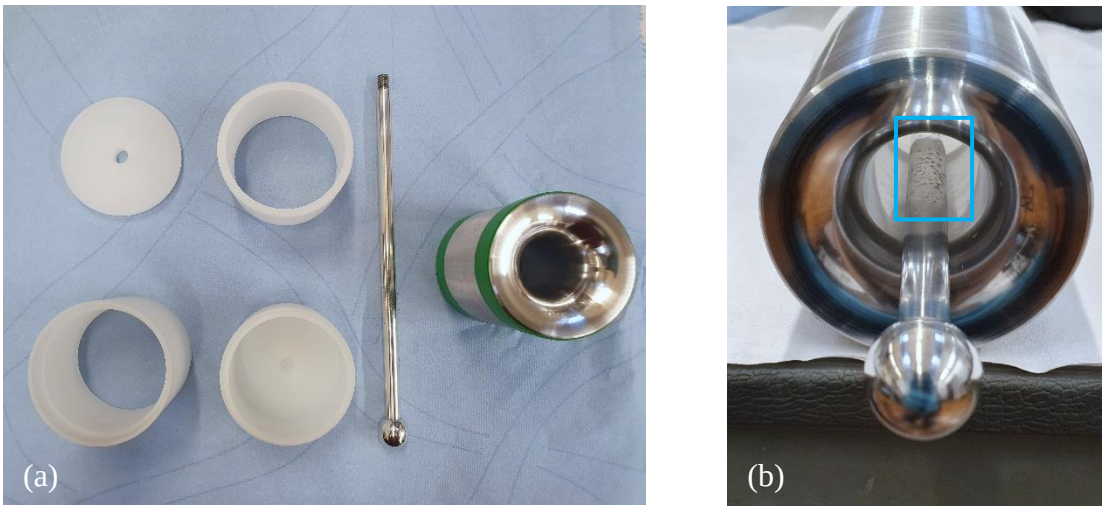

Figure 3-18. Fabricated components of the reduced-scale prototype (a) individual parts and (b) photography on the location of coaxial breakdowns.

3.3.1.5 Conductor Surface Roughness

The surface finish of the reduced-scale prototype conductor was machine turned and the surface roughness measurement was taken along the length of the conductor. An electrode may visually appear to be smooth, but the use of a magnifying device reveals a more complex structure. Surface roughness finish is commonly described as two amplitude parameters in accordance to BS EN/IEC 1134:2010 [82]: average surface roughness ($R_{average}$) and

maximum surface roughness (R_z). Usually, average surface roughness is labelled as R_a. However, since R_a is used for the conductor diameter notation in this thesis, it will be labelled as $R_{average}$.

$R_{average}$ is the arithmetic mean of the absolute ordinate values, Zi, within the measured sampling length (L), which can be expressed mathematically as follows [82]:

$$R_{average} = \frac{1}{n}\sum_{i=1}^{n}|Z_i| \tag{3-5}$$

where n is the number of measured points within a sampling length, Z_i is the ordinate values within L and i is the measurement point number. These parameters are depicted graphically in Figure 3-19 [82].

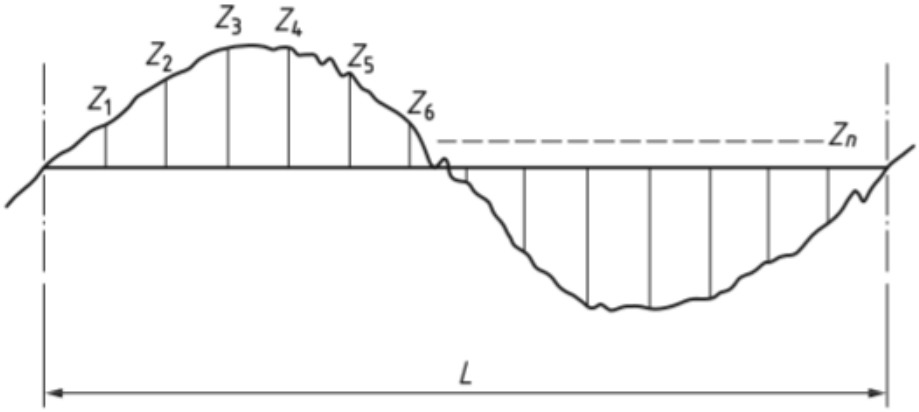

Figure 3-19. $R_{average}$ surface roughness calculation parameters obtained from [82].

R_z is the average value of the ten largest peak height (Z_p) to valley depth (Z_v) within L. In other words, R_z is the average value of the ten largest irregularity peak-to-peak values of the surface roughness curve within L. This can be expressed mathematically in equation 3-6 [83]:

$$R_z = \frac{(Z_{p1} + Z_{p2} + \cdots + Z_{p10}) + (Z_{v1} + Z_{v2} + \cdots + Z_{v10})}{10} \tag{3-6}$$

The parameters of equation (3-6) are shown in Figure 3-20 [83].

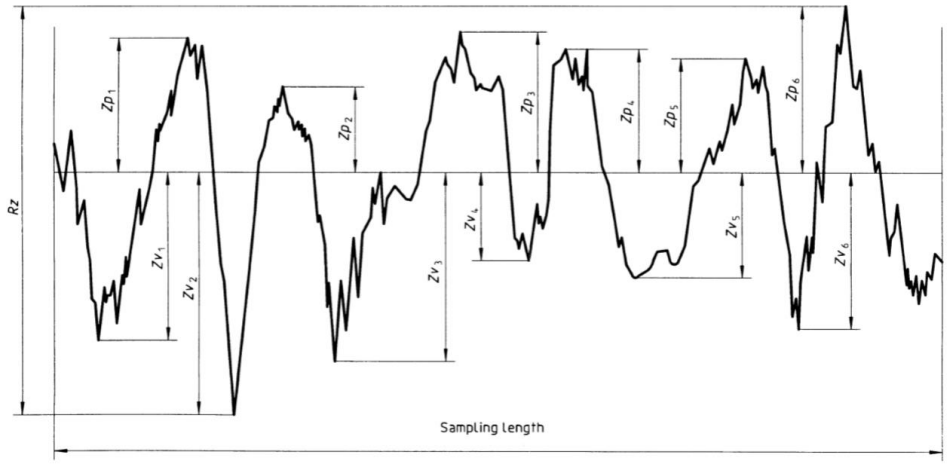

Figure 3-20. R_z surface roughness calculation parameters [83].

Laser confocal scanning microscopy (LCSM) was used to define the surface roughness of the reduced-scale prototype conductor. Precise profile measurements were carried out using a Keyence VK-X200 series laser microscope with a total magnification up to 24,000 times. As shown in Figure 3-21, measurements were taken for a sampling length of approximately 6000 μm. Figure 3-21(a) shows the optical image of the conductor which illustrates the machine turned surface finish. Figure 3-21(b) shows the height image from the laser microscope where red colour indicates the highest peaks and blue the deepest valleys. The image shown is mostly covered with red colour within the sampling length since the difference of height for this mirror-finished conductor is negligible. Figure 3-21(c) shows the surface roughness profile of the conductor within the sampling length measured. As shown, the detailed structure of the conductor involves multiple peaks and valleys as was defined in the surface roughness parameters above. The conductor was found to have a $R_{average}$ of 0.596 μm and R_z of 10.234 μm. Note that all electrodes were surface polished to these specific $R_{average}$ and R_z values prior to any tests. As was described in Chapter 2, field emission electrons released from the cathode can increase with the presence of electrode protrusions and microdefects which is why it is important to start the tests with the same initial $R_{average}$ and R_z values in order for the surface roughness to have negligible impact on the results.

3.3.2 Hemispherical Rod-plane and Coaxial Configurations – Weakly-Quasi Uniform Fields

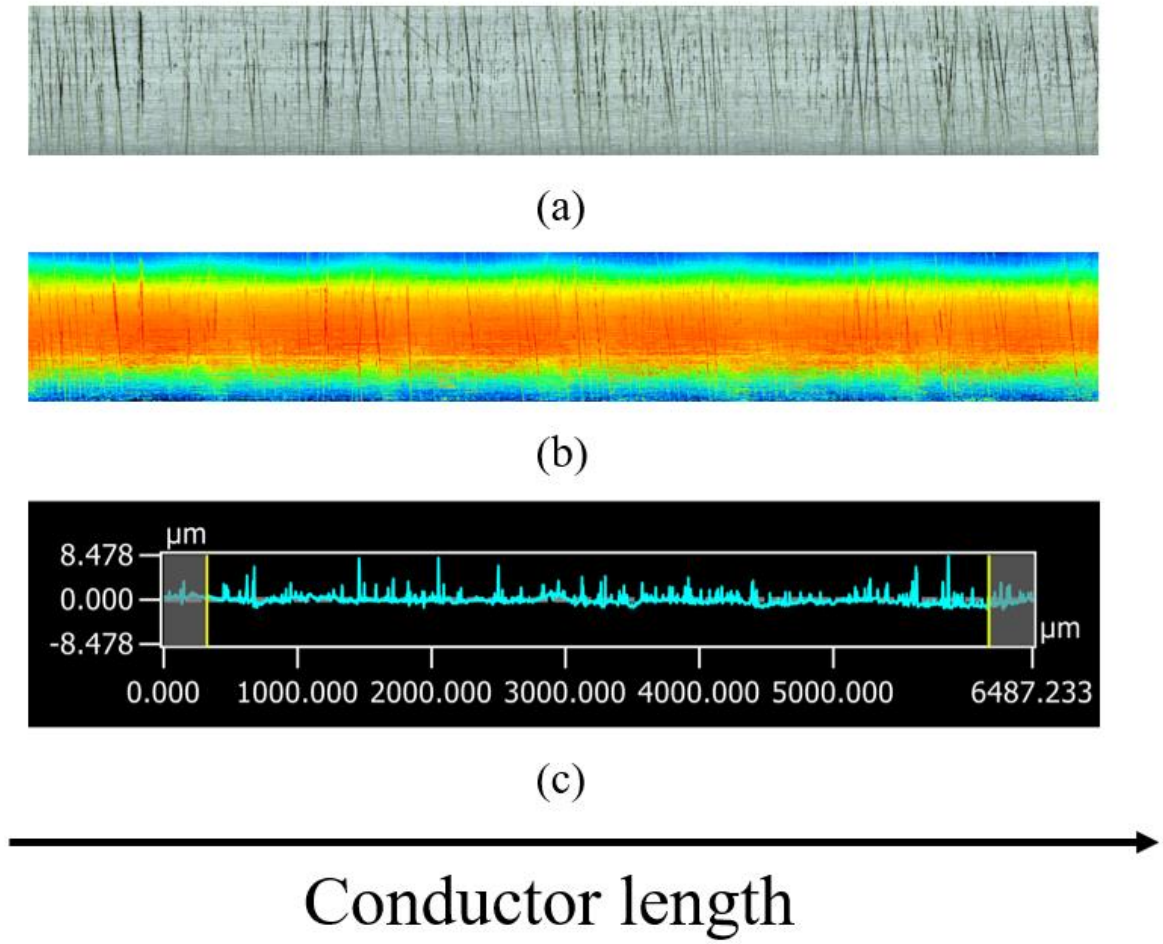

Figure 3-21. Surface roughness measurements of reduced-scale prototype conductor using laser confocal scanning microscopy over the sampling of 6000 µm (a) optical image illustrating the machine turned surface finish (b) height image where red colour indicates the highest peaks and blue the deepest valleys and (c) roughness profile.

For C_3F_7CN gas mixtures to be adopted as a retro-fill solution, it is important to determine the breakdown characteristics of the test gas under different field configurations and voltage waveforms. Coaxial and hemispherical rod-plane electrode configurations were designed based on field utilisation calculations to provide a similar non-uniformity factor despite the use of two distinctly different test electrode systems. COMSOL simulations have been used to compare the f and E_{max} of the two electrode configuration designs and define their field uniformity.

FEA simulations were carried out to investigate the effect of the conductor diameter on the E_{max} and f of a coaxial configuration. Using an enclosure with a fixed inner diameter of 60 mm, and a conductor diameter varying from 4 to 40 mm the E_{max} and f were calculated. E_{max} was found to decrease until it reached a minimum point with the lowest electric field

intensity and then increased with increasing conductor diameter. The *f* decreased almost linearly with decreasing conductor diameter, which suggests that geometrically the electric field is becoming more non-uniform. The lowest *f*, in this coaxial configuration, was found with a conductor diameter of 4 mm. Due to the fabrication difficulty of ensuring a straight 4 mm conductor, the second highest non-uniform 8 mm diameter conductor was chosen for this experimental investigation. The inner enclosure diameter of 60 mm was chosen as it was the maximum diameter possible due to the size limitation of the pressure vessel. Figure 3-22(a) shows the full dimensions for the coaxial electrode configuration. Figure 3-22(b) shows that the proposed coaxial design meets the requirements of giving a weakly quasi-uniform field while ensuring that E_{max} is located in the central region.

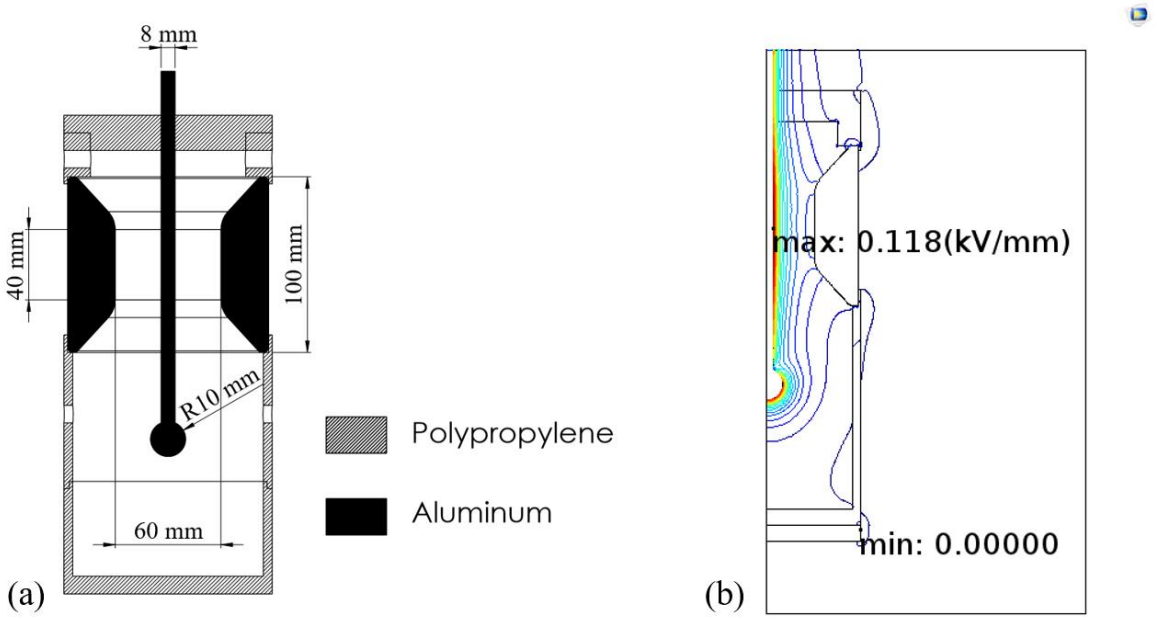

Figure 3-22. (a) Dimensions of coaxial configuration and (b) electric field (kV/mm) simulation result for 1 kV applied voltage.

A hemispherical rod with 30 mm diameter and 15 mm tip radius was found to have several common *f* values to the coaxial configuration. Figure 3-23 shows that by plotting the *f* of both geometries in the same graph, a common field utilization area where both geometries overlap each other can be identified. Figure 3-23 shows that a conductor of 8 mm diameter has approximately the same *f* with a gap distance of 40 mm using this specific rod-plane design.

Figure 3-24(b) illustrates the electric field distribution for the rod-plane electrode configuration with a 40 mm gap distance. Using E_{max} value and the generic field utilization factor equation (equation 2-6), the *f* of ≈0.3 for the coaxial design [Figure 3-22(a)] can be

matched by the hemispherical rod-plane design with a gap spacing of 40 mm [(Figure 3-24(a)]. The electric field uniformity of these two electrode configurations is going to be addressed as weakly quasi uniform. As with the reduced-scale prototype, the electrodes are made of aluminium and polypropylene is used to fabricate the support insulators so that the inner conductor is centred from the coaxial enclosure. The electrodes were polished with $R_{average}$ of 0.6 μm.

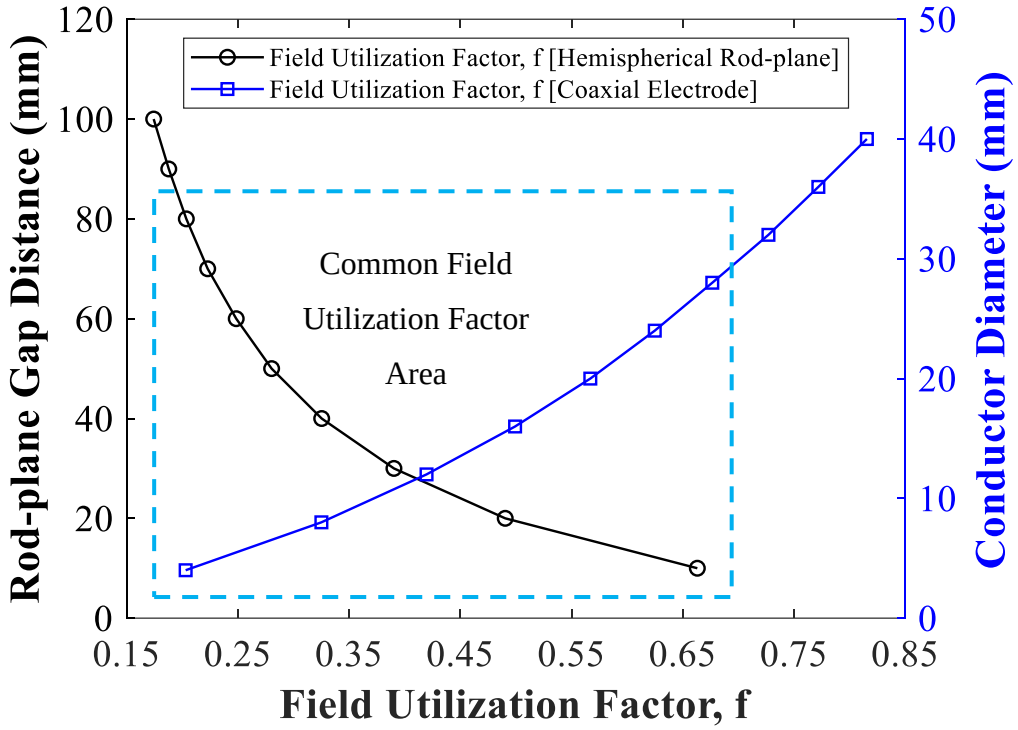

Figure 3-23. Hemispherical rod-plane and coaxial designs plotted against *f*.

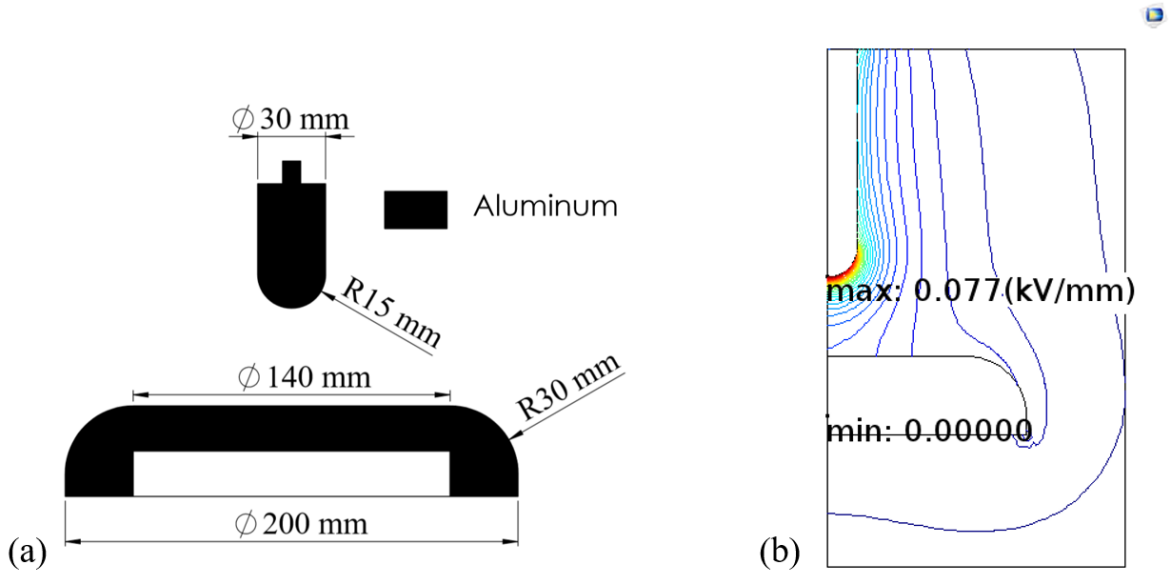

Figure 3-24. (a) Dimensions of the hemispherical rod-plane configuration and (b) electric field (kV/mm) simulation result for 1 kV applied voltage.

3.3.3 Needle Configurations – Divergent and Highly Divergent Fields

3.3.3.1 PD Sources in Practical GIL/GIB Equipment

PD detection and monitoring can be used to provide information about the condition of a dielectric medium in high voltage equipment prior to failure. In gas insulated equipment, there are several possible PD sources associated with the conductor, enclosure and insulating spacers. Figure 3-25 illustrates several faults that can cause PD activities in practical GIL/GIB equipment. PD activities can occur by the following [84]–[87]:

1. *Protrusion on the conductor/enclosure* – a protrusion on the high voltage conductor or grounded enclosure can create a localised field enhancement. This can create corona discharges which can deteriorate the long-term dielectric property of a gas in GIL/GIB equipment and eventually lead to insulation failure.
2. *Floating particles in gas or on insulator* – free conducting particles might start to bounce off the enclosure after gaining charge at operating voltage in GIL/GIB equipment. If the charge acquired becomes sufficiently high, the particle can cross the gas insulation gap between the enclosure and conductor where it can touch the latter one and cause a breakdown. The particle can also land on the insulating spacer which can deteriorate its surface and reduce its dielectric strength. Initiation of a surface discharge is also possible which can lead to a flashover within the equipment.
3. *Insulator with internal defect/void* – voids and defects within the spacer can initiate discharges once their inception voltage is exceeded. These can give rise to electrical trees with the final result being a breakdown.

Artificial defects were developed, using needles, in order to represent extreme case scenarios of two types of PD faults found in practical GIL/GIB equipment as illustrated in Figure 3-25. Electrode configurations were fabricated to model the PD faults of protrusion on conductor (POC) and protrusion on enclosure (POE). Figure 3-26 shows the electrode configurations for the PD experiments in this thesis. Two types of electrode configurations were fabricated: hemispherically capped rod-plane and plane-plane.

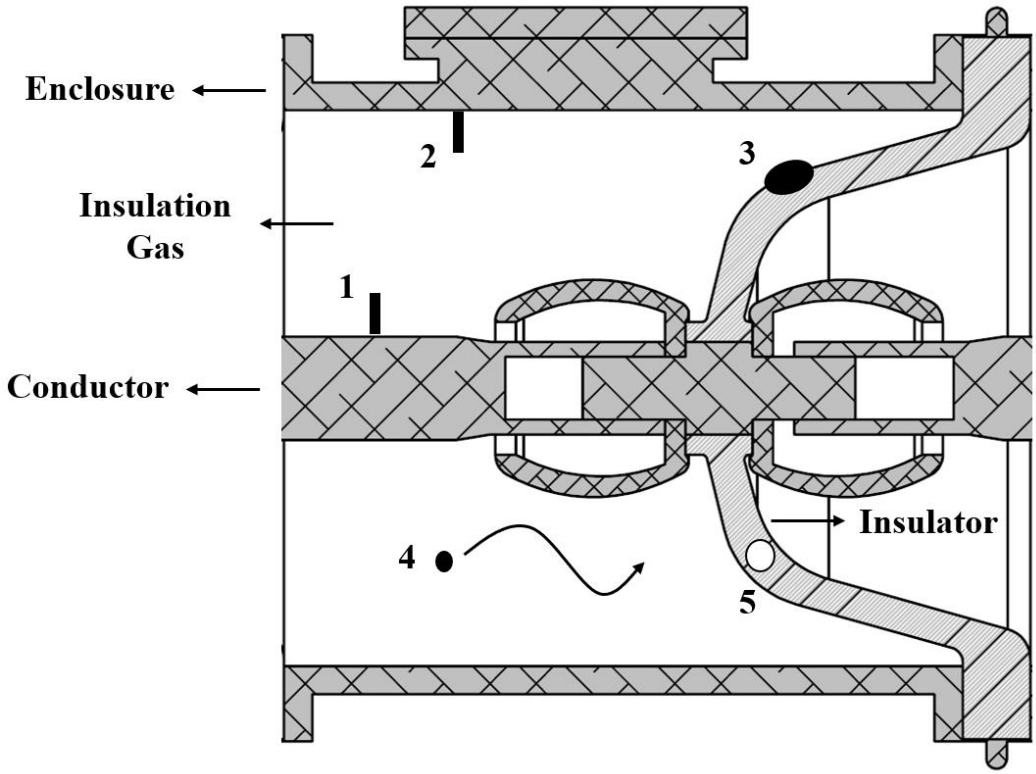

Figure 3-25. Typical insulation defects in practical GIL/GIB equipment that can cause PD activities (1) protrusion on conductor (2) protrusion on enclosure (3) particle on the insulator (4) floating particle and (5) void in the insulator.

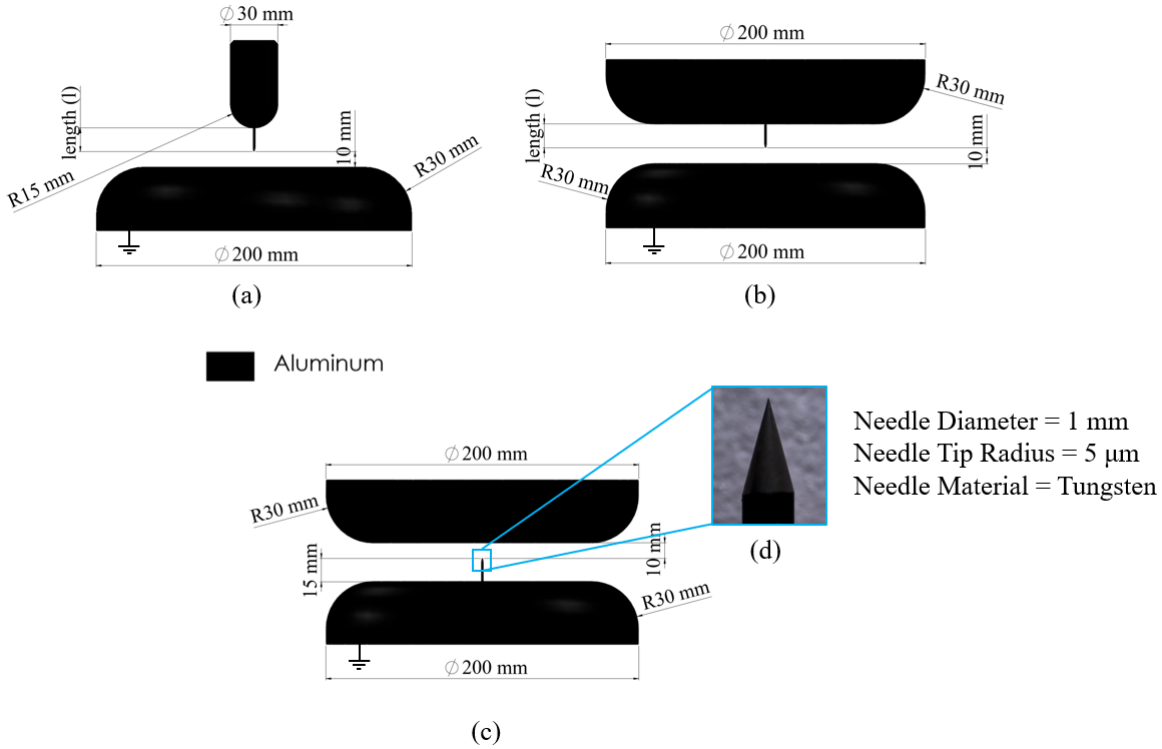

Figure 3-26. Artificial defects on electrode configurations for modelling PD sources of practical GIL/GIB equipment (a) rod-plane with a needle on the HV rod (b) plane-plane with a needle on the HV plane (c) plane-plane with a needle on the grounded plane and (d) needle used for protrusions.

For the POC experiments, the needle was placed on the HV hemispherically capped rod or plane of the electrode configurations as shown in Figures 3-26(a) and 3-26(b). Two needle lengths were used to vary the field uniformity of the electrode configurations. The needle lengths used were 5 mm and 15 mm. The gap spacing between the needle and the plane was always kept constant at 10 mm. The rod-plane and plane-plane electrode spacing was 25 mm and 15 mm with a needle length of 15 mm and 5 mm respectively. For the POE experiements, the needle was placed on the grounded plane of the electrode configuration as shown in Figure 3-26(c). The needle length was constant at 15 mm and the needle-to-plane gap spacing was kept at 10 mm. All electrodes shown in Figure 3-26 were made of aluminium while the needle was made of tungsten. The needle had a 1 mm diameter and a tip radius of 5 μm. Figure 26(d) shows a microscope image of the needle used for the PD experiments.

3.3.3.2 Effect of Needle Length on E_{max} (kV/mm)

FEA simulations were carried out on the PD electrode configurations to examine the change in electric field uniformity with different needle lengths and electrode configurations. Mesh refinement study was performed to ensure the subsequent simulation results are mesh independent. The minimum element quality was also ensured to be over 0.5 for all the FEA simulations in this section. A voltage of 1 kV was applied to the HV electrode for all the simulations. Figure 3-27(a) illustrates that a finer meshing was used close to the needle region. Figure 3-27(b) shows the E_{max} value for the rod-plane electrode configuration with a needle of 15 mm length attached to the HV rod.

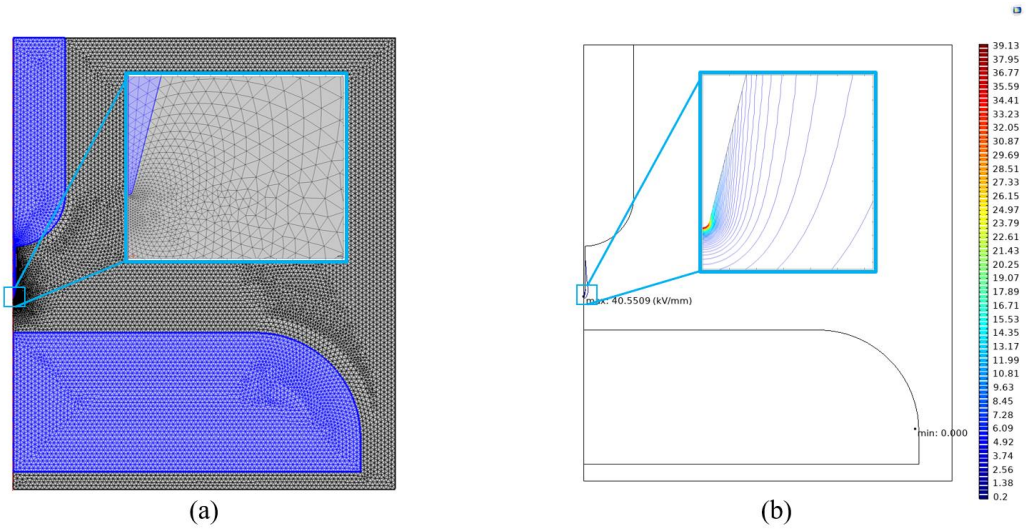

(a) (b)

Figure 3-27. Rod-plane FEA simulation with a needle of 15 mm length attached to the HV rod and a needle-to-plane gap distance of 10 mm (a) Geometry meshing and (b) E_{max} (kV/mm) value for 1 kV voltage applied to the HV electrode.

Figure 3-28 illustrates the effect of needle length on the electric field distribution for the rod-plane and plane-plane electrode configurations. It is shown that the highest electric field is at the HV needle-tip region. The figure illustrates that the most significant change in electric field magnitude, when the needle length is changed from 5 mm to 15 mm, occurs close to the needle tip region for both electrode configurations. Moving away from the needle tip, it can be seen that the electric field of 15 mm needle length is still higher than the 5 mm but marginally. In general, fields using the rod-plane electrode configuration appear to be more non-uniform than the plane-plane electrode configuration under the same needle length.

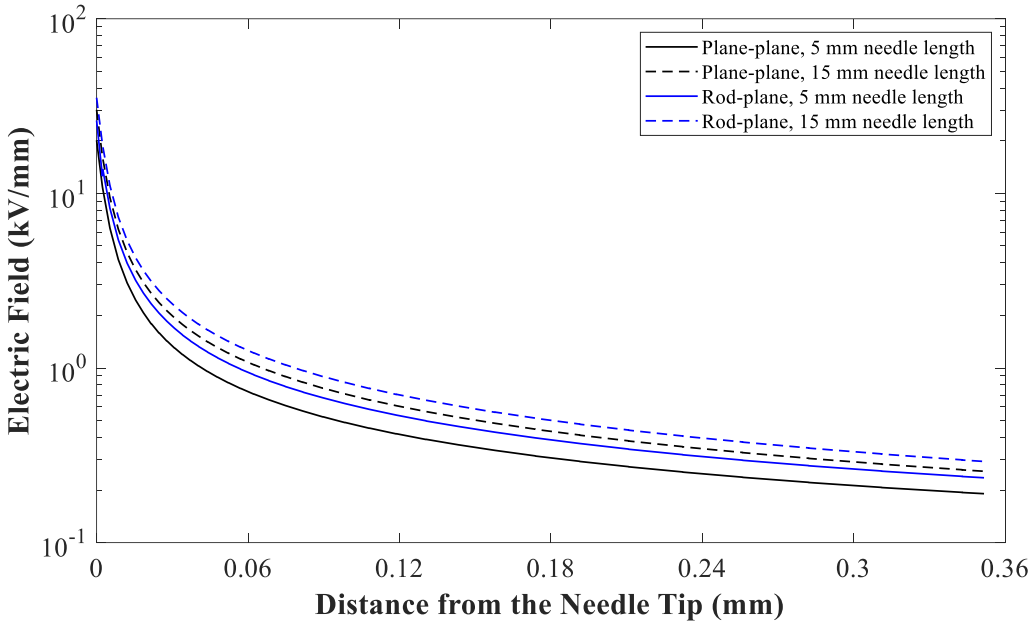

Figure 3-28. Electric field distribution (kV/mm) for 1 kV applied voltage in the needle-to-plane gap spacing of both electrode configurations starting from the needle tip and moving towards the plane.

Simulations were used to determine the field uniformity of each electrode configuration with the values shown in Table 3-4. E_{max} was computed using COMSOL and the f value was calculated using equation (3-7) where U is the applied voltage and d is the needle-to-plane distance (10 mm).

$$f = \frac{E_{mean}}{E_{max}} = \frac{U/d}{E_{max}} = \frac{U}{d \cdot E_{max}} \tag{3-7}$$

Table 3-4 illustrates that the most non-uniform electric field in the specific PD experiments was provided by the rod-plane electrode configuration with a needle length of 15 mm and a f value of 0.0025. In contrast, the most uniform field for these experiments was given by the

plane-plane configuration with a needle length of 5 mm and a resulting *f* value of 0.0043. Regardless of the electrode configuration, it can be seen from Table 3-4 that the reduction of needle length from 15 to 5 mm can increase the *f* value as much as 48%. This percentage value is derived from the increase in *f* by changing the needle length in the plane-plane electrode configuration. The values in this table show that the electrode configuration and needle length being used can have a significant impact on the field uniformity being tested.

Table 3-4. E_{max} and field utilisation factor values for all electrode configurations used in PD experiments for 1 kV applied voltage.

Electrode Configuration	Needle Length (mm)	Maximum electric field, E_{max} (kV/mm)	Field Utilisation Factor, *f*
Rod-plane (POC)	5	30.04	0.0033
	15	40.55	0.0025
Plane-plane (POC)	5	23.14	0.0043
	15	34.58	0.0029
Plane-plane (POE)	15	34.58	0.0029

3.3.4 Summary of Electrode Configurations Developed

Due to the different electrode field configurations developed, a summary is given in this section which clarifies the field uniformity category of each electrode configuration.

Electric fields are often classified into two main categories; uniform and non-uniform fields. Non-uniform fields can be further divided into two smaller groups: weakly and extremely non-uniform fields. However, there is no clear distinction of boundaries between these classifications. Table 3-5 shows the electrode configurations developed that covers a plethora of field uniformities.

The electrode configurations developed mainly belong to the non-uniform electric field section. The electrode configurations developed for breakdown experiments belong to the weakly non-uniform category while the ones developed for PD experiments are placed in the extremely non-uniform category. The weakly and extremely non-uniform categories were further broken down to quasi-uniform and weakly quasi-uniform as well as divergent and highly divergent groups respectively

Table 3-5. Classification of electric field categories for the electrode configurations developed for the breakdown and the PD experiments in this thesis.

<table>
<tr><td colspan="5">Electric Fields</td></tr>
<tr><td>Uniform Field</td><td colspan="4">Non-uniform field</td></tr>
<tr><td rowspan="3">No electrode designs for uniform field testing were developed in this thesis</td><td colspan="2">Weakly Non-uniform</td><td colspan="2">Extremely Non-uniform</td></tr>
<tr><td>Quasi-uniform</td><td>Weakly Quasi-uniform</td><td>Divergent</td><td>Highly Divergent</td></tr>
<tr><td> 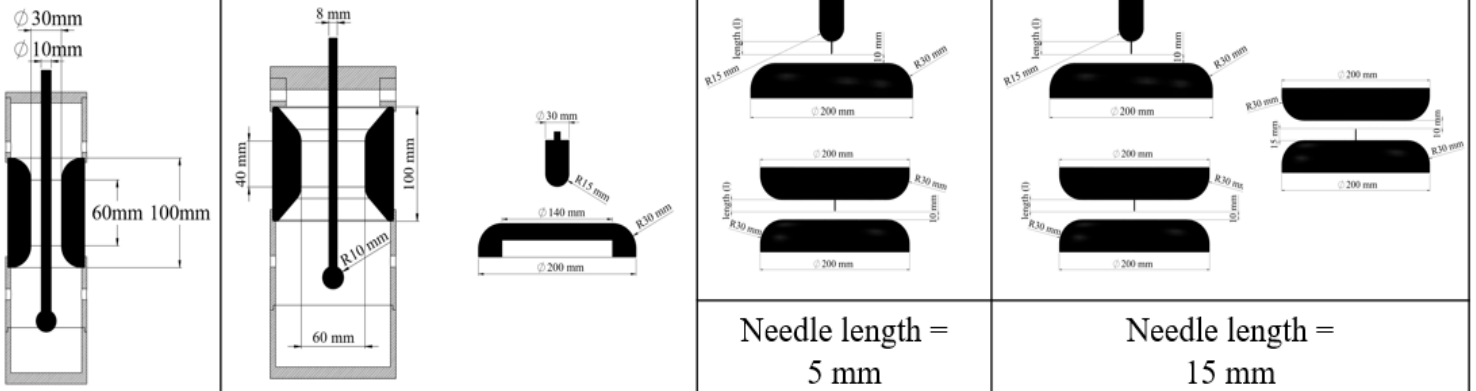
</td><td>Needle length = 5 mm</td><td>Needle length = 15 mm</td></tr>
<tr><td>$f \approx 1$</td><td>$0.5 < f$</td><td>$0.1 < f \leq 0.5$</td><td>$0.003 < f \leq 0.1$</td><td>$f \leq 0.003$</td></tr>
<tr><td></td><td colspan="2">Breakdown Experiments</td><td colspan="2">PD Experiments</td></tr>
</table>

3.4 Gas Handling Setup and Procedures

3.4.1 SF_6 and C_3F_7CN Gas Handling Setup

3.4.1.1 Gas Carts

Gas carts are being used for recycling and evacuation of air from the gas compartment. In this PhD project, SF_6 and C_3F_7CN/CO_2 gas mixtures were tested and separate gas carts were used for: (i) prevention of cross contamination and (ii) avoidance of material compatibility issues as C_3F_7CN gas reacts with the filter material used in the SF_6 gas cart.

It is important to minimise potential leak of SF_6 being released from gas handling due the environmental concerns of the gas. Figure 3-29 shows the DILO mini-series gas cart, designed for handling small gas quantities. The gas cart includes four main components: compressor (1.6 m^3/h), vacuum compressor (3.3 m^3/h) and suction pump (3 m^3/h), pre filter and vacuum pump (16 m^3/h). All the compartments are connected with gas tight hoses which minimised the likelihood of SF_6 emission.

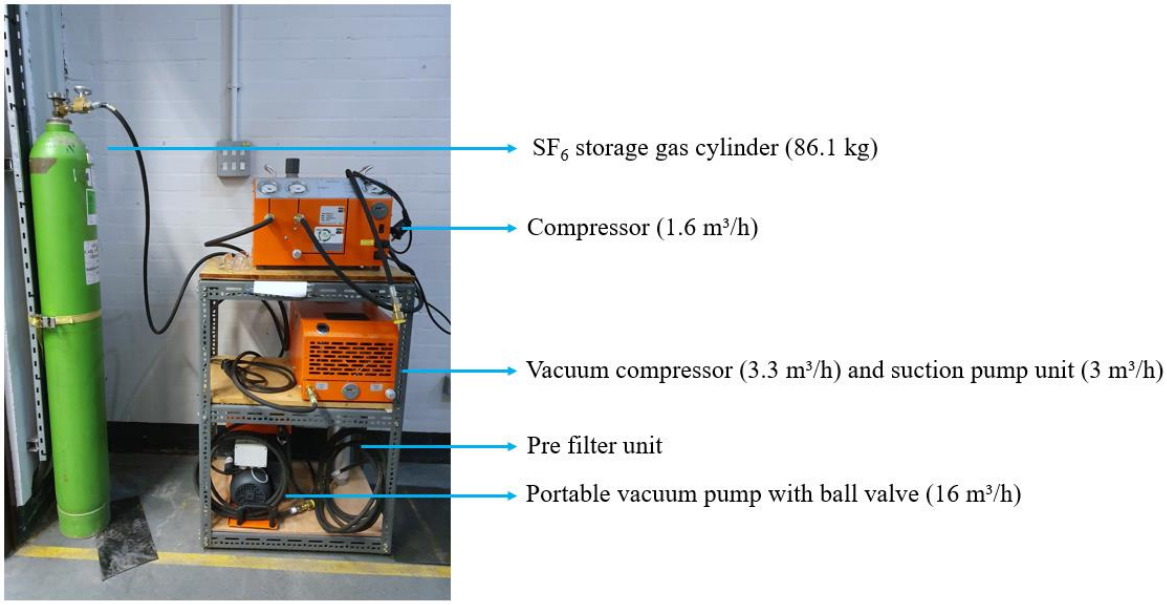

Figure 3-29. DILO SF_6 mini-series gas cart with individual units.

C_3F_7CN/CO_2 gas mixtures handling provides an eco-friendly and economic solution of re-using the gas mixtures for several tests. Even though alternative gas mixtures have a considerably lower impact to the environment, when compared to SF_6, they still have to be handled within a closed loop system to avoid unnecessary releases to the atmosphere. Additionally, careful gas handling has to be carried out for these gas mixtures within a gas tight system in order to avoid any air ingression. For these purposes, a bespoke DILO C_3F_7CN Piccolo-series gas cart was used.

Figure 3-30 shows the C_3F_7CN gas cart that consists of the control unit to perform gas operations and the inlet and outlet connections. The three-way ball valve can be used to switch between filling and recovery procedures and a pressure regulator is used to control the flow of gas during filling. Finally, the ball valve with a hand wheel can be used to allow the gas to escape from the gas cart in case of an over-pressurisation fault.

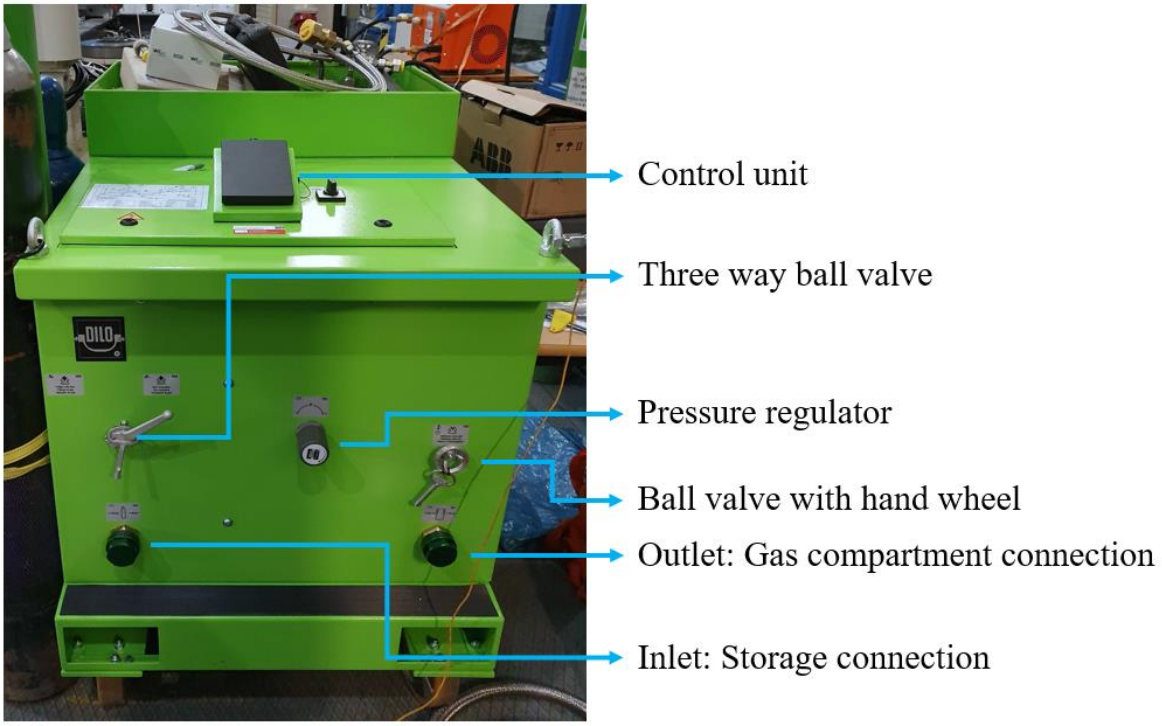

Figure 3-30. DILO C_3F_7CN Piccolo-series bespoke gas cart.

Contrary to the mini-series SF_6 gas cart, the Piccolo-series gas cart has all of its modular units encompassed within the metallic body. The interconnections between the modular units allow automatic gas handling operation and can interface with external units such as the storage cylinder or the pressure vessel.

The C_3F_7CN gas cart was designed for larger gas volumes and has a compressor capacity of 3.2 m^3/h. The suction pump unit has a delivery rate of 3 m^3/h, and the vacuum pump has a higher capability than the mini-series with a rate of 25 m^3/h. Both gas carts can recover gas and evacuate air down to < 1 mbar. However, different handling time is required due to the difference in the capacity of the modular units.

3.4.1.2 Gas Analysers

In the case of SF_6, a gas analyser is used for measuring the gas purity which is necessary for maintaining its dielectric properties. Based on BS EN/IEC 60480:2004 [88], SF_6 purity will reduce due to: (i) moisture/air impurities from mishandling or gas leak and (ii) gaseous decomposition by-products generated from PD and breakdown incidences. The standard also specifies that SF_6 should not be used for dielectric applications if its purity reduces below 97%. Figure 3-31 illustrates a DILO SF_6 volume percentage measuring device used to ensure that SF_6 gas purity was always above acceptable level. The measuring device uses the velocity of sound principle to detect the impurities in SF_6 gas. Its measuring range is from 0 to 100% SF_6 with a measuring accuracy of ±0.5% and can be used for a pressure range of 1.7 to 10 bar (abs). Note that the SF_6 gas used in this PhD project was always higher than 99% purity level as illustrated in Figure 3-31.

Figure 3-31. DILO SF_6 volume percentage measuring device.

The WIKA GA11 gas analyser, shown in Figure 3-32, can measure up to three parameters: (i) C_3F_7CN concentration (ii) humidity content and (iii) oxygen level. The C_3F_7CN concentration is measured using the velocity of sound. Optical and polymer-based capacitive humidity sensors are used to measure the oxygen and humidity contents within the gas mixtures respectively. The measuring range of the oxygen sensor is from 0 to 10% with a measuring accuracy of ±0.3%. The humidity sensor can measure between -55 to 0°C with the deviation varying according to the range of the measurement. The deviation is ±2°C from -25 to 0°C, ±3°C from -35 to -25°C and ±4°C from -55 to -35°C. As this is a prototype unit and larger tolerances are expected, the requirements to use a mixture for experiments in this project was to have an accurate C_3F_7CN concentration of ±1% accuracy and an oxygen level of 0%.

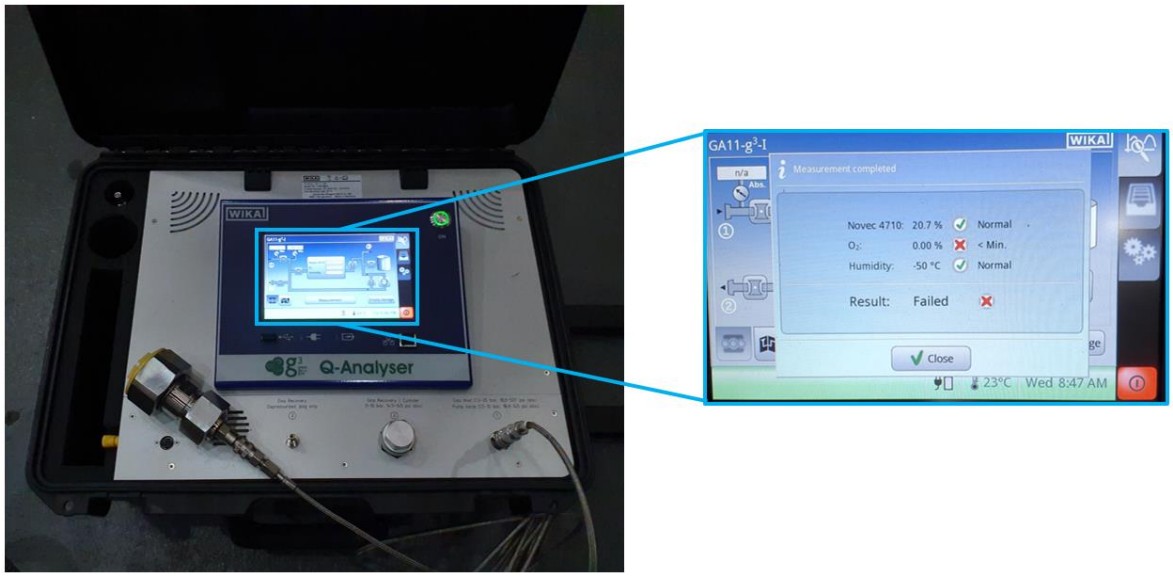

Figure 3-32. WIKA GA11 alternative gases analysis instrument for C_3F_7CN/CO_2 gas mixtures.

3.4.1.3 Gas Cylinders

Figure 3-33 shows the gas cylinders used for the preparation and storage of new C_3F_7CN/CO_2 gas mixtures. Pure C_3F_7CN gas cylinders were provided by 3M and pure CO_2, with 99.8% purity, was supplied from BOC. Different sizes of storage gas cylinders were used from Solvay and DILO including 10 l and 40 l capacity as shown in the figure.

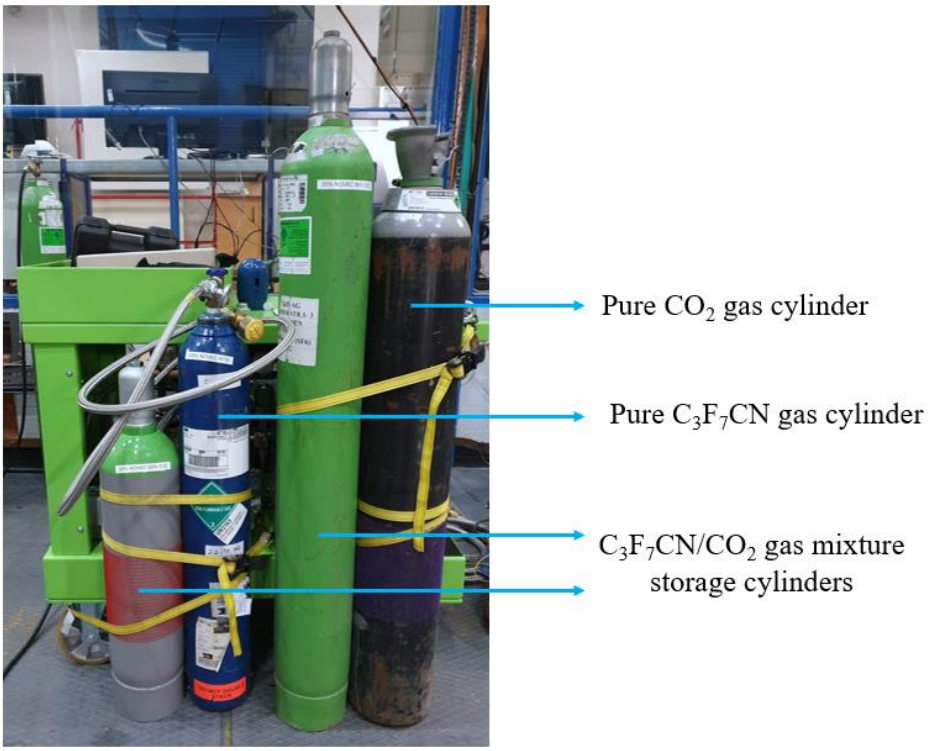

Figure 3-33. Gas storage cylinders used for pure C_3F_7CN, CO_2 and C_3F_7CN/CO_2 gas mixtures.

3.4.2 SF_6 and C_3F_7CN/CO_2 Mixtures Gas Handling Procedures

3.4.2.1 SF_6 Gas Handling

SF_6 gas handling involves evacuation of air, filling and recovery procedures. SF_6 filling is straight forward in comparison to C_3F_7CN/CO_2 gas mixtures since it only involves a single gas. Figure 3-34 shows the filling procedure for SF_6 gas. Evacuation of air was performed on the vessel until the pressure reached below 0.5 mbar. The filling of SF_6 gas was carried out by connecting the gas cylinder to the inlet and the pressure vessel to the outlet of the compressor unit respectively. This was done to control the flow of SF_6 with the compressor unit's pressure regulator to avoid any overpressure in the vessel which was necessary as SF_6 gas is stored at high pressure (≈20 bar absolute).

The compressor unit is also necessary when filling large-volume gas compartments. This is because when filling large volumes, such as the GIB demonstrator, the pressure of the storage cylinder and the gas compartment will reach a point of equilibrium where the gas can no longer flow from the high-pressure to the low-pressure environment (as both will be

at equal pressure). This is where the compressor is used to extract the residual SF_6 gas from the gas cylinder until 1 bar (abs) is reached. After filling, the purity of the SF_6 gas was always measured using the volume percentage measuring device shown in Figure 3-31.

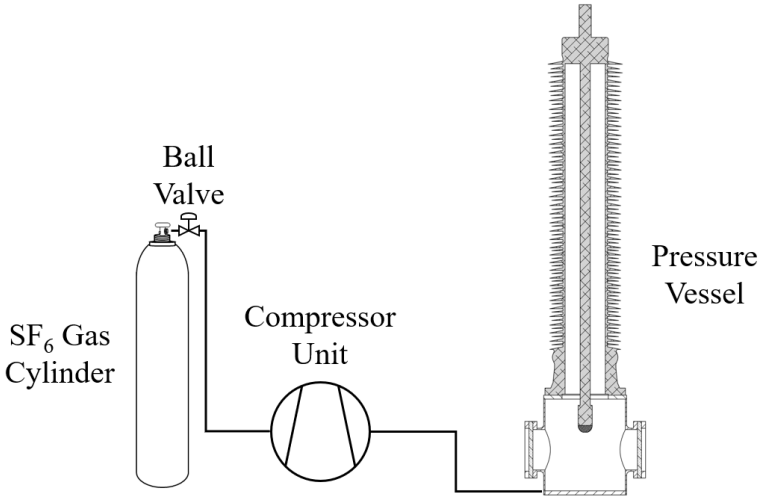

Figure 3-34. SF_6 filling procedure.

The recovery procedure of extracting and storing SF_6 is shown in Figure 3-35. The pre filter unit is used to absorb moisture, solid and gaseous decomposition products from used SF_6 after testing. The vacuum compressor is activated in conjunction with the compressor when the pressure of the gas compartment reaches 400 mbar. Similarly, the suction unit turns on when the pressure of the gas compartment reaches 5 mbar. These two units work concurrently with the compressor in order to extract the gas out of the gas compartment down to 1 mbar.

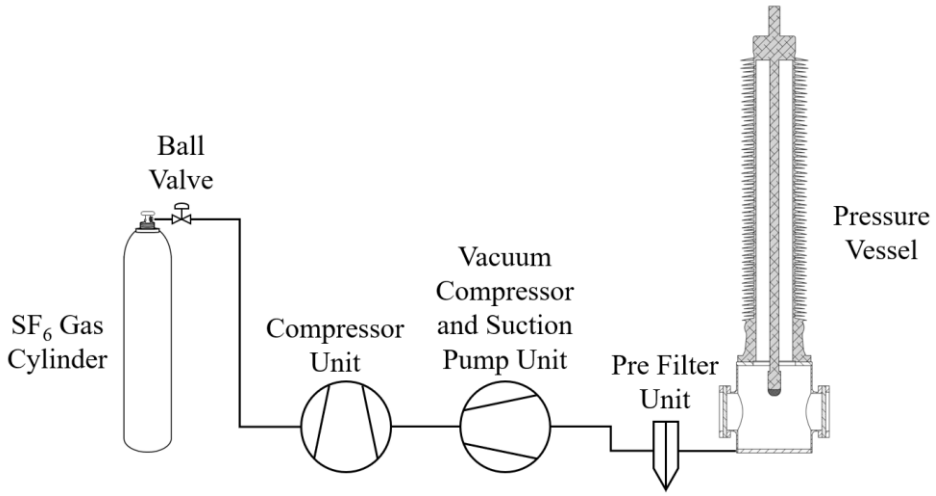

Figure 3-35. SF_6 recovery procedure.

3.4.2.2 C_3F_7CN/CO_2 Gas Mixtures Handling

C_3F_7CN/CO_2 gas mixtures handling complement extra procedures since the complexity of handling two gases increases compared to SF_6. In addition to filling and recovery procedures, handling C_3F_7CN/CO_2 gas mixtures involves mixing and refilling procedures. As with the SF_6 gas cart, the Piccolo-series gas cart was vacuumed down to < 0.5 mbar before the first usage to make sure there is no air impurities within the gas cart after transportation.

Figure 3-36 portrays the filling procedure for the C_3F_7CN/CO_2 gas mixtures. The Manometric method based on the Dalton's law of partial pressures was adopted, which states that the total pressure of a mixture of non-reacting gases is equal to the sum of the partial pressures of individual gases [89]. This can be expressed mathematically as follows:

$$P_{total} = \sum_{i=1}^{n} p_i \qquad or \qquad P_{total} = P_1 + P_2 + P_3 + \cdots + P_n \tag{3-8}$$

where P_1, P_2, ..., P_n represent the partial pressures of individual gases and P_{total} the total pressure of the gas mixture. Prior to filling, the pressure chamber was first vacuumed down to < 0.5 mbar and then filled with dry CO_2 to absorb moisture and minimise air impurities. The chamber was then vacuumed again down to < 0.5 mbar before filling the test gas mixture. C_3F_7CN was first filled up to the required partial pressure and then topped up with CO_2 to reach the desired total pressure of the gas mixture. A pressure regulator was used to control the flow of CO_2 due to the high storage pressure.

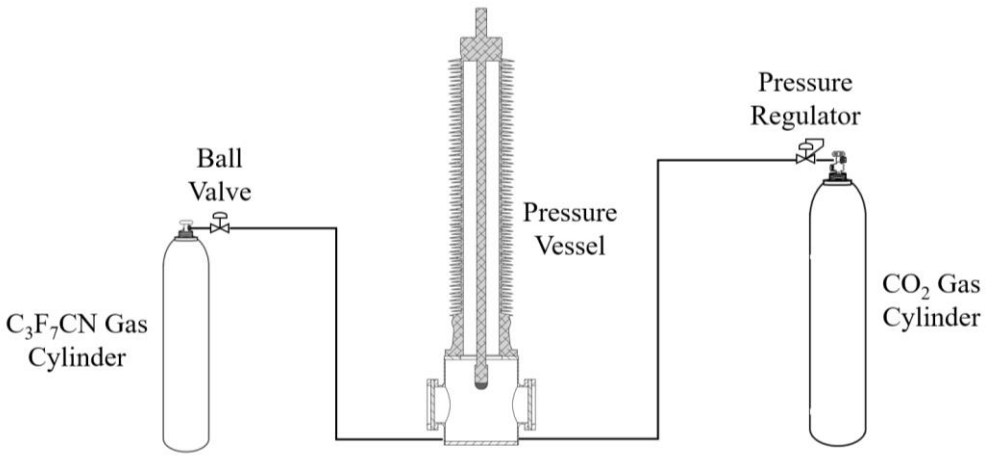

Figure 3-36. C_3F_7CN/CO_2 gas mixtures filling procedure.

Following the gas mixture filling procedure, a recirculation loop was connected using the two gas filling points on the pressure vessel with the inlet and the outlet of the DILO alternative gas Piccolo cart series as shown in Figure 3-37.

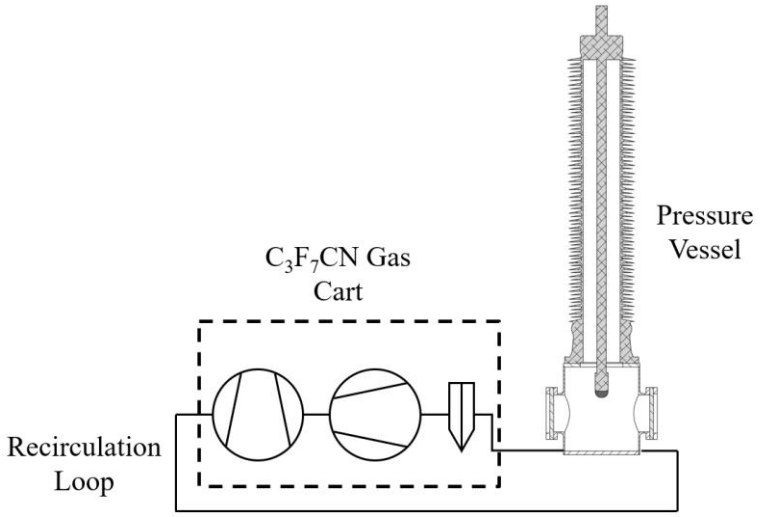

Figure 3-37. C_3F_7CN/CO_2 gas mixtures mixing procedure.

The loop was used to circulate the entire volume of gas inside the gas compartment for a minimum of two cycles to ensure that the C_3F_7CN/CO_2 gas mixture is homogeneously mixed. Based on the compressor rating (3.2 m^3/h) and the vessel volume of 114 l, it was calculated that the recirculation time for a gas mixture at 4.5 bar (abs) is approximately 20 minutes. This is given by:

$$Mixture\ circulation\ time\ per\ cycle = \frac{pressure\ vessel\ capacity\ (m^3) * pressure\ of\ gas\ mixture\ (abs) * 60}{compressor\ rating\ (m^3/h)}\ (minutes) \qquad (3\text{-}9)$$

After the completion of the filling and mixing procedures, the gas analyser, shown in Figure 3-32, was used to validate the mixture ratio and check whether there is any oxygen contamination.

Figure 3-38 shows the recovery and refiling procedures for C_3F_7CN/CO_2 gas mixtures. Each mixture was recovered into a storage gas cylinder which was used for the specific mixture concentration e.g. 20% C_3F_7CN / 80% CO_2 gas mixture storage cylinder. The pre-mixed gas could be used to refill or top up the pressure vessel when additional gas was necessary for tests at higher pressures. As C_3F_7CN within a gas mixture tends to liquefy when its partial

pressure exceeds ≈2.5 bar (abs), a heating blanket was always used when the pre-mixed storage gas cylinder was used to fill the pressure vessel. The purpose of the heating blanket was to pre-heat the bottle ensuring that the gas mixture remains in a homogeneous gaseous state prior to filling. This avoids the risk of C_3F_7CN gas liquefying and therefore giving a different ratio of gas mixture than the one expected. To avoid any liquefaction problems in this thesis, the 20% C_3F_7CN / 80% CO_2 gas mixture was stored in the GIB demonstrator (used as a storage vessel) of which the volume was about 10 times larger than the one of the pressure vessel. This assisted in having enough gas to fill the pressure vessel up to more than 10 bar (abs) while keeping the pressure of the storage vessel smaller than 4.5 bar (abs) pressure to avoid any liquefaction issues since the liquefaction pressure for the overall 20/80 gas mixture is about 12.5 bar (abs).

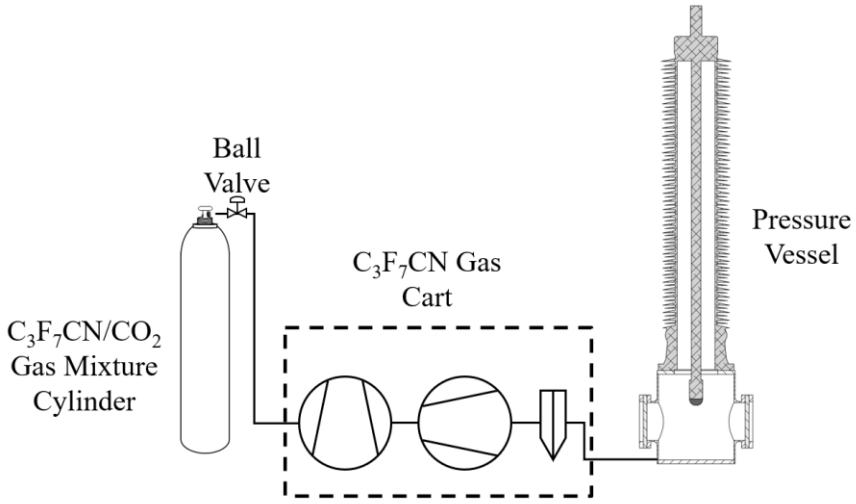

Figure 3-38. C_3F_7CN/CO_2 gas mixtures recovery and refilling procedures.

3.5 Summary

This chapter summarises the development of the test setups and gas handling procedures used for the experimental works described in this thesis.

Coaxial and hemispherical rod-plane electrode configurations were developed through calculation, simulation, preliminary test and design modification. Needles were attached on electrode configurations to mimic PD defects as found in practical GIL/GIB equipment and to determine the PD characteristics of C_3F_7CN/CO_2 gas mixtures versus SF_6.

A detailed description was given for the gas handling setups and procedures used for SF_6 gas and C_3F_7CN/CO_2 gas mixtures. The SF_6 gas used is always above 99% purity level and the C_3F_7CN/CO_2 mixtures were homogeneously mixed with minimal oxygen content. All gases are handled carefully to ensure a closed loop and avoid accidental leakage. Test gases were measured using the SF_6 and the alternative gas analysers to measure the gas purity before an experiment.

Chapter 4 Breakdown Characteristics of SF_6 Gas and C_3F_7CN/CO_2 Gas Mixtures

4.1 Introduction

Breakdown tests can be used to examine the difference in insulation performance between dielectric mediums. In this chapter, the hemispherical rod-plane, the reduced-scale 10/30 mm and 8/60 mm coaxial electrode configurations were tested under different test conditions to compare the breakdown characteristics of SF_6 gas and C_3F_7CN/CO_2 gas mixtures. Lightning impulse and AC voltage waveforms were tested in this chapter.

The breakdown characteristics of two C_3F_7CN/CO_2 gas mixtures were compared to SF_6 to identify the more suitable ratio for retro-fill applications. Tests were conducted on the reduced-scale 10/30 mm coaxial prototype which replicates quasi-uniform electric fields as found in practical GIL/GIB equipment. The 20% C_3F_7CN / 80% CO_2 gas mixture was chosen based on the trade-off of breakdown performance and liquefaction temperature. The same mixture was further evaluated experimentally in weakly quasi-uniform electric fields using the 8/60 mm coaxial and the hemispherical rod-plane electrodes.

4.2 Generation and Measurement of Lightning Impulses and AC Voltage Waveforms

4.2.1 Test Setup for Lightning Impulse Breakdown Experiments

Two types of Marx impulse generators were used for standard LI voltage applications: (i) BHT 8-stage and (ii) Haefely 10-stage impulse generators. The choice of impulse generator was dependent on the voltage range required for the tests. For tests up to 400 kV, the BHT impulse generator was used which has a capability to charge up to 100 kV per stage with a maximum capability of 800 kV when all stages are connected. Every stage has a low, 0.5 kJ

rated, energy which minimises the surface damage on the electrodes post breakdown. For tests where higher voltages were necessary, the Haefely impulse generator was used which has a capability to charge up to 200 kV per stage with a maximum voltage capability of 2 MV. Each stage has a rated energy of 15 kJ which results to more damage on the electrodes. As a result, the BHT impulse generator was preferred when the testing voltage range was ≤ 400 kV. The BHT impulse generator voltage was limited to a four-stage configuration with a maximum test voltage of 400 kV due to clearances in the lab.

Marx impulse generators are used when the voltage range required for testing is more than what a single-stage impulse generator can supply. This kind of generators give the flexibility of changing the voltage range supplied by varying the number of stages connected. These impulse generators are charged by having multiple impulse capacitors, C_{imp}, connected in parallel which are charged through the DC voltage source coming from a rectified unit. In the case of the BHT generator, LIs can be produced by using eight 100 kV rated capacitors, one per stage. The Haefely generator has two 100 kV capacitors in each stage, which allows it to charge up to a maximum 200 kV per stage. The impulse capacitors are charged through the charging resistors which are used to limit the charging current. As soon as all the capacitors are charged, the spark gap (SG) of the first stage is externally triggered from the impulse generator control unit causing an almost instantaneous in-series discharge for all stages connected. This provides the impulse application applied onto the HV connection of the pressure vessel. Front, R_F and tail, R_T resistors are used to alter the front and tail time of the voltage waveform. Impulse applications of both positive and negative polarities can be applied by changing the diode orientation. Figure 4-1 shows the circuit diagram for the LI breakdown tests using the Haefely impulse generator. The pressure vessel is connected in parallel to the impulse generator and a Haefely capacitive voltage divider (C_{VD}). The voltage measurement was taken through the capacitive voltage divider that has a conversion ratio of 1107/1 and is connected to the Highest Resolution Impulse Analysing System (HiAS) 744 system. HiAS is the control and measurement unit which can be used to trigger the impulse generator but also record the voltage parameters of every impulse shot.

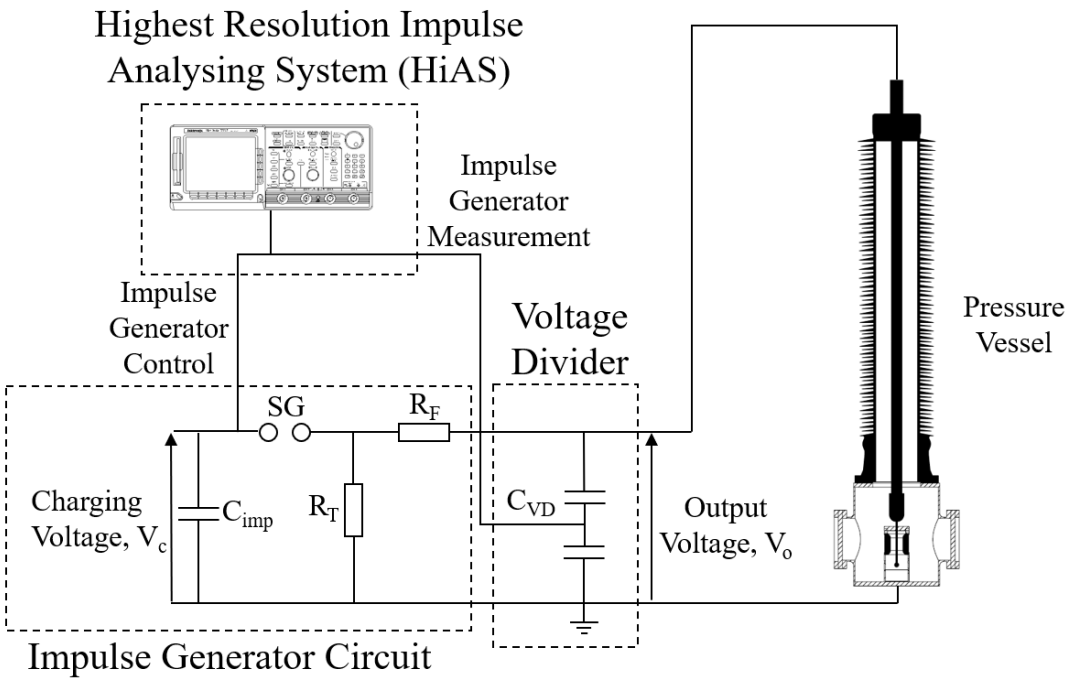

Figure 4-1. LI breakdown tests circuit diagram including the pressure vessel, impulse generator, voltage divider and the HiAS.

4.2.2 Standard Lightning Impulse Waveform

According to BS EN/IEC 60060-1:2010 [90], a standard lighting impulse waveform has a front time (T_1) of 1.2 μs, with a tolerance of ±30%, and a time to half-value (T_2) of 50 μs with a tolerance of ±20%. T_1 is calculated by dividing the time taken from the 30% value to the 90% value of the peak voltage (U_{peak}) by 0.6, denoted as T in Figure 4-2. Another parameter which should be within ±3% tolerance is the U_{peak} of the LI waveform. Figure 4-2 shows an example of an impulse shot used in the breakdown experiments where 252.2 kV were applied from the impulse generator control unit. As shown in the figure, the time and voltage parameters of the waveform applied for the breakdown tests in this chapter are within the tolerances specified by the standard.

4.2.3 Test Setup for AC Voltage Breakdown Experiments

A High Volt 2-stage cascade transformer AC generator was used for the AC breakdown tests. The application of a two-stage cascade AC transformer is taken to consideration when voltages up to 800 kV are necessary for testing. In addition to the primary and secondary winding of the transformer, a transfer winding is used to feed the primary winding of the

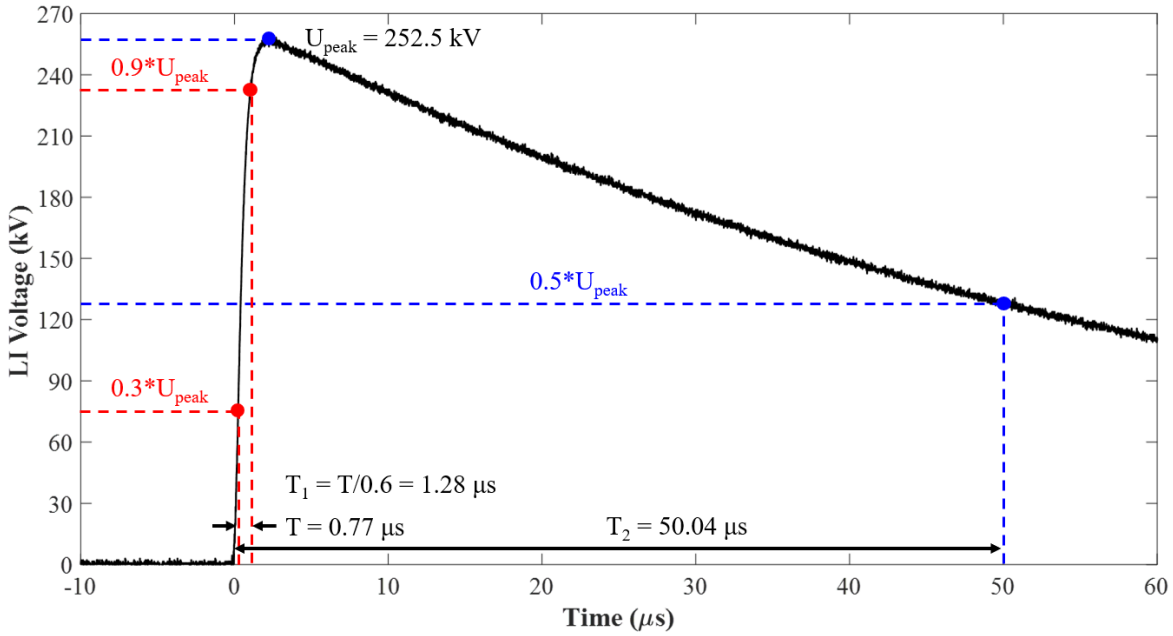

Figure 4-2. Measurement of a 252.2 kV LI withstand waveform with voltage and time parameters.

second stage transformer with a ratio of 1:1. With this generator, the first stage can produce 400 kV and the second stage can produce an additional 400 kV. Combined together, the High Volt AC generator has the capability of producing voltage up to 800 kV. The specific AC generator can provide a voltage stability of ±1% which satisfies the requirements of BS EN/IEC 60060-1:2010 standard.

Figure 4-3 shows the circuit diagram for the AC breakdown tests in this chapter using the High Volt AC generator. A capacitive voltage divider, C_{VD}, is connected in parallel to the two-stage cascade transformer configuration using a blocking impedance (B_i). The purpose of the impedance is to protect the sample being tested from damage that can occur due to high energy breakdowns. The generator is also equipped with an automatic post breakdown switch-off which preserves the electrode and the gas quality by protecting them from being exposed to continuous high voltage discharges. The control and measurement unit is connected to the AC generator and the capacitive voltage divider and can be used to control and record the AC_{RMS} input and output voltages respectively.

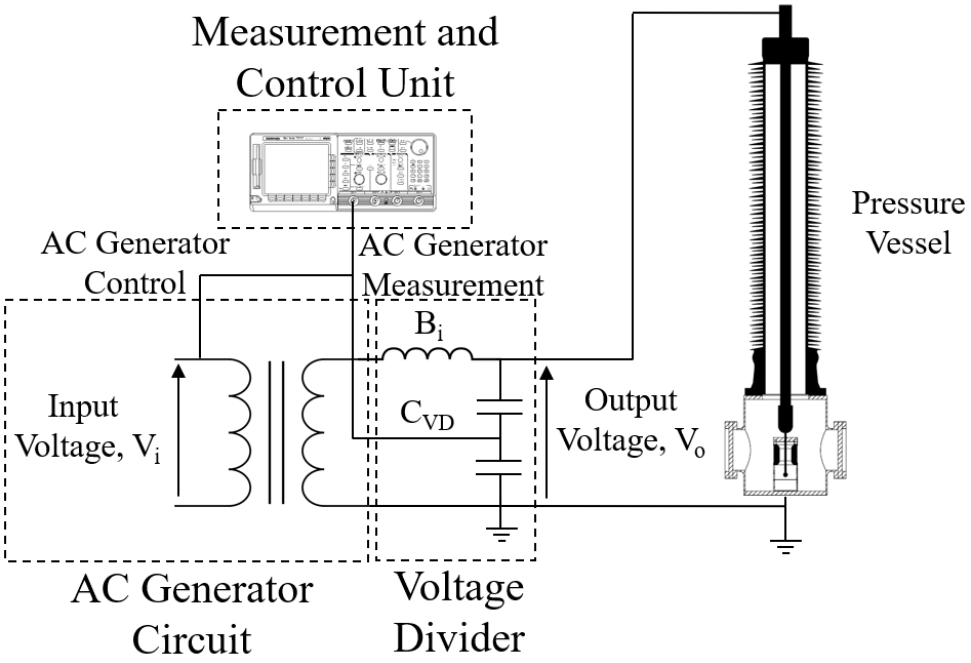

Figure 4-3. AC breakdown tests circuit diagram including the pressure vessel, voltage divider, AC generator and the measurement and control unit.

4.3 Experimental Techniques and Statistical Analysis

Two experimental techniques were carried out for the breakdown experiments. The up-and-down method was used for LI breakdown experiments and to obtain the 50% breakdown voltage, U_{50}. The progressive stress procedure was used for AC breakdown tests and to determine the average AC breakdown voltage. Both techniques were carried out and analysed in accordance to BS EN/IEC 60060-1:2010 [90] and 'Statistical Techniques for High-Voltage Engineering' [91].

4.3.1 Up-and-down Procedure for Lightning Impulse Breakdown Tests

The up-and-down procedure provides an accurate estimate for the U_{50} with reduced number of breakdowns and time requirements compared to other experimental techniques. This is important since it preserves the electrode surface roughness and the gas mixture quality by the end of a full set of experiments. This allows the user to have reliable and repeatable results when testing gas insulation materials without surface roughness and reduced quality of a gas mixture influencing the results. It is important to state that, for SF_6, the quality of the gas was reduced by less than 0.5% after approximately 150 breakdowns. Similarly, the

C_3F_7CN concentration in C_3F_7CN/CO_2 gas mixtures reduced by less than 0.5% for the same number of breakdowns. The $R_{average}$ of the electrode, regardless of the test gas, was only increased by approximately 0.4 μm. Both factors were changed marginally and no significant drop in breakdown performance was observed. Electrodes were changed and polished to the initial 0.6 μm, $R_{average}$, mirror finish after roughly 150 breakdowns in order to reduce the impact of increased conductor surface roughness on the breakdown results. Likewise, a new set of test gas was used after roughly 150 breakdowns.

Figure 4-4 shows a typical set of tests following the up-and-down procedure. For every test, a set of 30 impulses was applied with a time interval of 2 minutes in-between each impulse. Note that when a new electrode system was first setup, the breakdown voltage was observed to increase for the initial 15-20 breakdowns before the results became less dispersed. This is described as the conditioning effect [91] where residual particles can initiate a breakdowns at much lower voltages. These particles reduce in size with the increasing number of breakdowns and eventually have little effect on the breakdown voltage [91]. At this point, the up-and-down procedure can be used to determine the U_{50} of the gas. Note that the 15-20 initial breakdowns were also used to condition the electrode and establish the 3% step voltage level (ΔU) after every new setup. The conditioning effect was only observed for the first test after a test cell reassembly process. Similar effect was not observed when testing the same gas inside the test cell for subsequent experiments.

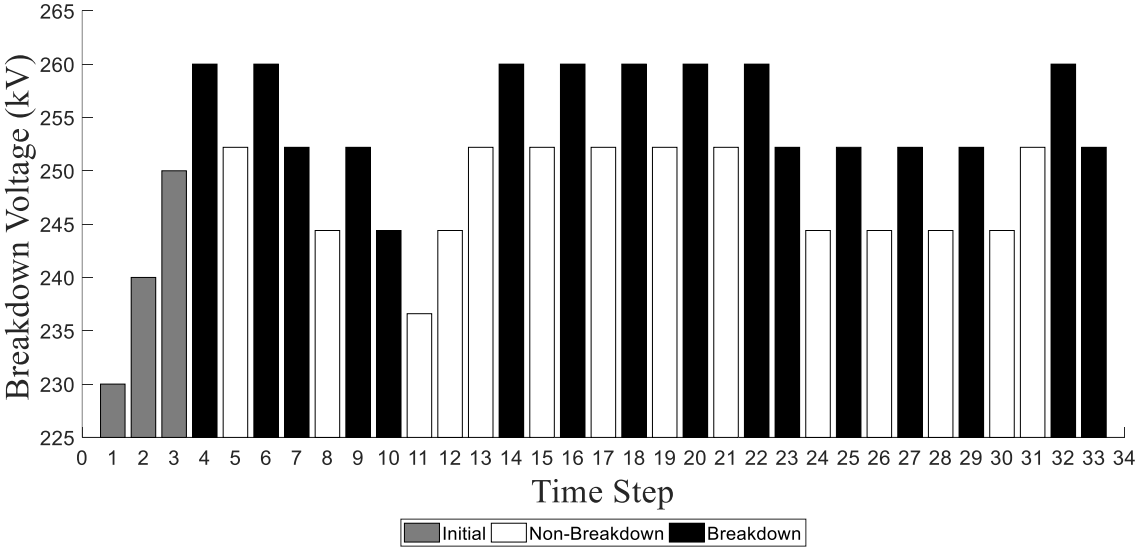

Figure 4-4. Example of an LI up-and-down procedure using 30 impulse shots.

The U_{50} and standard deviation (σ) can be calculated using equations (4-1) and (4-2) [27], [91]:

$$U_{50} = U_0 + \Delta U(\frac{A}{N} \pm \frac{1}{2}) \tag{4-1}$$

$$Standard\ Deviation, \sigma = 1.62 \cdot \Delta U(\frac{NB - A^2}{N^2} + 0.029) \tag{4-2}$$

where U_0 is the lowest breakdown voltage that occurred (or non-breakdown depending on which is the rarer), ΔU is the 3% step voltage and N is the number of rarer events. If the rarer events are breakdowns, the sign in equation (4-1) will be negative, or in the case of non-breakdowns the sign will be positive. The values of the constants N, A and B are determined using the following equations [27]:

$$N = \sum_{i=0}^{k} n_{iw} \ or \ \sum_{i=0}^{k} n_{ib} \tag{4-3}$$

$$A = \sum_{i=0}^{k} i n_{iw} \ or \ \sum_{i=0}^{k} i n_{ib} \tag{4-4}$$

$$B = \sum_{i=0}^{k} i^2 n_{iw} \ or \ \sum_{i=0}^{k} i^2 n_{ib} \tag{4-5}$$

where i is referring to the voltage level, n_{iw} to the number of non-breakdowns (chosen when non-breakdowns are the rarer event) and n_{ib} (chosen when breakdowns are the rarer event) to the number of breakdowns at that level.

4.3.2 Progressive Stress Procedure for AC Voltage Breakdown Tests

The progressive stress procedure was carried out for the AC breakdown tests in accordance to BS EN/IEC 60060-1:2010 [90]. This procedure always leads to a breakdown and the test voltage can be increased in steps or continuously with the latter selected for this project. For every test, a set 30 breakdowns was carried out. For every new set of tests, the first breakdown voltage was carried out by ramping up the voltage at a constant rate of 0.5 kV/s throughout the range in order to estimate the values where the breakdown will most likely occur. Following the first breakdown, to optimise the test time, the voltage was increased

with a rate of 5 kV/s up to 40% of the applied test voltage and the rest of the range was covered with a rate of 0.5 kV/s until breakdown. A 2-minute rest interval was applied from the instant of a breakdown to the next ramping of the AC voltage. Figure 4-5 shows an example of an AC breakdown test procedure using the progressive stress method and a set of 30 breakdowns.

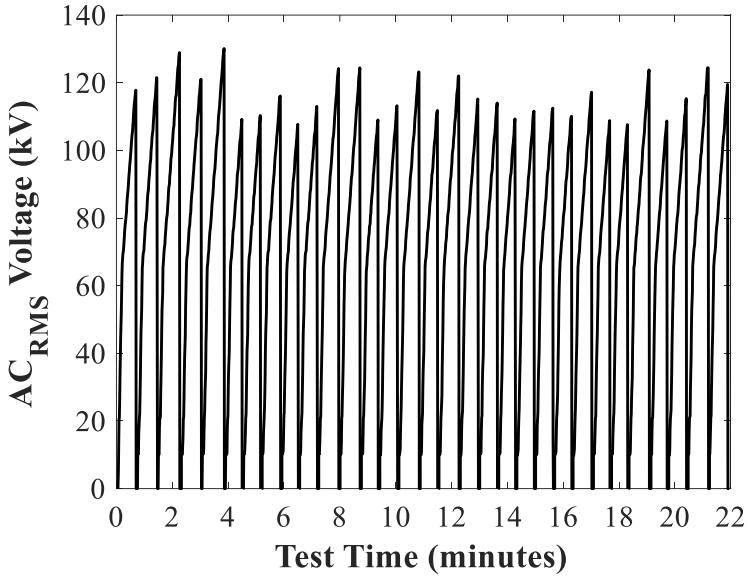

Figure 4-5. Example of an AC progressive stress test procedure using 30 breakdowns.

The results of the test in Figure 4-5 usually consist of a total number of breakdowns, *n*, and the voltages where those individual breakdowns occur, U_i. From these parameters, the values of average breakdown voltage, U_{avg}, and the standard deviation, σ, can be calculated. For a Gaussian (or Normal) distribution, U_{avg} can also be a good estimation for U_{50}. These parameters were calculated using the following equations [90]:

$$U_{avg} = U_{50} = \sum \frac{U_i}{n} \tag{4-6}$$

$$Standard\ Deviation, \sigma = \sqrt{\frac{\sum (U_i - U_{avg})^2}{n-1}} \tag{4-7}$$

4.3.3 Voltage-time Characteristics Analysis

Voltage-time (V-t) characteristic is an important property to assess the breakdown behaviour of insulating materials under different experimental conditions. The time parameter,

commonly given as time lag, in V-t characteristics is given by the time difference between the time of a voltage application to a gap, which is sufficient to cause a breakdown, and the time of breakdown. The voltage parameter is the value which the chop, point where the voltage rapidly collapses to zero during a breakdown, of the LI waveform occurs. Factors like the rate of rise of voltage and the field geometry are known to influence the V-t characteristics of an insulating material [27]. In this thesis, the V-t characteristics of SF_6 gas and C_3F_7CN/CO_2 gas mixtures were analysed for various experimental conditions such as pressure, LI polarity and gas type.

The V-t characteristics analysis was conducted with the guidance of BS EN/IEC 60060-1:2010. There are two kinds of breakdowns cases when using LI waveforms: (i) breakdown at the front with a time lag of less than ≈1.2 μs and (ii) breakdown at the tail with a time lag of more than ≈1.2 μs. Figure 4-6 shows an example of a breakdown at the front while Figure 4-7 shows the case of a breakdown at the tail. Depending on the case, V-t characteristics are analysed differently. A full guide on the analysis of the two cases can be found in BS EN/IEC 60060-1:2010 [90]. The key analysis parameters are shown in Figures 4-6 and 4-7. These parameters are the 10%, 30%, 70% and 90% values of the curve. In the case of a front breakdown, all the aforementioned percentage values are calculated from the U_{peak} of the waveform. For the tail breakdown, the 30% and 90% values are calculated from the U_{peak} while the 10% and 70% values are calculated from the chopping voltage, U_C.

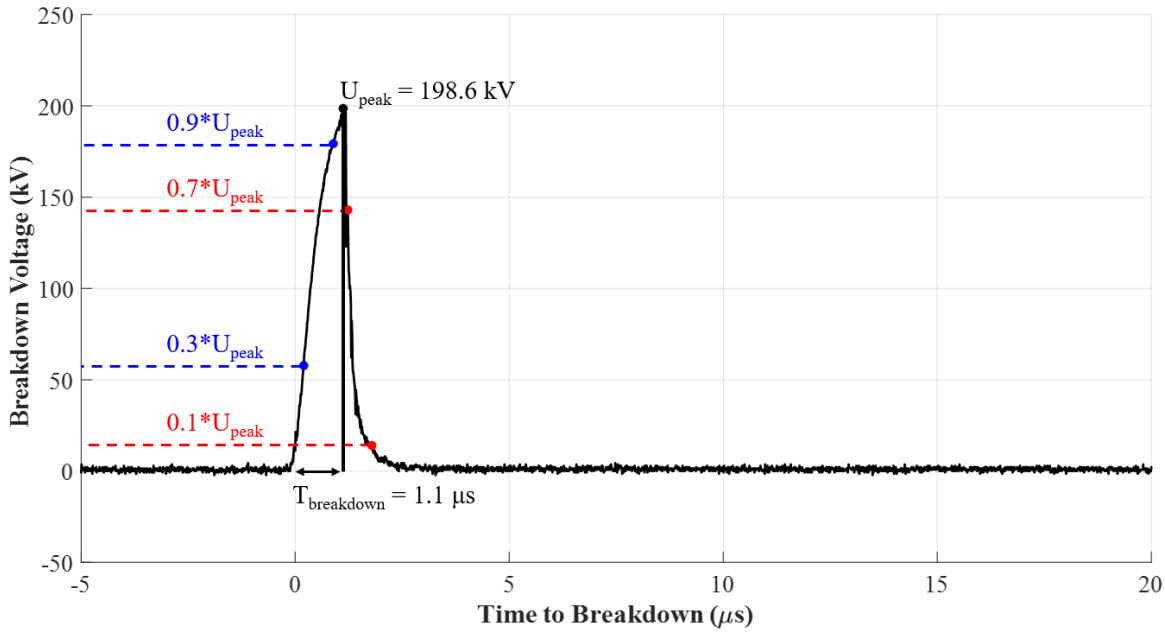

Figure 4-6. Example of a LI breakdown voltage where the chop occurred at the front of the waveform.

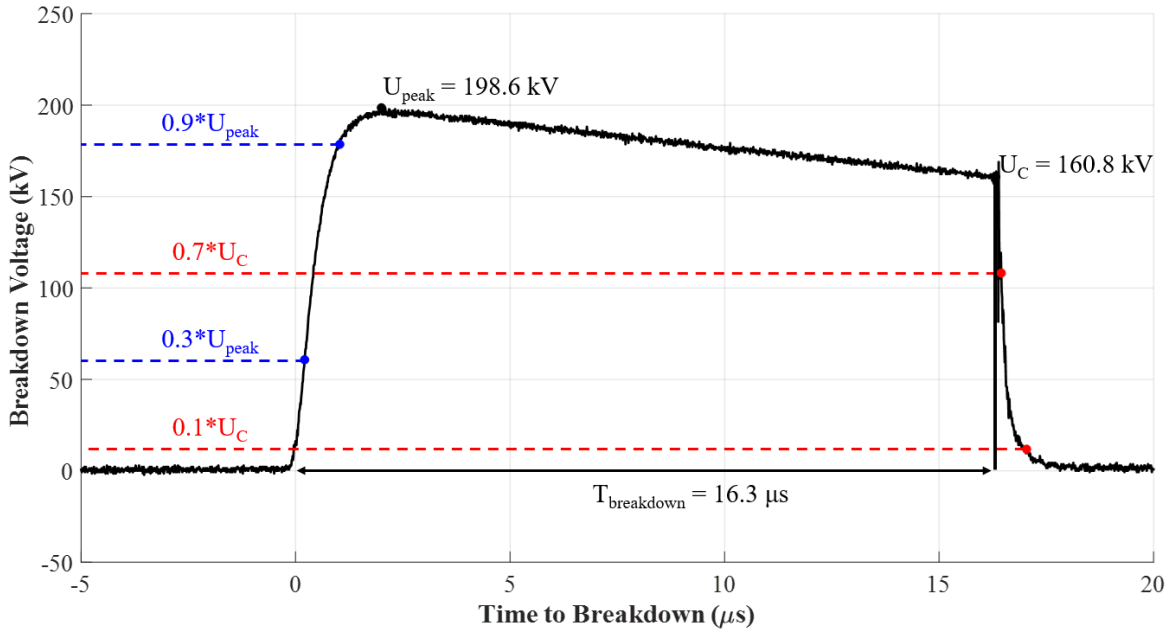

Figure 4-7. Example of a LI breakdown voltage where the chop occurred at the tail of the waveform.

A Matlab code was developed to acquire the V-t characteristics and plot them for SF_6 and the C_3F_7CN/CO_2 gas mixtures.

4.4 Breakdown Characteristics of the 10/30 mm Coaxial Configuration

This section describes the results acquired from the 10/30 mm coaxial configuration. The relation of U_{50} and pressure was plotted for different voltage waveforms, LI polarities and C_3F_7CN/CO_2 mixtures. For these tests, the main focus is on two mixtures: 16% C_3F_7CN / 84% CO_2 and 20% C_3F_7CN / 80% CO_2. As mentioned earlier, a 20/80% mixture was chosen because it was reported to have an equivalent dielectric strength to SF_6. The 16/84% mixture was chosen since the reduction in C_3F_7CN ratio can lower the liquefaction temperature by approximately 5°C. The operating pressure of GIL/GIB practical equipment used in the UK power network is 4.5 bar (abs) and the liquefaction temperatures for both C_3F_7CN mixtures and SF_6 at pressures of 1 to 4.5 bar (abs) are shown in Table 4-1.

Table 4-1. Liquefaction point for 16% and 20% C_3F_7CN Gas Mixtures and SF_6 for 1-4.5 bar (abs).

Gas / Gas Mixture	Liquefaction Temperature (°C)			
	1 bar	2 bar	3 bar	4.5 bar
20% C_3F_7CN / 80% CO_2	-42.0	-28.6	-19.8	-10.1
16% C_3F_7CN / 84% CO_2	-45.9	-33.2	-24.8	-15.6
SF_6 [52]	-63.8	-49.4	-40.8	-32.2

4.4.1 Effect of C_3F_7CN Content and Pressure

In figures 4-8 and 4-9, the U_{50} and the standard deviations, as error bars, are given against pressure for a direct comparison between the two C_3F_7CN/CO_2 gas mixtures and 100% SF_6. Figure 4-8 compares the breakdown performance of SF_6 to the gas mixtures with 16% and 20% C_3F_7CN concentrations under positive LI. The breakdown voltage of 100% SF_6 and the 20% C_3F_7CN / 80% CO_2 mixture increases almost linearly with pressure in the investigated range. However, the 16% C_3F_7CN / 84% CO_2 gas mixture increases linearly up to 3 bar (abs) and then shows signs of saturation towards 4.5 bar (abs).

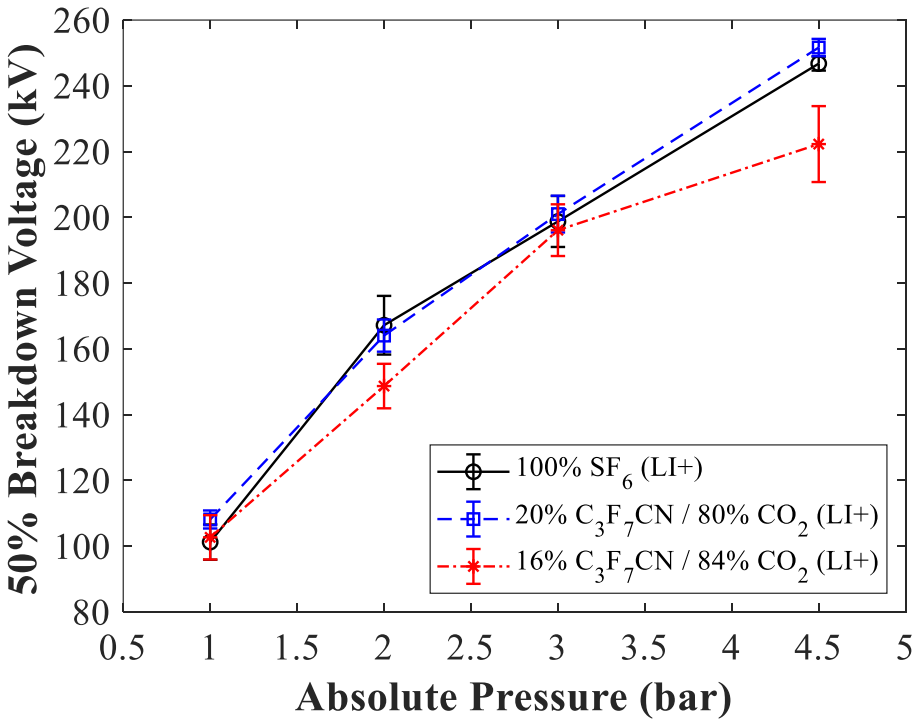

Figure 4-8. U_{50} as a function of absolute pressure for the reduced-scale coaxial prototype of 10 mm conductor and 30 mm inner enclosure diameters using SF_6 and C_3F_7CN/CO_2 mixtures with 20% and 16% C_3F_7CN concentration under positive lightning impulse (LI+).

The non-linear increase of breakdown voltage at higher pressures was also observed in previous studies on other gases [52]. This trend could be due to the increased gas density at higher pressures, where density change will not make as much difference to the ionisation process as it did at lower pressures since the gas molecules are more densely populated.

In Figure 4-8, the breakdown characteristics of 100% SF_6 and the 20% C_3F_7CN / 80% CO_2 gas mixture under positive LI are almost identical to each other with the two curves overlapping. The 16% C_3F_7CN / 84% CO_2 has a slightly lower breakdown voltage than the other two gases and appear to saturate at a lower pressure. This is in good agreement with previous studies [4], [9] where it was stated that a C_3F_7CN/CO_2 gas mixture with a 18-20% C_3F_7CN concentration can have an equivalent dielectric strength to pure SF_6 under uniform electric fields. Figure 4-9 shows the breakdown characteristics of the same gases under negative LI. As with the positive LI, the breakdown characteristics of 100% SF_6 and the 20% C_3F_7CN / 80% CO_2 gas mixture are comparable under negative polarity. The mixture with 16% C_3F_7CN concentration has a slightly weaker breakdown performance than SF_6 and the mixture with 20% C_3F_7CN concentration.

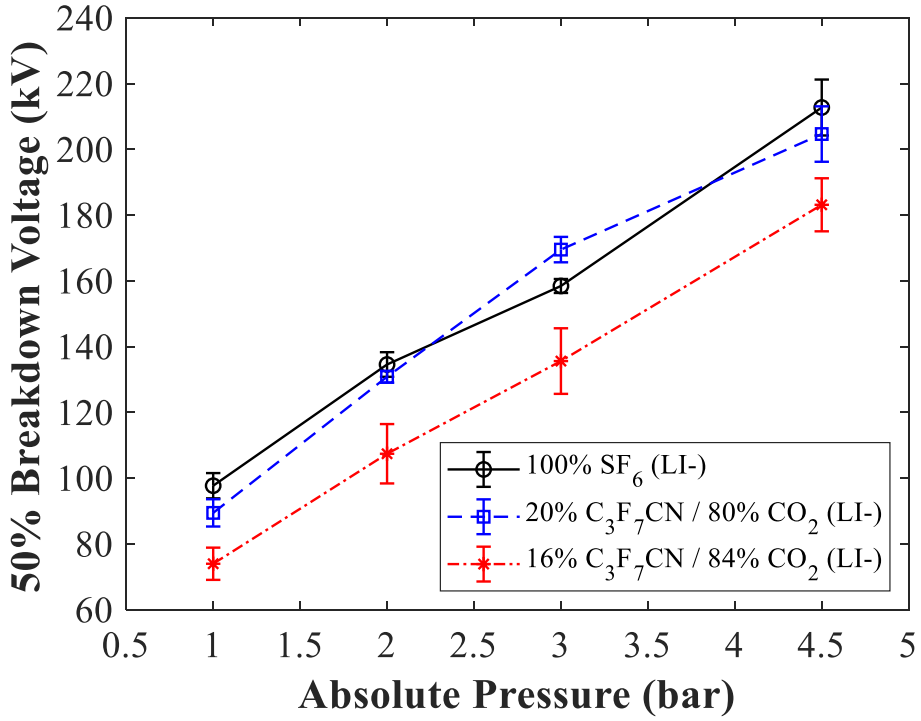

Figure 4-9. U_{50} as a function of absolute pressure for the reduced-scale coaxial prototype of 10 mm conductor and 30 mm inner enclosure diameters using SF_6 and C_3F_7CN/CO_2 mixtures with 20% and 16% C_3F_7CN concentration under negative lightning impulse (LI-).

Figure 4-10 compares the breakdown performance of the three candidates at 4.5 bar (abs). The 20% C_3F_7CN / 80% CO_2 gas mixture slightly outperforms SF_6 under positive polarity but SF_6 has a higher negative LI breakdown voltage. The 16% C_3F_7CN gas mixture demonstrates a comparatively lower breakdown performance than the other two gases at this pressure under both polarities.

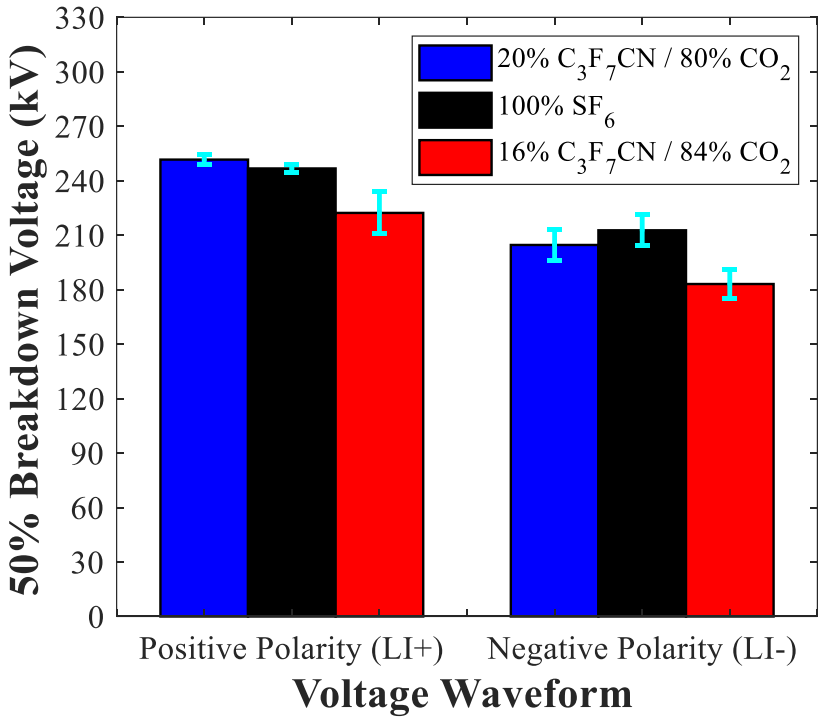

Figure 4-10. U_{50} for 100% SF_6, 20% C_3F_7CN / 80% CO_2 and 16% C_3F_7CN / 84% CO_2 for the reduced-scale coaxial prototype of 10 mm conductor and 30 mm inner enclosure diameters at 4.5 bar (abs).

4.4.2 Effect of Voltage Waveform

Figures 4-11 and 4-12 show that, regardless of the gas being used, the negative polarity LI breakdown voltages tend to be lower than the positive polarity in coaxial configurations. This agrees with the previous study [52]. With the conductor being negatively charged, it can be considered as an additional source of electrons which results in an electron avalanche initiated at a lower electric field. In the case of a positively charged conductor, an electron is initiated from detachment from a negative ion or ionising a neutral molecule which may require a higher electric field. This is an indication that gas insulated busbars have a higher failure probability under a negative LI as opposed to a positive LI. This highlights the importance of the 20% C_3F_7CN / 80% CO_2 gas mixture having the same breakdown performance with 100% SF_6 under both LI polarities as shown in Figure 4-11.

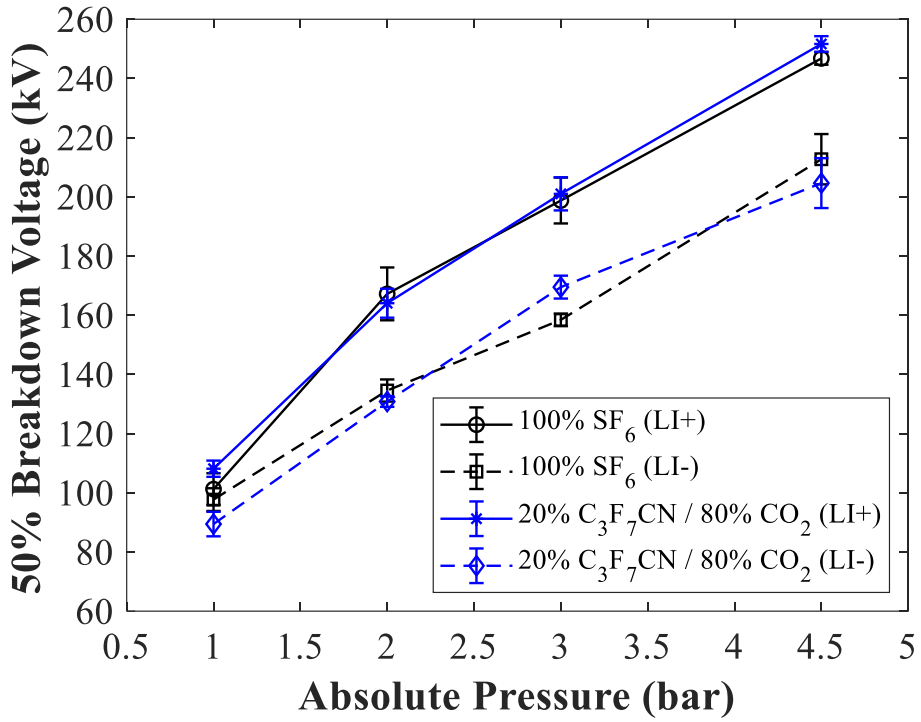

Figure 4-11. U_{50} as a function of absolute pressure for the reduced-scale coaxial prototype of 10 mm conductor and 30 mm inner enclosure diameters using SF_6 and 20% C_3F_7CN / 80% CO_2 gas mixture under lightning impulse of both polarities.

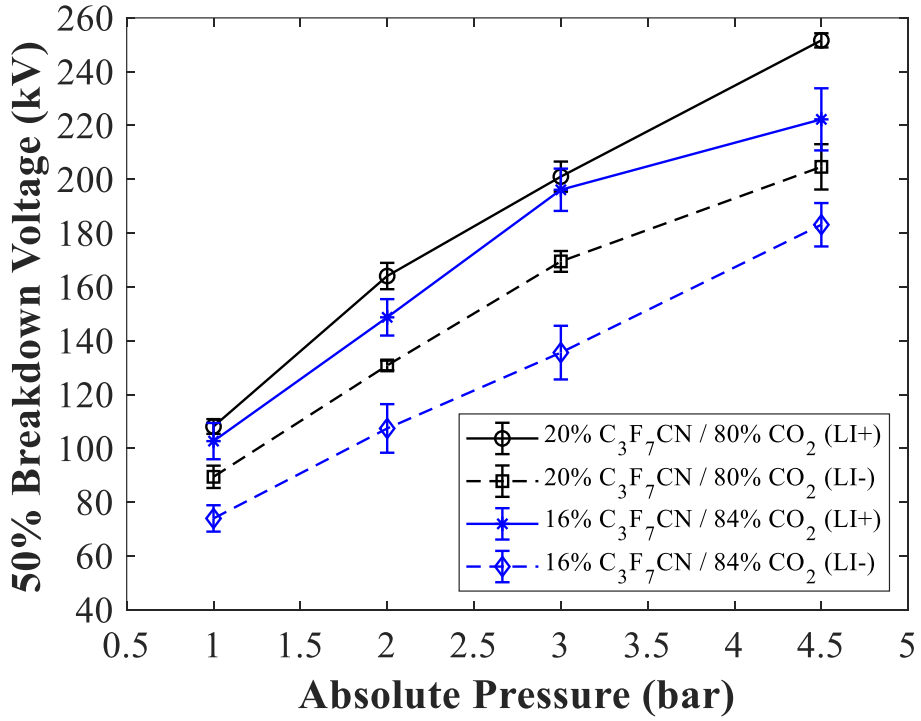

Figure 4-12. U_{50} as a function of absolute pressure for the reduced-scale coaxial prototype of 10 mm conductor and 30 mm inner enclosure diameters using 20% C_3F_7CN / 80% CO_2 and 16% C_3F_7CN / 84% CO_2 gas mixtures under lightning impulse of both polarities.

The breakdown characteristics of 100% SF_6 and the 20% C_3F_7CN / 80% CO_2 gas mixture were further investigated by applying AC waveform to the reduced-scale prototype coaxial configuration shown in Figure 4-13. The impulse to AC breakdown voltage ratio is approximately 2 which is similar to what has been found previously [52]. Like the LI breakdown characteristics, the mixture with 20% C_3F_7CN concentration demonstrates a comparable AC breakdown performance to pure SF_6. The AC breakdown voltage of both gases rises almost linearly with pressure. The largest difference in breakdown voltage between the two gases is at 4.5 bar (abs) where SF_6 is about 10 kV (9%) higher than the 20% C_3F_7CN / 80% CO_2 gas mixture.

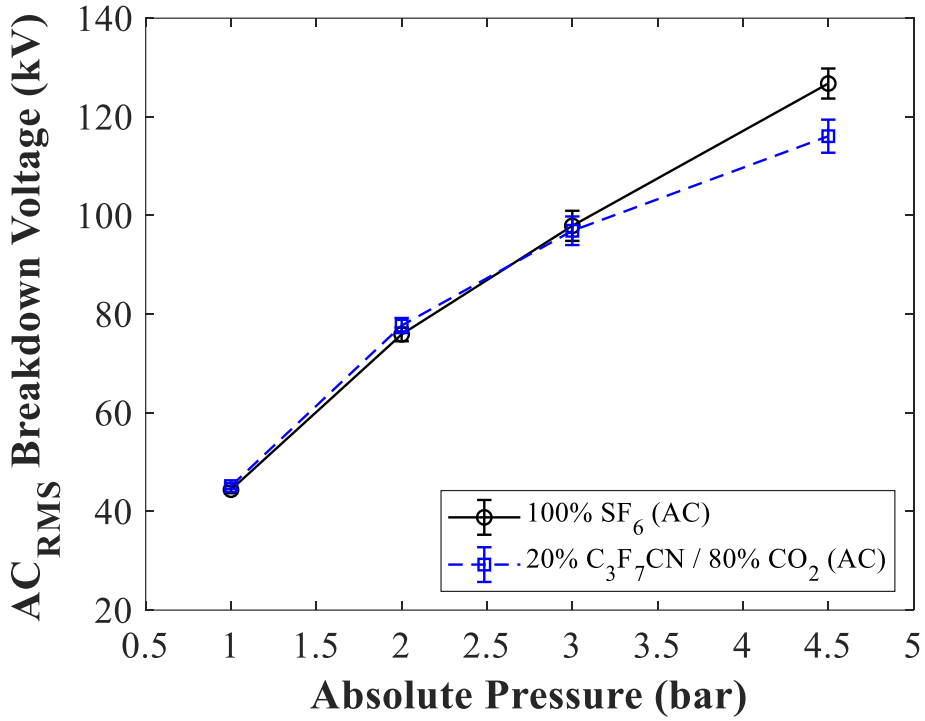

Figure 4-13. U_{avg} as a function of absolute pressure for the reduced-scale coaxial prototype of 10 mm conductor and 30 mm inner enclosure diameters using SF_6 and 20% C_3F_7CN / 80% CO_2 gas mixture under AC voltage.

4.4.3 V-t Characteristics

The V-t characteristics of the 10/30 mm coaxial prototype tested for SF_6, 20% C_3F_7CN / 80% CO_2 and 16% C_3F_7CN / 84% CO_2 gas mixtures are depicted in Figures 4-14, 4-15 and 4-16 respectively. All the figures plot the breakdown voltage against the time to breakdown (T_b) for different pressures and polarities. As was shown in Figures 4-6 and 4-7, the breakdown voltage is equal to U_{peak} in the case of a front breakdown and equal to U_C in the case of a tail breakdown. For all three figures, as anticipated, the average breakdown voltage

increases with pressure under any given polarity. As explained previously in this chapter, with increased pressure and density, a higher applied voltage is necessary to start the ionisation process and eventually cause a breakdown in the gas medium.

Figure 4-14 shows the V-t characteristics for SF_6 gas. The average T_b value is consistent under negative polarity with the majority of breakdowns occurring below 6 μs, regardless of the pressure being used. However, under positive polarity, the average T_b increases with pressure. As observed in Figure 4-14, at 4.5 bar (abs) all the breakdown events are located on the tail of the voltage waveform.

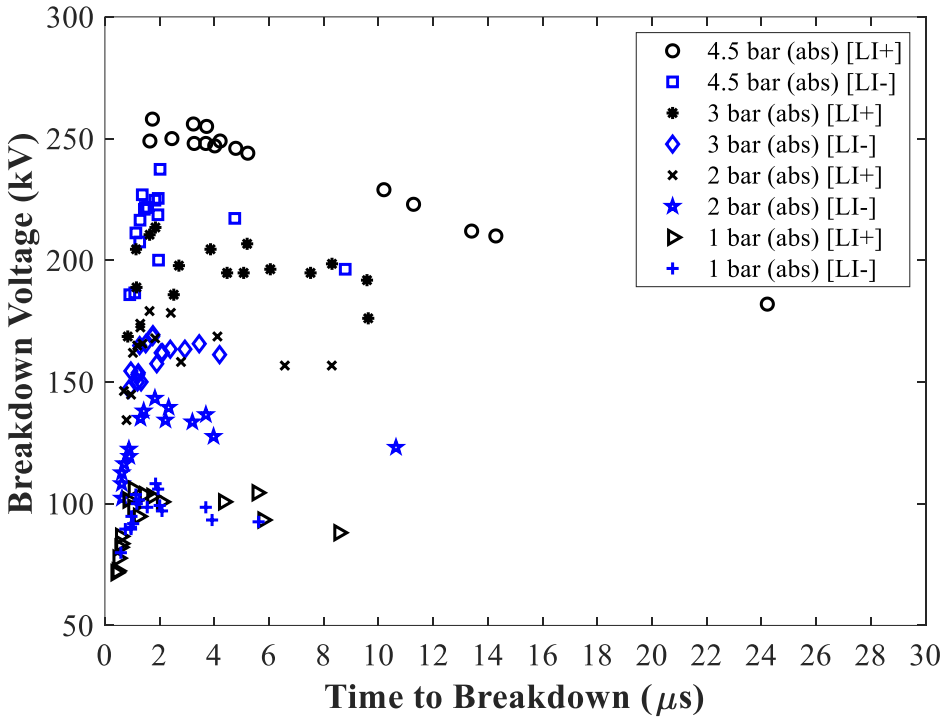

Figure 4-14. V-t characteristics for SF_6 from 1 to 4.5 bar (abs) pressure, tested on the reduced-scale coaxial prototype of 10 mm conductor and 30 mm inner enclosure diameters under both lightning impulse polarities.

Figures 4-15 and 4-16 show the V-t characteristics for the gas mixtures with 20% and 16% C_3F_7CN content respectively. For the 20% C_3F_7CN / 80% CO_2 gas mixture, the average T_b is shorter at 4.5 bar (abs) under both positive and negative polarities. The average T_b value from 1 to 3 bar (abs) is consistently longer than at 4.5 bar (abs), with pressure and polarity impacting it marginally. Under this range of pressures, a large number of breakdowns occurs after 4 μs which is contrary to 4.5 bar (abs) where most breakdowns occur before this time value.

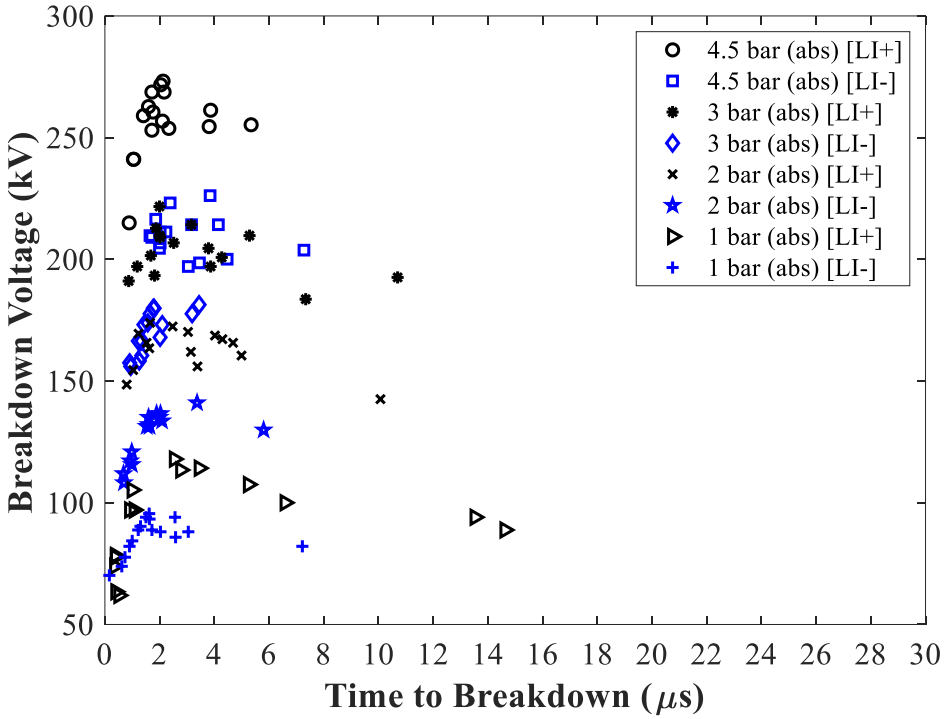

Figure 4-15. V-t characteristics for the 20% C_3F_7CN / 80% CO_2 gas mixture from 1 to 4.5 bar (abs) pressure, tested on the reduced-scale coaxial prototype of 10 mm conductor and 30 mm inner enclosure diameters under both lightning impulse polarities.

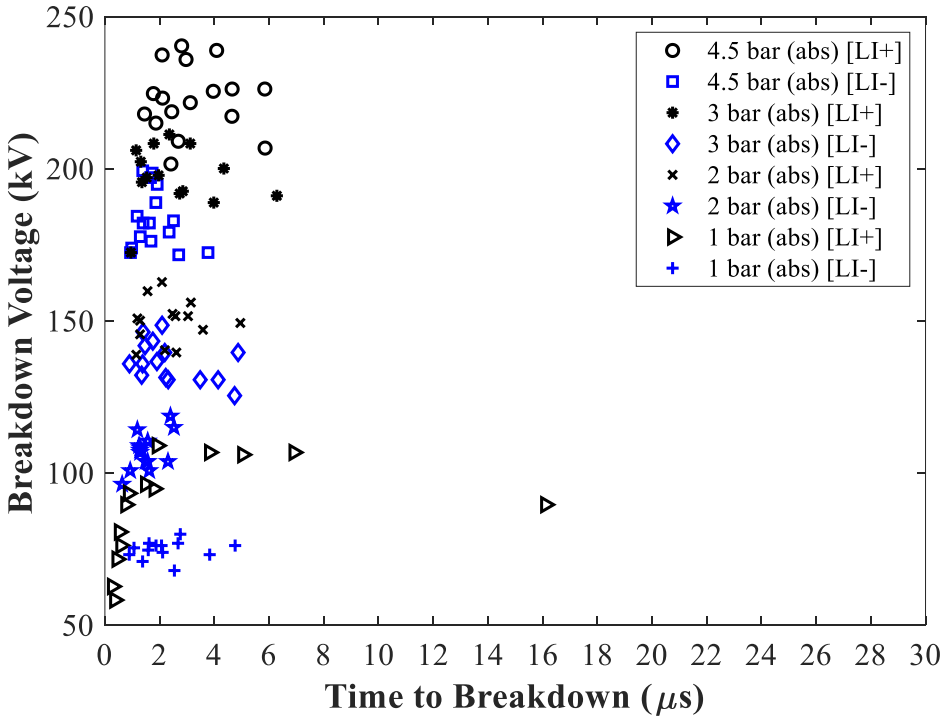

Figure 4-16. V-t characteristics for the 16% C_3F_7CN / 84% CO_2 gas mixture from 1 to 4.5 bar (abs) pressure, tested on the reduced-scale coaxial prototype of 10 mm conductor and 30 mm inner enclosure diameters under both lightning impulse polarities.

For the 16% C_3F_7CN / 84% CO_2 gas mixture, shown in Figure 4-16, polarity and pressure have shown to negligibly influence the T_b value. As shown in Figure 4-16, almost all breakdowns, with the exception of one, occur below 8 μs with the result of average T_b being similar at all pressures and both polarities.

Figures 4-17, 4-18 and 4-19 have been plotted to compare the frequency of breakdown events for all three gases based on their T_b values and impulse polarity. T_b is the sum of two components: statistical (T_s) and formative (T_f) time lags. T_s is defined as the time required for a primary electron to appear and initiate a critical avalanche. T_f is the time required for the critical avalanche to develop into a self-sustained breakdown which will bridge the gap of insulation. Numerous factors can affect these two parameters which in turn will result to different T_b values [27], [92].

For all three gases and under negative polarity, most of the breakdown events have shown to be concentrated below 8 μs. Most breakdowns occur below 2 μs indicating that the negative impulse polarity is predominated with front case breakdowns regardless of the gas medium being used. A negatively charged conductor, where electrons are readily available, could possibly result in the reduction of T_f. Electron production in the vicinity of the cathode can assist in faster development of a self-sustained breakdown process which will decrease T_f and in turn the overall T_b values for negative polarity LIs [92], [93].

For the positive polarity, a correlation between the type of gas medium and T_b values has been observed. For SF_6, which is a purely electronegative gas, breakdowns show to be more evenly distributed in relationship to the T_b values. Breakdown events occur mostly below 10 μs but there are also events exceeding this value and reach as high as approximately 25 μs. For the 20% C_3F_7CN / 80% CO_2 gas mixture, which is a mixture of strongly and weakly electronegative gases, the breakdown events have shown to occur mostly below 10 μs with very few exceptions exceeding this value. For the 16% C_3F_7CN / 84% CO_2 gas mixture, where there is a further reduction in the concentration of the strongly electronegative gas, the breakdown events are all concentrated below 8 μs with only one breakdown event exception exceeding the 10 μs threshold value.

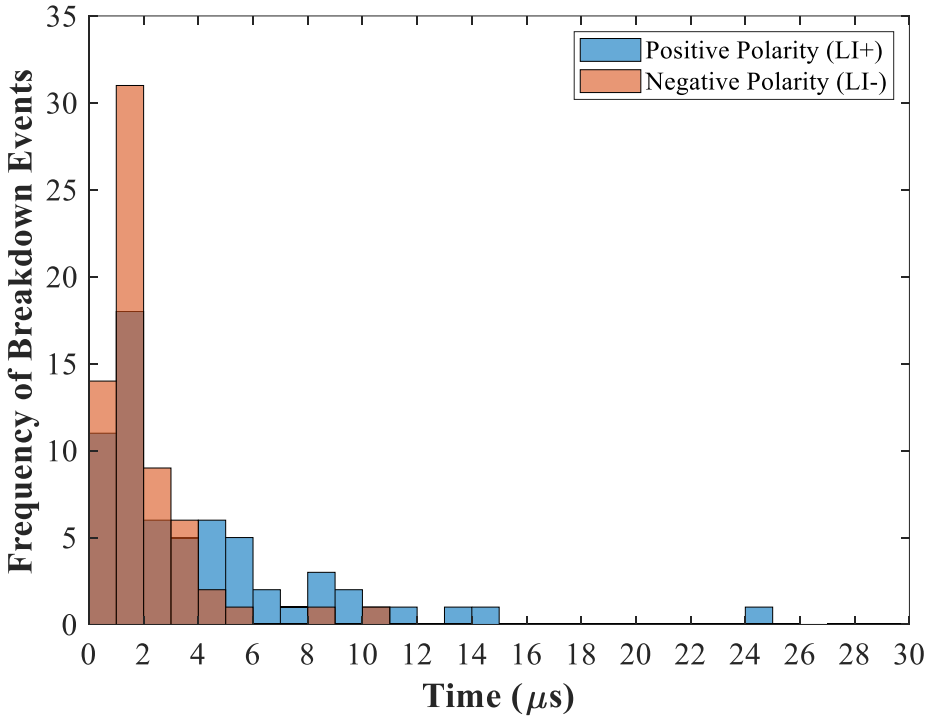

Figure 4-17. Frequency of breakdown events as a function of time for SF_6 gas tested in the reduced-scale prototype coaxial prototype of 10 mm conductor and 30 mm inner enclosure diameters under both lightning impulse polarities.

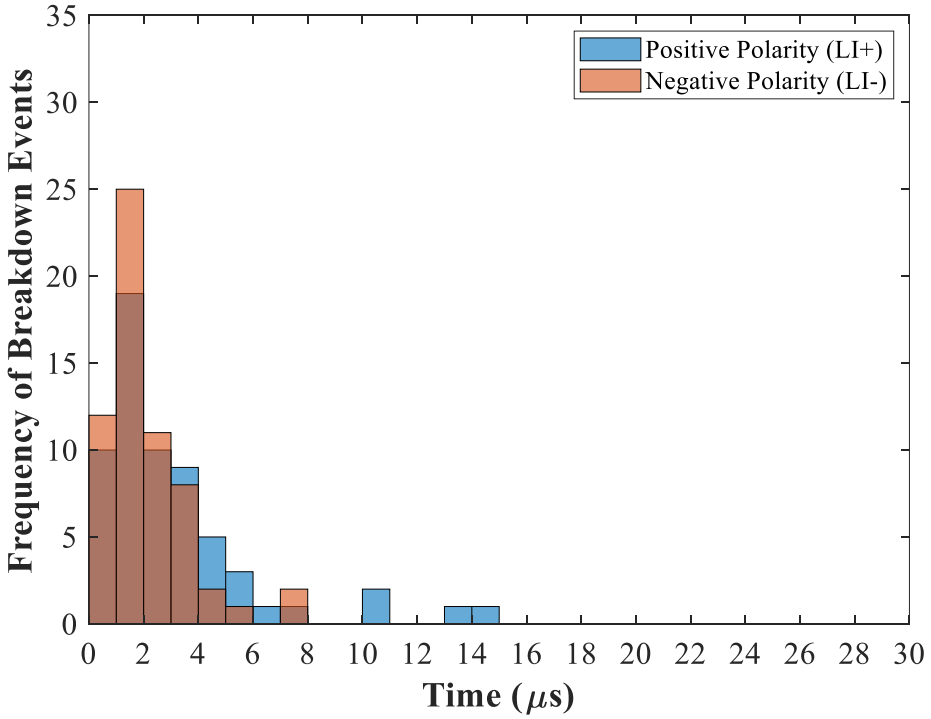

Figure 4-18. Frequency of breakdown events as a function of time for the 20% C_3F_7CN / 80% CO_2 gas mixture tested in the reduced-scale coaxial prototype of 10 mm conductor and 30 mm inner enclosure diameters under both lightning impulse polarities.

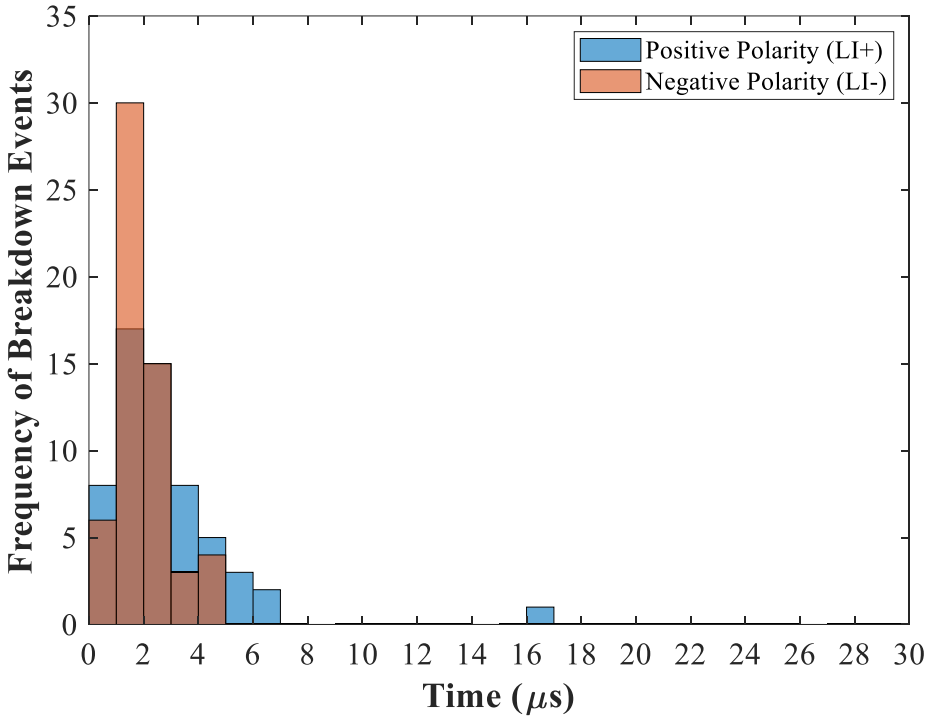

Figure 4-19. Frequency of breakdown events as a function of time for the 16% C_3F_7CN / 84% CO_2 gas mixture tested in the reduced-scale coaxial prototype of 10 mm conductor and 30 mm inner enclosure diameters under both lightning impulse polarities.

A general trend that can be derived from Figures 4-17, 4-18 and 4-19 is that, under positive polarity, T_b reduces with the electronegative gas concentration. SF_6, which is a purely electronegative gas, has a higher average T_b than the two C_3F_7CN/CO_2 gas mixtures. The addition of a weakly attaching gas, such as CO_2, in a gas mixture can potentially influence both the T_s and T_f values. Under a positive conductor, field emission primary free electrons could come from the detachment of a negative ion or the ionisation of a neutral molecule prior to the formation of electron avalanches. For a C_3F_7CN/CO_2 gas mixture, there is a higher probability to detach electrons from a CO_2 neutral molecule or a negative ion than with either C_3F_7CN or SF_6 which can lead to a faster initiation of a critical avalanche and in turn a reduction of the T_s value. As reported in [27], long and highly scattered T_b values have been found to occur in strongly electronegative gases. This could be affected by the complex nature of the breakdown development in highly electron attaching gases which could increase T_f and in turn the overall T_b values under positive LI polarity. Concluding, the heavily electronegative property of SF_6 gas could potentially lead to longer T_b times under positive polarities compared to C_3F_7CN/CO_2 gas mixtures.

4.4.4 Pressure-reduced Breakdown Field Strength

The pressure-reduced breakdown field strength $(E_b/p)_{max}$ is calculated using (4-8) by assuming that the breakdown field strength of the reduced-scale coaxial electrode is exceeded with the breakdown voltage value (U_b) where $U_b = U_{50}$:

$$(E_b/p)_{max} = \frac{U_b}{R_a \cdot \ln(\frac{R_b}{R_a}) \cdot p} \; (kV/mm) \tag{4-8}$$

Figures 4-20 and 4-21 show that $(E_b/p)_{max}$ reduces as pressure increases and, for the investigated range, the negative polarity values of both SF_6 and the C_3F_7CN/CO_2 gas mixtures fall slightly below the $(E/p)_{crit}$ value of SF_6 gas. The $(E/p)_{crit}$ value is where the attachment coefficient (η) of an electronegative gas is equal to the ionisation coefficient (α) [α=η] and discharge growth is not likely to occur at this value.

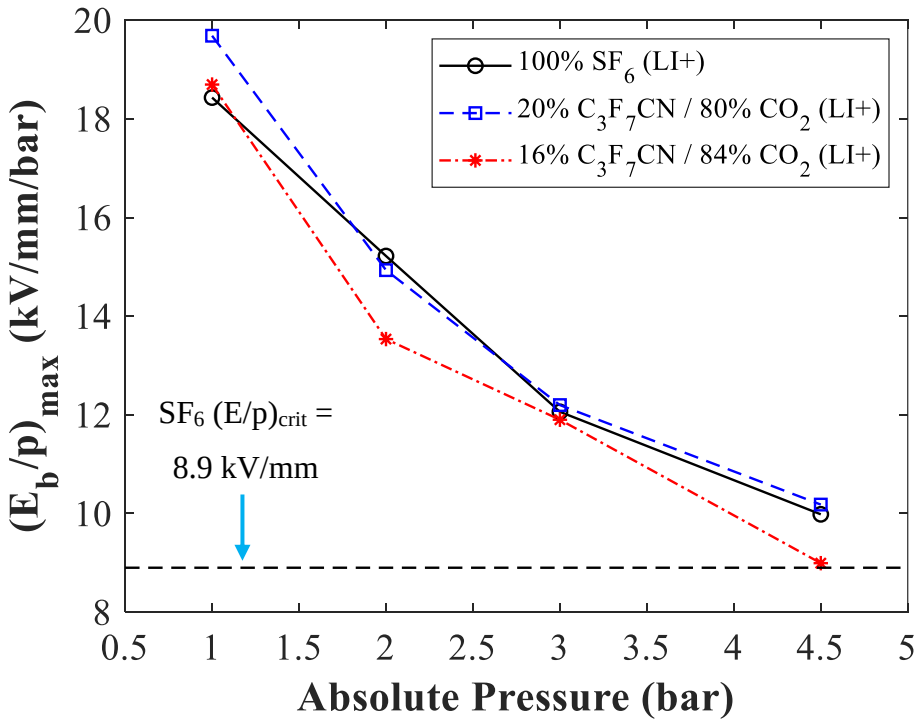

Figure 4-20. $(E_b/p)_{max}$ as a function of absolute pressure for the reduced-scale coaxial prototype of 10 mm conductor and 30 mm inner enclosure diameters using SF_6 and C_3F_7CN/CO_2 mixtures with 20% and 16% C_3F_7CN concentration under positive lightning impulse (LI+).

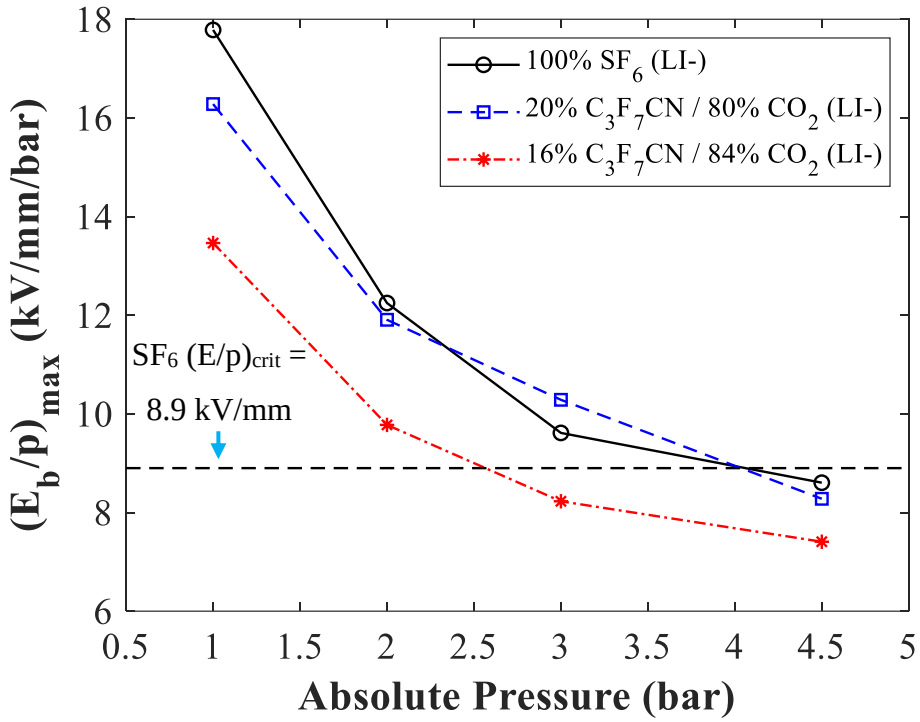

Figure 4-21. $(E_b/p)_{max}$ as a function of absolute pressure for the reduced-scale coaxial prototype of 10 mm conductor and 30 mm inner enclosure diameters using SF_6 and C_3F_7CN/CO_2 mixtures with 20% and 16% C_3F_7CN concentration under negative lightning impulse (LI-).

An electric field higher than this critical point [$E/p > (E/p)_{crit}$] brings an imbalance between α and η (α > η) which leads to cumulative ionisation and most likely a breakdown. In contrast, electric fields lower than this value [$E/p < (E/p)_{crit}$] are not likely to lead to a breakdown since attachment is greater than the ionisation coefficient (η > α). Figures 4-20 and 4-21 show that $(E_b/p)_{max}$ curve of the 20% C_3F_7CN / 80% CO_2 gas mixture behaves identically to pure SF_6 tested in the 10/30 mm coaxial configuration. The 16% C_3F_7CN / 84% CO_2 gas mixture is weaker when compared to the other two gases.

4.5 Breakdown Characteristics of Weakly Quasi-uniform Field Configurations

The results from the breakdown characteristics in Section 4.4 have demonstrated that the mixture of 20% C_3F_7CN / 80% CO_2 is a more technically viable alternative to SF_6 than the 16% C_3F_7CN / 84% CO_2 gas mixture. Therefore, the 20% C_3F_7CN content gas mixture was further investigated using the 8/60 mm coaxial and the hemispherical rod-plane coaxial configurations.

4.5.1 8/60 mm Coaxial Configuration – Effect of Gas Pressure and Impulse Polarity

Figure 4-22 portrays the U_{50} of SF_6 and the 20% C_3F_7CN / 80% CO_2 gas mixture as a function of pressure using the coaxial electrode configuration. The breakdown voltage increases with pressure for both SF_6 and 20% C_3F_7CN / 80% CO_2. These results agree with previous studies which showed a similar rate of change for breakdown voltage with pressure [9], [55].

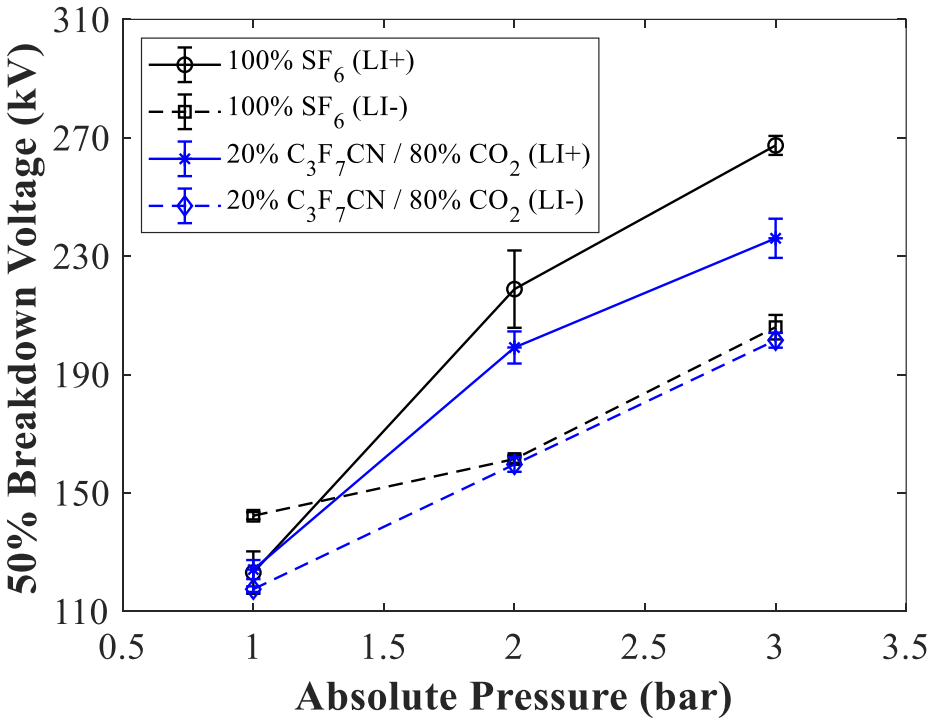

Figure 4-22. U_{50} as a function of absolute pressure for the coaxial configuration of 8 mm conductor and 60 mm inner enclosure diameters using SF_6 and 20% C_3F_7CN / 80% CO_2 gas mixture under lightning impulse of both polarities.

Figure 4-23 compares CO_2, SF_6 gases and 20% C_3F_7CN / 80% CO_2 mixture at 3 bar (abs) tested for the 8/60 mm coaxial configuration. The 20% C_3F_7CN / 80% CO_2 mixture has a comparable breakdown performance to SF_6 under negative polarity but lower breakdown voltage than SF_6 under positive polarity. As reported in [9], CO_2 as a weakly electron attaching gas has roughly half the breakdown voltage when compared to SF_6 and the 20% C_3F_7CN / 80% CO_2 mixture under the same experimental conditions. This demonstrates the improvement in breakdown voltage by using a 20% C_3F_7CN / 80% CO_2 mixture in comparison to pure CO_2 gas.

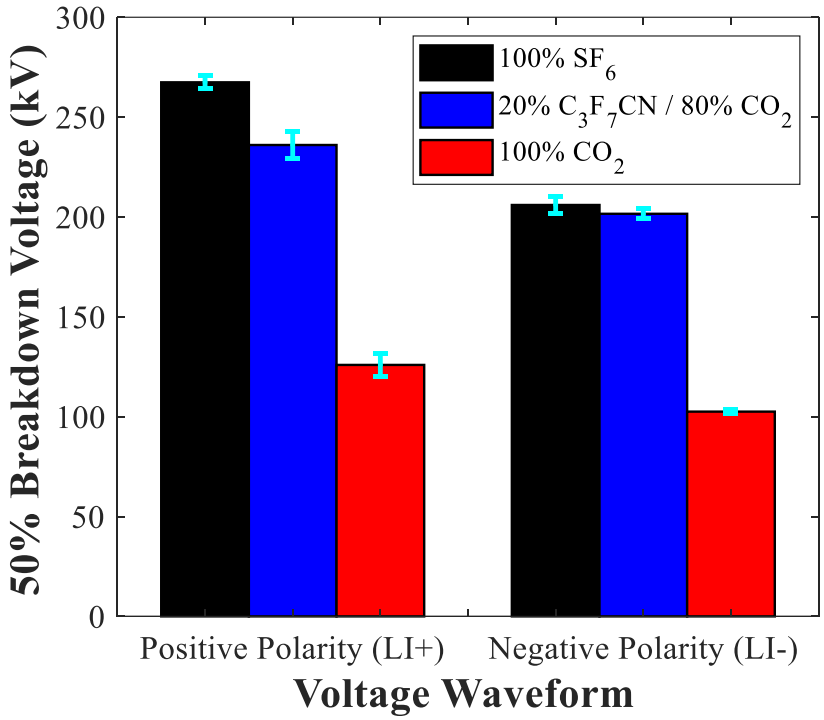

Figure 4-23. U_{50} for SF_6, CO_2 and 20% C_3F_7CN / 80% CO_2 gas mixture for the 8 mm conductor and 60 mm inner enclosure diameter coaxial electrode configuration at 3 bar (abs).

Figures 4-22 and 4-23 show that regardless of the gas medium, for coaxial configuration, the positive LI breakdown results were higher than the corresponding negative ones. At 1 bar (abs), both polarities of the 20% C_3F_7CN / 80% CO_2 mixture demonstrate a similar breakdown voltage with no prominent polarity effect.

The breakdown voltage of SF_6 under negative polarity at 1 bar (abs), displays a higher breakdown voltage than the positive ones. This is consistent with results reported in [94] where it was found that for a hemispherical rod-plane configuration of similar *f*, a 'polarity reversal' can occur at lower pressures with the negative breakdown voltage of SF_6 being higher than its positive breakdown voltage. As the pressure increases, the emission of electrons from the negatively charged conductor leads to an increased rate of ionisation, which resulted in the negative breakdown voltage to be lower than their positive counterpart. In the case of a positive conductor, electrons are initiated by detachment from a negative ion or ionising a neutral molecule, which requires a higher electric field.

4.5.2 Hemispherical Rod-plane Configuration – Effect of Gas Pressure, Gap Distance and Impulse Polarity

Figure 4-24 shows the effect of gap distance and impulse polarity on the U_{50} of SF_6 and 20% C_3F_7CN / 80% CO_2 mixture. The LI breakdown voltage increases significantly from 10 to 30 mm for both gases. However, the trend saturates slightly when the gap distance was further increased beyond 30 mm. This characteristic is observed for both gases and under both polarities. Figure 4-24 also shows that SF_6 has higher LI breakdown voltages than 20% C_3F_7CN / 80% CO_2 mixture under positive polarity. Contrastingly, negative LI breakdown results for both gases were nearly identical.

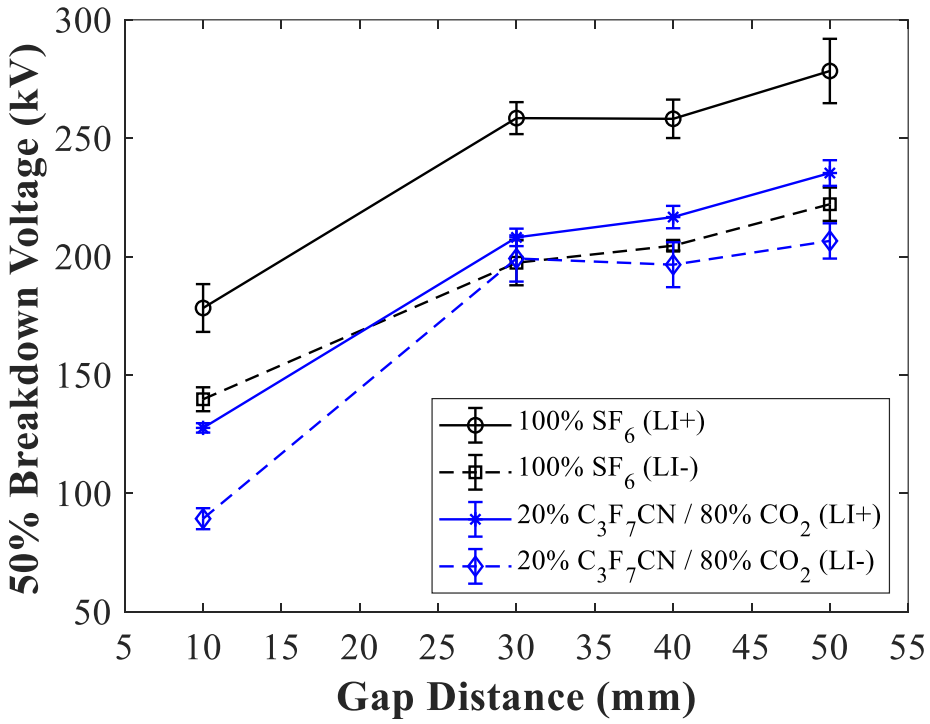

Figure 4-24. U_{50} as a function of gap distance for the hemispherical rod-plane configuration using SF_6 and 20% C_3F_7CN / 80% CO_2 gas mixture under lightning impulse of both polarities.

The difference in positive LI breakdown results can be attributed to the breakdown mechanism. For a positively charged hemispherical rod, free electrons come from the detachment of a negative ion or the ionisation of a neutral molecule prior to the formation of electron avalanches. For a 20% C_3F_7CN / 80% CO_2 gas mixture, there is a higher probability to detach electrons from a CO_2 neutral molecule or a negative ion, being a weakly electronegative gas, than with either C_3F_7CN or SF_6. Hence, a lower applied field is potentially required to initiate the avalanche formation.

In the case of a negative polarity, a large number of electrons can be emitted from the cathode which can initiate an electron avalanche process more readily under a lower applied field. Additionally, secondary processes such as photoemission or positive ion bombardment can further assist in making the electron avalanche process self-sustained and in turn result to a breakdown. These processes have led to the lower negative LI voltages than their positive counterpart. This also results in SF_6 and 20% C_3F_7CN / 80% CO_2 mixture having similar breakdown performance under negative LI.

Note that, even though the *f* factor decreases from 0.66 (10 mm gap) to 0.28 (50 mm gap) which makes the field more non-uniform, there is no evident change in the difference between positive and negative LI breakdown voltage for both SF_6 and 20% C_3F_7CN / 80% CO_2. The positive breakdown results were consistently higher than the negative results within the range of gap spacing tested. This can occur since the *f* range of 0.28-0.66 may be considered within the same category of weakly quasi-uniform field. Results in [58] have shown that for the same electrode configuration, but for hemispherically capped rods with smaller diameters (3.16 mm and 6.3 mm), the negative breakdown results were higher than the positive, which is different to the results shown in Figure 4-24. This indicates that with increasing diameter of the high voltage rod, thereby increasing the *f*, a reversed polarity effect on the breakdown voltage can be attained. The polarity effect on breakdown voltage is heavily dependent on *f*, which can be varied by other design parameters such as the rod diameter for the same electrode configuration.

Figure 4-24 also shows that SF_6 demonstrates a significantly better breakdown performance under positive polarity, whilst the 20% C_3F_7CN / 80% CO_2 mixture shows that the difference between positive and negative breakdown voltages is not as prominent as in SF_6 under weakly quasi-uniform fields. As shown in Figure 4-23, this could be attributed to the fact that the 20% C_3F_7CN / 80% CO_2 gas mixture behaves very similarly to CO_2 gas under the specific electric field uniformity range, with small difference in the positive and negative breakdown voltages. Therefore, the difference of polarity behaviour between SF_6 and the 20% C_3F_7CN / 80% CO_2 gas mixture can occur due to the high concentration of CO_2 (a weakly attaching gas) used. Importantly, this establishes that the polarity effect does not only depend on the field utilization factor but also on the insulating gas medium used.

Figure 4-25 shows the U_{50} as a function of pressure for SF_6 and 20% C_3F_7CN / 80% CO_2 mixture. LI breakdown voltage increases almost linearly with pressure except that the 20% C_3F_7CN / 80% CO_2 mixture shows a slight saturation from 2 to 3 bar, under positive polarity. As with the gap distance, SF_6 performs better than the 20% C_3F_7CN / 80% CO_2 gas mixture under positive polarity but the breakdown voltages of the two gases are more comparable under negative polarity. The polarity effect can also be seen in Figure 4-25 where the positive breakdown voltages are higher than the negative ones.

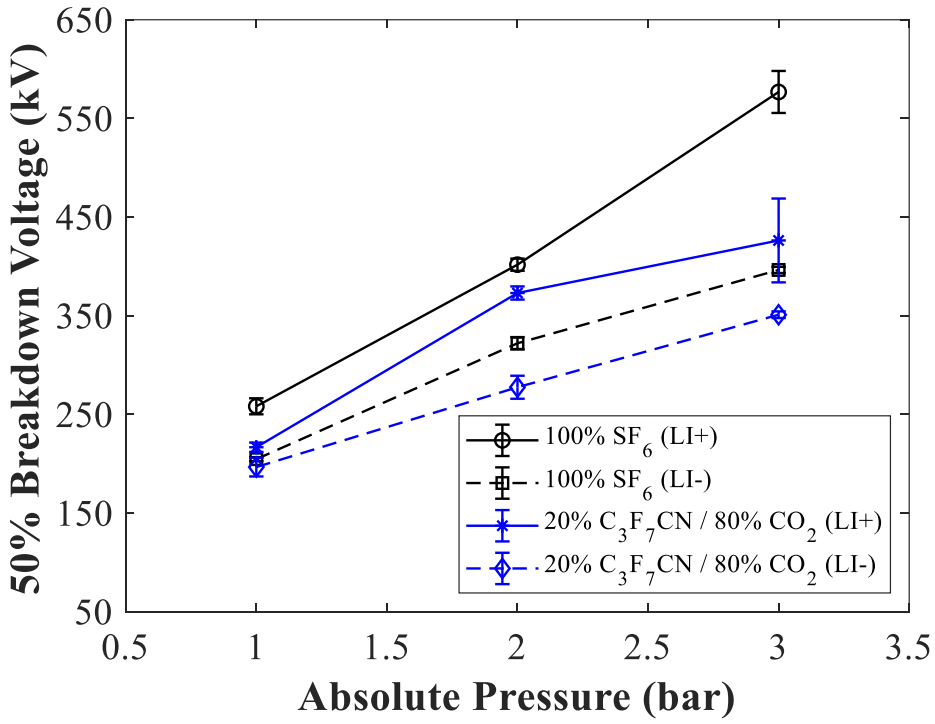

Figure 4-25. U_{50} as a function of absolute pressure for the hemispherical rod-plane configuration using SF_6 and 20% C_3F_7CN / 80% CO_2 gas mixture under lightning impulse of both polarities.

Figure 4-26 depicts the correlation between U_{50} and the pressure spacing product for SF_6 and 20% C_3F_7CN / 80% CO_2 gas mixture using the hemispherical rod-plane electrode configuration. This figure contains all of the presented hemispherical rod-plane breakdown data in this section. Figures 4-24 to 4-26 show that the rate of change for U_{50} with increasing pressure is much higher than the case for U_{50} with widening gap spacing.

For the range exceeding 50 bar·mm, a clear increase of breakdown voltage is seen for both gas candidates and under both polarities. In the case of a fixed gap and increasing pressure, the higher pressure-spacing values lead to increase in gas density and a reduced mean free path, which is in agreement with the Paschen's Law. Therefore, electrons undergo more

frequent collisions at shorter distance with the densely packed neutral gas molecules and are unable to attain sufficient energy to ionise the gas. A higher applied voltage is therefore required to start a self-sustained ionisation process and subsequently result to a higher breakdown voltage at higher pressure spacing values.

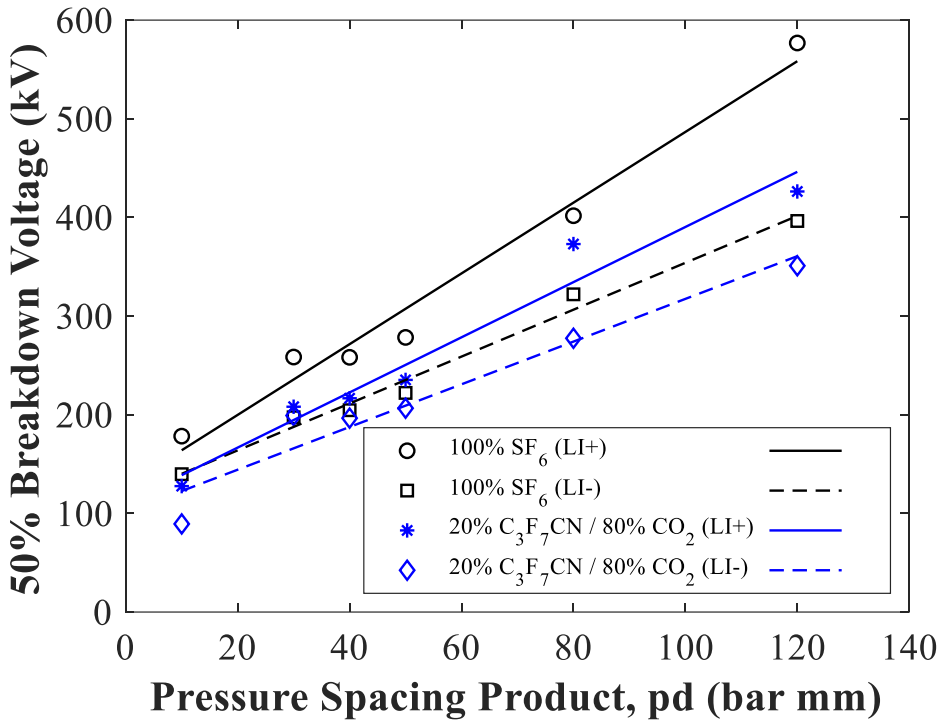

Figure 4-26. U_{50} as a function of pressure spacing product comparing SF_6 and 20% C_3F_7CN / 80% CO_2 gases for the hemispherical rod-plane electrode configuration.

4.5.3 Polarity Effect for 8/60 mm Coaxial and Hemispherical Rod-plane Electrode Configurations

Figures 4-27 and 4-28 compare the breakdown characteristics of SF_6 and 20% C_3F_7CN / 80% CO_2 mixture under different electrode geometries of similar f value. Figure 4-27 compares the characteristics of SF_6 gas under the hemispherical rod-plane and the 8/60 mm coaxial electrode configurations. The rod-plane electrode configuration shows that positive LI breakdown is higher than the negative LI breakdown over the pressure range investigated. In [58], hemispherical rod-plane configurations with smaller diameter rods (3.16 mm and 6.3 mm diameter) show that the negative LI breakdowns were consistently higher than the positive for LI breakdown results. This indicates that the size of the hemispherical rod electrode can make a significant difference to the polarity effect as it can change the electric

field from extremely to weakly quasi-uniform. The coaxial configuration could undergo a 'polarity reversal' effect around 1 bar (abs) where negative LI marginally exceeds the positive LI. Similar trend was also reported in [52] for coaxial configurations tested at lower pressures, where the positive LI breakdowns are almost identical to the negative LI breakdown results. As the pressure increases, the positive LI breakdown voltages are consistently higher than the negative LI.

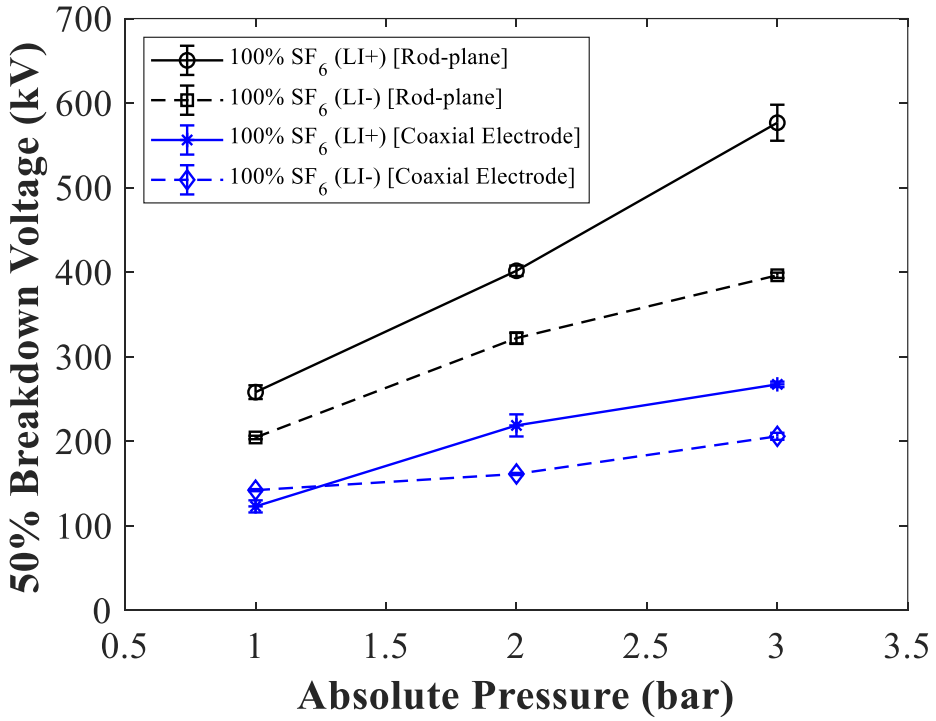

Figure 4-27. U_{50} as a function of absolute pressure comparing the 8/60 mm coaxial and hemispherical rod-plane electrode configurations under positive and negative lightning impulses tested using SF_6.

Figure 4-28 compares the characteristics of 20% C_3F_7CN / 80% CO_2 mixture under the hemispherical rod-plane and the 8/60 mm coaxial electrode configurations. The C_3F_7CN/CO_2 gas mixture behaves similarly to SF_6 where for both electrode configurations the positive LI breakdown is at higher voltages than the corresponding negative LI at higher pressures. However, at 1 bar (abs), the polarity effect becomes less evident. This shows that pressure has a significant impact on the polarity effect of both gases since it reduces considerably at lower pressures. The C_3F_7CN/CO_2 gas mixture also shows a smaller difference between positive and negative LI breakdown voltages than SF_6, which suggests that the use of a non-attaching gas like CO_2 can also make a difference on the polarity effect.

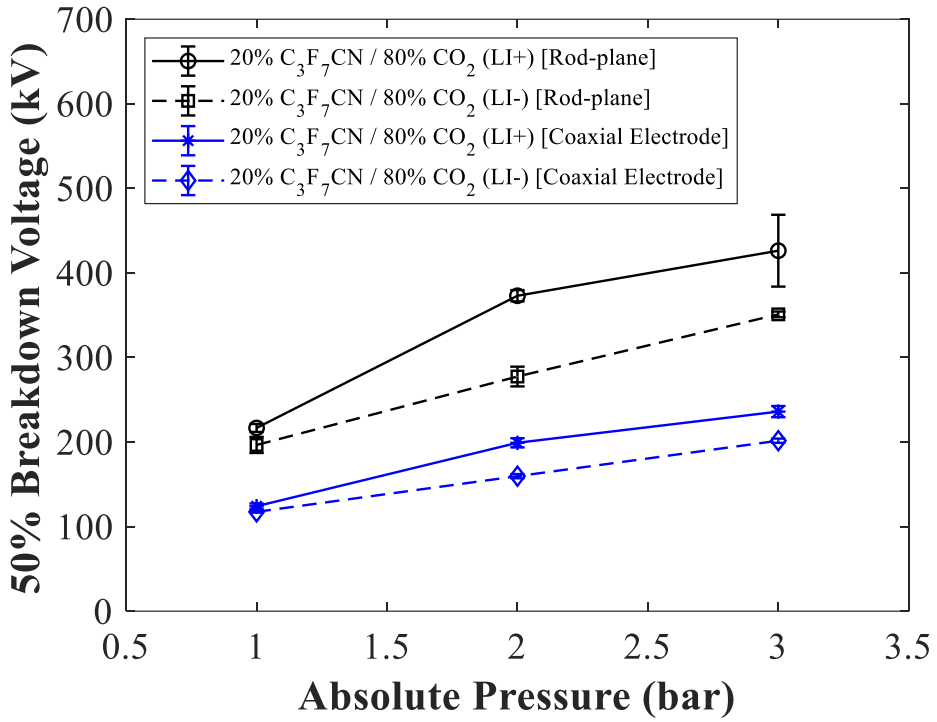

Figure 4-28. U_{50} as a function of absolute pressure comparing the 8/60 mm coaxial and hemispherical rod-plane electrode configurations under positive and negative lightning impulses tested using 20% C_3F_7CN / 80% CO_2 gas mixture.

4.5.4 Pressure-reduced Breakdown Field Strength

Figure 4-29 plots the pressure reduced breakdown field strength, $(E_b/p)_{max}$, of the coaxial electrode configuration with increasing pressure. The $(E_b/p)_{max}$ is calculated using equation (4-8). The figure illustrates that $(E_b/p)_{max}$ reduces with increasing pressure. For a positive conductor, a higher applied electric field is required to start an electron avalanche and the values of $(E_b/p)_{max}$ lie above the $(E/p)_{crit}$ of SF_6 gas for the investigated pressure range.

Results under negative polarity for both SF_6 and the 20% C_3F_7CN / 80% CO_2 mixture demonstrate an equivalent performance throughout the investigate pressure range and at 3 bar (abs) both curves fall slightly below the critical electric field $(E/p)_{crit}$ of SF_6 gas. As described previously in this chapter, no breakdown should occur at an electric field value below the $(E/p)_{crit}$ as the attachment coefficient exceeds the ionisation coefficient of the gas. However, for negative polarity, the cathode provides an additional source of electrons which leads to a greater ionisation process than the attachment ($\alpha > \eta$). At higher pressures, the $(E_b/p)_{max}$ obtained through experiments can also fall below the $(E/p)_{crit}$ of the gas medium. Therefore, it is important to

design the gas insulated equipment at its rated pressure to have a working stress well below the $(E/p)_{crit}$ of the chosen gas medium to avoid insulation failure. For gas insulated lines and busbars of coaxial geometries, the equipment insulation level must be designed to withstand the lower negative LI voltage. As shown throughout this chapter, the negative polarity breakdown voltages are consistently lower than the positive ones. Therefore, it can be concluded that the negative polarity for GIL/GIB representative electric fields is the most critical since it has the highest probability of causing a breakdown. From these observations, it is of significant importance that the 20% C_3F_7CN / 80% CO_2 gas mixture has a comparable negative LI performance to SF_6 since it establishes a safety level for the polarity with the highest probability of failure.

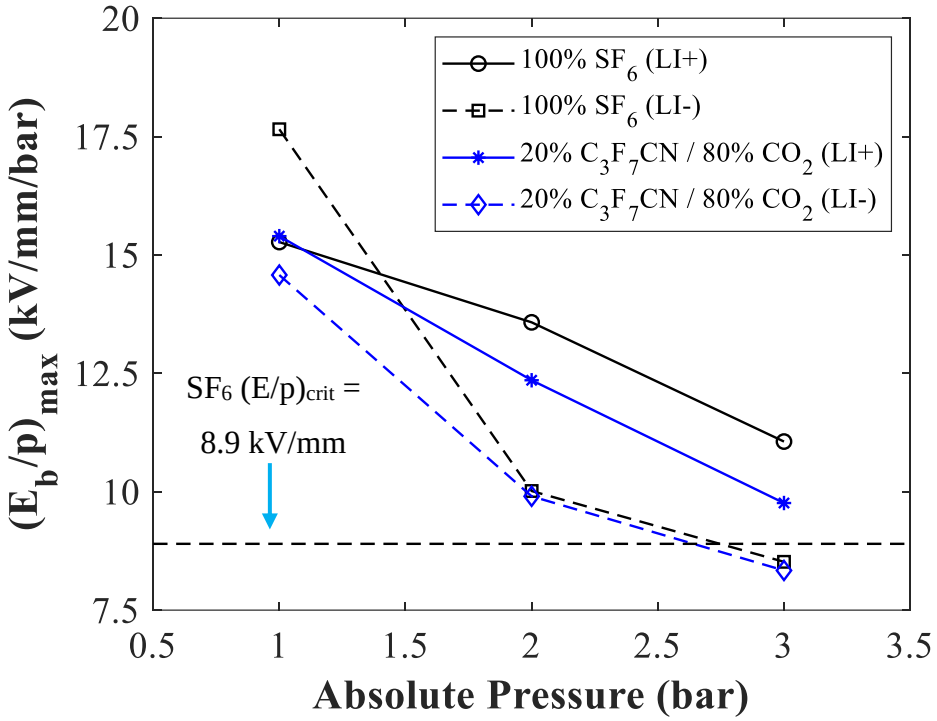

Figure 4-29. $(E_b/p)_{max}$ as a function of absolute pressure for the coaxial configuration of 8 mm conductor and 60 mm inner enclosure diameters using SF_6 and 20% C_3F_7CN / 80% CO_2 gas mixture under lightning impulse of both polarities.

Figure 4-30 shows the $(E_b/p)_{max}$ as a function of absolute pressure for the hemispherical rod-plane configuration which was computed using COMSOL. It shows that $(E_b/p)_{max}$ for both gases reduces gradually under positive and negative LI polarities. Unlike the breakdown characteristics of the coaxial configuration, the experimentally determined $(E_b/p)_{max}$ values for the hemispherical rod-plane configuration do not fall below the $(E/p)_{crit}$ of SF_6 for higher pressures within the investigated pressure range. This behaviour could be attributed to the large diameter of the high voltage hemispherical rod electrode.

The large diameter of the hemispherical rod electrode resulted in a lower E_{max} at a given voltage and a higher applied voltage is required to cause a breakdown. Conversely, reducing the size of the hemispherical rod can lead to a higher E_{max} at the rod tip, which can cause the insulating medium to breakdown at a lower applied voltage. In the case of the coaxial configuration, an 8 mm conductor was used within a 60 mm inner enclosure diameter which results in a gap spacing of 26 mm. The small conductor diameter leads to a high electric field intensification at the conductor surface and results in a comparatively lower breakdown performance than the hemispherical rod-plane electrode.

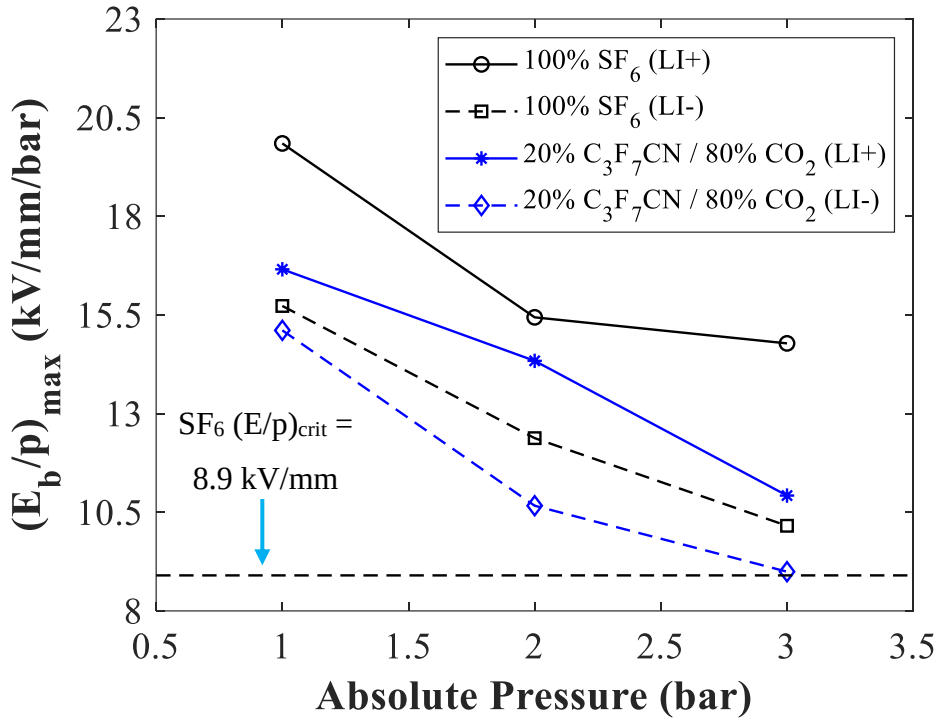

Figure 4-30. $(E_b/p)_{max}$ as a function of absolute pressure for the hemispherical rod-plane configuration using SF_6 and 20% C_3F_7CN / 80% CO_2 gas mixture under lightning impulse of both polarities

4.6 Summary

This chapter investigated the breakdown characteristics of C_3F_7CN/CO_2 mixtures in comparison to SF_6 as potential replacements for high voltage insulation applications. The results have shown that a mixture of 20% C_3F_7CN / 80% CO_2 can be a promising SF_6-alternative. Using the 10/30 mm reduced-scale coaxial configuration, the 20% C_3F_7CN / 80% CO_2 gas mixture has demonstrated to have an AC and LI breakdown performance comparable to SF_6. A mixture with 16% C_3F_7CN concentration can provide a lower

liquefaction temperature of 5°C than the 20% C_3F_7CN gas mixture but with a noticeably lower breakdown strength. This chapter has also shown that negative polarity LI breakdown voltage tends to be lower than positive using this reduced-scale prototype coaxial configuration. This indicates that for gas insulated equipment with a coaxial geometry, the negative polarity is more critical in the design consideration.

This chapter further investigated the breakdown characteristics of SF_6 and 20% C_3F_7CN / 80% CO_2 gas mixture under weakly quasi-uniform field configurations. This was carried out since these two gases were found to have a comparable electrical performance under quasi-uniform electric fields. Two different electrode configurations, coaxial and hemispherical rod-plane, with similar f values were developed to investigate the LI breakdown characteristics of both gases. The results have shown that SF_6 has higher breakdown voltages than the 20% C_3F_7CN / 80% CO_2 gas mixture for positive polarity under weakly quasi-uniform fields. The negative breakdown voltages are comparable for both gases. Even though the 20% C_3F_7CN / 80% CO_2 gas mixture has a lower positive breakdown voltage under weakly quasi-uniform field configurations, the equal behaviour under negative polarity provides a safety margin that this mixture can be used in GIL/GIB applications. This is because, as shown in this chapter, the negative polarity has a higher probability of failure using coaxial configurations. Therefore, equal performance of the two mediums under the weakest performing polarity shows that it can be tested in full-scale equipment with confidence.

The polarity effect does not exclusively depend on the field uniformity but other parameters such as pressure and gas medium (electronegativity) can significantly affect the polarity effect. The 20% C_3F_7CN / 80% CO_2 gas mixture has shown a smaller polarity difference in breakdown voltage than SF_6 between both LI polarities under weakly quasi-uniform electric fields. At a low pressure (1 bar abs), the breakdown voltages of the C_3F_7CN/CO_2 gas mixture for both LI polarities were found to be almost identical. All these factors should be taken into consideration to adopt a SF_6-alternative for retro-fill applications.

Blank Page

Chapter 5 Partial Discharge Characteristics of SF_6 Gas and 20% C_3F_7CN / 80% CO_2 Gas Mixture

5.1 Introduction

Manufacturing defects such as small protrusions on conductor and enclosure as well as the presence of floating metallic particles can lead to field enhancements within the GIL and GIB equipment [28], [95]. These flaws and contaminations will stress the gas and slowly deteriorate its insulation capability over time which could eventually lead to catastrophic failure of equipment. This localised breakdown of insulation results in discharge activities which are known as partial discharge (PD). These defects are better prevented in the modern equipment since, with the advancement in technology, the technical finish in new assets can be treated more cautiously. However, when dealing with a retro-fill investigation for replacing SF_6 in equipment operating since the 1960s, it is a vital performance parameter to take into consideration. Therefore, it is important to experimentally compare the PD behaviour of the 20% C_3F_7CN / 80% CO_2 gas mixture against SF_6.

Chapter 3 has described the development of PD test configurations using needles on electrodes to represent defects on conductor and enclosure in practical equipment. In this chapter, the PD behaviour of SF_6 and 20% C_3F_7CN / 80% CO_2 gas mixture were characterised in terms of PDIV and PDEV values. Different needle lengths and electrode configurations were used to vary the field uniformity from divergent to highly divergent electric fields. Finally, the PD behaviour of SF_6 and 20% C_3F_7CN / 80% CO_2 gas mixture under varying field uniformities were analysed through the usage of PRPD patterns.

5.2 Test Circuit and Test Procedure

5.2.1 Ultra-High Frequency (UHF) Method

The UHF method has become increasingly popular for onsite condition monitoring due to its high sensitivity and improved signal-to-noise (S/N) ratio compared to other methods as well as the ability to locate the PD fault using time of flight measurements [28], [95]. PDs lead to currents with a rise time of less than a nanosecond, which radiate electromagnetic (EM) waves with frequencies up to about 2000 MHz [28]. Practical GIL/GIB assets do not always have preinstalled UHF sensors for capturing these EM waves, especially equipment that was installed in the 1960s. Therefore, external UHF sensors as shown in Figure 5-1, can be positioned over an exposed area of an insulating support to detect PDs within the GIL/GIB [95]. The UHF sensor used in this work has a bandwidth of 300-2000 MHz.

Figure 5-1. UHF barrier sensor used for the PD experiments [96].

5.2.2 Test Circuit Diagram

The PD experiments were carried out with the same stainless-steel pressure vessel used for the breakdown experiments. A 150 kV transformer was used to generate the AC waveform. The voltage measurement was taken through a capacitive voltage divider as shown in Figure 5-2. Hemispherically capped rod-plane and plane-plane electrode configurations incorporated with needles, described in Chapter 3, were used to provide a point of enhanced field and to initiate PD activities at a chosen location. To model a protrusion-on-the-conductor (POC) fault in GIB, a needle was inserted into the HV electrode. Similarly, a needle was placed on the ground electrode to model a protrusion-on-the-enclosure (POE) defect. All needles tested have a tip radius of 5 μm and can be repositioned to vary the needle length. The needle-to-plane gap distance was always kept constant at 10 mm.

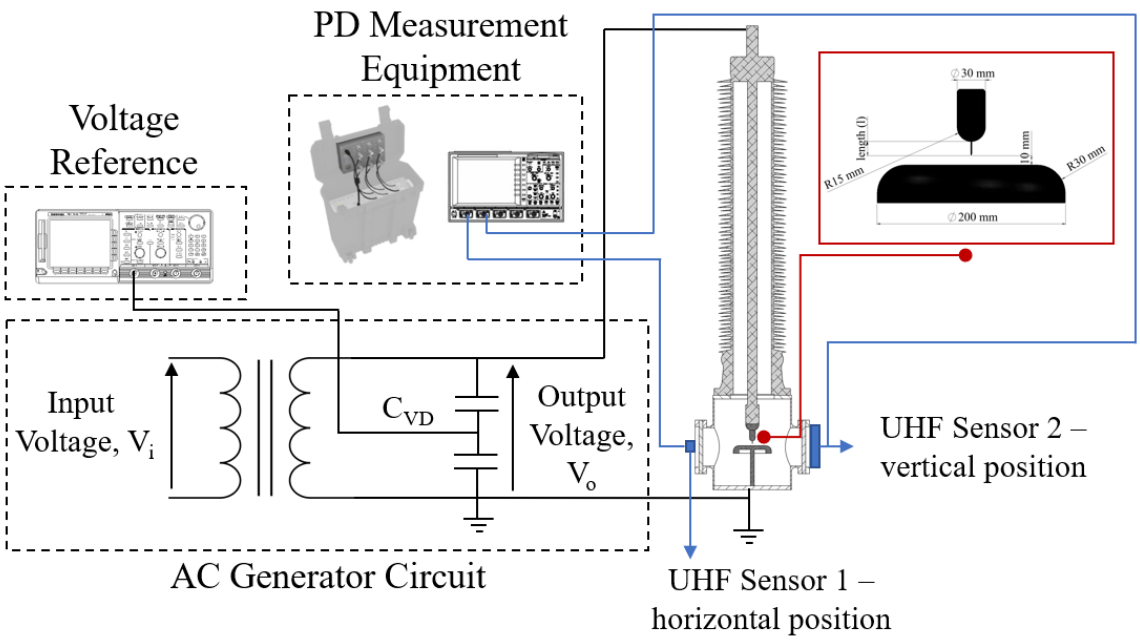

Figure 5-2. PD experimental test circuit including the AC generator circuit and PD measurement equipment.

5.2.3 Position Orientation and Sensitivity Check of UHF Sensors

UHF sensors, shown in Figure 5-1, were attached onto the two viewing windows of the pressure vessel. As the viewing windows are circular in shape, the UHF barrier sensors can be placed in several different positions by rotating around the axis of the window. These UHF sensors are linearly polarised, which means that their orientation relative to the PD electrode configuration inside the pressure vessel makes a significant difference to the amplitude of the signal received. Therefore, it is important to optimise the position of the UHF sensors relative to the PD defect to acquire the best signal possible.

Sensors with a specific polarisation are ineffective in receiving EM signals of a different polarisation. A linearly polarised sensor that is placed at 90° angle difference relative to the polarisation of the EM wave is known to be cross-polarised, which results into a negligible amplitude signal being received. In contrast, an incoming EM wave matching the polarisation of the UHF sensor will result in a maximum amplitude signal being recorded [97], [98]. Therefore, the sensors were placed in different positions to cover both directions of EM wave propagation due to PD activities. Sensor 1 had a horizontal alignment, shown in Figure 5-3(a), which was perpendicular to the needle direction. Sensor 2 was placed in a

vertical position, shown in Figure 5-3(b), and was parallel in relation to the needle direction. The two sensors had a 90° orientation difference.

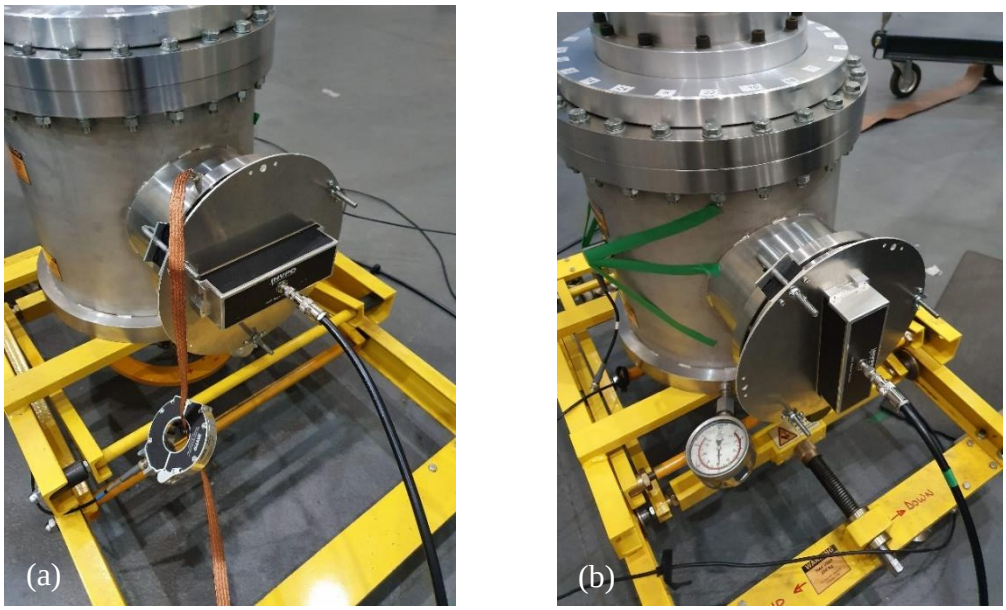

Figure 5-3. UHF barrier sensor orientation (a) Sensor 1 - perpendicular relative to the needle (horizontal) and (b) Sensor 2 - parallel to the needle (vertical).

A sensitivity check, as described in [99], was carried out to ensure that both UHF sensors can measure PD signals equally with the setup used. A signal generator in combination with a pulse sharpener were used to generate a fast rise signal (< 5 ns) similar to those produced by PDs. An example of the signal is shown in Figure 5-4.

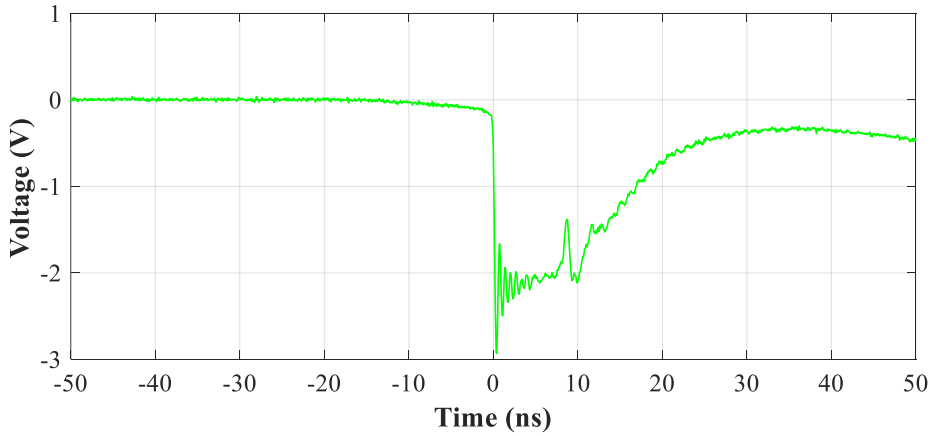

Figure 5-4. Pulse sharpener output signal with a fast-rise time of less than 5 ns which was used for the sensitivity check.

The sensitivity verification procedure was performed using one UHF sensor as a transmitter and the remaining sensor as a receiver. In order to illustrate the effect of the position on the

sensors, the sensors were firstly aligned with each other in horizontal orientation. A signal was first injected into Sensor 2 and received from Sensor 1 and then vice versa. Measurements from the UHF sensors represent a PD pulse and both cases are illustrated in Figures 5-5(a) and 5-5(b). As shown in Figure 5-5, the peak-to-peak amplitude values for the same input signal are 146 mV and 143 mV when Sensor 1 and Sensor 2 were used as receivers respectively. This shows that both sensors have almost identical performance and can detect PD with the same sensitivity. The PD measurement signals shown in Figure 5-5 are the maximum amplitude signals possible since the input signals and the UHF sensors have matching polarisations in this case.

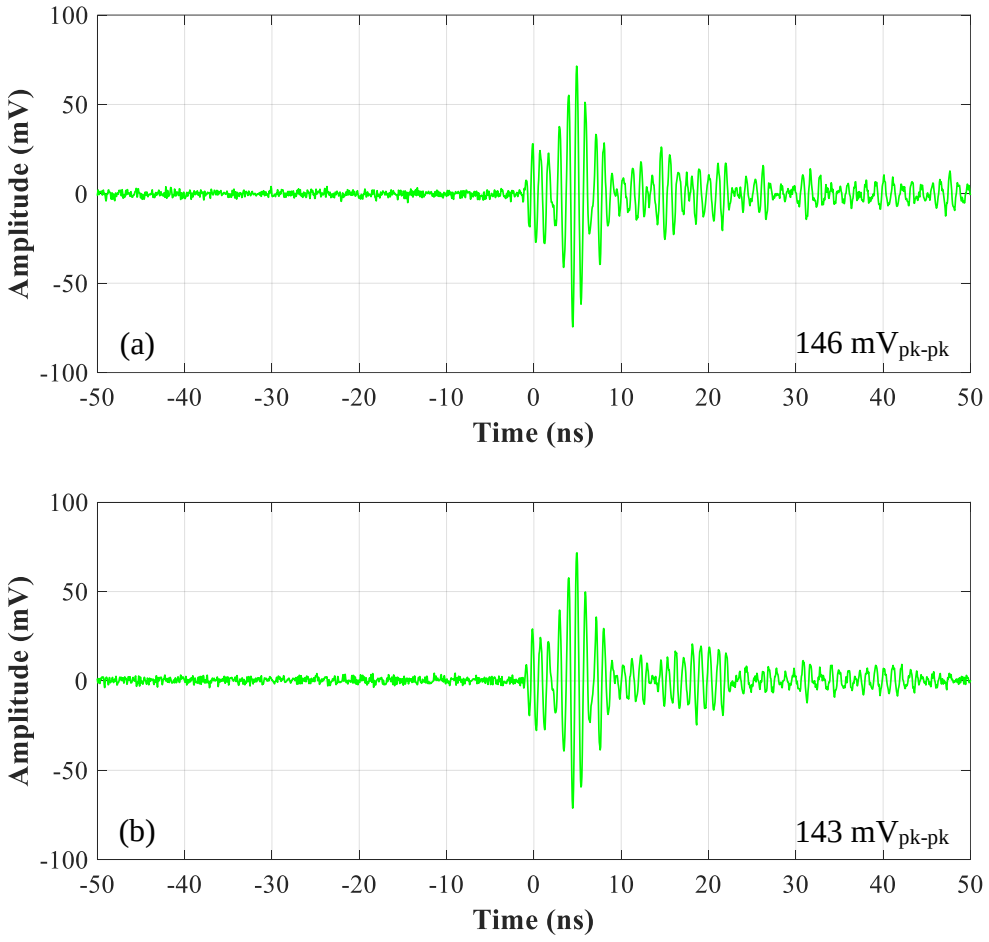

Figure 5-5. UHF sensors PD measurement responses to the fast-rise signal with their orientation aligned (a) Sensor 1 used as a receiver (horizontal) and Sensor 2 used as a transmitter (horizontal) and (b) Sensor 2 used as a receiver (horizontal) and Sensor 1 used as a transmitter (horizontal).

The position of the sensors was later adjusted to a 90° orientation difference for the sensitivity check, as initially shown in Figure 5-3, with Sensor 1 as horizontal and Sensor 2 as vertical. The signal was first injected to Sensor 2 and received from Sensor 1, shown in Figure 5-6(a), and then vice versa which is shown in Figure 5-6(b). Figure 5-6 shows that

regardless of the sensor chosen as the receiver, the signal reading is almost identical indicating that both sensors provide repeatable PD detection. The 90° orientation difference of the sensors' position results in a significant difference from the signals in Figure 5-5 that demonstrates the effect of position mismatch. A mismatch in polarisation of almost 90° will lead to the peak-to-peak reading of the signal to be about 10 times smaller.

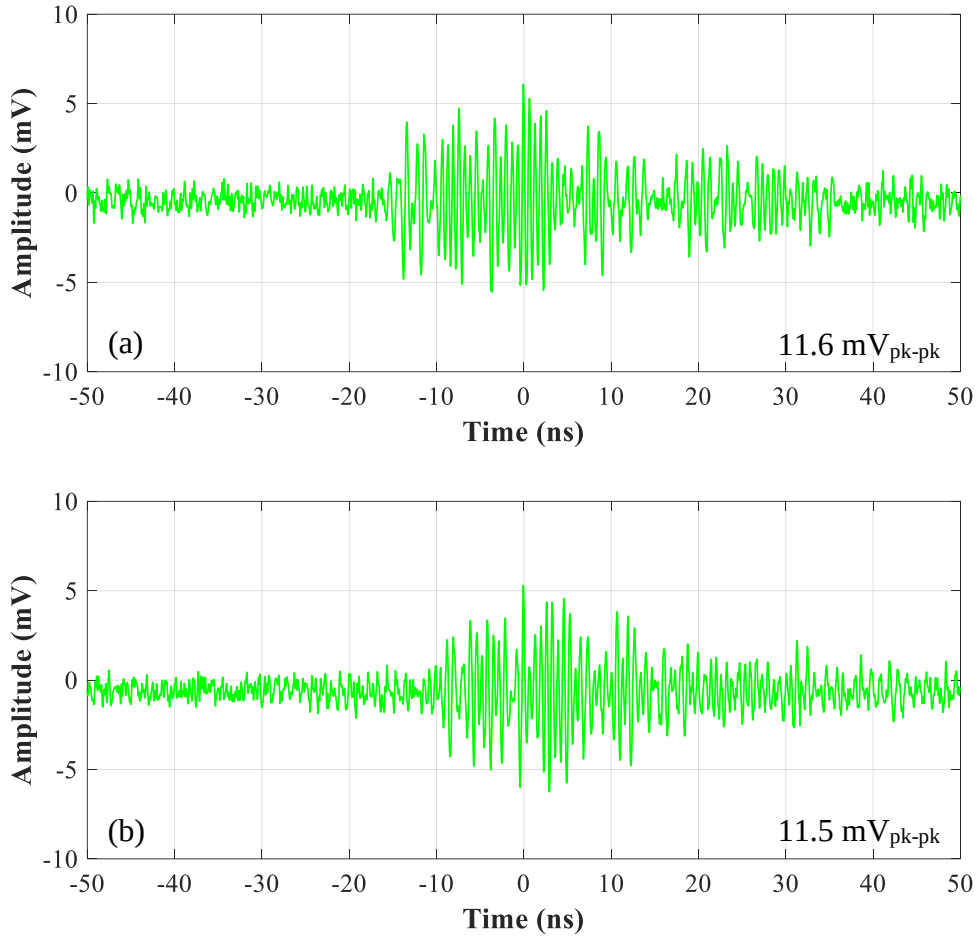

Figure 5-6. UHF sensors PD measurement responses to the fast-rise signal with a 90° orientation difference (a) Sensor 1 used as a receiver (horizontal) and Sensor 2 used as a transmitter (vertical) and (b) Sensor 2 used as a receiver (vertical) and Sensor 1 used as a transmitter (horizontal).

Since the polarisation of the incoming signals occurring from the PD configuration inside the test vessel was unknown, the sensor positions as shown in Figure 5-3 were adopted. This helps to avoid any case of cross-polarisation and to cover both polarisations of wave oscillation. After some initial tests, Sensor 1 (horizontal orientation) was found to be more sensitive to PD activity and was used to acquire the results described in the following sections. Note that sensitivity checks were carried out with both test gases and negligible difference was observed.

5.2.4 PD Measuring Equipment and UHF Test Procedures

The UHF sensors were connected to the measurement equipment using 15 meters of low-loss RG213 coaxial cable. In the first instance, a Lecroy 4 GHz oscilloscope was used to determine the PDIV and PDEV values. Subsequently, for frequency scans and PRPD measurements, the UHF sensors were connected to a HVPD Kronos Spot Tester coupled with a UHF converter. The UHF converter is used to convert the high frequency (≈1000 MHz) PD signals into the 50 MHz bandwidth of the acquisition system and has a programmable frequency sweep setting.

The voltage was raised from zero at a rate of ≈1 kV every 3 seconds (stepwise voltage increase). This provided sufficient time for the oscilloscope to trigger on PD activity. The trigger of the oscilloscope was set at 5 mV and signals above this voltage level (10 mV_{pk-pk}) were classified as PD activity. An example of a PD signal with the specific setup is shown in Figure 5-7.

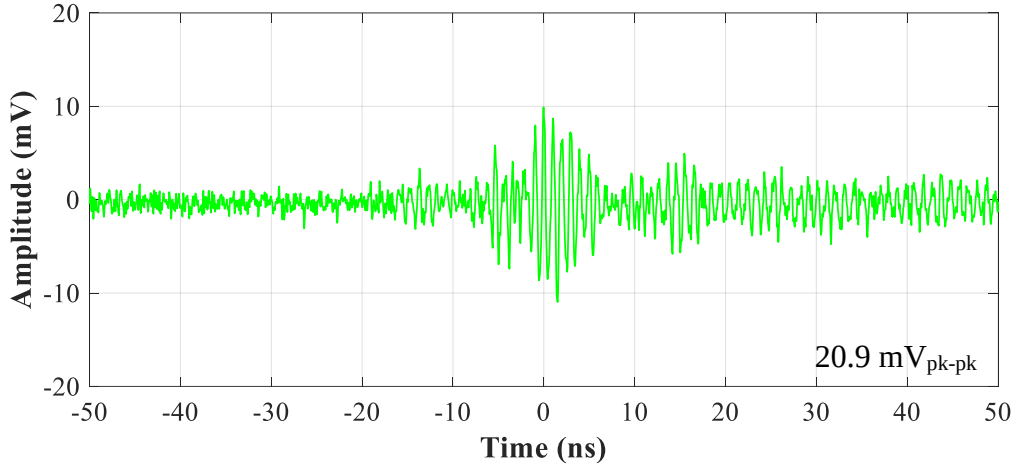

Figure 5-7. PD signal example recorded from the UHF sensors with a 20.9 mV_{pk-pk} value.

The PD signal is very distinctive from the maximum noise level detected in the lab. Note that the noise signals in the lab never exceeded 8 mV_{pk-pk}. A typical noise type signal detected during these experiments is shown in Figure 5-8. The PDIV in this study was considered the voltage level where repeated PD activities were observed (signals above the 5 mV trigger level, equivalent to 10 mV_{pk-pk}). Similarly, PDEV was considered the voltage level where PD signals above 5 mV (equivalent to 10 mV_{pk-pk}) ceased to occur. This procedure was

performed 5 times to calculate the average PDIV and PDEV values and their standard deviation using equations (4-6) and (4-7).

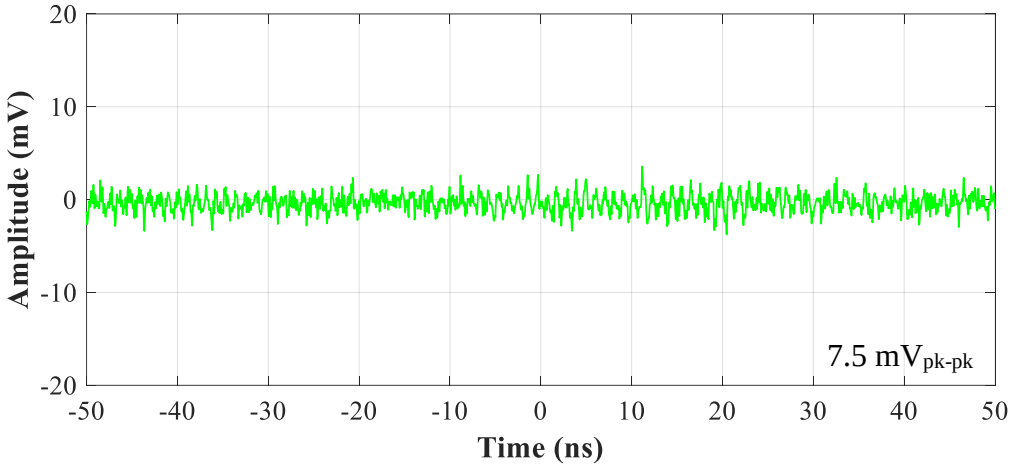

Figure 5-8. Noise level example recorded from the UHF sensors with a maximum of 7.5 mV_{pk-pk}.

5.2.5 Full Bandwidth Scan of PD Activities

A full bandwidth scan was carried out from 300 to 2000 MHz with a 50 MHz step increase to determine the frequencies where signals with the highest S/N ratio occur for SF_6 and 20% C_3F_7CN / 80% CO_2 with the setup being used. A good indication of the S/N ratio is the intensity (V_{peak}/V_{RMS} ratio) of the down converted signal of the acquisition unit as shown in Figures 5-9 and 5-10. Figures 5-9 and 5-10 illustrate the PD activity scans for both SF_6 and 20% C_3F_7CN / 80% CO_2 at 5 bar (abs) pressure. Figure 5-9 shows that SF_6 demonstrated a more wideband PD behaviour than the 20% C_3F_7CN / 80% CO_2 gas mixture as the signals with the best S/N ratio for SF_6 span across the frequencies between 1050 to 1300 MHz.

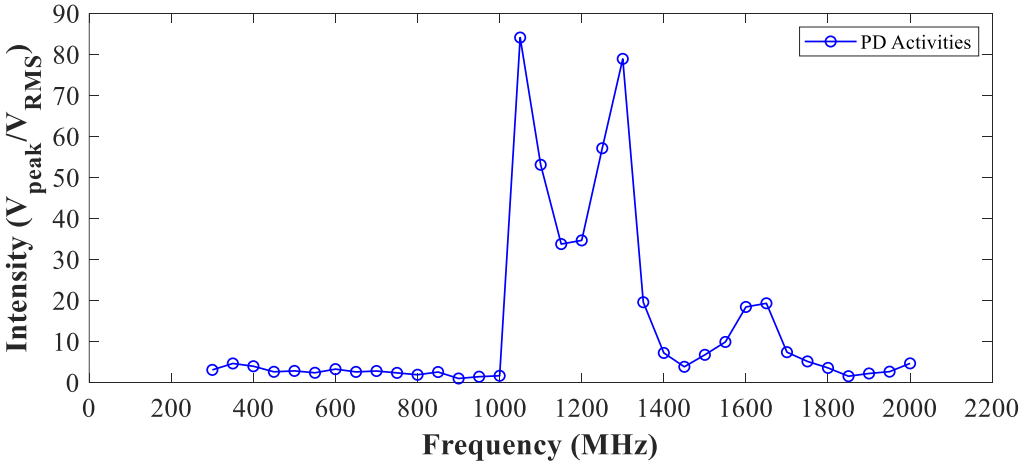

Figure 5-9. Full bandwidth scan of PD activities for SF_6.

Figure 5-10 shows that for the 20% C_3F_7CN / 80% CO_2 gas mixture the signals with the best S/N ratio occurred between 1050 to 1100 MHz. To optimise test time while providing sufficient detail on PD activity, the frequencies of 1050, 1100 and 1150 MHz were chosen for recording the PRPD patterns as it provided the highest intensity of PDs and the best S/N ratio for both gases. For each PRPD pattern, 15-cycle measurements were taken for the 1050, 1100 and 1150 MHz frequencies where the acquisition system scanned 15 times through each individual frequency and recorded the PD activity. Note that choosing a different bandwidth for PRPD recordings could have an impact on the shape of the patterns as different S/N ratios will be used for the measurements.

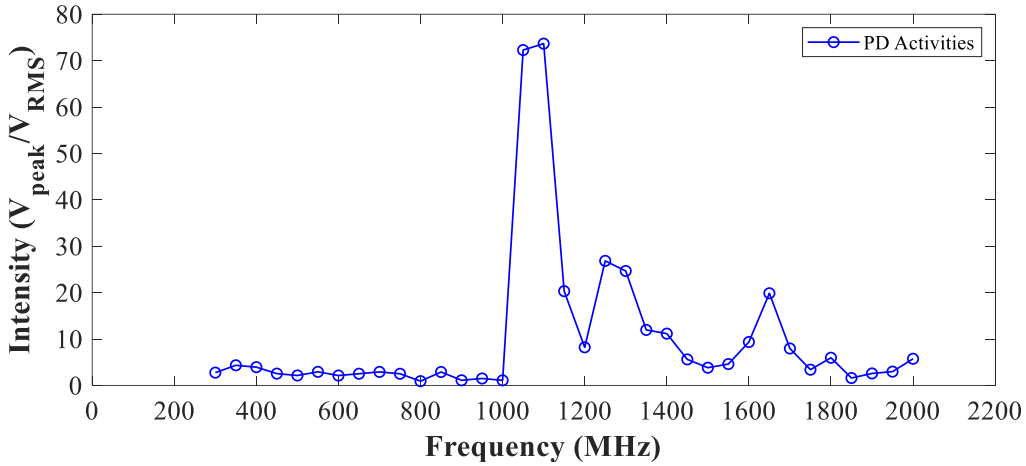

Figure 5-10. Full bandwidth scan of PD activities for 20% C_3F_7CN / 80% CO_2.

Also, note that the amplitude (mV) of the PRPD patterns is smaller than the actual amplitude values of the UHF signals recorded directly from the UHF sensors (due to the down scale from the UHF converter). Therefore, the noise level of 8 mV is not applicable for the PRPD patterns shown in this chapter since the amplitude of the signals is plotted in relative values. Noise in the PRPD patterns was up to 0.2 mV and was removed after processing.

5.3 Results of Hemispherical Rod-plane Electrode Configuration

5.3.1 Effect of Pressure, Gas Type and Field Uniformity on the PDIV and PDEV Characteristics

Figures 5-11 and 5-12 illustrate the AC_{RMS} PDIV and PDEV values as a function of pressure for SF_6 and 20% C_3F_7CN / 80% CO_2. Figure 5-11 displays the values using the rod-plane configuration with a 15 mm needle attached on the HV electrode. As shown in the figure, from 1 to 4 bar (abs), SF_6 has almost double the inception and extinction voltages of the 20% C_3F_7CN / 80% CO_2 gas mixture. However, at 5 bar (abs), the difference between the 20% C_3F_7CN / 80% CO_2 gas mixture and SF_6 reduces significantly. As the pressure increased from 4 to 5 bar, the PDIV and PDEV values of 20% C_3F_7CN / 80 % CO_2 gas mixture increase by 46% and 50% from 4 to 5 bar respectively. For the same pressure change, SF_6 only attains a small increase of 11% and 2% for PDIV and PDEV, respectively. This shows that SF_6 has almost linear correlation with pressure change, throughout the range investigated, using the rod-plane configuration with a needle of 15 mm. In contrast, the 20% C_3F_7CN / 80% CO_2 gas mixture seems to be more sensitive to highly divergent fields than SF_6 for pressures of 1 to 4 bar (abs) but at 5 bar (abs) the PDIV and PDEV values are getting close to SF_6.

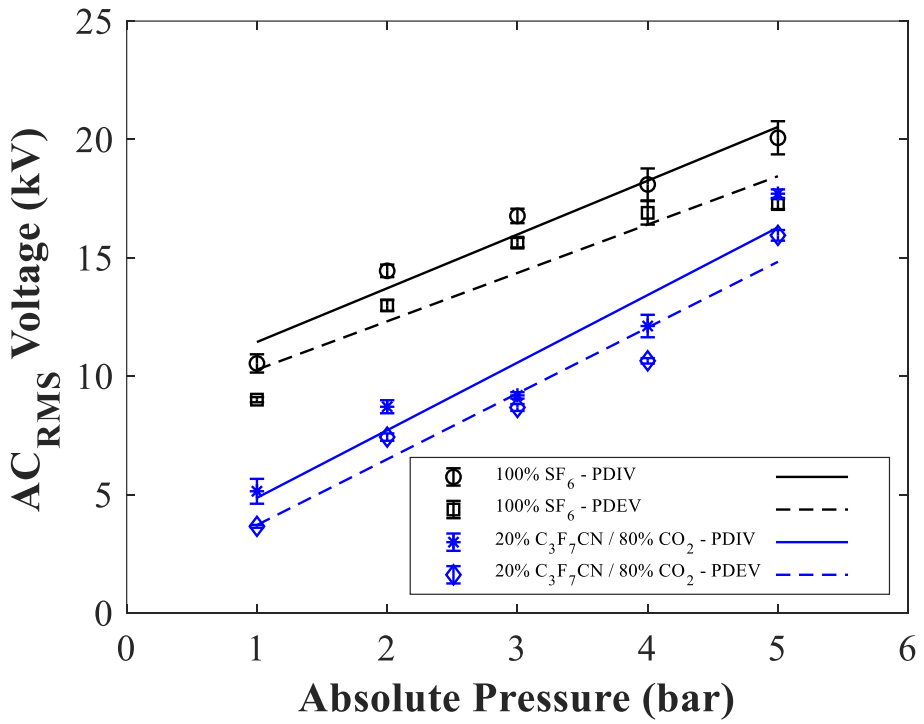

Figure 5-11. AC_{RMS} PDIV and PDEV of SF_6 and 20% C_3F_7CN / 80% CO_2 as a function of absolute pressure using the hemispherical rod-plane electrode configuration with a needle attached on the HV electrode with a length of 15 mm and a needle-plane gap distance of 10 mm.

Figure 5-12 displays the PDIV/EV characteristics of the rod-plane configuration when the length of the needle attached on the HV electrode was reduced to 5 mm. By reducing the needle length, the electric field of the configuration essentially becomes more uniform. The

increased field uniformity has resulted in much closer PDIV/EV values between SF_6 and the 20% C_3F_7CN / 80% CO_2 gas mixture. Figure 5-12 illustrates that, except for the values at 1 bar (abs) which were marked as outliers and therefore excluded from the line of best fit, the 20% C_3F_7CN / 80% CO_2 gas mixture demonstrates a PD performance that is much closer to SF_6 than using the 15 mm needle length. The PDIV/EV values of both SF_6 and the 20% C_3F_7CN / 80% CO_2 demonstrate a fairly linear correlation with increasing pressure with the exception of 1 bar (abs).

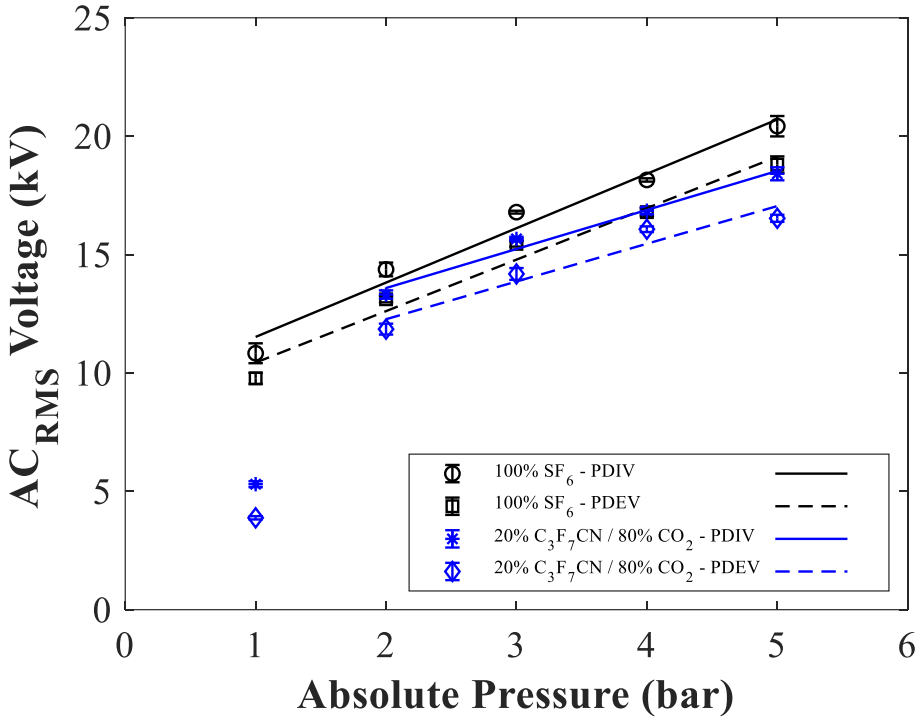

Figure 5-12. AC_{RMS} PDIV and PDEV of SF_6 and 20% C_3F_7CN / 80% CO_2 as a function of absolute pressure using the hemispherical rod-plane electrode configuration with a needle attached on the HV electrode with a length of 5 mm and a needle-plane gap distance of 10 mm.

Figures 5-13 and 5-14 plot the PDIV/EV values for SF_6 and the 20% C_3F_7CN / 80% CO_2 gas mixture respectively to illustrate the effect of varying field uniformity with a reduction of the needle length. Figure 5-13 shows that negligible effect was observed for SF_6 and the PDIV/EV values are almost identical for both needle lengths. Figure 5-14 shows that the PD performance of the 20% C_3F_7CN / 80% CO_2 gas mixture significantly improves with increased field uniformity. The ability for SF_6 to sustain discharges, regardless of the field uniformity might be attributed to the strong attachment nature of the fluorine element in its molecule. In the case of the gas mixture, it is comprised predominantly of CO_2 gas, with carbon being a weakly attaching element, and discharges can be initiated more readily under

more non-uniform electric fields. Therefore, the critical threshold of SF_6 for PD initiation, or PD inception level, appears to be higher than the C_3F_7CN/CO_2 gas mixture.

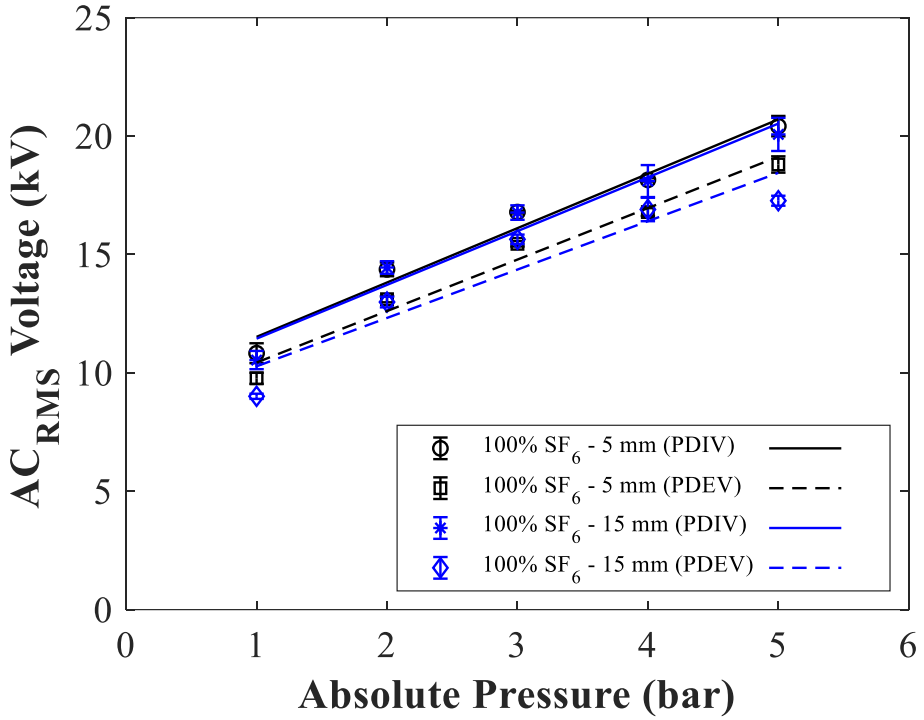

Figure 5-13. AC_{RMS} PDIV and PDEV of SF_6 as a function of absolute pressure using the hemispherical rod-plane electrode configuration with a needle attached on the HV electrode with 5- and 15-mm lengths.

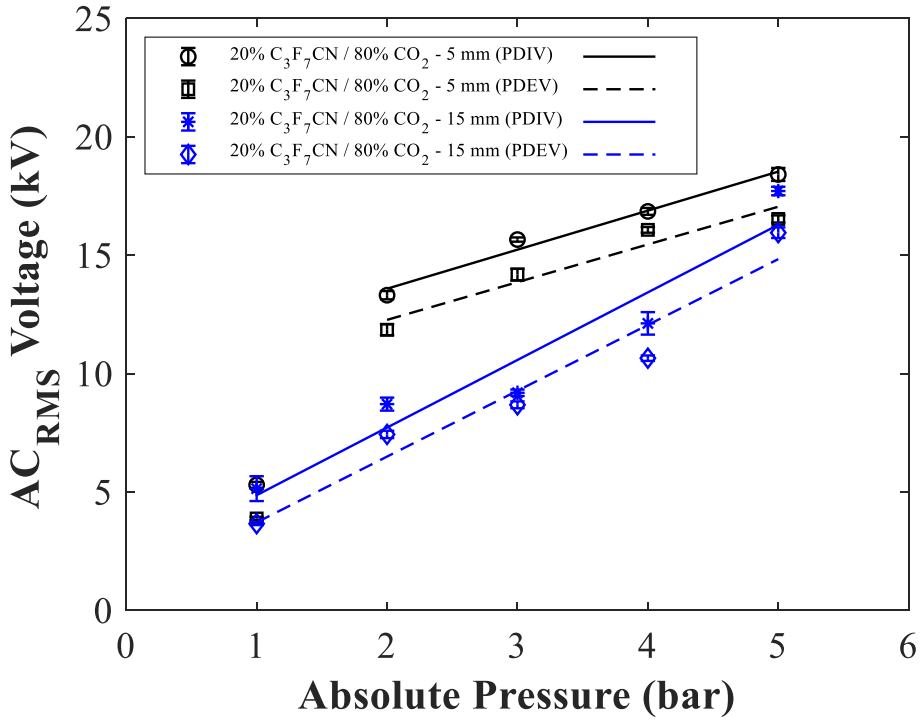

Figure 5-14. AC_{RMS} PDIV and PDEV of 20% C_3F_7CN / 80% CO_2 as a function of absolute pressure using the hemispherical rod-plane electrode configuration with a needle attached on the HV electrode with 5- and 15-mm lengths.

5.3.2 PRPD Pattern Analysis

5.3.2.1 Effect of Pressure

Figure 5-15 illustrates the PRPD patterns for 20% C_3F_7CN / 80% CO_2 and SF_6 recorded at 20 kV for pressures in the range of 2 to 5 bar (abs) using a rod-plane configuration with a needle of 15 mm. PD activities mostly occurred on the positive half-cycle between 45° and 135° phase angles. Both SF_6 and the 20% C_3F_7CN / 80% CO_2 gas mixture appear to suppress the PD activity more effectively with increased pressure as was also shown in Figures 5-11 and 5-12. By applying a fixed voltage at different pressures, the effect of gas density on PD activities can be demonstrated through PRPD patterns. Discharges in PDs develop similarly to a breakdown as described in Chapter 2. At low pressures, the mean free path between the gas molecules is significant. This provides the electrons enough space to accumulate the required ionisation energy and create electron avalanches that lead to discharges at low voltages. As the pressure is increased, density increases within a fixed volume and this will result in a reduced mean free path between the gas molecules. Due to insufficient space in between the gas molecules, electrons undergo more frequent collisions with neutral molecules thus being unable to accumulate enough energy to ionise the gas. Therefore, a higher applied voltage is required to provide electrons with enough energy for ionisation and to lead to the initiation of PD activity as illustrated by PRPD patterns in Figure 5-15.

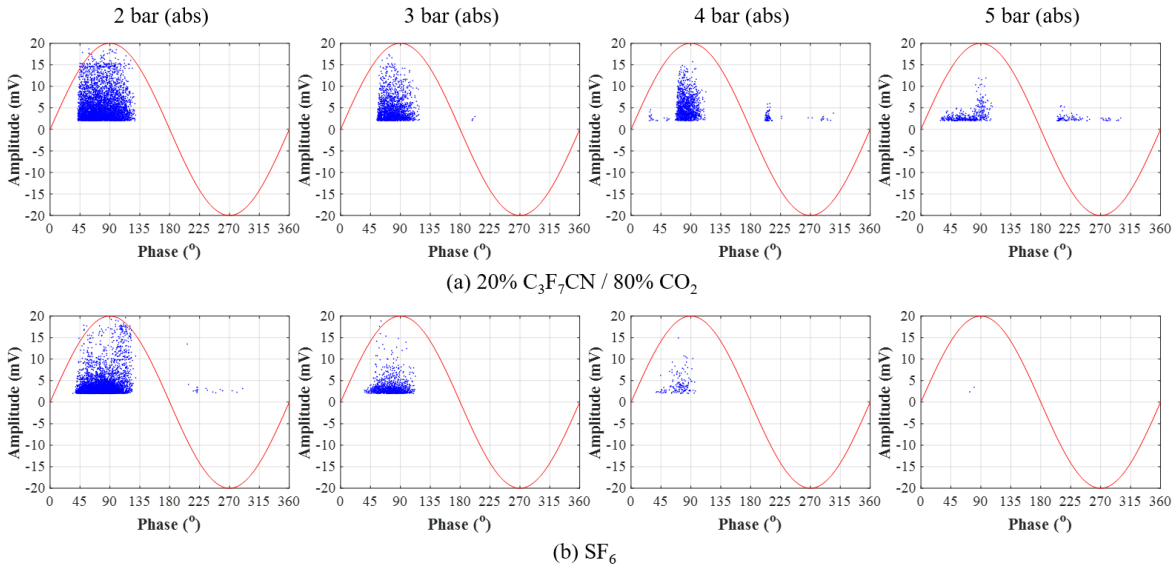

Figure 5-15. PRPD patterns comparing (a) 20% C_3F_7CN / 80% CO_2 and (b) SF_6 at 20 kV for pressure range from 2 to 5 bar (abs) using the hemispherical rod-plane configuration with a 15 mm needle on the HV electrode.

Inception of PD activities at a lower voltage for a gas could lead to a lower breakdown voltage as well since the initiation of a discharge occurs at a lower voltage. However, this is not certain since additional processes, such as attachment, can affect the growth of an electron avalanche to a complete breakdown as was described in Chapter 2.

5.3.2.2 Effect of Field Uniformity

Figure 5-16 shows the effect of reduced needle length on the PD behaviour of SF_6 at 5 bar (abs) using the rod-plane configuration. For both needle lengths, PDs mostly occurred on the positive half-cycle of the AC waveform. With a 15 mm needle being used, negative activities (PDs on the negative half-cycle of the AC waveform) gradually appear with an increase in voltage such as 150% and 200% of their PDIV values. Using a 5 mm needle, PDs on the negative half-cycle appear to be fairly stable regardless of the voltage increase. The most significant difference between Figures 5-16(a) and 5-16(b) is the magnitude of the PDs recorded from the PRPD acquisition unit. Despite their PDIV values being similar, as was shown in Figure 5-13, the PD activities using 15 mm needle length have a considerably higher amplitude than the 5 mm ones. PDs using the 15 mm needle length spread up to 20 mV, while a maximum amplitude of approximately 5 mV was recorded for the 5 mm needle length.

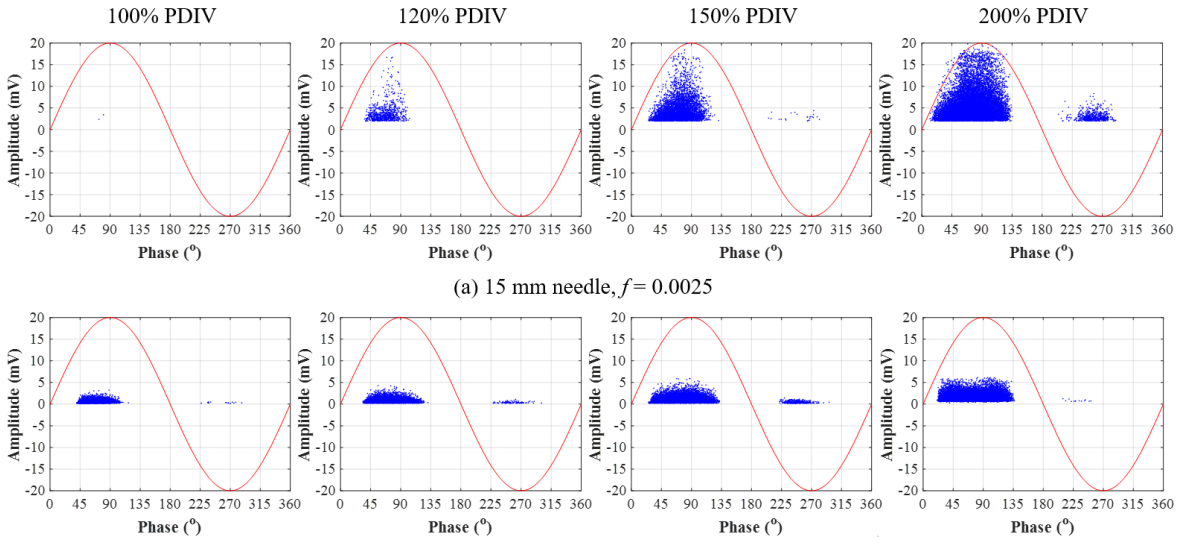

(a) 15 mm needle, $f = 0.0025$

(b) 5 mm needle, $f = 0.0033$

Figure 5-16. PRPD patterns comparing SF_6 with (a) 15 mm and (b) 5 mm needle lengths on the HV electrode at 5 bar (abs) for 100, 120, 150 and 200% of its PDIV values using the hemispherical rod-plane configuration.

The same observation was found with the UHF signals recorded on the 4 GHz oscilloscope directly from the sensors. Figure 5-17 shows the maximum amplitude signals recorded out of a total of 50 recordings for each needle. The figure shows that the 5- and 15-mm needle signals have peak-to-peak values of 25.1 mV_{pk-pk} and 74.5 mV_{pk-pk} respectively. This suggests that a highly divergent field can lead PD activities with high amplitude.

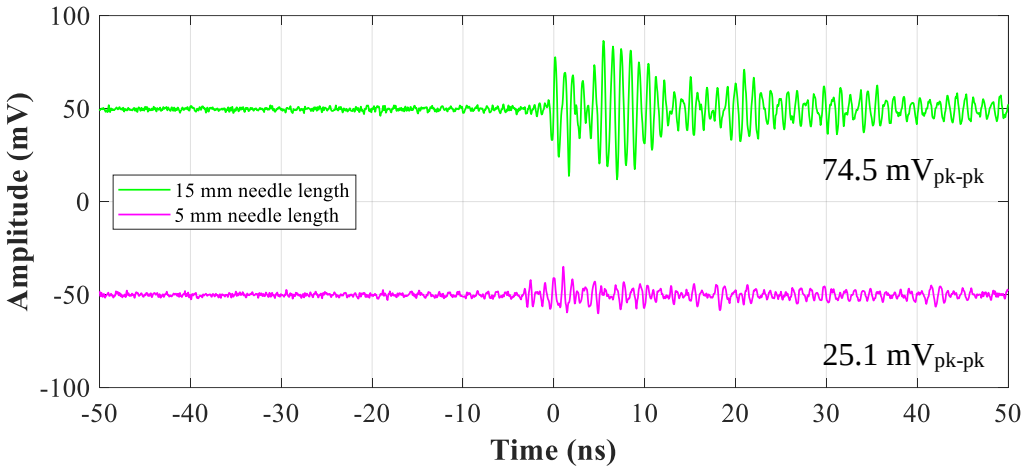

Figure 5-17. Maximum UHF signal comparison for SF_6 at 5 bar (abs) using 15- and 5-mm needle lengths recorded directly from the UHF sensors at the PDIV value with the 4 GHz oscilloscope.

Figure 5-18 compares the PRPD patterns of the 20% C_3F_7CN / 80% CO_2 gas mixture at 5 bar (abs) for 5- and 15-mm needle lengths using the rod-plane configuration.

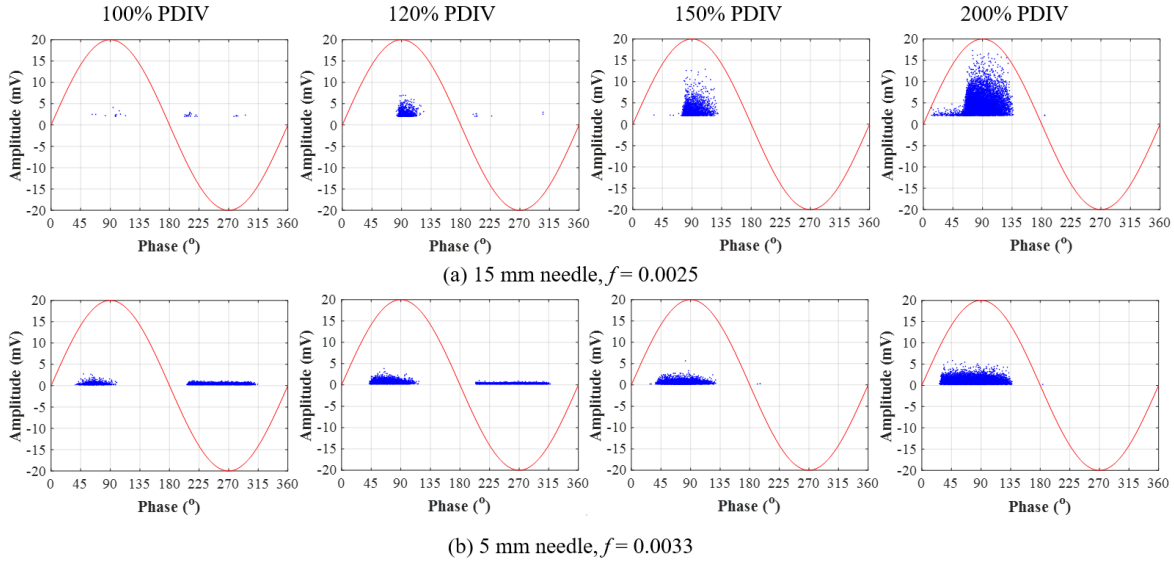

Figure 5-18. PRPD patterns comparing 20% C_3F_7CN / 80% CO_2 with (a) 15 mm and (b) 5 mm needle lengths on the HV electrode at 5 bar (abs) for 100, 120, 150 and 200% of its PDIV values using the hemispherical rod-plane configuration.

For the 15 mm needle length, the majority of PD activities occurred on the positive half-cycle. Both positive and negative PDs are observed to take place initially using the 5 mm needle length. However, at higher voltages, the PDs were observed to occur in the positive half-cycle of the AC waveform. Similar to SF_6, the magnitude of PDs for the 15 mm needle length is comparatively higher than the 5 mm. The amplitude of PDs using the 5- and 15-mm needles extend up to 5 mV and 15 mV respectively, indicating a similar PD performance to SF_6.

Figure 5-19 illustrates the UHF signals at 100% PDIV recorded directly from the sensors for the 20% C_3F_7CN / 80% CO_2 gas mixture at 5 bar (abs) for 5 mm and 15 mm needle lengths using the rod-plane configuration. Once again, the signals shown in Figure 5-19 are the maximum out of a total of 50 recordings for each needle. Like SF_6, the 15 mm needle length signal peak-to-peak value is higher than the 5 mm. However, the change in the amplitude of the signals for the C_3F_7CN/CO_2 gas mixture due to different needle lengths, is not as evident as observed with SF_6.

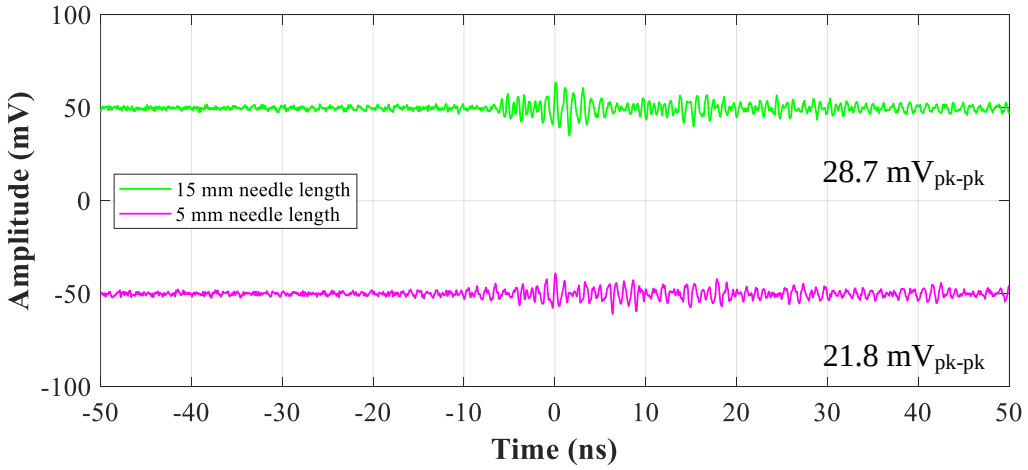

Figure 5-19. Maximum UHF signal comparison for 20% C_3F_7CN / 80% CO_2 at 5 bar (abs) using 15- and 5-mm needle lengths recorded directly from the UHF sensors at the PDIV value with the 4 GHz oscilloscope.

The recorded maximum peak-to-peak values for the 5 mm needle are comparable for both the 20% C_3F_7CN / 80% CO_2 gas mixture and SF_6. Nevertheless, with the 15 mm needle, the signals using SF_6 appear to have much higher peak-to-peak values than the 20% C_3F_7CN / 80% CO_2 gas mixture. A potential reason is the high electronegativity of SF_6, which suppresses PDs up to a critical threshold very effectively, leading to a higher PDIV value than the 20% C_3F_7CN / 80% CO_2 gas mixture. However, SF_6 is considered as a 'brittle' insulation gas in the sense that ionisation builds up quickly when its critical field strength is

exceeded. As the PDIV threshold is exceeded, ionisation activity of SF_6 could rapidly increase in the presence of a sharp protrusion such as the needle being used in this configuration [28]. Therefore, this can be considered as an important factor influencing the PD activity quantity as well as the amplitude for SF_6 and the 20% C_3F_7CN / 80% CO_2 gas mixture.

5.3.2.3 Effect of Gas Medium

Figure 5-20 compares SF_6 and the 20% C_3F_7CN / 80% CO_2 gas mixture using their PRPD patterns to illustrate the effect of different gas mediums on their PD behaviour. Both gases were plotted at 200% of their PDIV values for the pressure range of 1 to 5 bar (abs) using the rod-plane configuration with a needle length of 5 mm. This is to clearly show the PD characteristics of both gases at a voltage value where sufficient number of PDs can occur.

Figure 5-20(a) shows that the PD activities for the 20% C_3F_7CN / 80% CO_2 gas mixture initially occur at the negative half-cycle of the AC waveform. As PDIV increases with pressure, the PD activities start to appear on the positive half-cycle. The 20% C_3F_7CN / 80% CO_2 gas mixture has been observed to go through a 3-stage transitional PRPD behaviour: (i) PDs appear on the negative cycle at relatively low pressures (ii) consistent PDs on both the positive and negative cycles at higher pressures and (iii) majority of PDs shift onto the positive half-cycle at very high pressures where it starts to behave like SF_6. Figure 5-20(b) illustrates that the PD activities for SF_6 mostly occurred on the positive half-cycle with some small activities on the negative half-cycle. As seen from the PRPD patterns, SF_6 does not go through a similar transitional phase to the 20% C_3F_7CN / 80% CO_2 gas mixture. The SF_6 results agree with findings reported in [70] where the majority of PDs are on the positive half-cycle.

To further examine the effect of gas medium on the PD behaviour, pure CO_2 and C_3F_7CN gases were tested using the rod-plane configuration with a 5 mm needle. This is to identify whether one of the two gases is the main contributing factor for the distinct PD behaviour of the 20% C_3F_7CN / 80% CO_2 gas mixture relative to SF_6. Figure 5-21 shows the PDs of CO_2 for 200% of its PDIV values at different pressures. As shown in the figure, PD activities in

pure CO_2 were mostly observed on the negative half-cycle for the pressures and voltages used.

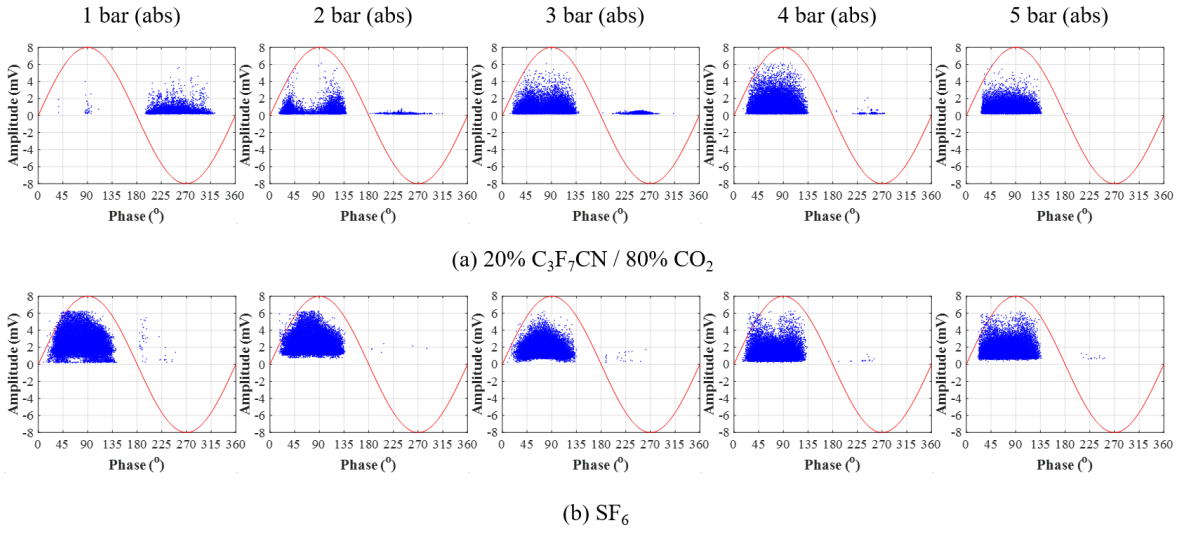

(a) 20% C_3F_7CN / 80% CO_2

(b) SF_6

Figure 5-20. PRPD patterns comparing (a) 20% C_3F_7CN / 80% CO_2 and (b) SF_6 at 200% of their PDIV values for the range of 1 to 5 bar (abs) pressure using the hemispherical rod-plane configuration with a 5 mm needle on the HV electrode.

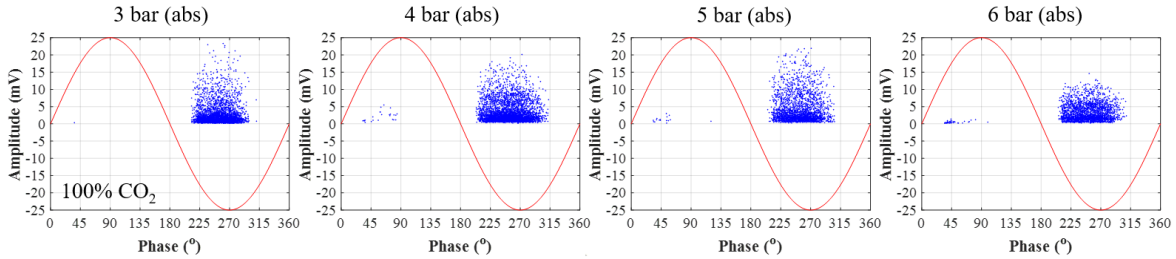

Figure 5-21. PRPD patterns comparing CO_2 for 3-6 bar (abs) at 200% PDIV to illustrate its PRPD behaviour using the hemispherical rod-plane configuration with a 5 mm needle on the HV electrode.

Figure 5-22 illustrates the PD activities for pure C_3F_7CN at 1 bar (abs) at different voltage levels. Tests for pure C_3F_7CN gas at high pressures cannot be performed due to its high boiling point limitation. The figure shows that pure C_3F_7CN demonstrates a similar PD performance to the C_3F_7CN/CO_2 gas mixture where PDs start on the negative half-cycle and shift to the positive with higher voltages. This shows that the different PD behaviour, relative to SF_6, observed in the PRPD patterns for the 20% C_3F_7CN / 80% CO_2 gas mixture can be caused by both C_3F_7CN and CO_2 gases. Positive PDs most probably arise due to the use of C_3F_7CN while negative PDs are a result from both gases. This suggests that the PD behaviour in PRPD patterns can potentially be affected by the type of gas being used and should be taken into consideration for future condition monitoring using SF_6-alternatives.

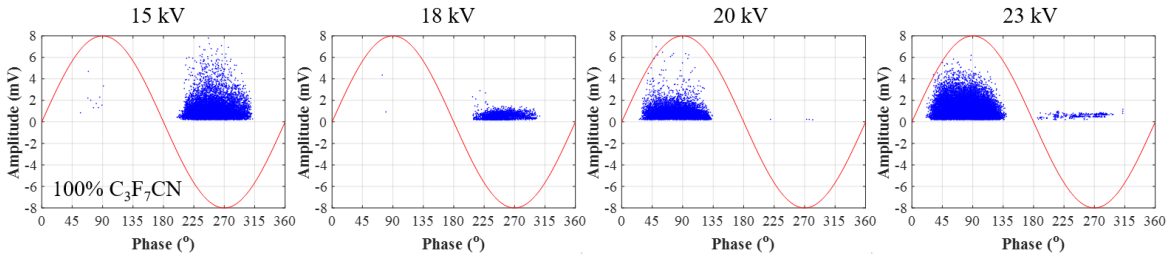

Figure 5-22. PRPD patterns comparing C_3F_7CN at 1 bar (abs) for different voltage levels to illustrate its PRPD behaviour using the hemispherical rod-plane configuration with a 5 mm needle on the HV electrode.

According to [28], [100], when a needle is attached on the HV conductor of a GIB there are three distinct phases in which corona discharges can develop in gas insulating mediums with increasing voltage:

1. Inception: This is the phase when the first discharges, of very low magnitude (approximately 0.5 to 1 pC), are initiated after the PDIV is exceeded. These low-level pulses appear on the negative half-cycle of the waveform.
2. Streamer: Higher voltages lead to a phase where streamers start to form and give rise to PD activities on the positive half-cycle. At the same time negative PDs still exist but are becoming more sporadic. Note that these streamers, under these experimental conditions, will not yet lead to a breakdown.
3. Leader: Further increase in the applied voltage leads to the final phase of the PD development process. With increasing voltage, larger discharges occur on the positive half-cycle of the AC waveform which indicates the formation of leaders. When leaders are present, there is a much higher probability of breakdown than phase two.

Figures 5-20 and 5-22 show that the pure C_3F_7CN and the 20% C_3F_7CN / 80% CO_2 gas mixture appear to go through all three phases of corona discharge development using this electrode configuration. In contrast, the strong attachment coefficient of SF_6 seems to inhibit the low magnitude streamer formation and could possibly go straight to the leader phase due to the short gap being used. Due to its electronegative nature, SF_6 has the ability to suppress PDs up to a critical threshold very effectively. However, once its critical field is exceeded, ionisation can build up rapidly and result in large magnitude discharges on the positive half-cycle. However, pure C_3F_7CN and the 20% C_3F_7CN / 80% CO_2 gas mixture both contain carbon elements in their molecular structure which is a weakly attaching element. This could potentially initiate ionisation activities at lower voltages and lead to all three phases of

corona discharges. As the voltage increases, low level-discharges and streamers develop into leaders and C_3F_7CN starts behaving similar to SF_6. This could also relate to the fact that SF_6 has been observed to have higher peak-to-peak signals once the PDIV value is exceeded. SF_6 has been noticed to go through the same 3-phase transition stage when tested in actual GIL/GIB equipment which means that the gap size between the HV and the grounded part could also influence the PRPD pattern behaviour of the gas [28].

The assumption that SF_6 can have higher magnitude discharges than the 20% C_3F_7CN / 80% CO_2 gas mixture can be further reinforced by the damage sustained on the test needle after the experiments. Figure 5-23 shows that the needle shape, when testing with the C_3F_7CN/CO_2 gas mixture, is more or less preserved after the experiments have finished. In contrast, the needle tested with SF_6 looks severely damaged and it also has a red colour deformation. However, the red colour deformation could also be attributed to the fact that tungsten might chemically react more with SF_6 than with the C_3F_7CN/CO_2 gas mixture.

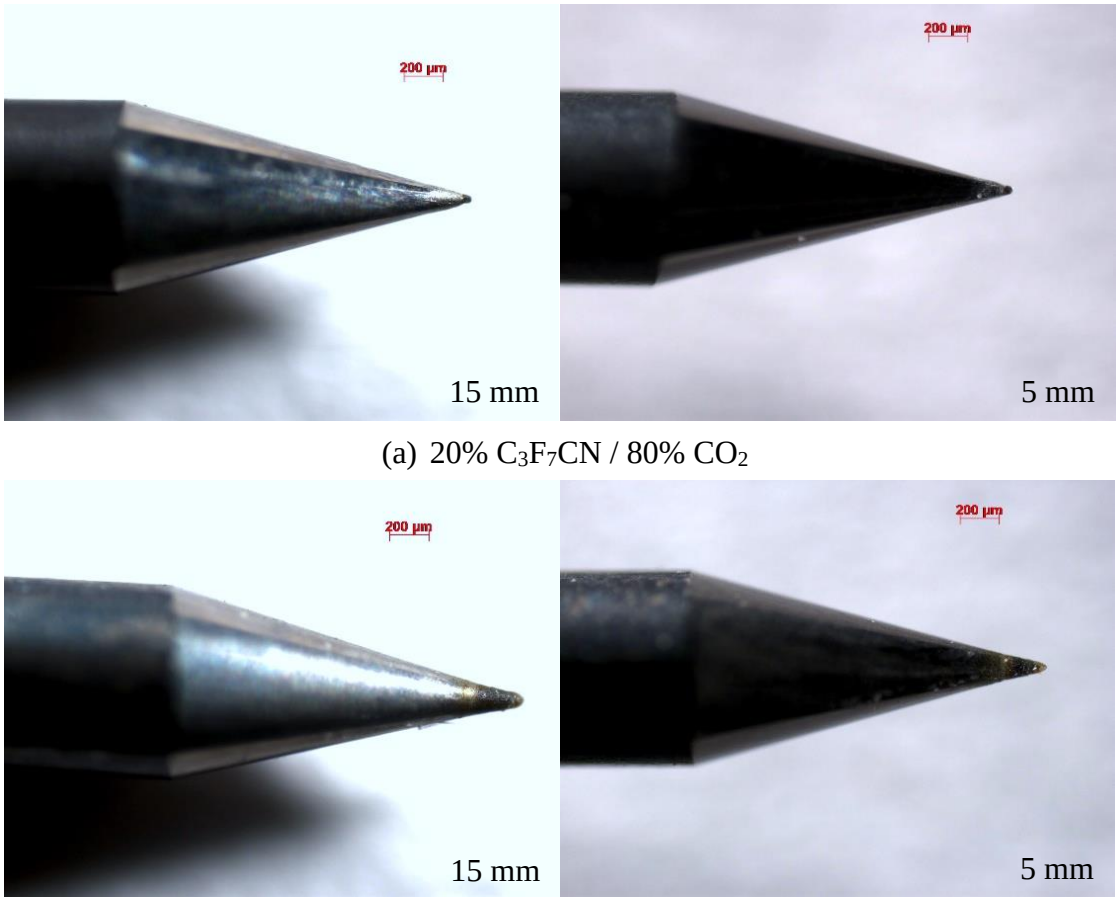

(a) 20% C_3F_7CN / 80% CO_2

(b) SF_6

Figure 5-23. Used needles microscope images for (a) 20% C_3F_7CN / 80% CO_2 and (b) SF_6.

5.4 Results of Plane-plane Electrode Configuration

5.4.1 Effect of Pressure, Gas Type, Defect Location and Field Uniformity on the PDIV and PDEV Characteristics

Figures 5-24 and 5-25 show the PDIV/EV characteristics as a function of pressure for SF_6 and the 20% C_3F_7CN / 80% CO_2 gas mixture using the plane-plane electrode configuration. Figure 5-24 illustrates the PD characteristics when a 15 mm needle is attached onto the HV plane of the configuration while Figure 5-25 shows the results when the needle is located on the grounded plane. With a *f* value of 0.0029, this plane-needle-plane configuration has a similar field uniformity to the rod-plane electrode configuration, with a needle length of 15 mm (f = 0.0025). This could be the reason of similar PDIV/EV performance, where the 20% C_3F_7CN / 80% CO_2 gas mixture is considerably lower than SF_6. As with the rod-plane configuration, when the needle is attached on the HV plane, the 20% C_3F_7CN / 80% CO_2 gas mixture has shown significant improvement in its PDIV/EV values, relative to SF_6, at 5 bar (abs). This could be attributed to the higher gas density at higher pressures and/or because of a higher absolute volume of C_3F_7CN used within the test object.

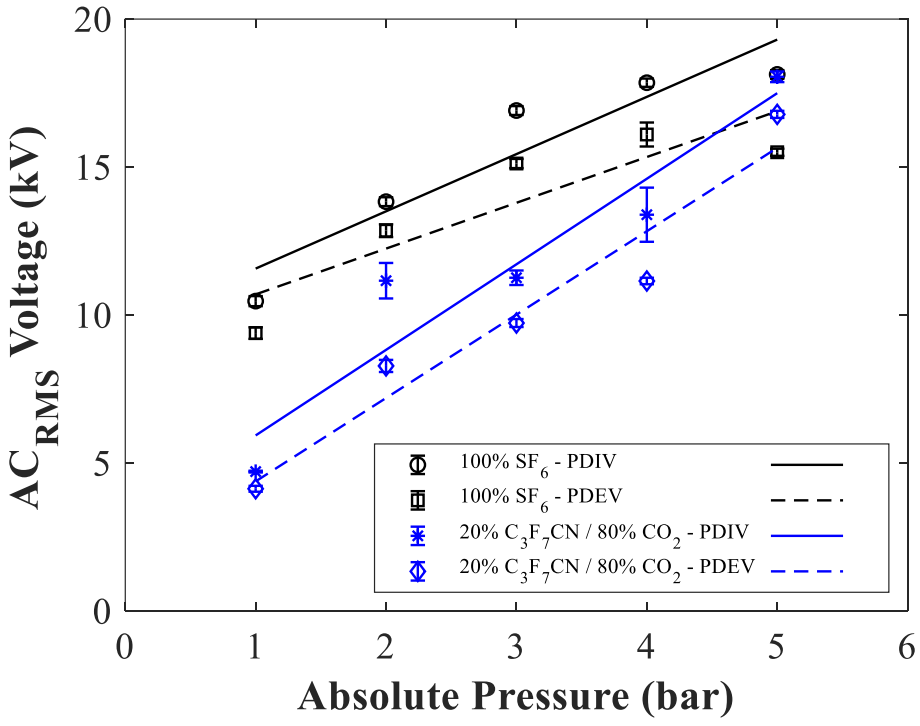

Figure 5-24. AC_{RMS} PDIV and PDEV of SF_6 and 20% C_3F_7CN / 80% CO_2 as a function of absolute pressure using the plane-plane electrode configuration with a needle attached on the HV electrode with a length of 15 mm and a needle-plane gap distance of 10 mm.

Figure 5-25 shows that the PDIV/EV values of the 20% C_3F_7CN / 80% CO_2 gas mixture are considerably lower than SF_6 regardless of the position of the defect. The SF_6 PDIV/EV values are marginally affected with the change in defect location since they are comparable with the HV electrode needle protrusion voltages. However, the 20% C_3F_7CN / 80% CO_2 gas mixture appears to be affected more by the change in defect location and specifically at 5 bar (abs) where it does not improve with the increase in pressure as before. Compared to the protrusion on the HV electrode, the PDIV/EV values for the 20% C_3F_7CN / 80% CO_2 gas mixture slightly decrease which is similar performance to findings reported in [70].

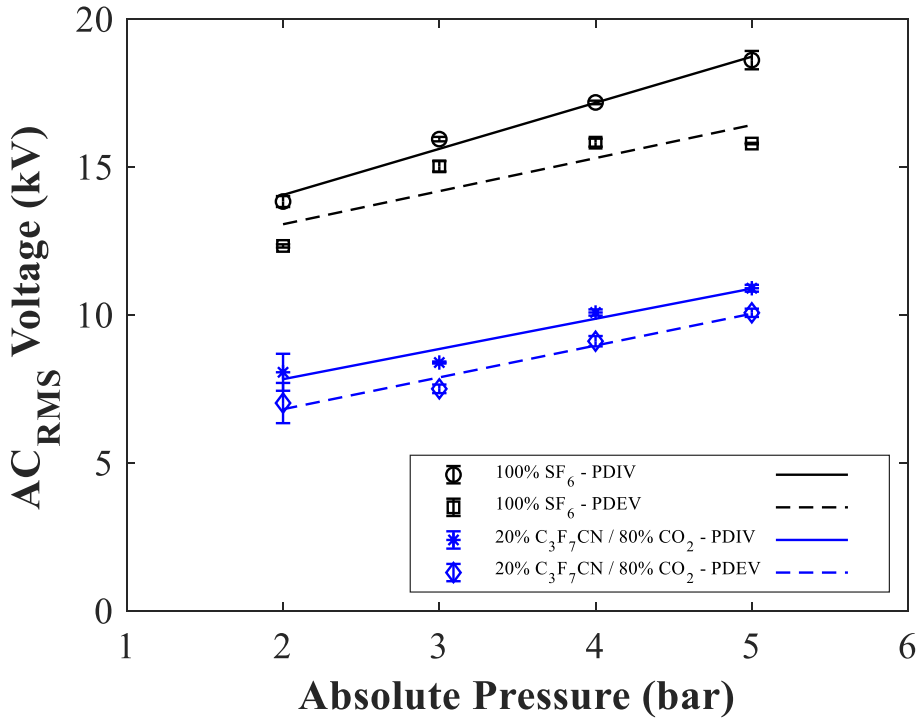

Figure 5-25. AC_{RMS} PDIV and PDEV of SF_6 and 20% C_3F_7CN / 80% CO_2 as a function of absolute pressure using the plane-plane electrode configuration with a needle attached on the ground electrode with a length of 15 mm and a needle-plane gap distance of 10 mm.

Figure 5-26 displays the PDIV/EV characteristics of SF_6 and the 20% C_3F_7CN / 80% CO_2 gas mixture for the plane-plane configuration with a 5 mm needle attached on the HV plane. The combination of the plane electrode and a 5 mm needle provides the most uniform electric field configuration used for PD characterisation with a f value of 0.0043. Based on the previous PD configurations tested in this chapter, it was shown that the 20% C_3F_7CN / 80% CO_2 gas mixture never exceeded the PDIV/EV values of SF_6. However, as shown in Figure 5-26, the PD performance of the 20% C_3F_7CN / 80% CO_2 gas mixture dramatically improved using a relatively more uniform electric field. The usage of a 5 mm needle length with a

plane has resulted to PDIV/EV values of the 20% C_3F_7CN / 80% CO_2 gas mixture to surpass SF_6 at pressures from 2 to 5 bar (abs). This agrees with results reported in [54], [68], where with the usage of a 2 mm needle the PD characteristics of SF_6 and the 20% C_3F_7CN / 80% CO_2 gas mixture were similar at a lower pressure range. At 1 bar (abs), just like with other configurations in this chapter, the gas mixture has almost half the PDIV/EV values of SF_6. However, with increasing pressure, the PDIV/EV values of 20% C_3F_7CN / 80% CO_2 gas mixture significantly increase with the result being higher than SF_6. The results at 1 bar (abs) for the 20% C_3F_7CN / 80% CO_2 gas mixture seem to be unaffected by the change of field uniformity since, regardless of the configuration used, the PDIV/EV values are almost equal. Therefore, future investigation is required to study the PD characteristics of the C_3F_7CN/CO_2 gas mixture at 1 bar (abs) in order to discover the reasons behind this difference with the rest of the pressure values.

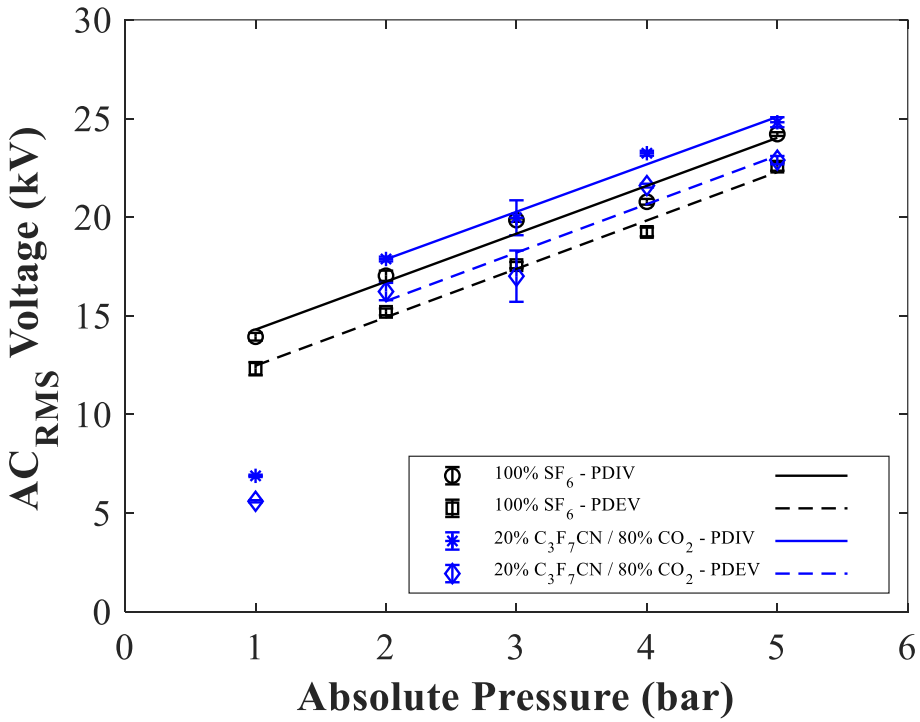

Figure 5-26. AC_{RMS} PDIV and PDEV of SF_6 and 20% C_3F_7CN / 80% CO_2 as a function of absolute pressure using the plane-plane electrode configuration with a needle attached on the HV electrode with a length of 5 mm and a needle-plane gap distance of 10 mm.

As with the rod-plane configuration, Figures 5-27 and 5-28 plot the PDIV and PDEV values for SF_6 and the 20% C_3F_7CN / 80% CO_2 gas mixture separately to demonstrate the effect of changing the needle length from 15 to 5 mm for each gas individually. Using the plane-plane configuration, the PDIV/EV values of SF_6 increase with a reduction in the needle length.

Similarly, the PD performance of the 20% C_3F_7CN / 80% CO_2 gas mixture also improved with the decrease in needle length.

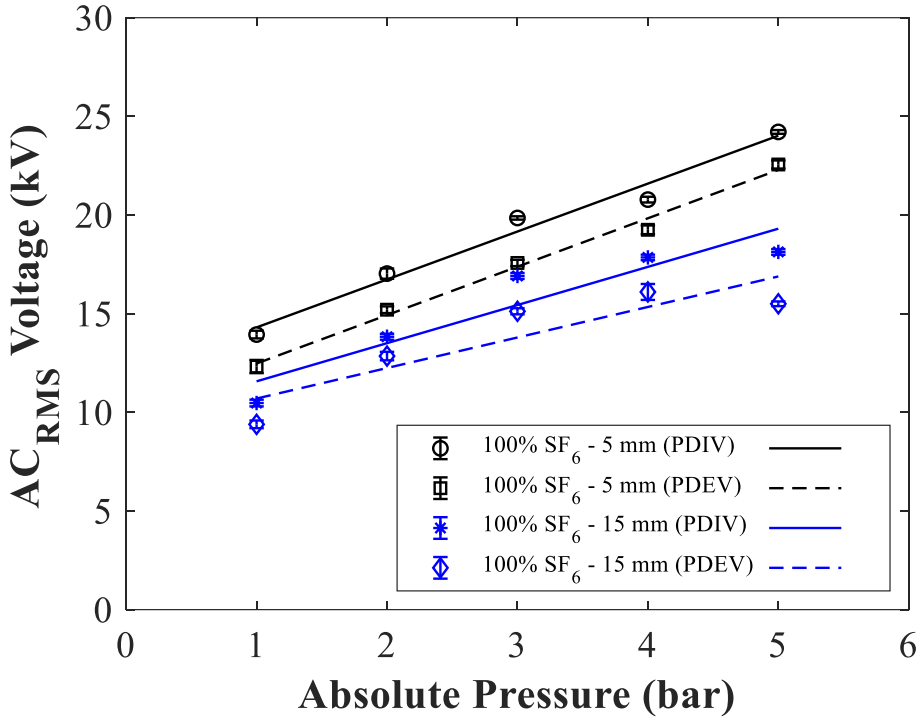

Figure 5-27. AC_{RMS} PDIV and PDEV of SF_6 as a function of absolute pressure using the plane-plane electrode configuration with a needle attached on the HV electrode with 5- and 15-mm lengths.

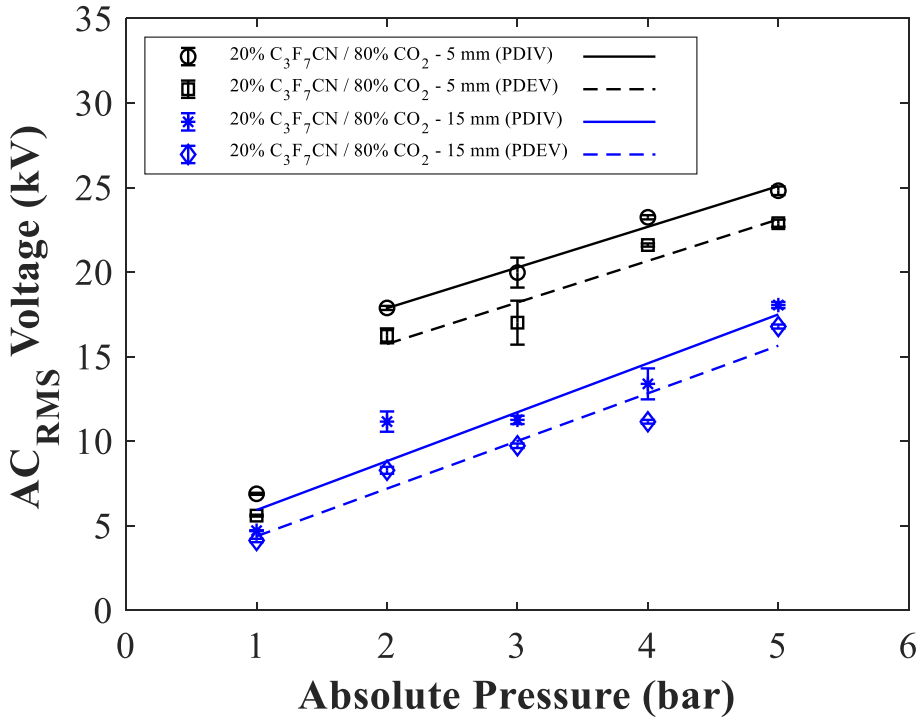

Figure 5-28. AC_{RMS} PDIV and PDEV of 20% C_3F_7CN / 80% CO_2 as a function of absolute pressure using the plane-plane electrode configuration with a needle attached on the HV electrode with 5- and 15-mm lengths.

As before, the 20% C_3F_7CN / 80% CO_2 gas mixture is influenced more with this change than SF_6 which shows that its PD performance is largely affected by a change in field uniformity. These results can also correlate to the breakdown results, shown in Chapter 4, where it was found that the 20% C_3F_7CN / 80% CO_2 gas mixture has comparable strength to SF_6 under more uniform fields (quasi-uniform fields). However, the gas mixture did not have similar performance to SF_6 under non-uniform fields. Unlike when using the rod-plane configuration, SF_6 improves its PD performance considerably with the reduction of needle length. This might be related with the fact that the field uniformity change of reducing the needle length from 15 to 5 mm in the plane-plane configuration (0.0029 to 0.0043) is greater than when using the rod-plane configuration (0.0025 to 0.0033).

5.4.2 PRPD Pattern Analysis

5.4.2.1 Effect of Pressure

Figure 5-29 illustrates the PRPD patters for 20% C_3F_7CN / 80% CO_2 and SF_6 at 20 kV for different pressures in the range of 2 to 5 bar (abs) using the plane-plane configuration with a needle of 15 mm. In general, the PD activities for both gases in this case mostly occur on the positive half-cycle between 45° and 135° phase angles. However, the 20% C_3F_7CN / 80% CO_2 gas mixture appears to have some PD activities on the negative half-cycle as well.

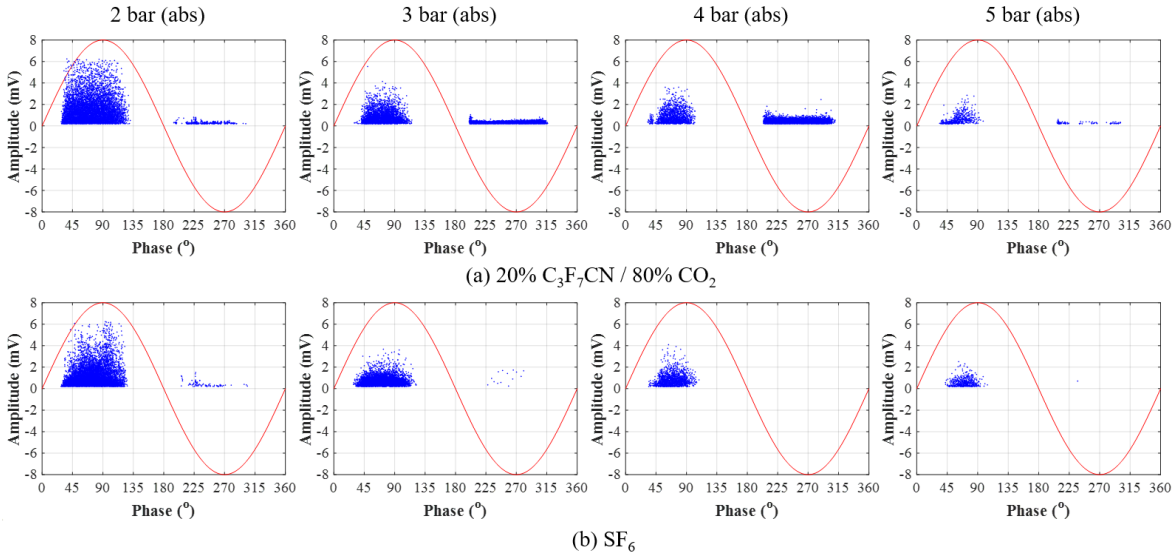

Figure 5-29. PRPD patterns comparing (a) 20% C_3F_7CN / 80% CO_2 and (b) SF_6 at 20 kV for the range of 2 to 5 bar (abs) pressure using the plane-plane configuration with a 15 mm needle on the HV electrode.

Both SF_6 and the 20% C_3F_7CN / 80% CO_2 gas mixture have been observed to suppress the PD activity more effectively with increased pressure. As explained earlier in this chapter, the suppression of PD activities with increasing pressure is expected since the gas density increases, and a higher applied voltage is required to initiate the ionisation process. Figure 5-29 also shows the 20% C_3F_7CN / 80% CO_2 gas mixture having more PDs than SF_6 from 2 to 4 bar (abs) with the exception at 5 bar (abs) where PD activities for both gases look similar. This is expected since the PDIV values of SF_6 are greater than the C_3F_7CN/CO_2 gas mixture in the investigated range except at 5 bar (abs).

5.4.2.2 Effect of Field Uniformity

Figure 5-30 uses PRPD patterns to show the influence of the needle length reduction on the PDs of SF_6 at 5 bar (abs) using the plane-plane configuration. For the 5 mm needle length, 170% PDIV was recorded instead of 200% which was measured for all other configurations. This was done to avoid having a breakdown since the PDIV values at 5 mm plane-plane were higher than the rest of the configurations. As with the rod-plane configuration, PDs mostly occur on the positive half-cycle of the AC waveform with some negative activities occurring at higher voltages such as 150% and 170/200% of their PDIV values.

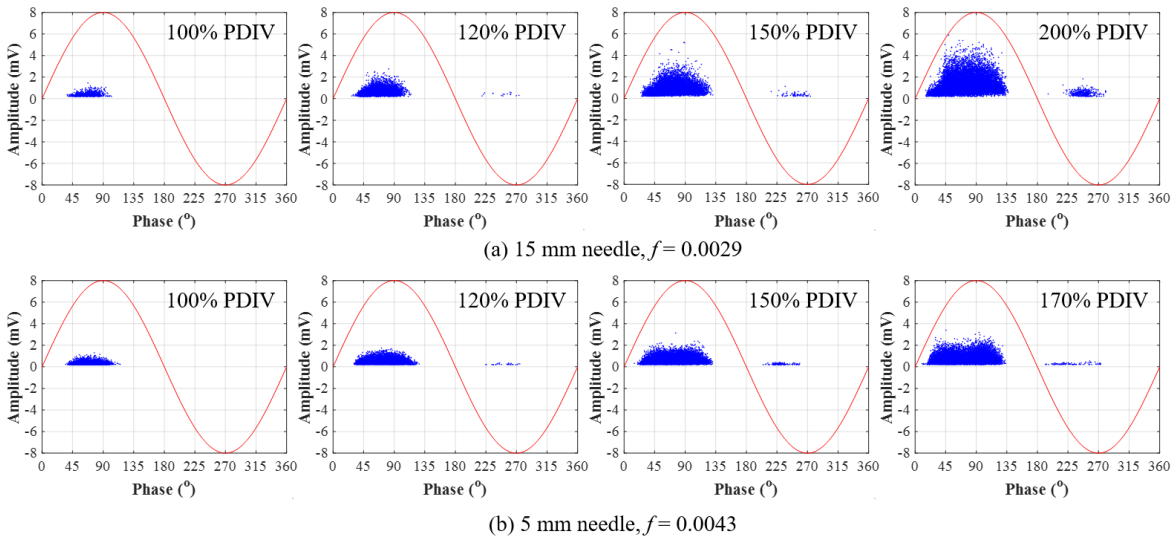

Figure 5-30. PRPD patterns comparing SF_6 with (a) 15 mm and (b) 5 mm needle lengths on the HV electrode at 5 bar (abs) for 100, 120, 150 and 170/200% of its PDIV values using the plane-plane configuration.

Unlike with the rod-plane configuration, Figure 5-30 shows that with the plane-plane there is negligible difference in the magnitude of the signals due to the needle length reduction. A

5 mm needle length still generates lower magnitude signals, and this can be due to the relatively more uniform electric field than the 15 mm needle configuration. No considerable difference was observed in the UHF signals with the plane-plane configuration using different needle lengths.

Figure 5-31 compares the PRPD patterns of the 20% C_3F_7CN / 80% CO_2 gas mixture at 5 bar (abs) for 15- and 5-mm needle lengths using the plane-plane configuration. Figure 5-31(a) shows that PD activities using the 15 mm needle length start on both half-cycles and then transition to the positive half-cycle with higher voltages. This behaviour is similar to the 5 mm rod-plane configuration at 5 bar (abs). This could be due to both the 15 mm plane-plane and 5 mm rod-plane having comparable field uniformities with *f* values of 0.0029 and 0.0033, respectively. Using the 5 mm plane-plane configuration, the C_3F_7CN/CO_2 gas mixture PD behaviour is comparable to SF_6 where discharges start on the positive half-cycle and the activity increases with applied voltage.

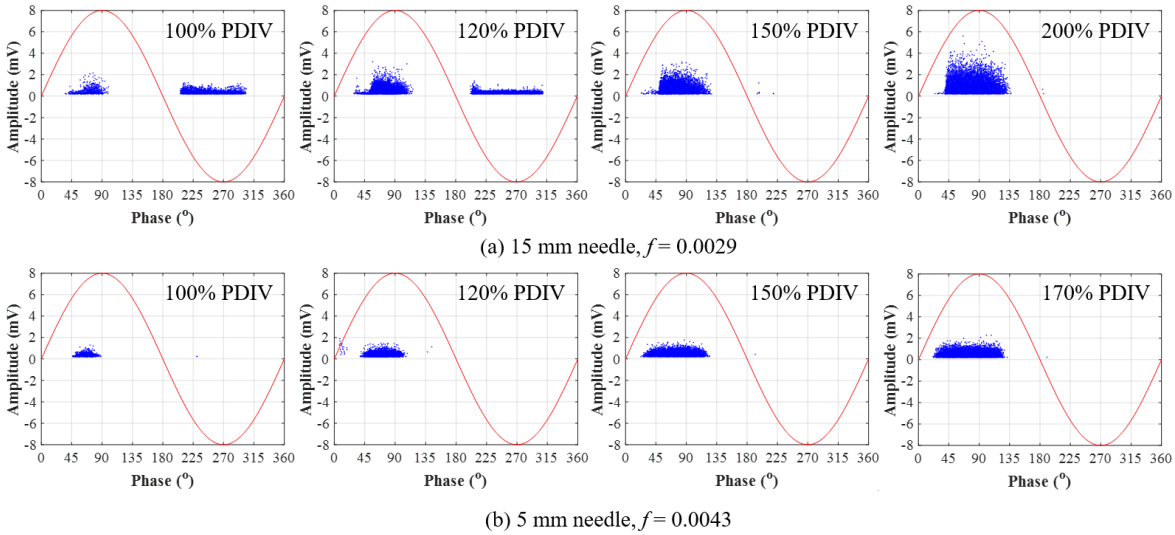

Figure 5-31. PRPD patterns comparing 20% C_3F_7CN / 80% CO_2 with (a) 15 mm and (b) 5 mm needle lengths on the HV electrode at 5 bar (abs) for 100, 120, 150 and 170/200% of its PDIV values using the plane-plane configuration.

5.4.2.3 Effect of Defect Location

Figure 5-32 compares the PRPD patterns for the 20% C_3F_7CN / 80% CO_2 gas mixture and SF_6 at 5 bar (abs) with a 15 mm needle on the grounded electrode of the plane-plane configuration. These PRPD patterns are to examine the reverse behaviour of the gases using

a needle on the grounded electrode. For SF_6, PDs started on the negative half-cycle of the AC waveform with some discharges on the positive half-cycle at higher voltages. For the 20% C_3F_7CN / 80% CO_2 gas mixture, the 3-stage transition phase, described earlier in this chapter, was once more observed. PDs initially started on the positive half-cycle, followed by discharges on both half-cycles and eventually at higher voltages the majority of PD activities occurred on the negative half-cycle.

As shown in Figure 5-32, by placing the needle on the grounded electrode the exact opposite PRPD pattern to the HV electrode is recorded for both gases. That means that the majority of PD activities occur when electrons are attracted to the vicinity of the needle regardless of its position. In the case of a needle on the HV plane, when the polarity of the AC waveform is positive, electrons are attracted to the vicinity of the needle where ionisation is greater and PD activities are more likely to develop. When the polarity is negative, electrons are repelled away from the needle to the low field area where they can be effectively captured by the insulation gas and therefore suppress PD activities. The discharge mechanism works similarly when the needle is placed on the grounded electrode. With a negative polarity of the HV electrode, electrons are repelled towards the high field area of the needle region resulting in PDs. With a positive polarity, electrons are attracted to the low field area which in turn results to lower activities on the positive half-cycle of the waveform.

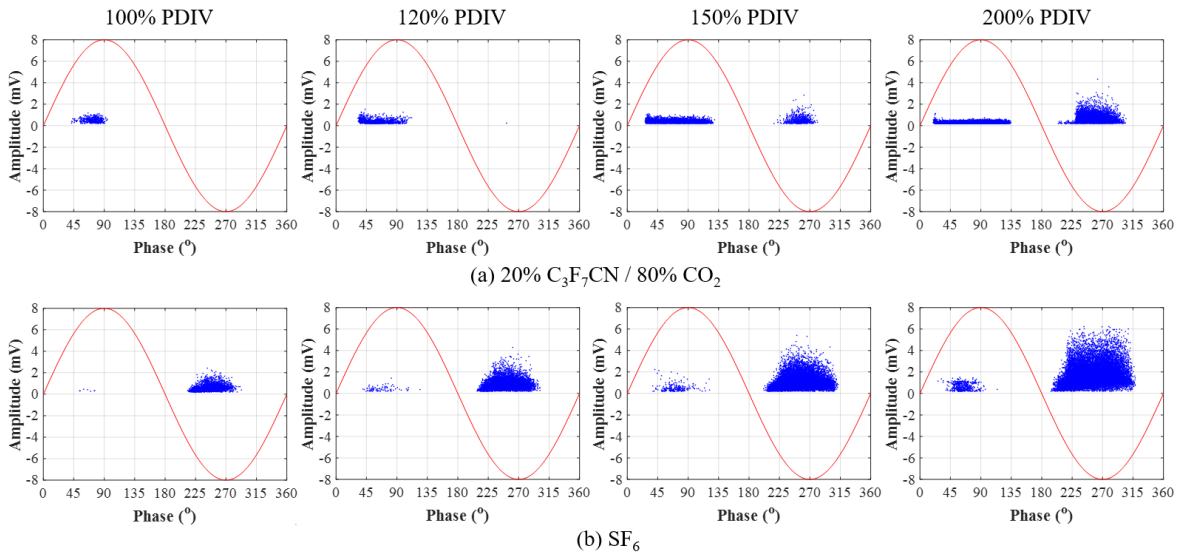

Figure 5-32. PRPD patterns comparing (a) 20% C_3F_7CN / 80% CO_2 and (b) SF_6 at 5 bar (abs) pressure at 100, 120, 150 and 200% of their PDIV values using the plane-plane configuration with a 15 mm needle on the grounded electrode.

This behaviour, however, varies depending on the gas insulation being used since it has been observed that SF_6 and the C_3F_7CN/CO_2 gas mixture have different characteristics in their PRPD patterns.

5.4.2.4 Effect of Gas Medium

Figures 5-33 and 5-34 illustrate the PRPD patterns recorded for SF_6 and 20% C_3F_7CN / 80% CO_2 gas mixture in the pressure range of 1-5 bar (abs) using the plane-plane configuration with a 5 mm needle attached on the HV electrode.

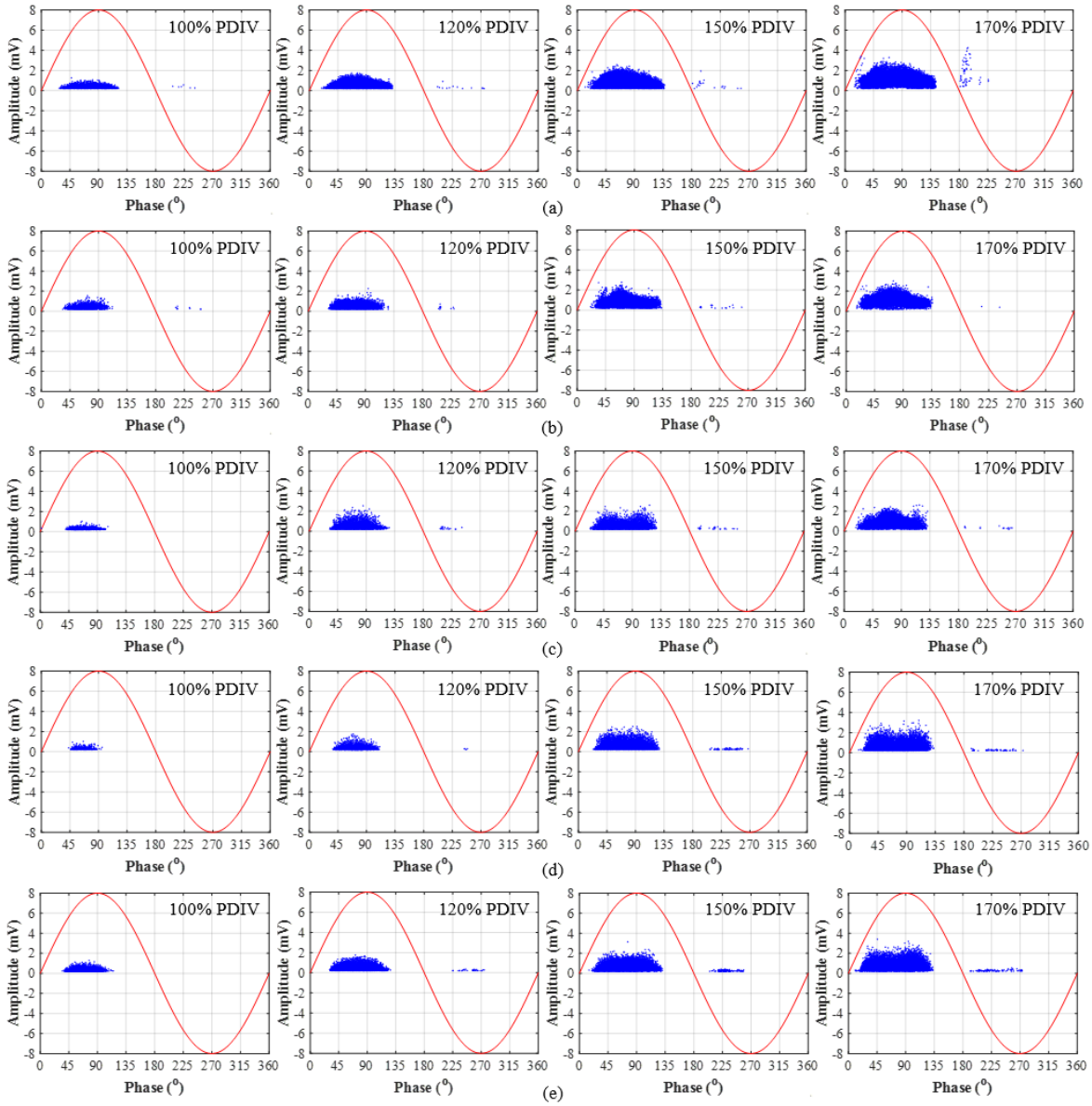

Figure 5-33. PRPD patterns comparing SF_6 at 100, 120, 150 and 170% of its PDIV values at (a) 1 bar (b) 2 bar (c) 3 bar (d) 4 bar and (e) 5 bar (abs) pressure using the plane-plane configuration with a 5 mm needle on the HV electrode.

Figure 5-33 shows that regardless of pressure and voltage magnitude, the majority of PDs for SF_6 occur on the positive half-cycle with some negative activities at higher voltages. The same observation has been made for all other configurations used in this chapter, which shows that the PRPD behaviour of SF_6 is not affected by field uniformity, pressure or voltage magnitude. When electrons are repelled towards the low field region, during the negative polarity of AC waveform, they are effectively captured by SF_6 molecules thereby minimising PD activities.

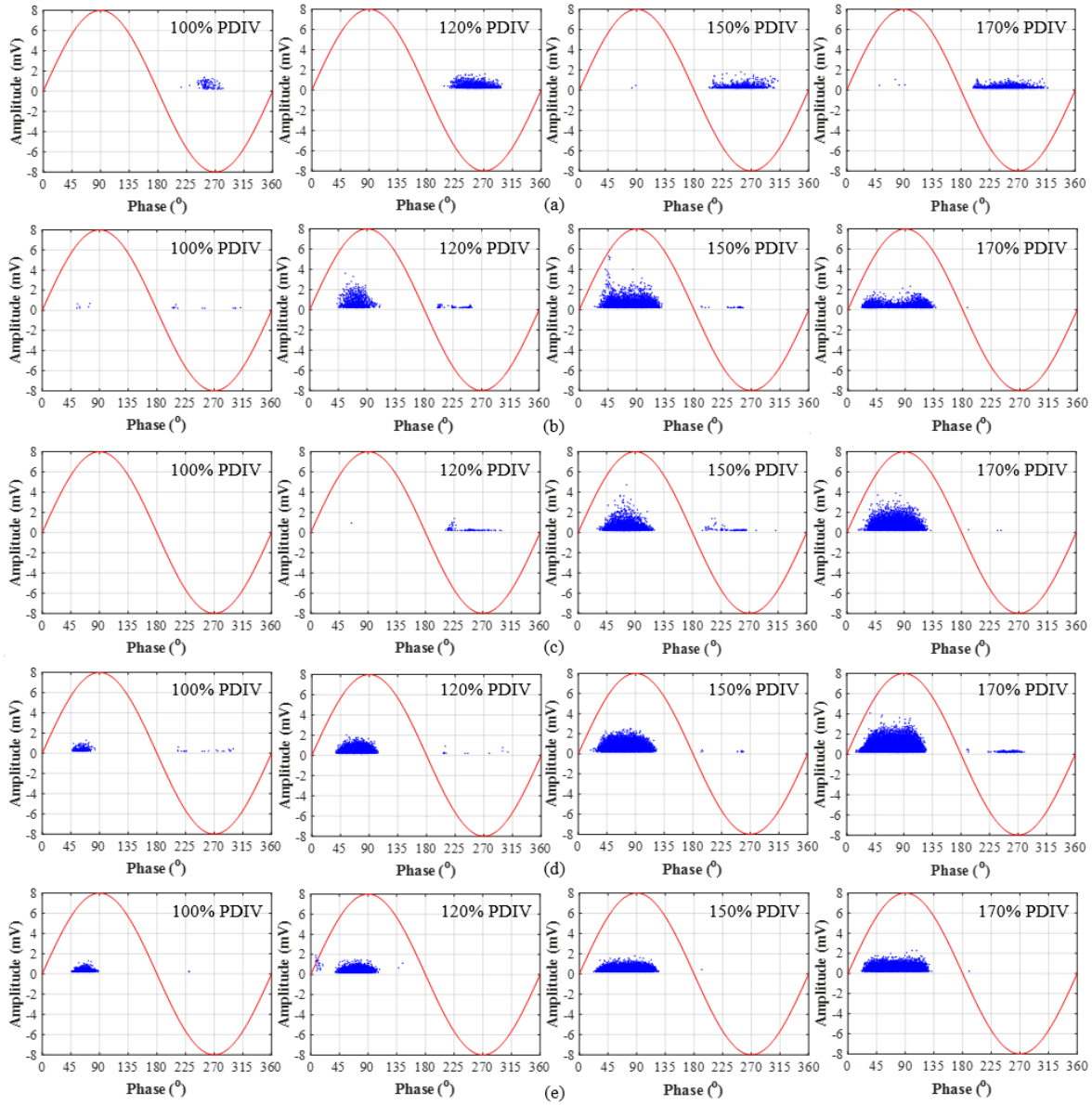

Figure 5-34. PRPD patterns comparing 20% C_3F_7CN / 80% CO_2 gas mixture at 100, 120, 150 and 170% of its PDIV values at (a) 1 bar (b) 2 bar (c) 3 bar (d) 4 bar and (e) 5 bar (abs) pressure using the plane-plane configuration with a 5 mm needle on the HV electrode.

Figure 5-34 shows that, with the exception of 1 bar (abs), the 20% C_3F_7CN / 80% CO_2 gas mixture behaves very similar to SF_6 using the plane-plane configuration with a 5 mm needle attached on the HV electrode. These PRPD patterns contradict the ones recorded from the rest of the electrode configurations used in this chapter with the 20% C_3F_7CN / 80% CO_2 gas mixture. For all cases, excluding the 15 mm rod-plane at 5 bar (abs), the PDs in the PRPD patterns appear to start on the negative half-cycle and with an increasing voltage to shift to the positive half-cycle via the 3-stage transition phase described earlier in this chapter. This is an indication that voltage magnitude, field uniformity and pressure/density can influence the PRPD pattern behaviour of the 20% C_3F_7CN / 80% CO_2 gas mixture.

5.5 Discussion

The PD results from this chapter, using varying electric field uniformities, are significantly important for the retro-fill of an alternative gas mixture in existing GIL/GIB equipment. The probability of having a protrusion with a length of 5 and 15 mm in GIL/GIB is considered extremely rare. Usually, imperfections in practical GIL/GIB are smaller than the tested scenarios but these specific needle lengths were tested to assess the behaviour of the 20% C_3F_7CN / 80% CO_2 gas mixture in comparison to SF_6 in the presence of extreme electric field enhancements. As shown from the results, under highly divergent fields (15 mm needle) the gas mixture behaves poorly in comparison to SF_6 but when the needle length is reduced, and the field uniformity is increased, its PD performance significantly improves. The PD performance of the C_3F_7CN/CO_2 gas mixture, however, needs to be validated in full-scale GIL/GIB equipment which will be shown on a later stage in this thesis.

As described earlier in this chapter, the 3-stage transition phase of the PRPD pattern behaviour, which was found for the C_3F_7CN/CO_2 gas mixture, can be associated with voltage magnitude and the development of streamers and leaders [28], [100]. However, as shown in this chapter, this can be further influenced by field uniformity, pressure/density as well as the gas medium since the 20% C_3F_7CN / 80% CO_2 gas mixture has a different PRPD behaviour to SF_6.

As mentioned before, pressure/density, field uniformity as well as voltage magnitude have no effect on SF_6 gas using small gaps since the PDs predominantly occur on the positive

half-cycle of the AC waveform. However, the 20% C_3F_7CN / 80% CO_2 gas mixture was found to behave differently to SF_6 with field uniformity, pressure/density and voltage magnitude having an effect on its PD behaviour. Taking all the PRPD patterns recorded into consideration, several observations have been found to affect the PD behaviour of the C_3F_7CN/CO_2 gas mixture:

- Voltage magnitude appeared to make a difference as in many cases the negative activities started at 100% PDIV values but they shift to the positive half-cycle with an increasing voltage up to 200% PDIV. This, as explained earlier, could be occurring because of low magnitude PDs at 100% PDIV but as voltage increases, and the development of streamers and leaders progresses, the PDs shift to the positive half-cycle.
- Field uniformity has been observed to affect the 3-stage transition phase of the gas mixture. With field uniformities of f values less than 0.0033, the transition phase occurred for almost all investigated pressures. Once this critical f value was exceeded, where only the 5 mm plane-plane configuration (f = 0.0043) does that, the C_3F_7CN/CO_2 gas mixture was able to suppress PD activities more effectively and this was demonstrated by the PDIV/EV values. Better PDIV/EV values for C_3F_7CN/CO_2 gas mixture were also associated with positive PD activities occurring within the range of 2-5 bar (abs). This shows that with more uniform fields, where 20% C_3F_7CN / 80% CO_2 has the ability to suppress PDs like SF_6, the PRPD patterns for the gas mixture start to appear SF_6-alike.
- Pressure or gas density have shown to influence the PD performance and PRPD pattern of the 20% C_3F_7CN / 80% CO_2 gas mixture. The gas mixture has demonstrated susceptibility to PDs at 1 bar (abs) where PDIV/EV values were consistently half of corresponding SF_6 values, regardless of field uniformity. This has also been associated with the PRPD patterns at 1 bar (abs) to be dominated with PDs on the negative half-cycle.

From the above observations, it can be derived that the PD behaviour of the 20% C_3F_7CN / 80% CO_2 mixture, unlike SF_6, can be influenced from factors such as field uniformity and pressure/density which is also reflected in its PRPD patterns. Highly divergent fields at lower pressures can initiate PD activities on the negative half-cycle of the AC waveform which was not observed in SF_6. The presence of negative PD activities could be correlated to lower

PDIV/EV values relative to SF_6. This is because the only electrode configuration that the 20% C_3F_7CN / 80% CO_2 gas mixture had comparable PD performance to SF_6 was the 5 mm plane-plane where PRPD patterns were dominated by positive PD activities. A reason for the gas mixture to be affected more from pressure/density and field uniformity could be the presence of weakly electronegative carbon molecules, as the C_3F_7CN/CO_2 gas mixture is predominantly filled with CO_2, which can result to PDs initiated at lower voltages than SF_6 which is a purely electronegative gas.

5.6 Summary

The PD characteristics of SF_6 gas and the 20% C_3F_7CN / 80% CO_2 gas mixture were experimentally investigated in this chapter using two external UHF sensors attached onto the viewing windows of the pressure vessel. Full bandwidth scans were carried out, over the range of 300-2000 MHz, which have shown that the two gases display the best signal-to-noise ratio PDs around 1050 to 1100 MHz. Therefore, PRPD measurements in this chapter were focused for the frequency range of 1050-1150 MHz.

PD behaviour for SF_6 and the 20% C_3F_7CN / 80% CO_2 gas mixture were compared using their PDIV and PDEV values. The characterisation was carried out using two different electrode configurations, namely plane-plane and rod-plane and two needle lengths of 5 and 15 mm, to vary the field uniformity from divergent to highly divergent. In general, SF_6 has shown to have higher PDIV and PDEV values than the 20% C_3F_7CN / 80% CO_2 gas mixture. Results have shown that the 20% C_3F_7CN / 80% CO_2 gas mixture can be more sensitive to highly divergent fields than SF_6 for the pressure range of 1-4 bar (abs). However, at 5 bar (abs), the 20% C_3F_7CN / 80% CO_2 gas mixture was found to reduce the difference in PDIV/EV values to SF_6 which indicates that it can perform better at higher pressures. Additionally, using a 5 mm needle on the HV electrode of the plane-plane configuration, which is the most uniform electrode arrangement in this chapter, has resulted in a significant improvement in the PD characteristics of the 20% C_3F_7CN / 80% CO_2 gas mixture relative to SF_6. The PDIV/EV values of the 20% C_3F_7CN / 80% CO_2 gas mixture under more uniform fields were found to exceed SF_6 in the pressure range of 2-5 bar (abs). This shows that the SF_6-alternative can potentially suppress PD activities equally well to SF_6 when having points

of electric field enhancement on the HV conductor in a high-pressure environment as found in practical GIL/GIB equipment.

Finally, SF_6 and 20% C_3F_7CN / 80% CO_2 were found to behave differently in their PRPD patterns at more non-uniform fields and lower pressure/density values. Most of the PD activity for SF_6 occurred on the positive cycle with a few discharges on the negative cycle at higher voltages, regardless of the field uniformity and pressure/density being used. On the contrary, the PRPD patterns using the 20% C_3F_7CN / 80% CO_2 gas mixture were significantly influenced by voltage magnitude, field uniformity and gas pressure/density. For more non-uniform fields and lower pressures, PD activities of the 20% C_3F_7CN / 80% CO_2 gas mixture started on the negative cycle and switched to the positive cycle at higher voltages when the needle was located on the HV electrode. A reverse behaviour was observed with a needle on the grounded electrode. A 3-stage transition behaviour was generally noticed when the applied voltage, pressure/density and field uniformity was changed for the 20% C_3F_7CN / 80% CO_2 gas mixture. This shows that different gas types, and more specifically a mixture of strong and weakly attaching gases such as C_3F_7CN and CO_2, can react otherwise with their PRPD patterns under varying conditions. This should be taken into consideration for future condition monitoring diagnostics, in case SF_6-alternatives are being used in high voltage equipment.

Chapter 6 Retro-fill Investigation of a GIB Demonstrator Rated for Transmission Voltages

6.1 Introduction

The purpose of this retro-fill investigation is to explore the feasibility of replacing SF_6 in existing GIL/GIB assets in the power network with a more environmentally friendly gas medium. Retro-filling is a time-saving and cost-efficient solution as only two major procedures have to be carried out on the equipment: (i) extraction of SF_6 from GIL/GIB assets and (ii) refill of equipment with the 20% C_3F_7CN / 80% CO_2 gas mixture. For a retro-fill investigation, two important studies have to be taken into consideration: (i) electrical type tests according to the International Electrotechnical Commission (IEC) standards using full-scale, SF_6-designed GIL/GIB equipment filled with the 20% C_3F_7CN / 80% CO_2 gas mixture and (ii) material compatibility tests for the new gas mixture with materials commonly found in full-scale GIL/GIB equipment, such as elastomer gaskets.

Type tests, or withstand voltage tests, on assets are usually performed to verify if the new product meets the IEC standard requirements. Equipment undergoes lightning impulse (LI), switching impulse (SI), power frequency (AC) and PD type tests prior to commissioning them to the network. Although breakdown voltage and PD characteristics tests provide useful information about an alternative insulation material, such as C_3F_7CN, it cannot be proposed as a potential solution unless it has passed the required type tests on practical equipment. National Grid plc, the transmission operator of Great Britain, uses 550 kV rated GIB equipment for the 400 kV England and Wales transmission network. To investigate the technical viability of the 20% C_3F_7CN / 80% CO_2 gas mixture, the new gas mixture was retro-filled in a full-scale GIB demonstrator and subjected to type tests. This can establish a level of confidence that the new gas mixture can indeed be retro-filled in SF_6-designed GIB in UK substations. This chapter focuses on three main investigations: (i) conduct type tests using a 420/550 kV, SF_6-designed GIB demonstrator filled with SF_6 and then 20% C_3F_7CN / 80% CO_2 gas mixture (ii) perform a material compatibility study for C_3F_7CN with a

common gasket material used within the gas-insulated equipment, and (iii) assess the impact of replacing SF_6 with the 20% C_3F_7CN / 80% CO_2 gas mixture in the UK transmission network and the overall carbon emission reduction.

6.2 Experimental Setup and Test Techniques

6.2.1 AC and Impulse Generators Test Setup

Power system assets, during type tests, are subjected to waveforms representing operational overvoltages as well as external and internal transients. Operational overvoltages, which stress the insulation under special circumstances such as light or no-load conditions, are tested through Power Frequency or AC waveform. External overvoltage transients can arise with lightning strike events on the network while internal transients are generated from connecting and disconnecting parts of the network through the occurrence of fault in the system [21], [27]. External and internal overvoltage transients are tested using lightning and switching impulses respectively. AC and impulse voltages were generated with the 800 kV High Volt and 2 MV Haefely generators described in Chapter 4.

Figure 6-1 shows the test circuit diagram including the AC and impulse generators. The same circuit diagram used for the breakdown tests was also implemented for the withstand voltage tests. The setup involved the full-scale GIB demonstrator, voltage dividers and measuring and control units. For the withstand voltage experiments the following voltage waveforms were used with tolerances as defined in BS EN/IEC 60060-1:2010:

- Standard AC (50 Hz) voltage waveform with ±1% of test voltage
- Switching Impulse (SI) [250 (±20%) / 2500 (±60%) μs] with ±3% of test voltage
- Lightning Impulse (LI) [1.2 (±30%) / 50 (±20%) μs] with ±3% of test voltage

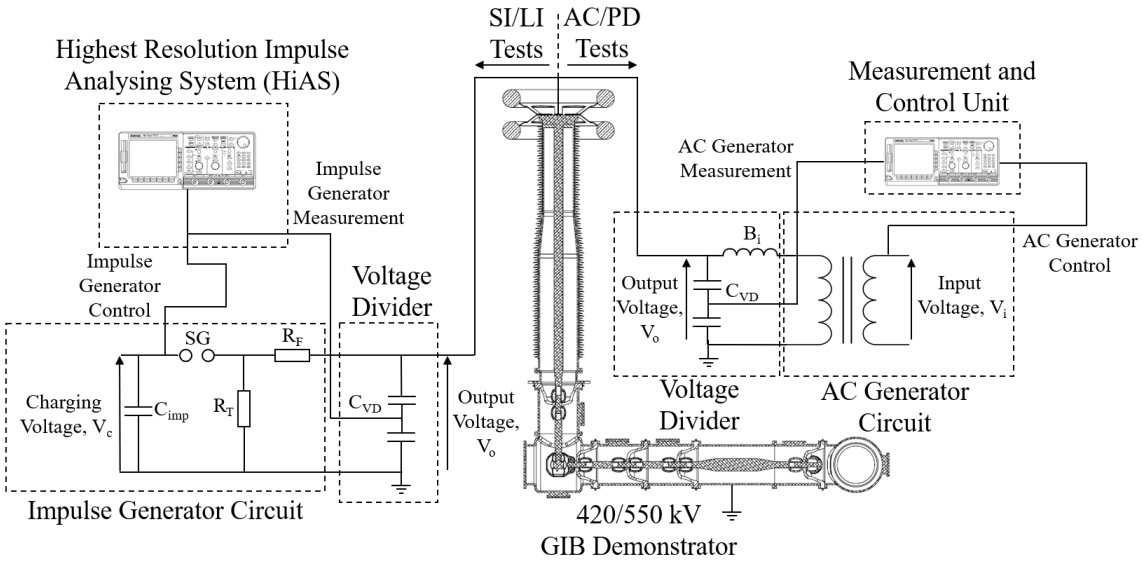

Figure 6-1. Type tests circuit diagram including the impulse and AC generator circuits.

6.2.2 Full-scale Demonstrator for Withstand Type Tests

Figure 6-2 illustrates the full-scale 420/550 kV GIB demonstrator setup used for the type tests in this thesis. Figures 6-2(a), (b) and (c) show the GIB demonstrator in individual components before being assembled and Figure 6-2(d) shows the assembly process. As shown in Figure 6-2(d), special caution was taken with the assembly of the demonstrator in order to avoid any damage on the conductor. All the components were vacuumed and cleaned thoroughly with isopropyl alcohol prior to assembly to prevent any contamination impurities.

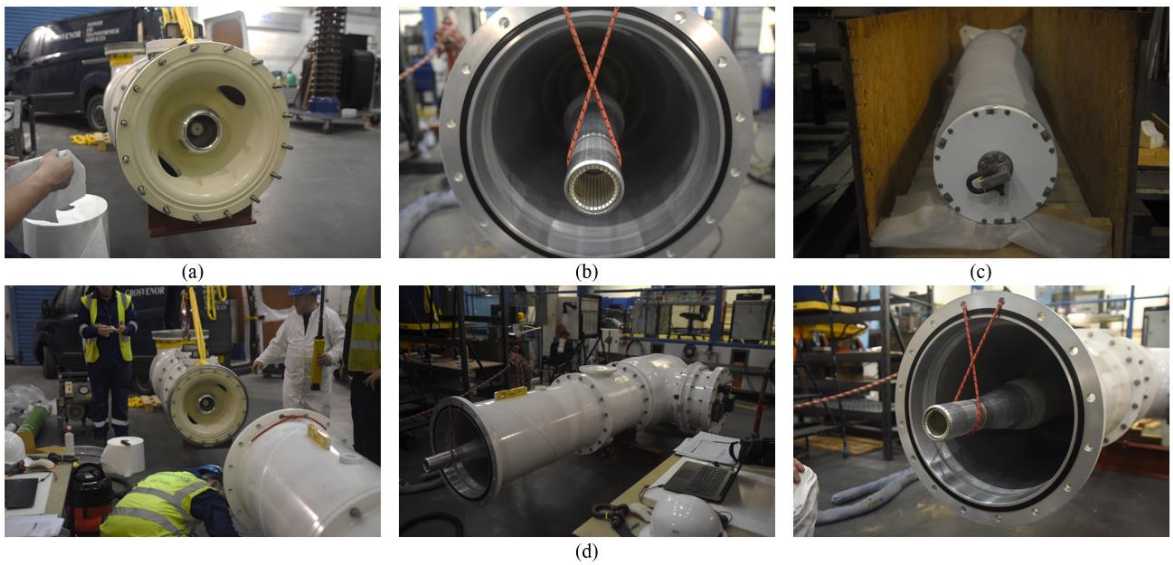

Figure 6-2. GIB demonstrator setup (a) insulating spacer (b) straight conductor section (c) HV bushing and (d) demonstrator assembly process.

After establishing the margin between pure SF_6 gas and C_3F_7CN/CO_2 mixtures in terms of breakdown performance and PD characteristics, the most technically viable mixture was the 20% C_3F_7CN / 80% CO_2 gas mixture, which was then retro-filled in the full-scale GIB demonstrator for type tests.

The 3D design of the full-scale 420/550 kV GIB demonstrator used is shown in Figure 6-3. As shown in Figure 6-3, the GIB demonstrator is separated into the bushing and the test zones using a non-permeable conical insulator. The bushing zone was always filled with SF_6 gas while the test zone was initially filled with SF_6 to validate the test setup and establish a benchmark prior to testing with the 20% C_3F_7CN / 80% CO_2 gas mixture. A rated operating pressure of 4.5 bar (abs) was set in both zones. The GIB was equipped with DN20 DILO gas filling points for carrying out the gas handling procedures. Elfab bursting discs, or pressure safety discs, rated at 7.6 bar (abs) are embedded onto the demonstrator for protection in the case of an over-pressurisation failure. Two corona rings were used to minimise corona activities at the top of the bushing and reduce external PD activity.

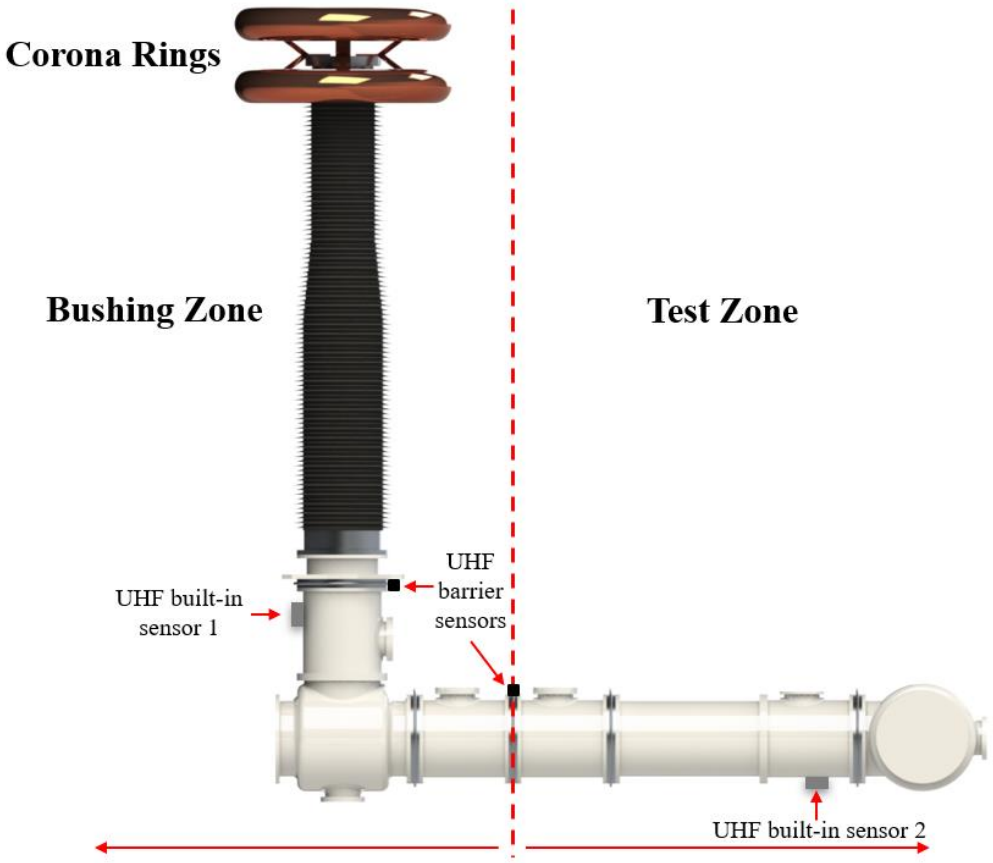

Figure 6-3. 3D design of the 420/550 kV GIB demonstrator with location for the UHF sensors.

For measuring PD monitoring, Areva built-in UHF PD couplers with a bandwidth of 200-1500 MHz were incorporated into the GIB demonstrator. Two additional external UHF sensors, described in Chapter 5, with a bandwidth of 300-2000 MHz were attached on the external enclosure of the GIB insulators [95]. The positions of the built-in and the barrier UHF sensors are shown in Figure 6-3. As described in Chapter 5, the expected frequencies of discharges for PD activities in insulating gases are in the GHz range. To measure these signals during the type tests, a Lecroy ultra-wide band oscilloscope with a bandwidth of 8 GHz was used. Prior to testing, a sensitivity verification procedure was performed using one UHF sensor as a transmitter and the remaining three sensors as receivers. Figure 6-4 shows the AC generator setup connected to the GIB demonstrator for testing.

Figure 6-4. 800 kV AC generator test setup connected to the 420/550 kV GIB demonstrator.

Figure 6-5 shows the Haefely Impulse generator connected to the 420/550 kV GIB demonstrator. Note that for the type tests, all ten stages of the impulse generator were connected to generate voltages up to 2 MV. Using the same impulse generator, by changing the resistor values, the voltage waveform could be altered to test both SI and LI.

Figure 6-5. 2 MV Impulse generator test setup connected to the 420/550 kV GIB demonstrator.

6.2.3 BS EN/IEC Standards Type Tests Procedures

Withstand type tests were conducted according to the following BS EN/IEC standards [90], [101]–[103]:

- BS EN/IEC 60060-1: 2010 [90]
- BS EN/IEC 62271-1: 2011 [101]
- BS EN/IEC 62271-204: 2011 [102]
- BS EN/IEC 62271-203: 2012 [103]

LI, SI, PD and AC type tests were carried out. As the equipment is rated for 420 and 550 kV, both voltage levels were type tested for the 20% C_3F_7CN / 80% CO_2 mixture. Test procedures for all voltage waveforms are shown below in Table 6-1.

Table 6-1. Type tests procedures for the full-scale GIB demonstrator.

Test	Description	Test Conditions and Pass Criteria
AC withstand voltage test	Maintain U_d for 1 min	U_d = 650 kV (U_r = 420 kV) U_d = 710 kV (U_r = 550 kV) No breakdown
AC + partial discharge test	$U_{pre\text{-}stress} = U_d$ for 1 min $U_{pd\text{-}test} = 1.2\ U_r / \sqrt{3}$ for > 1 min	$U_{pd\text{-}test}$ = 291 kV (U_r = 420 kV) $U_{pd\text{-}test}$ = 381 kV (U_r = 550 kV) No indication for PD
Lightning impulse (LI) voltage test	15 impulses of both polarities	±1425 kV LI (U_r = 420 kV) ±1550 kV LI (U_r = 550 kV) Breakdowns < 2/15
Switching impulse (SI) voltage test	15 impulses of both polarities	±1050 kV SI (U_r = 420 kV) ±1175 kV SI (U_r = 550 kV) Breakdowns < 2/15
U_r:	*rated voltage for equipment*	
U_d:	*AC withstand test voltage*	
$U_{pre\text{-}stress}$:	*pre-stress voltage*	
$U_{pd\text{-}test}$:	*test voltage for PD measurement*	

6.3 420/550 kV Gas Insulated Busbar Demonstrator

Following the PD characteristics comparison of 20% C_3F_7CN / 80% CO_2 and SF_6, the specific gas mixture was later retro-filled in the full-scale GIB demonstrator in order to carry out the type tests described in Table 6-1. As new gases were used for filling SF_6 and the C_3F_7CN/CO_2 mixture in the GIB demonstrator, it was important to make sure that SF_6 had a satisfactory gas purity and the 20% C_3F_7CN / 80% CO_2 mixture ratio was successfully achieved prior to testing. Following the gas handling procedures and using the equipment described in Chapter 3, SF_6 was recorded to have a 99.8% purity while the gas mixture had a ratio of 20.7% C_3F_7CN / 79.3% CO_2 without any trace of O_2. This shows that both gases complied with the tolerances specified in the gas handling procedures which are: (a) always use SF_6 above 97% purity and (b) a gas mixture with a ±1% margin of the stated C_3F_7CN concentration.

6.3.1 Type Test Results

For electrical tests performed on equipment using lightning and switching impulses, it is important to keep the waveforms within the time and voltage tolerances specified in the BS EN/IEC 60060-1:2010 standard. This ensures that the tests conform to international standards and that factors like shorter/longer front or tail time do not affect the results. Tables 6-2 and 6-3 show the recorded voltage and time values for the impulses measured from HiAS to provide evidence that the waveforms used were within acceptable limits.

Table 6-2 shows examples of SI waveforms recorded for type tests of 420 kV and 550 kV rating. For a positive polarity voltage application of 1050 kV, the waveform was 0.1% higher than the specified voltage and 12.8% and 9.9% lower than the standard peak time and time to half-value respectively. Similarly, for the positive polarity 1175 kV voltage waveform, the values were 0.3%, 15.2% and 9.4% lower than the applied voltage, peak time and time to half-value. As shown in Table 6-2, voltage and time values under negative polarity impulse applications had a negligible difference from the positive. Evidently, all SI applied were within the tolerances specified.

Table 6-2. Switching impulse voltage and time values recorded with the HiAS for voltage applications of (a) 1050 kV (420 kV rating) and (b) 1175 kV (550 kV) rating.

Rated Voltage	Applied SI Voltage	Recorded Peak Voltage, U_{pk}	Recorded Front Time, T_p	Recorded Time to Half-Value, T_2
420 kV	+1050 kV	1051 kV	218.489 μs	2252 μs
	-1050 kV	1052 kV	215.279 μs	2247 μs
550 kV	+1175 kV	1171 kV	212.368 μs	2265 μs
	-1175 kV	1175 kV	213.429 μs	2252 μs

Table 6-3 shows examples of LI voltage and time values recorded for 420 kV and 550 kV rating type tests. For a positive polarity LI shot of 1425 kV, the recorded waveform was 0.1%, 5.5% and 3.2% different than the applied voltage, front time and time to half-value. Likewise, for the positive 1550 kV voltage (550 kV rating tests), the voltage, front time and time to half-value were 0.3%, 4.3% and 4.2% away from the applied values. As with the SI applications, there was marginal difference between the negative and positive polarity values. Once again, this shows that the LI applications were all within the acceptable limits set by the BS EN/IEC standards.

Table 6-3. Lightning impulse voltage and time values recorded with the HiAS for voltage applications of (a) 1425 kV (420 kV rating) and (b) 1550 kV (550 kV) rating.

Rated Voltage	Applied LI Voltage	Recorded Peak Voltage, U_{pk}	Recorded Front Time, T_1	Recorded Time to Half-Value, T_2
420 kV	+1425 kV	1424 kV	1.134 μs	51.619 μs
	-1425 kV	1428 kV	1.142 μs	51.288 μs
550 kV	+1550 kV	1555 kV	1.149 μs	52.112 μs
	-1550 kV	1547 kV	1.145 μs	50.902 μs

Table 6-4 shows that the 20% C_3F_7CN / 80% CO_2 gas mixture has passed the type tests for 420 kV rating successfully like SF_6. There was no breakdown occurrence during the SI, LI and power frequency withstand tests at the specified BS EN/IEC voltage levels. For the UHF sensor setup, PD discharges emit a signal of at least 16 mV_{pk-pk} and a signal exceeding this value was defined as a PD discharge in the equipment. Following the pre-stress procedure at 650 kV AC_{RMS} for 1 minute, the GIB was energised at 291 kV AC_{RMS} voltage for more than 30 minutes for the PD type test. The maximum noise level recorded from the UHF sensors during this period was 8.01 mVpk-pk which indicates no PD activity in the GIB at the BS EN/IEC voltage level.

Table 6-4. Type test results for the full-scale GIB demonstrator at 420 kV rated voltage tests.

Rated Voltage	Test	20% C_3F_7CN / 80% CO_2	100% SF_6
420 kV	±1050 kV SI	0/15	0/15
	±1425 kV LI	0/15	0/15
	650 kV AC	No breakdown	No breakdown
	291 kV PD	Signals < 16 mV_{pk-pk}	Signals < 16 mV_{pk-pk}

Following the completion of the 420 kV type tests, the 20% C_3F_7CN / 80% CO_2 gas mixture was pushed up to the voltage levels specified for the 550 kV equipment rating in accordance to the BS EN/IEC standards mentioned earlier. Table 6-5 shows that no breakdown occurrence was recorded, even at an elevated voltage level for all voltage waveforms. No PD pulses were detected from the UHF sensors since the maximum signal recorded was 11.42 mV_{pk-pk} at 381 kV AC_{RMS} voltage (energised for 30 minutes) for SF_6 and the 20%

C_3F_7CN / 80% CO_2 gas mixture, indicating a comparable dielectric performance for both dielectrics in full-scale industrial equipment. This shows that SF_6-designed GIB practical equipment can be PD-free using both SF_6 and the 20% C_3F_7CN / 80% CO_2 gas mixture.

Table 6-5. Type test results for the full-scale GIB demonstrator at 550 kV rated voltage tests.

Rated Voltage	Test	20% C_3F_7CN / 80% CO_2	100% SF_6
550kV	±1175 kV SI	0/15	0/15
	±1550 kV LI	0/15	-
	710 kV AC	No breakdown	No breakdown
	381 kV PD	Signals < 16 mV_{pk-pk}	Signals < 16 mV_{pk-pk}

Finally, after finishing the standard type tests according to the guidance from the BS EN/IEC standards [90], [101]–[103], the GIB demonstrator was subjected to non-standard type tests. Non-standard type tests involved increasing the impulse shot applications from 15 to 30 in order to investigate the behaviour of the 20% C_3F_7CN / 80% CO_2 gas mixture under an increased amount of overvoltage transient events. Table 6-6 shows that despite increasing the number of impulse applications, the 20% C_3F_7CN / 80% CO_2 gas mixture successfully passed the non-standard type tests with no breakdown occurrence. These type tests, both standard and non-standard, have effectively established that the 20% C_3F_7CN / 80% CO_2 gas mixture can be retro-filled with a sizeable safety margin in the specific SF_6-designed equipment for the 400 kV UK transmission network. Similar test approach could be adopted for the remaining SF_6-designed GIB makes used in the UK transmission network in order to examine whether the 20% C_3F_7CN / 80% CO_2 gas mixture could replace SF_6.

Table 6-6. Non-standard type test results for the full-scale GIB demonstrator at 420 kV rated voltage tests.

Rated Voltage	Test	20% C_3F_7CN / 80% CO_2	100% SF_6
420 kV	±1050 kV SI	0/30	-
	±1425 kV LI	0/30	-

6.3.2 Material Compatibility of Gaskets

C_3F_7CN gas compatibility with the O-ring material was evaluated by 3M using a sample of an EPDM elastomer used in the existing GIL/GIB [104]. A small sample of the EPDM elastomer was placed into a dried 50 mL glass vial and sealed with a PTFE-lined septum cap as shown in Figure 6-6.

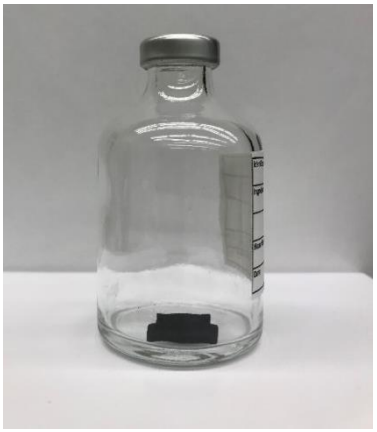

Figure 6-6. EPDM elastomer sample tested for compatibility with C_3F_7CN gas.

An approximate 27% C_3F_7CN mixture in air was created by adding 0.1122 g of C_3F_7CN to this vial. The test sample was placed in an oven for more than 3 months. The oven was operating at 105°C which according to [12], [101] is the maximum operating temperature SF_6 can be exposed to within a GIL/GIB configuration. The conditions for the material compatibility test are shown in Table 6-7.

Table 6-7. Material compatibility test conditions.

O-ring Material	EPDM
Gas Concentration	27% C_3F_7CN mixed in air
Operating Temperature	105°C
Duration	112 days
Analysis Method	Gas Chromatography (GC)

The purity of C_3F_7CN was assessed by extracting 100 µL samples from the vial using a gas-tight syringe. The samples were analysed using gas chromatography (GC). The purity results of the gas corresponding to the time interval taken after the placement of the sample in the oven are shown in Table 6-8. Table 6-8 illustrates that the purity of the gas is not affected

by the elastomer material even when exposed to elevated temperatures. The purity of C_3F_7CN is reduced by less than 0.2% after 112 days exposure at 105°C. The test results highlight that there should not be any degradation to the EPDM elastomer gasket or to C_3F_7CN gas when they are exposed to elevated temperatures over an extended period of time. This shows that the C_3F_7CN/CO_2 mixture does not have any risk of losing its insulation capability through degradation or gas leakage because of damaged EPDM elastomer gaskets when retro-filled in SF_6-designed equipment.

Table 6-8. C_3F_7CN purity when aged at 105°C in contact with the EPDM elastomer sample.

Time (days)	C_3F_7CN GC area (%)
0	99.99
15	99.84
28	99.85
55	99.9
90	99.86
112	99.86

6.4 Impact of Retro-fill Solution for UK Transmission Network

6.4.1 SF_6 National Grid Inventory and Leakage Rates

The main aim of this project is to investigate the possibility of extracting all the SF_6 gas currently being used in UK network assets and replace it with a more environmentally friendly gas mixture. As the focus of this thesis is the insulation applications as opposed to arc-quenching applications, the electrical and material compatibility capabilities of the 20% C_3F_7CN / 80% CO_2 gas mixture in GIBs were thoroughly studied, and its performance was assessed compared to SF_6. Following the findings that the gas mixture could be a potential SF_6-alternative, the impact of replacing SF_6 in passive components within the UK network was evaluated to assess the CO_2 equivalent (tCO_2e) emission reduction in case a new environmentally friendly gas medium is adopted.

Ofgem's recent reports have shown that the total SF_6 volume used in the network is still increasing with new assets being installed regularly [105]. According to data provided by

National Grid, the total transmission SF_6 inventory up to date is approximately 906 tons. From the total inventory, the division of passive (i.e. non-breaking chambers such as GIB equipment) and active (i.e. arc-quenching units such as circuit breakers) components is shown in Figure 6-7. As reported by National Grid, the majority of SF_6 used in the UK transmission network is for passive components accounting for 84% of the total, while the remaining 16% of the assets is for active components.

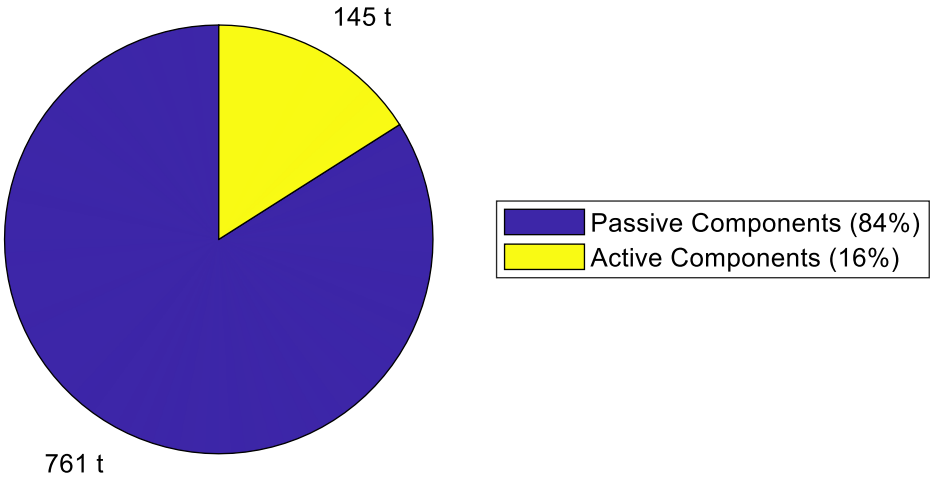

Figure 6-7. Total SF_6 inventory in the UK transmission network divided in passive and active components.

Figure 6-8 shows that roughly 25% of SF_6 in the inventory of passive components (approximately 761 t), is filled in the same equipment model as the demonstrator investigated in this project for the 20% C_3F_7CN / 80% CO_2 gas mixture. The figure below illustrates the impact that retro-filling the SF_6-designed GIB equipment can have in the UK network, leading to a potential replacement of 190 t of SF_6.

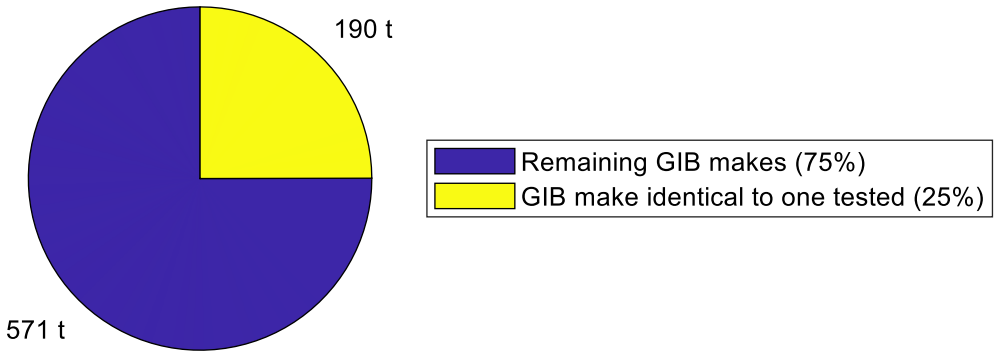

Figure 6-8. Total SF_6 passive components inventory in the UK transmission network and the volume of SF_6 being used for the GIB demonstrator type tested in this chapter.

Table 6-9 shows the recorded SF_6 leakages from 2014 to 2019 as documented from National Grid in the UK [106]. Ofgem has reported that there has been a 12% reduction in relative SF_6 leakage rates in the UK from all utilities between 2013/2014 to 2017/2018 [105]. Nevertheless, Table 6-9 shows that the absolute volume of SF_6 leaking into the atmosphere, from National Grid plc only, is still increasing which is attributed to the increasing number of SF_6 assets installed in the network. The SF_6 leakage rate in 2018/2019 was approximately 1.6%, which is considerably higher than the target leakage of 0.5% recommended by the BS EN/IEC 62271-203:2012 [103] standard. This indicates the necessity of a retro-fill solution in order to significantly reduce the tCO_2e emissions from installed gas insulated equipment.

Table 6-9. SF_6 yearly losses as reported from National Grid.

Year	SF_6 losses (t)
2014/2015	12.4
2015/2016	12.0
2016/2017	14.7
2017/2018	14.0
2018/2019	14.4

6.4.2 GWP Calculation and CO_2 Equivalent Emissions

As reported from IPCC [3], SF_6 has a GWP that is 23,500 times higher than CO_2. C_3F_7CN has a GWP of 2,090 [7] in its pure form but this reduces when the gas is used in low concentrations as part of a mixture. Figure 6-9 shows the calculated GWP values based on the reduced density of the gas mixture. As anticipated, it shows that the GWP of a mixture decreases with lower C_3F_7CN concentrations. Figure 6-9 shows the GWP of g^3 used by General Electric which uses a 4% C_3F_7CN concentration and reduces CO_2 emissions up to 98% compared to SF_6 [6], [8]. The mixture investigated in this thesis has a 20% C_3F_7CN content with a GWP of ≈1,100, which represents a 95% reduction of SF_6.

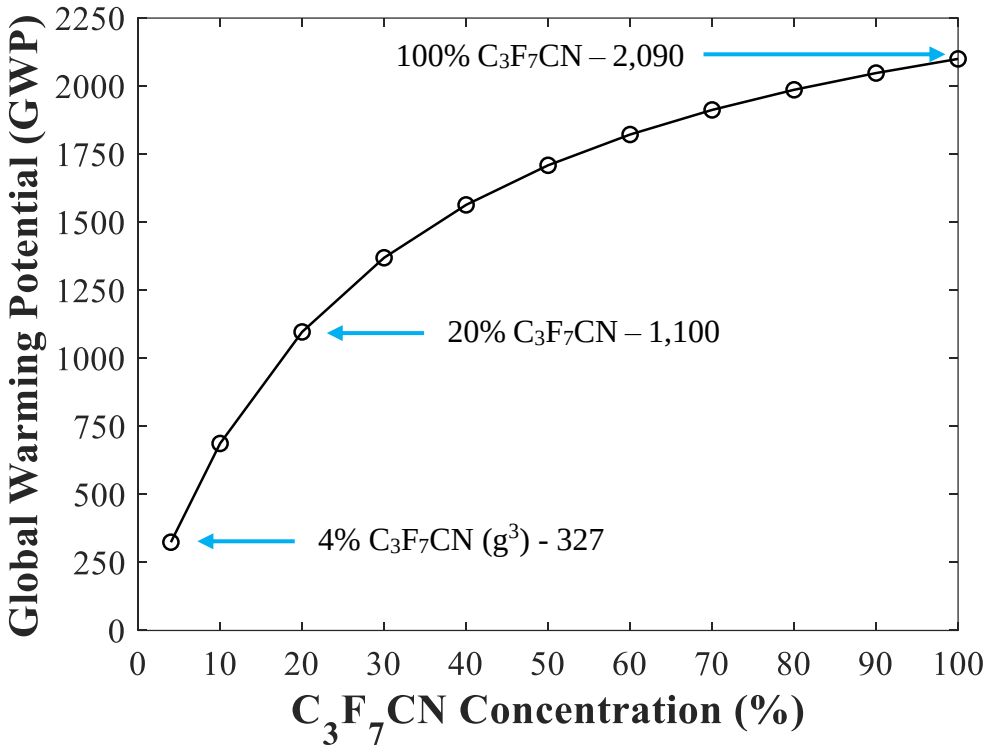

Figure 6-9. Calculated GWP as a function of C_3F_7CN concentration in a mixture.

Using the calculated GWP values, the tCO_2e quantity of SF_6 and the 20% C_3F_7CN / 80% CO_2 gas mixture can be calculated using the following equation [107]:

$$tCO_2e = \left(\frac{Mass\ of\ F\ gas\ (kg)}{1000}\right) \cdot F\ gas\ GWP \tag{6-1}$$

Using equation (6-1), a comparison can be made for the tCO_2e of SF_6 and the 20% C_3F_7CN / 80% CO_2 gas mixture. Figure 6-10 shows the impact of replacing the SF_6 inventory in National Grid with the C_3F_7CN/CO_2 gas mixture. As shown in Figure 6-10, assuming the leakage rates continue as indicated in Table 6-9, by adopting a 20% C_3F_7CN / 80% CO_2 mixture instead of SF_6 will significantly reduce the tCO_2e emissions. Finally, Figure 6-10 illustrates that the tCO_2e emissions from annual SF_6 leakages can go up to 350,000 t while by adopting the 20% C_3F_7CN / 80% CO_2 gas mixture there can be a significant reduction in yearly tCO_2e to approximately 25,000 t.

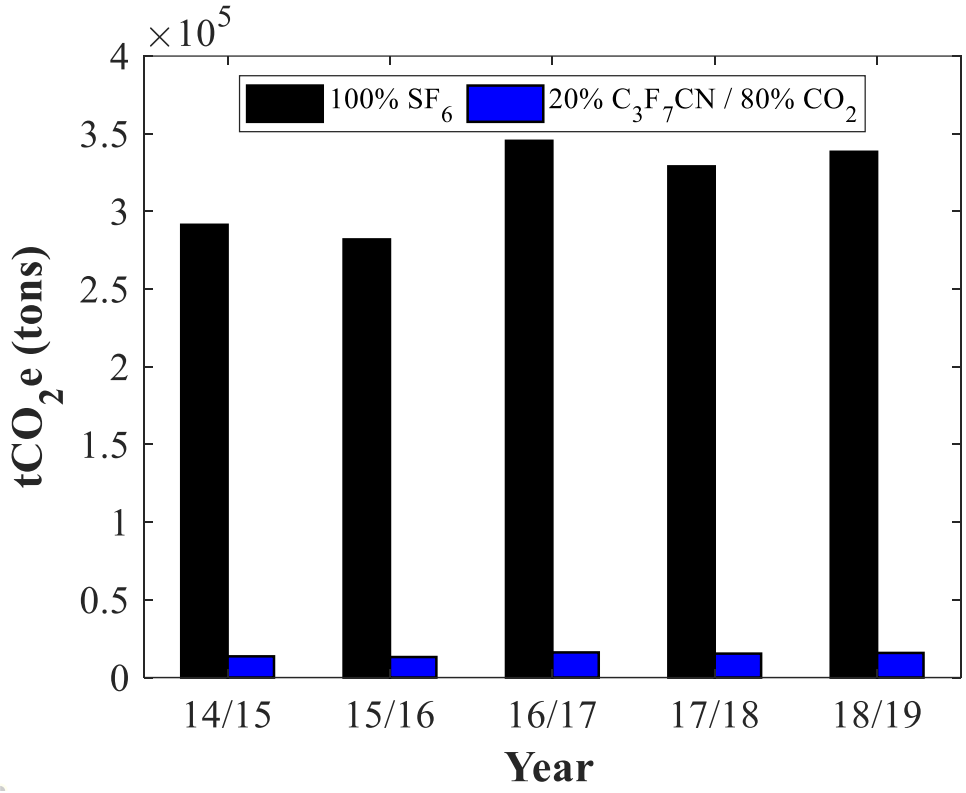

Figure 6-10. Comparison of SF_6 and 20% C_3F_7CN / 80% CO_2 gases tCO_2e using leakages from 2014 to 2019 from Table 6-6.

6.4.3 Potential Retro-fill Locations in the UK and Temperature Profiles

Outdoor gas insulated equipment retro-filled with 20% C_3F_7CN / 80% CO_2 can be operated down to -10°C (liquefaction point for the mixture at 4.5 bar absolute). This can be considered as acceptable since the internal conductor carries several thousands of amps during high-load conditions and will inherently heat up the insulating medium. However, the temperature is still considerably higher than the maximum liquefaction point assigned by the BS EN/IEC standards (-25°C) [103] and there will also be cases where the current flowing through the conductor is at minimum due to light or no-load conditions. Therefore, it is important to assess the probability of reaching this temperature in potential retro-fill locations in the UK.

Table 6-10 reports information provided by National Grid about the transmission level substations in the UK that use large amounts of SF_6, and each has an inventory of more than 20 t. The specific substations are the highest ones in terms of SF_6 usage and, when combined, they form about 40% of the total National Grid SF_6 inventory in the UK.

Table 6-10. National Grid substations in the UK with SF_6 inventory that exceeds 20 t.

Map Location	Substation Name and Voltage Rating	SF_6 Inventory (t)
1	BRAMFORD, 400 kV	53
2	ST JOHNS WOOD, 400 kV	37
3	CONNAHS QUAY, 400 kV	31
4	WEST HAM, 400 kV	28
5	HACKNEY, 400 kV	27
6	SELLINDGE, 400 kV	26
7	NORTON, 400 kV	26
8	LITTLEBROOK, 400 kV	25
9	KILLINGHOLME, 400 kV	24
10	BARKING, 400 kV	22
11	SIZEWELL, 400 kV	22
12	GRAIN, 400 kV	22
13	NEW CROSS, 275 kV	21

In order to evaluate whether the high boiling point of the 20% C_3F_7CN / 80% CO_2 gas mixture will pose any difficulties for a retro-fill solution in the UK, historic temperature data have been obtained from weather stations close to the substations' location shown in Table 6-10. The weather stations shown in Table 6-11 have been capturing temperature data for almost 100 years and the information is publicly available on the Met Office website [108].

Table 6-11. Met Office weather stations located nearby the substations reported in Table 6-10 [108].

Map Location	Weather Station Location
A	Durham
B	Sheffield
C	Lowestoft
D	Heathrow
E	Manston

The geographical locations of both the substations and weather stations have been graphically pinpointed in Figure 6-11. As shown in the figure, the majority of the substations reported in Table 6-10 are sited in the South East region of the UK with a smaller number located further north. Locations of weather stations have been chosen to cover the temperature profiles of regions throughout UK and close to the substations shown in Table 6-10.

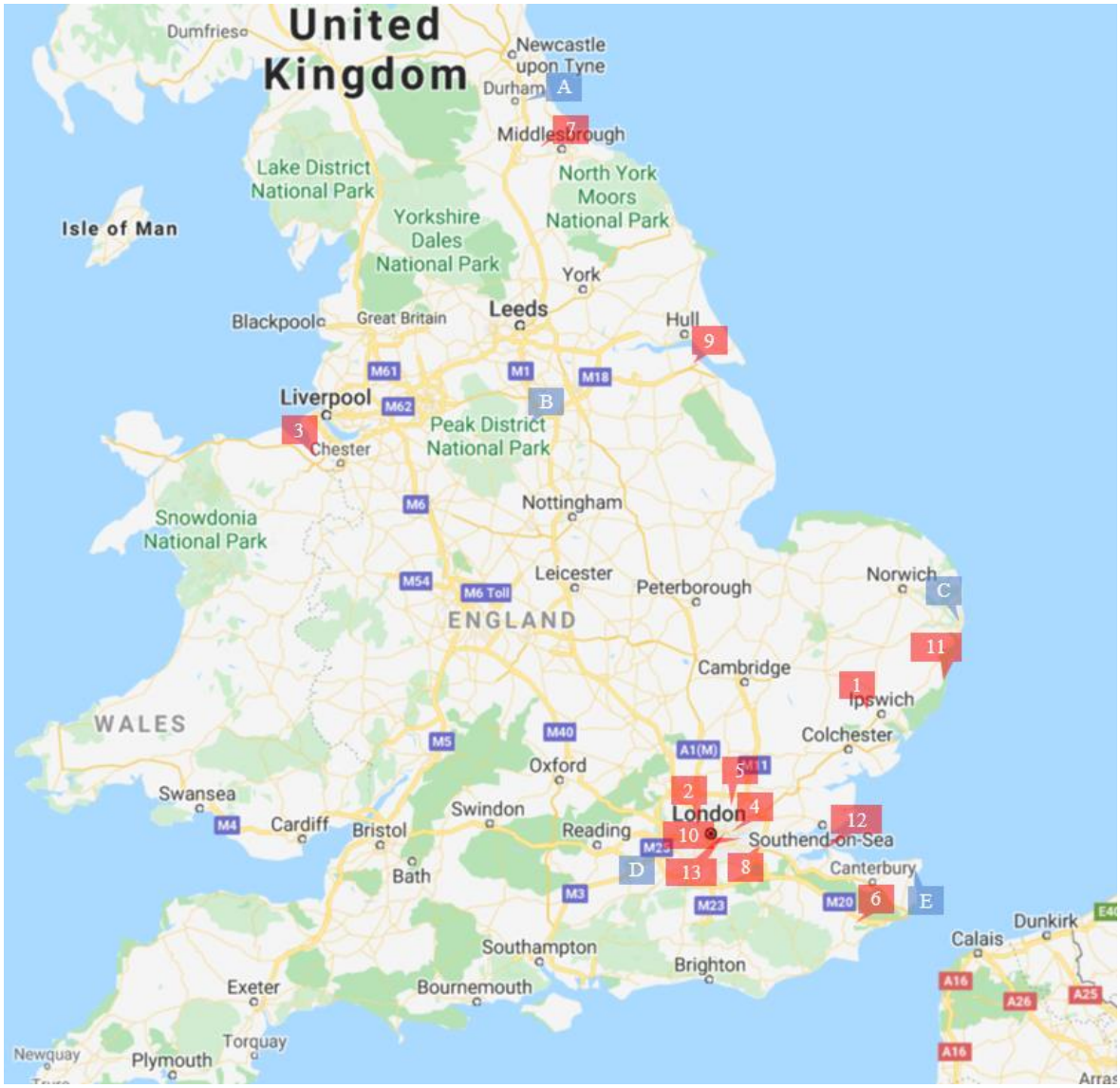

Figure 6-11. Geographical locations of National Grid substations and Met Office weather stations reported in Table 6-10 and Table 6-11 [109].

Figures 6-12 and 6-13 portray the mean daily minimum temperature recorded for every month from 1990 to 2018 in the weather stations labelled A and B in Figure 6-11. The Durham and Sheffield weather stations represent the temperatures that mostly occur in the Northern region of England. As shown in both figures, for temperature data recorded in a time period of almost 20 years, the mean daily minimum temperatures reached their lowest points in December 2010 where the temperatures were -3.4°C and -1.9°C for Durham and Sheffield stations respectively.

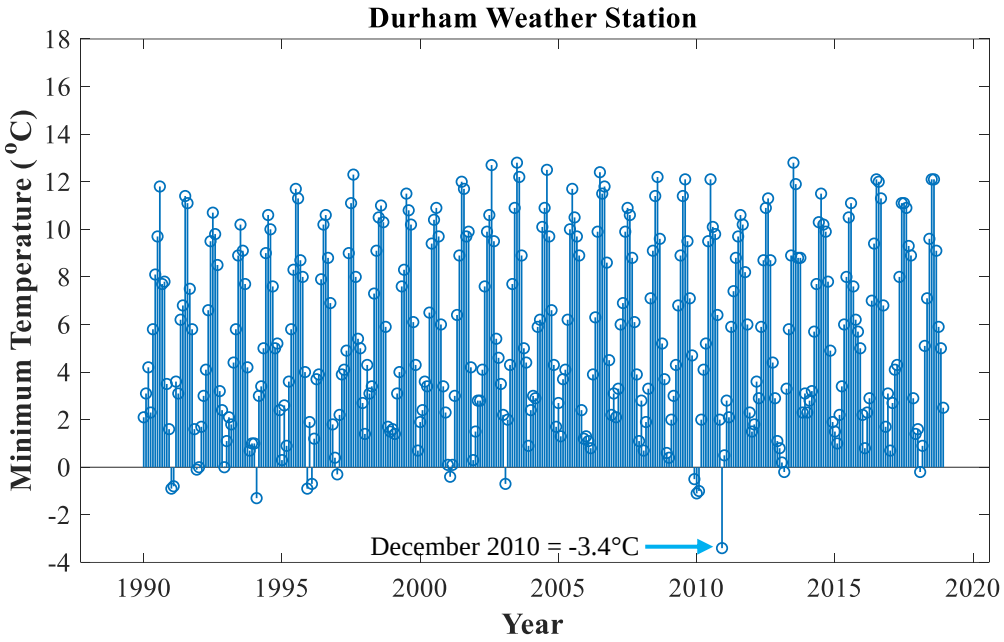

Figure 6-12. Mean daily minimum temperature for every month from 1990 to 2018 recorded from Durham weather station.

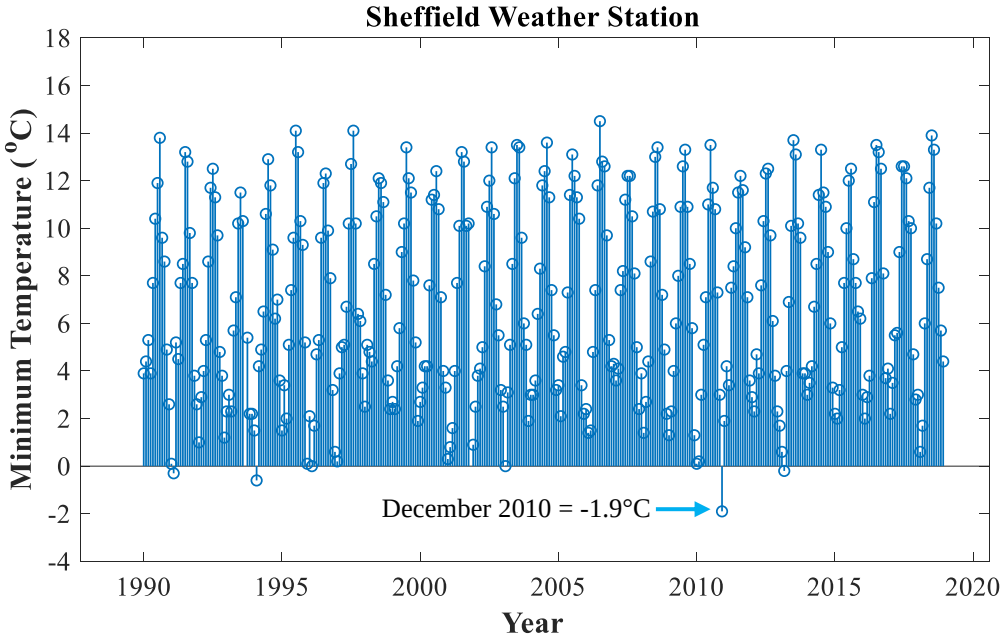

Figure 6-13. Mean daily minimum temperature for every month from 1990 to 2018 recorded from Sheffield weather station.

Figures 6-14, 6-15 and 6-16 illustrate the mean daily minimum temperature data measured for every month from 1990 to 2018 in the Lowestoft, Heathrow and Manston weather stations respectively. These stations represent the temperatures in the South Eastern region of the UK. Similar to the Durham and Sheffield stations, the lowest temperature recorded by

the South Eastern weather stations in the past 20 years was in December 2010. The minimum temperatures were -1.4°C, -1.5°C and -1°C for Lowestoft, Heathrow and Manston respectively.

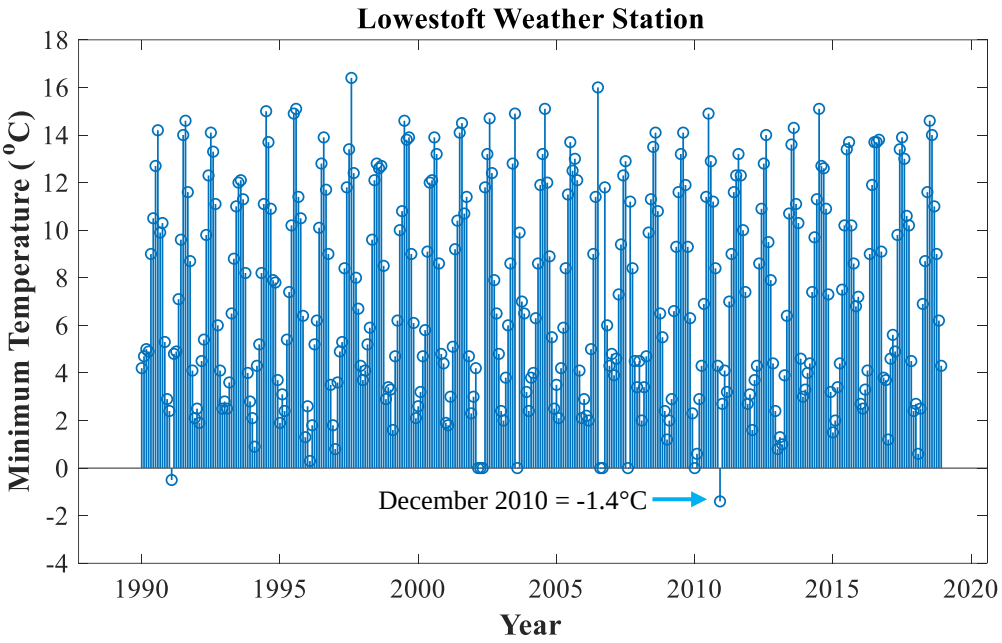

Figure 6-14. Mean daily minimum temperature for every month from 1990 to 2018 recorded from Lowestoft weather station.

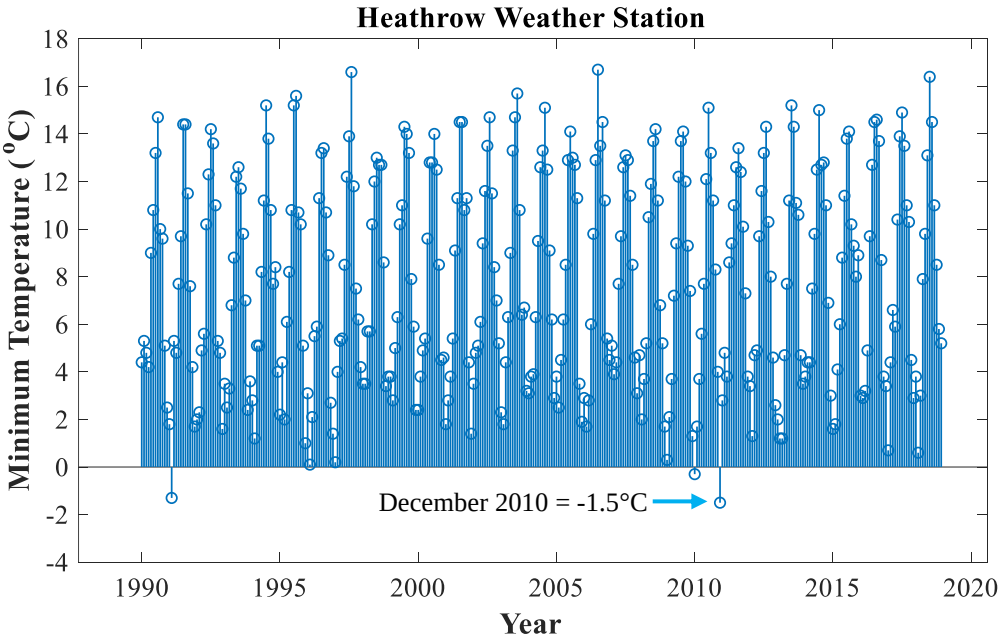

Figure 6-15. Mean daily minimum temperature for every month from 1990 to 2018 recorded from Heathrow weather station.

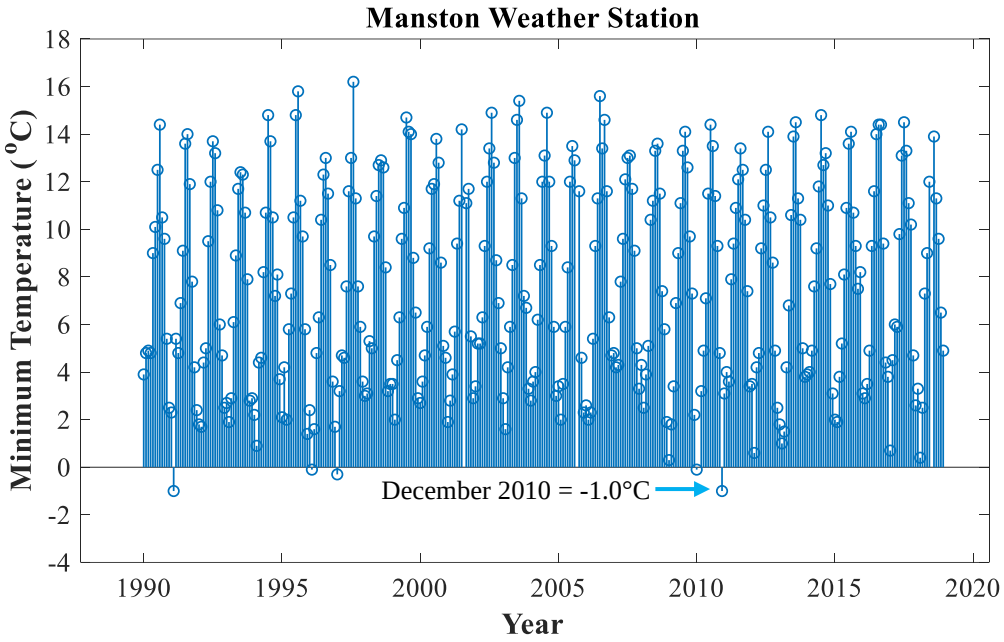

Figure 6-16. Mean daily minimum temperature for every month from 1990 to 2018 recorded from Manston weather station.

As shown in the above figures, temperatures tend to be slightly higher in the South East region of England than the Northern region. Nevertheless, the mean daily minimum temperature data analysed from weather stations over the past 20 years from several regions in the UK show that it is unlikely that the atmospheric temperature can drop below -10°C. The lowest mean daily minimum temperature recorded (-3.4°C) was in Durham weather station in December 2010.

6.5 Summary

This chapter presents results of retro-fill research on the 20% C_3F_7CN / 80% CO_2 gas mixture as a potential alternative to SF_6 for high voltage insulation applications in GIL and GIB. The type test and material compatibility results demonstrate strong potential for replacing SF_6-filled network assets with the more environmentally friendly medium of 20% C_3F_7CN / 80% CO_2 gas mixture. The main conclusions drawn are as follows:

- Type tests with a GIB demonstrator showed that the 20% C_3F_7CN / 80% CO_2 gas mixture passed all the required type tests as SF_6, indicating that the two gases have the same electrical performance for 420/550 kV rated equipment. Experiments with the GIB

demonstrator were further extended with non-standard type tests which involved increasing the SI and LI applications and in turn the failure probability. No breakdown occurrence was recorded for the 20% C_3F_7CN / 80% CO_2 gas mixture which establishes a level of confidence for its dielectric performance when retro-filled in SF_6-designed equipment.

- A material compatibility test showed no clear sign of C_3F_7CN purity degradation when in contact with a common gasket material EPDM elastomer and subjected to the maximum operating temperature of GIL/GIB practical equipment. This shows that the 20% C_3F_7CN / 80% CO_2 gas mixture could maintain its purity under extreme operating conditions in the long term when retro-filled in SF_6-designed GIL/GIB equipment.
- The use of a 20% C_3F_7CN / 80% CO_2 gas mixture at 4.5 bar (abs) with a -10°C liquefaction temperature can be considered as a potential retro-fill solution for SF_6-designed equipment installed in the UK network and can achieve a potential tCO_2e reduction of up to 95% when compared to SF_6.
- The retro-fill of 20% C_3F_7CN / 80% CO_2 gas mixture in SF_6-designed GIB models identical to the one tested in this chapter can lead to the replacement of 190 t of SF_6 in the UK transmission network. Similar research approach can be adopted to address the remaining 571 t of passive components in the UK transmission inventory.
- The main limitation of the gas mixture is the liquefaction point of -10°C which is higher than the BS EN/IEC defined level of -25°C. However, through investigation of the mean daily minimum temperature profiles from relevant substation locations in the UK over the past 20 years, it was found that it is very rare that the atmospheric temperature can go down to -10°C. The lowest mean daily minimum temperature recorded in the past 20 years in the UK, from weather stations located close to National Grid substations with the largest SF_6 inventory (specified in Table 6-10), is -3.4°C in December 2010 at Durham station.

Chapter 7 Conclusions and Future Work

7.1 Research Aim and Objectives

Research about finding a viable SF_6-alternative has intensified over the past few years with several gas candidates being investigated. The main aim of this study was to investigate the possibility of adopting a suitable C_3F_7CN/CO_2 gas mixture as a retro-fill solution in existing SF_6-designed GIL/GIB assets at transmission voltage levels in the power network. The quest of finding the ideal SF_6 replacement focuses on reducing the overall carbon emissions arising from using one of the most potent greenhouse gases as an insulation material in the power industry. However, most SF_6-alternative gases come with a major drawback, such as low dielectric strength, high GWP, high toxicity or high boiling point which prevents a like-for-like replacement for SF_6 in high voltage equipment. This thesis evaluated the feasibility of the 20% C_3F_7CN / 80% CO_2 gas mixture being used as a SF_6 replacement by addressing the following key points:

1. Breakdown strength assessment of C_3F_7CN/CO_2 gas mixtures compared to SF_6 and identification of the ideal C_3F_7CN/CO_2 concentration ratio which has a comparable electrical performance to SF_6 gas under GIL/GIB representative electric fields.
2. PD characteristics evaluation for the 20% C_3F_7CN / 80% CO_2 gas mixture and SF_6 to examine how the gas mixture performs in suppressing PD activities with the presence of protrusions causing microscopic electric field enhancements within the equipment.
3. Type test performance investigation of the 20% C_3F_7CN / 80% CO_2 gas mixture compared to SF_6 when retro-filled in full-scale 420/550 kV GIB equipment and subjected to BS EN/IEC defined electrical type tests. Tests were also performed for elastomers currently being used in GIL/GIB equipment in order to examine whether the SF_6-alternative gas is compatible and does not deteriorate when in contact with the existing materials in assets.
4. Limitation analysis of the solution and the impact of a retro-fill adoption to the carbon emissions reduction in the UK power network.

7.2 Summary of Results and Research Findings

7.2.1 Breakdown Characteristics

The breakdown characteristics of CO_2 gas and two C_3F_7CN/CO_2 gas mixtures were compared to SF_6 gas under weakly non-uniform electric fields tested under LI and AC voltages. The two C_3F_7CN/CO_2 gas mixtures were compared to SF_6 using a coaxial electrode configuration which represents a quasi-uniform field as found in GIL/GIB equipment. Out of the two gas mixtures, 20% C_3F_7CN / 80% CO_2 was found to be a more technically viable SF_6-alternative with a comparable breakdown performance to SF_6. The 16% C_3F_7CN / 84% CO_2 gas mixture was found to have a slightly lower breakdown performance but with the benefit of an additional 5°C margin to the liquefaction point when compared to the 20% C_3F_7CN / 80% CO_2 gas mixture.

The 20% C_3F_7CN / 80% CO_2 gas mixture and CO_2 gas were then compared to pure SF_6 using coaxial and hemispherical rod-plane electrode configurations with a more non-uniform fields under LI voltages. The results demonstrated that CO_2 has half the breakdown voltage in comparison to 20% C_3F_7CN / 80% CO_2 mixture and SF_6 gas, which demonstrates the significant insulation improvement by the addition of C_3F_7CN content in the gas mixture. It was also found that, under positive LI polarity, the breakdown voltage of SF_6 was consistently higher than the 20% C_3F_7CN / 80% CO_2 gas mixture. In the case of negative LI polarity, the performance of the 20% C_3F_7CN / 80% CO_2 mixture was more comparable to SF_6.

Finally, the LI polarity influence on the breakdown voltage of different gas mixtures was evaluated using the coaxial and hemispherical rod-plane electrode configurations. Under the category of weakly non-uniform electric fields, which is described by *f* values between 0.28 to 0.66 in this thesis, the negative LI breakdown voltages were consistently lower than their positive counterparts. In addition to field uniformity, gas type and pressure were also found to affect the breakdown voltage for different LI polarities. The difference of breakdown voltages between positive and negative polarities was found to be larger in SF_6 than in the 20% C_3F_7CN / 80% CO_2 gas mixture and CO_2. At 1 bar (abs), the polarity effect was not as prominent as in higher pressures with the breakdown voltages being similar under both

polarities. Nevertheless, the negative polarity was found to be more critical and have a higher probability to cause a breakdown within this field uniformity category, which should be taken into consideration for future design of gas insulated equipment.

7.2.2 Partial Discharge Characteristics

The PD characteristics of SF_6 gas and the 20% C_3F_7CN / 80% CO_2 gas mixture were compared under divergent and highly divergent electric fields (defined in Chapter 3) using UHF sensors. Two electrode configurations, namely hemispherical rod-plane and plane-plane with different needle lengths were used to vary the electric field uniformity and initiate PD activity. SF_6 has shown to have comparatively higher PDIV/EV values than the 20% C_3F_7CN / 80% CO_2 gas mixture under highly divergent fields caused by using a 15 mm needle. The difference in PDIV/EV values between the two gases reduced using a 5 mm needle length. In fact, the PDIV/EV values of the 20% C_3F_7CN / 80% CO_2 gas mixture exceeded SF_6 when a plane-plane configuration was used with a 5 mm needle attached on the HV electrode. This indicates that with the presence of microscopic irregularities on the HV conductor resulting in localised field enhancements in a high-pressure environment like in GIL/GIB equipment, the 20% C_3F_7CN / 80% CO_2 gas mixture has the potential to suppress PD activities as effectively as SF_6.

SF_6 and the 20% C_3F_7CN / 80% CO_2 gas mixture were also observed to behave differently in their PRPD patterns. The 20% C_3F_7CN / 80% CO_2 gas mixture has shown to be significantly affected by different pressures/densities, voltage magnitude and field uniformities which is the opposite to SF_6. Using a needle on the HV electrode, SF_6 appeared to have most of its PD activity in the positive half-cycle of the AC waveform with some PD activities in the negative half-cycle at higher voltages. In contrast, the 20% C_3F_7CN / 80% CO_2 gas mixture appeared to go through a 3-phase transition stage in its PRPD patterns where the PD activity started on the negative half-cycle and shifted to the positive. As was shown in Chapter 5, pressure/density, voltage magnitude and field uniformity can all affect the transition phase in the PRPD pattern of the 20% C_3F_7CN / 80% CO_2 gas mixture and this could be due to the combination of a strongly and weakly attaching gas as opposed to SF_6 which is a strongly attaching gas.

7.2.3 Type Tests and Material Compatibility Analyses

The 20% C_3F_7CN / 80% CO_2 gas mixture was retro-filled and type tested in a 420/550 kV, SF_6-designed GIB demonstrator following the voltage levels specified by the BS EN/IEC standards. The C_3F_7CN/CO_2 gas mixture passed the LI, SI, AC and PD type tests, which indicate a comparable performance to SF_6 in a full-scale SF_6-designed GIL/GIB equipment. The type tests for the GIB demonstrator involved subjecting it to standard and non-standard type tests, for both 420 kV and 550 kV equipment ratings, where no breakdown event or PD activity was observed for the 20% C_3F_7CN / 80% CO_2 gas mixture.

A material compatibility test took place by exposing a sample of the EPDM elastomer material as found in the GIB equipment to C_3F_7CN gas. The sample was placed in an oven for more than 3 months at a temperature of 105°C, which is the maximum temperature in practical GIL/GIB equipment in accordance to BS EN/IEC standards. The measured results show that there is no noticeable sign of degradation for C_3F_7CN over a 3-month exposure at elevated temperatures. This is a strong indication that the C_3F_7CN/CO_2 gas mixture not only can maintain its insulation capability, but also pose little risk of leakage due to damaged O-rings when used as a retro-fill solution in SF_6-degined equipment.

7.2.4 Environmental Assessment

The impact of a retro-fill solution with the 20% C_3F_7CN / 80% CO_2 gas mixture in SF_6-designed equipment in the UK network was evaluated. As this thesis focuses more on passive components, such as GIB and GIL, it was important to quantify the SF_6-inventory used for this purpose in the UK. Out of a total inventory of 906 t of SF_6 installed by National Grid to date, roughly 84% is used on passive units. A further 25% of the passive components inventory, accounting for approximately 190 t of SF_6, is used for insulation in the specific GIB make that was type tested in this project. This means that this retro-fill solution could potentially lead to at least 190 t of SF_6 being replaced with the 20% C_3F_7CN / 80% CO_2 gas mixture which, with a GWP of 1,100, could lead to a 95% reduction in the tCO_2e.

The retro-fill solution being recommended in this work is: the use of the 20% C_3F_7CN / 80% CO_2 gas mixture at an operating pressure of 4.5 bar (abs) with a -10°C liquefaction point,

which could result in 95% reduction in tCO_2e arising from SF_6 usage in gas insulated equipment. However, the big concern of this solution is the liquefaction temperature which is considerably higher than the -25°C limit set in the BS EN/IEC standards. Despite that, after a thorough analysis of the mean daily minimum temperature profiles of multiple locations in the UK for the past 20 years, it was found that the temperature of -10°C can only be reached in extreme weather scenarios. The lowest temperature recorded in potential retro-fill substation locations in the UK over the past 20 years (with SF_6 inventory greater than 20 t), according to historic data recorded, was -3.4°C which is considerably higher than the liquefaction point of -10°C for the gas mixture.

7.3 Future Work

The research work conducted in this thesis has mainly investigated the potential of using the 20% C_3F_7CN / 80% CO_2 gas mixture as a retro-fill solution in existing SF_6-designed GIB equipment. The work has compared the characteristics of the C_3F_7CN/CO_2 gas mixture to SF_6 in terms of breakdown, PD and withstand type tests in practical equipment. However, future work can further characterise the mixture and identify any problems that might arise with its implementation in practical equipment.

- **Effect of Surface Roughness on the Inception and Breakdown Voltage of Coaxial Configurations**

Several previous studies were carried out on the effect of the HV electrode surface roughness and pressure on the breakdown voltage of SF_6. The purpose of these investigations was to identify the maximum threshold value that the product of surface roughness and pressure does not impact the insulation capability of SF_6, when used in practical equipment. It was found that when the product of maximum surface roughness and pressure was below 40 bar·μm, the breakdown voltage of the gas was marginally affected. In contrast, any value exceeding this could significantly reduce the breakdown performance of SF_6.

To retro-fill C_3F_7CN/CO_2 gas mixtures, it is important to establish the same threshold value as SF_6 since the existing GIB equipment has been in operation for more than 50 years. Technical surface finish in equipment in the 1960s was not as smooth as modern installations

and this could potentially influence the insulation capability of the mixture if it does not behave as well as SF_6. The surface roughness study can be done by modifying the reduced-scale coaxial prototype used in the breakdown tests, where several conductors with different surface roughness values can be experimentally examined. The external UHF sensors used in the PD chapter can also be exploited to determine the corona inception voltage of the coaxial configuration under different pressures and surface roughness values. This study could result in three important analyses: (i) evaluate the effect of pressure and surface roughness on C_3F_7CN/CO_2 mixtures (ii) establish a threshold value for when the surface roughness and pressure product does not influence the insulation capability of the chosen C_3F_7CN/CO_2 gas mixture and (iii) identify the margin between inception and breakdown voltage for different surface roughness and pressures for the C_3F_7CN/CO_2 gas mixture.

- **Breakdown Tests for Needle Electrode Configurations**

PD needle configurations in this thesis were used to compare the PDIV/EV characteristics of the 20% C_3F_7CN / 80% CO_2 gas mixture to SF_6. These tests can be further extended by pushing the voltage until a breakdown occurs in the needle configuration. Breakdown tests using the PD electrode configurations can be useful in establishing the gap from inception to breakdown voltage for these gases and investigate their behaviour with the existence of a protrusion in the equipment. In general, the C_3F_7CN/CO_2 gas mixture in the PD chapter was found to have lower PDIV/EV values compared to SF_6 with the presence of a protrusion. However, this does not necessarily mean that the gas mixture can fail easier than SF_6 when used in practical equipment. By carrying out breakdown voltage tests using the same electrode configurations can help determine if lower PDIV/EV values also lead to inferior breakdown voltages for the C_3F_7CN/CO_2 gas mixture compared to SF_6. Otherwise, in the case that the C_3F_7CN/CO_2 gas mixture has lower PDIV/EV values but similar breakdown performance, the lower PD inception level can be used to its advantage for future condition monitoring of the gas insulated equipment. By having lower PDIV/EV values but similar breakdown values means that a defect in equipment can be detected long before failure when using C_3F_7CN/CO_2 gas mixtures instead of SF_6. This could potentially lead to earlier fault detection and repair of the asset which would assist in the prevention of its total failure.

➢ PD Characterisation of Artificial Defects in the GIB Demonstrator

Using several internal and external UHF sensors, a full-scale 420/550 kV GIB demonstrator was found to be PD-free using either SF_6 or the 20% C_3F_7CN / 80% CO_2 gas mixture up to the voltage levels specified by the BS EN/IEC standards. However, the full-scale GIB demonstrator can be used more extensively to characterise and compare SF_6 and the C_3F_7CN/CO_2 gas mixture in the presence of defects that can lead to PDs in the practical equipment. Defects such as protrusion on conductor/enclosure, free metallic particles or a fault on the epoxy insulator can be used to characterise the behaviour of the 20% C_3F_7CN / 80% CO_2 gas mixture under live energisation. This study could lead to the following important findings:

- PDIV/EV values comparison between SF_6 and the 20% C_3F_7CN / 80% CO_2 gas mixture at operational pressure which will reveal more about the ability of the gas to suppress PD activity with the presence of a defect in a full-scale equipment.
- Characterisation of UHF signals and PRPD patterns to show how the gases react to different types of PD defects. This knowledge can be used for on-site condition monitoring in order to identify the cause of PDs in gas insulated equipment.
- Comparison on the effectiveness of PD capturing between the internal UHF sensors and the external ones placed on insulators. This will show the capability of the external sensors to be used for on-site condition monitoring of gas insulated equipment that are not equipped with internal UHF sensors.
- Time of flight measurements, by placing defects at different distances from the sensor in the GIB equipment, can be used to establish a standardised procedure for identifying the defect location within the equipment.

Blank Page

References

[1] EPA, "Overview of SF_6 Emissions Sources and Reduction Options in Electric Power Systems," 2018.

[2] H. Koch, *Gas Insulated Substations*. United Kingdom: John Wiley & Sons, 2014.

[3] IPCC, "Climate Change 2013: The Physical Science Basis. Working Group I Contribution to the Fifth Assessment Report on Interngovernmental Panel on Climate Change," 2013.

[4] Y. Kieffel, T. Irwin, P. Ponchon, and J. Owens, "Green Gas to Replace SF_6 in Electrical Grids," *IEEE Power and Energy Magazine*, vol. 14, no. 2, pp. 32–39, 2016.

[5] Earth System Research Laboratories. (2020). *Sulfur hexafluoride (SF_6) — Combined Data Set* [Online]. Available: https://www.esrl.noaa.gov/gmd/hats/combined/SF6.html.

[6] Y. Kieffel, "Characteristics of g^3 - An alternative to SF_6," in *IEEE International Conference on Dielectrics (ICD)*, Montpellier, France, 2016, pp. 880–884.

[7] 3M Electronics Materials Solutions Division, "3M™ Novec™ 4710 Insulating Gas." 2017.

[8] Y. Kieffel, "Characteristics of g^3 - an alternative to SF_6," *CIRED, Open Access Proc. J.*, vol. 2017, no. 1, pp. 54–57, 2017.

[9] J. G. Owens, "Greenhouse Gas Emission Reductions through use of a Sustainable Alternative to SF_6," in *IEEE Electrical Insulation Conference (EIC)*, Montreal, QC, 2016, pp. 535–538.

[10] Siemens, "Gas-Insulated Transmission Lines (GIL)," 2016.

[11] H. Meinecke, "High voltage gas insulated switchgear: an overview," in *IEE Colloquium on GIS (Gas-Insulated Switchgear) at Transmission and Distribution Voltages*, Nottingham, UK, 1995, pp. 3/1–3/8.

[12] H. Koch, *Gas-Insulated Transmission Lines (GIL)*. United Kingdom: John Wiley & Sons, 2012.

[13] J. Riedl and T. Hillers, "Gas-Insulated Transmission Lines," *IEEE Power Eng. Rev.*, vol. 20, no. 9, pp. 15–16, 2000.

[14] EU. (2015). *EU legislation to control F-gases* [Online]. Available: https://ec.europa.eu/clima/policies/f-gas/legislation_en#tab-0-0.

[15] UK Government. (2019). *Fluorinated gases (F gases)* [Online]. Available: https://www.gov.uk/guidance/fluorinated-gases-f-gases.

[16] J. Wada, G. Ueta, S. Okabe, and M. Hikita, "Dielectric Properties of Gas Mixtures with Per-Fluorocarbon Gas and Gas with Low Liquefaction Temperature," *IEEE Trans. Dielectr. Electr. Insul.*, vol. 23, no. 2, pp. 838–847, 2016.

[17] M. Hyrenbach, T. Hintzen, P. Müller, and J. Owens, "Alternative Gas Insulation in Medium-voltage switchgear," in *CIRED, 23rd International Conference on Electricity Distribution*, Lyon, France, 2015, pp. 1–5.

[18] A. Beroual and A. Haddad, "Recent advances in the quest for a new insulation gas with a low impact on the environment to replace Sulfur Hexafluoride (SF_6) gas in high-voltage power network applications," *Energies*, vol. 10, pp. 1–20, 2017.

[19] Toshiba. *Substation Equipment that secures the quality of electric power* [Online]. Available: https://www.toshiba-energy.com/en/transmission/product/.

[20] P. Bolin and H. Koch, "Gas Insulated Switchgear GIS - State of the Art," in *IEEE Power Engineering Society General Meeting*, Tampa, FL, 2007, pp. 1–3.

[21] N. H. Malik, A. A. Al-Arainy, and M. I. Qureshi, *Electrical Insulation in Power Systems*. Taylor & Francis, 1998.

[22] H. Koch, "Gas Insulated Transmission Lines - GIL," in *IEEE Power Engineering Society General Meeting*, Tampa, FL, 2007, pp. 1–5.

[23] H. Koch, D. Kunze, S. Pohler, L. Hofmann, C. Rathke, and A. Mueller, "Gas Insulated Lines - Reliable Power Transmission Toward New Wolrdwide Challenges in Hydro and Wind Power Generation," in *Cigre, B3-210*, Paris, France, 2008, pp. 1–6.

[24] H. Koch, "Basic information on gas insulated transmission lines (GIL)," in *IEEE Power and Energy Society General Meeting - Conversion and Delivery of Electrical Energy in the 21st Century*, Pittsburgh, PA, 2008, pp. 1–4.

[25] T. Hillers, "Second-generation gas-insulated line," *IET Power Eng. J.*, vol. 16, no. 3, pp. 111–116, 2002.

[26] T. Hillers, "Gas insulated transmission lines (GIL): ready for the real world," in *IEEE Power Engineering Society Winter Meeting*, 2000, pp. 575–579.

[27] Solvay, "Sulphur Hexafluoride."

[28] A. Haddad and D. Warne, *Advances in High Voltage Engineering*. The Institution of Engineering and Technology (IET), 2007.

[29] UNFCCC. *The Kyoto Protocol* [Online]. Available: https://unfccc.int/kyoto_protocol.

[30] S. Okabe, J. Wada, and G. Ueta, “Dielectric Properties of Gas Mixtures with C_3F_8/C_2F_6 and N_2/CO_2,” *IEEE Trans. Dielectr. Electr. Insul.*, vol. 22, no. 4, pp. 2108–2116, 2015.

[31] Y. Kieffel *et al.*, “SF_6 Alternative Development for High Voltage Switchgears,” in *Cigre, D1-305*, Paris, France, 2014.

[32] 3M Electronics Materials Solutions Division, “3M™ Novec™ 5110 Insulating Gas.” 2017.

[33] J. D. Mantilla, N. Gariboldi, S. Grob, and M. Claessens, “Investigation of the Insulation Performance of a New Gas Mixture with Extremely Low GWP,” in *IEEE Electrical Insulation Conference (EIC)*, Philadelphia, Pennsylvania, 2014, pp. 469–473.

[34] M. S. Kamarudin *et al.*, “CF_3I Gas and Its Mixtures : Potential for Electrical Insulation,” in *Cigre, D1-308*, Paris, France, 2014, pp. 1–9.

[35] L. Chen *et al.*, “Breakdown Characteristics of CF_3I/CO_2 Gas Mixtures Under Fast Impulse In Rod-Plane And GIS Geometries,” in *International Symposium on High Voltage Engineering (ISH)*, Pilsen, Czech Republic, 2015, pp. 1–6.

[36] L. Chen, P. Widger, M. S. Kamarudin, H. Griffiths, and A. Haddad, “Potential of CF_3I Gas Mixture as an Insulation Medium in Gas-Insulated Equipment,” in *IEEE Conference on Electrical Insulation and Dielectric Phenomena (CEIDP)*, Ann Arbor, MI, 2015, pp. 868–871.

[37] L. Chen, H. Griffiths, A. Haddad, and M. S. Kamarudin, “Breakdown of CF_3I Gas and its Mixtures under Lightning Impulse in Coaxial-GIL Geometry,” *IEEE Trans. Dielectr. Electr. Insul.*, vol. 23, no. 4, pp. 1959–1967, 2016.

[38] L. Chen, P. Widger, M. S. Kamarudin, H. Griffiths, and A. Haddad, “CF_3I Gas Mixtures : Breakdown Characteristics and Potential for Electrical Insulation,” *IEEE Trans. Power Deliv.*, vol. 32, no. 2, pp. 1089–1097, 2017.

[39] A. Xiao, J. Bonk, and J. G. Owens, “Emission Reductions Through Use of Sustainable SF_6 Alternatives,” in *CIRED, 23rd International Conference on Electricity Distribution*, Madrid, Spain, 2019, pp. 1–5.

[40] T. Kawamura, S. Matumoto, M. Hanai, and Y. Murayama, “SF_6/N_2 Mixtures for HV Equipment and Practical Problems,” in *Gaseous Dielectrics VIII*, 1998, pp. 333–342.

[41] H. Koch, F. Goll, T. Magier, and K. Juhre, “Technical Aspects of Gas Insulated Transmission lines and Application of New Insulating Gases,” *IEEE Trans. Dielectr. Electr. Insul.*, vol. 25, no. 4, pp. 1448–1453, 2018.

[42] 3M, “3M Novec 4710 Insulating Gas Safety Datasheet,” 2020.

[43] The British Standards Institution, “Determination of toxicity of a gas or gas mixture,” *BS ISO 10298*, 2010.

[44] Y. Li *et al.*, “Assessment on the toxicity and application risk of C_4F_7N: A new SF_6 alternative gas,” *J. Hazard. Mater.*, vol. 368, pp. 653–660, 2019.

[45] T. Uchii, Y. Hoshina, H. Kawano, K. Suzuki, T. Nakamoto, and M. Toyoda, “Fundamental Research on SF_6-free Gas Insulated Switchgear Adopting CO_2 Gas and Its Mixtures,” in *International Symposium on EcoTopia Scienece (ISET)*, Nagoya, Japan, 2007, pp. 516–520.

[46] D. Y. Peng and D. B. Robinson, “A New Two-Constant Equation of State,” *Ind. Eng. Chem. Fundam.*, vol. 15, no. 1, pp. 59–64, 1976.

[47] N. H. Malik and A. H. Qureshi, “Breakdown Mechanisms in Sulphur Hexafluoride,” *IEEE Trans. Electr. Insul.*, vol. EI-13, no. 3, pp. 135–145, 1978.

[48] S. Hu, W. Zhou, J. Yu, R. Qiu, Y. Zheng, and H. Li, “Synergistic Effect of i-C_3F_7CN/CO_2 and i-C_3F_7CN/N_2 Mixtures,” *IEEE Access*, vol. 7, pp. 50159–50167, 2019.

[49] X. Zhang *et al.*, “Experimental Study on Power Frequency Breakdown Characteristics of C_4F_7N/CO_2 Gas Mixture Under Quasi-Homogeneous Electric Field,” *IEEE Access*, vol. 7, pp. 19100–19108, 2019.

[50] Y. Kawaguchi, K. Sakata, and S. Menju, “Dielectric Breakdown of Sulphur Hexafluoride in Nearly Uniform Fields,” *IEEE Trans. Power Appar. Syst.*, vol. PAS-90, no. 3, pp. 1072–1078, 1971.

[51] S. Menju, H. Aoyagi, K. Takahashi, and H. Qhno, “Dielectric Breakdown of High Pressure SF_6 in Sphere and Coaxial Cylinder Gaps,” *IEEE Trans. Power Appar. Syst.*, vol. PAS-93, no. 5, pp. 1706–1712, 1974.

[52] B. Zhang, N. Uzelac, and Y. Cao, “Fluoronitrile/CO_2 Mixture as an Eco-Friendly Alternative to SF_6 for Medium Voltage Switchgears,” *IEEE Trans. Dielectr. Electr. Insul.*, vol. 25, no. 4, pp. 1340–1350, 2018.

[53] R. Arora and M. Wolgang, *High Voltage and Electrical Insulation Engineering*. Hoboken, New Jersey: John Wiley & Sons, 2011.

[54] H. E. Nechmi, A. Beroual, A. Girodet, and P. Vinson, “Fluoronitriles/CO_2 Gas Mixture as Promising Substitute to SF_6 for Insulation in High Voltage Applications,” *IEEE Trans. Dielectr. Electr. Insul.*, vol. 23, no. 5, pp. 2587–2593, 2016.

[55] C. Wang *et al.*, “Characteristics of C_3F_7CN/CO_2 as an Alternative to SF_6 in HVDC-

GIL Systems," *IEEE Trans. Dielectr. Electr. Insul.*, vol. 25, no. 4, pp. 1351–1356, 2018.

[56] Y. Tu, Y. Cheng, C. Wang, X. Ai, F. Zhou, and G. Chen, "Insulation Characteristics of Fluoronitriles / CO_2 Gas Mixture under DC Electric Field," *IEEE Trans. Dielectr. Electr. Insul.*, vol. 25, no. 4, pp. 1324–1331, 2018.

[57] N. H. Malik and A. H. Qureshi, "The Influence of Voltage Polarity and Field Non-Uniformity on The Breakdown Behavior of Rod-Plane Gaps Filled with SF_6," *IEEE Trans. Electr. Insul.*, vol. EI-14, no. 6, pp. 327–333, 1979.

[58] B. S. Manjunath, K. Dwarakanath, and M. . Naidu, "Influence of Polarity and Field Non-Uniformity on the Breakdown Votlage Characteristics of SF_6 Gas Under Impulse Voltages," in *IEEE International Symposium on Electrical Insulation*, Pittsburgh, PA, 1994, pp. 485–488.

[59] E. Kuffel, W. S. Zaengl, and J. Kuffel, *High Voltage Engineering - Fundamentals*, 2nd ed. Great Britain: Pergamon Press, 2000.

[60] T. Zhang, W. Zhou, and J. Yu, "Insulation Properties of C_4F_7N/CO_2 Mixtures under Lightning Impulse," *IEEE Trans. Dielectr. Electr. Insul.*, vol. 27, no. 1, pp. 181–188, 2020.

[61] A. Pedersen, "The Effect of Surface Roughness on Breakdown in SF_6," *IEEE Trans. Power Appar. Syst.*, vol. PAS-94, no. 5, pp. 1749–1754, 1975.

[62] A. Pedersen, "Limitations of Breakdown Voltages in SF_6 caused by Electrode Surface Roughness," in *IEEE Conference on Electrical Insulation and Dielectric Phenomena (CEIDP)*, Downingtown, PA, 1974, pp. 457–464.

[63] X. Yan, Y. Zheng, K. Gao, X. Xu, W. Wang, and J. He, "The Criterion of Conductor Surface Roughness in Environment-friendly C_4F_7N/CO_2 Gas Mixture," in *IEEE Sustainable Power and Energy Conference (iSPEC)*, Beijing, China, 2019, pp. 377–381.

[64] Y. Zheng *et al.*, "Influence of conductor surface roughness on insulation performance of C_4F_7N/CO_2 mixed gas," *IEEE Trans. Dielectr. Electr. Insul.*, vol. 26, no. 3, pp. 922–929, 2019.

[65] X. Ai *et al.*, "The effect of electrode surface roughness on the breakdown characteristics of C_3F_7CN/CO_2 gas mixtures," *Elsevier*, pp. 1–6, 2020.

[66] Z. Li *et al.*, "Surface Flashover Characteristics of Epoxy Insulator in C_4F_7N/CO_2 Mixtures in a Uniform Field under AC Voltage," *IEEE Trans. Dielectr. Electr. Insul.*, vol. 26, no. 4, pp. 1065–1072, 2019.

[67] The British Standards Institution, “High-voltage test techniques - Partial Discharge measurements,” *BS EN 60270*, 2016.

[68] B. Zhang and Y. Cao, “Comparison of Partial Discharges in SF_6 and Fluoronitrile/CO_2 Gas Mixtures,” in *Cigre*, Paris, France, 2017, pp. 1–7.

[69] Y. I. Li *et al.*, “Study on the Dielectric Properties of C_4F_7N/N_2 Mixture Under Highly Non-Uniform Electric Field,” *IEEE Access*, vol. 6, pp. 42868–42876, 2018.

[70] G. Wang, W.-H. Kim, G. Kil, S.-W. Kim, and J.-R. Jung, “Green Gas for a Grid as An Eco-Friendly Alternative Insulation Gas to SF_6 : From the Perspective of Partial Discharge Under AC,” *Appl. Sci.*, vol. 9, no. 651, pp. 1–10, 2019.

[71] Y. Kieffel, F. Biquez, and P. Ponchon, “Alternative Gas to SF_6 for Use in High Voltage Switchgears: g^3,” in *CIRED, 23rd International conference on electricity distribution*, Lyon, France, 2015, no. 0230, pp. 1–5.

[72] Y. Zhou *et al.*, “Comparison of Decomposition By-products of C_4F_7N/CO_2 Mixed Gas under AC Discharge Breakdown and Partial Discharge,” in *International Conference on Electric Power Equipment - Switching Technology (ICEPE-ST)*, Kitakyushu, Japan, 2019, pp. 82–85.

[73] P.Simka, C. B. Doiron, S.Scheel, and A. Di-Giann, “Decomposition of alternative gaseous insulation under partial discharge,” in *International Symposium on High Voltage Engineering (ISH)*, Buenos Aires, Argentina, 2017, pp. 1–6.

[74] K. Pohlink *et al.*, “Characteristics of a Fluoronitrile/CO_2 Mixture - An Alternative to SF_6,” in *Cigre, D1-204*, Paris, France, 2016, pp. 1–11.

[75] Lapp Insulators GmbH, “High Voltage GIS Bushing with composite housing.” 2015.

[76] COMSOL. (2016). *The Finite Element Method (FEM)* [Online]. Available: https://www.comsol.com/multiphysics/finite-element-method.

[77] L. Chen, “Investigation on the Feasibility of Trifluoroiodomethane (CF_3I) for Application in Gas-Insulated Lines,” Ph.D. dissertation, Cardiff Univ, Cardiff, UK, 2015.

[78] W. Frei. (2013). *Meshing Considerations for Linear Static Problems* [Online]. Available: https://www.comsol.com/blogs/meshing-considerations-linear-static-problems/.

[79] A. Griesmer. (2014). *Size Parameters for Free Tetrahedral Meshing in COMSOL Multiphysics* [Online]. Available: https://www.comsol.co.in/blogs/size-parameters-free-tetrahedral-meshing-comsol-multiphysics/.

[80] COMSOL. (2016). *Finite Element Mesh Refinement* [Online]. Available:

https://www.comsol.com/multiphysics/mesh-refinement.

[81] H. Gothall. (2017). *How to Inspect Your Mesh in COMSOL Multiphysics®* [Online]. Available: https://uk.comsol.com/blogs/how-to-inspect-your-mesh-in-comsol-multiphysics/.

[82] The British Standards Institution, "Assessment of Surface Texture - Guidance and General Information," *BS 1134*, 2010.

[83] The British Standards Institution, "Geometrical product specification (GPS) - Surface texture : Profile method - Terms , definitions and surface texture parameters," *BS EN ISO 4287*, 2009.

[84] I. A. Metwally, "Status review on partial discharge measurement techniques in gas-insulated switchgear/lines," *Elsevier*, vol. 69, no. 1, pp. 25–36, 2004.

[85] N. De Kock, B. Coric, and R. Pietsch, "UHF PD detection in gas-insulated switchgear - Suitability and sensitivity of the UHF method in comparison with the IEC 270 method," *IEEE Electr. Insul. Mag.*, vol. 12, no. 6, pp. 20–26, 1996.

[86] G. Wang and G. S. Kil, "Measurement and Analysis of Partial Discharge Using an Ultra-high Frequency Sensor for Gas Insulated Structures," *Metrol. Meas. Syst.*, vol. 24, no. 3, pp. 515–524, 2017.

[87] T. Prabakaran, S. Usa, and A. Santosh Kumar, "Analysis of Partial Discharge Signals in 420 kV Gas Insulated Substation," in *IEEE International Conference on Condition Assessment Techniques in Electrical Systems (CATCON)*, Kolkata, India, 2013, pp. 249–254.

[88] The British Standards Institution, "Guidelines for the checking and treatment of sulphur hexafluoride (SF_6) taken from electrical equipment and specification for its re-use," *BS EN 60480*, 2004.

[89] M. S. Silberberg, *Chemistry: The Molecular Nature of Matter and Change*, 5th ed. Boston: McGraw-Hill, 2009.

[90] The British Standards Institution, "High-Voltage test techniques, Part 1: General Definitions and test requirements," *BS EN 60060-1*, 2010.

[91] W. Hauschild and W. Mosch, *Statistical Techniques for High-voltage Engineering*. Peter Peregrinus Ltd, 1992.

[92] F. Rizk and M. Eteiba, "Impulse Breakdown Voltage-Time Curves of SF_6 and SF_6-N_2 Coaxial-Cylinder Gaps," *IEEE Trans. Power Appar. Syst.*, vol. PAS-101, no. 12, pp. 4460–4471, 1982.

[93] S. R. Naidu and P. D. T. Mederos, "Volt-Time Curves For A Coaxial Cylindrical Gap

In SF_6-N_2 Mixtures," *IEEE Trans. Electr. Insul.*, vol. EI-22, no. 6, pp. 755–762, 1987.

[94] T. Wen *et al.*, "Discussion on lightning impulse test waveform according to breakdown characteristics of SF_6 gas gaps," *IEEE Trans. Dielectr. Electr. Insul.*, vol. 24, no. 4, pp. 2306–2313, 2017.

[95] C. Zachariades, R. Shuttleworth, and R. Giussani, "A Dual-Slot Barrier Sensor for Partial Discharge Detection in Gas-Insulated Equipment," *IEEE Sens. J.*, vol. 20, no. 2, pp. 860–867, 2020.

[96] HVPD. *Ultra High Frequency Detection for Partial Discharge* [Online]. Available: https://www.hvpd.co.uk/products/uhf-barrier-sensor/.

[97] J. Shipman, J. Wilson, C. Higgins, and O. Torres, *An Introduction to Physical Science*, 14th ed. Boston: Cengage Learning, 2016.

[98] P.-S. Kildal, *Foundations of Antenna Engineering: A Unified Approach for Line-of-sight and Multipath*. Kildal Antenn AB, 2015.

[99] M. Albiez *et al.*, "Partial Discharge Detection System for GIS: Sensitivity Verification for the UHF Method and the Acoustic Method," *Cigre, Electra*, vol. 183, pp. 77–87, 1999.

[100] J. S. Pearson, O. Farish, B. F. Hampton, M. D. Judd, and D. Templeton, "Partial Discharge Diagnostics for Gas Insulated Substations," *IEEE Trans. Dielectr. Electr. Insul.*, vol. 2, no. 5, pp. 893–905, 1995.

[101] The British Standards Institution, "High-voltage switchgear and controlgear, Part 1: Common specifications," *BS EN 62271-1*, 2011.

[102] The British Standards Institution, "High-voltage switchgear, Part 204: Rigid gas-insulated transmission lines for rated voltage above 52kV," *BS EN 62271-204*, 2011.

[103] The British Standards Institution, "High-voltage switchgear and controlgear, Part 203: Gas-insulated metal-enclosed switchgear for rated voltages above 52kV," *BS EN 62271-203*, 2012.

[104] L. Loizou, L. Chen, Q. Liu, I. Cotton, M. Waldron, and J. Owens, "Technical Viability of Retro-filling C_3F_7CN/CO_2 Gas Mixtures in SF_6-designed Gas Insulated Lines and Busbars at Transmission Voltages," *IEEE Trans. Power Deliv.*, pp. 1–9, 2020.

[105] Ofgem, "RIIP-ET1 Annual Report," 2019.

[106] National Grid. *Performance - environmental sustainability: Sulphur Hexafluoride* [Online]. Available: https://www.nationalgrid.com/group/responsibility-and-sustainability/our-progress/our-performance/performance-environmental.

[107] UK Government. (2014). *Calculate the carbon dioxide equivalent quantity of an F*

gas [Online]. Available: https://www.gov.uk/guidance/calculate-the-carbon-dioxide-equivalent-quantity-of-an-f-gas.

[108] UK Government. *Met Office* [Online]. Available: https://www.metoffice.gov.uk/.

[109] Google. *Google Maps* [Online]. Available: https://www.google.com/maps.

Blank Page

List of Publications

Peer-reviewed Journal Papers

1. L. Loizou, L. Chen, Q. Liu and M. Waldron, "Lightning impulse breakdown characteristics of SF_6 and 20% C_3F_7CN / 80% CO_2 mixture under weakly non-uniform electric fields," in IEEE Transactions on Dielectrics and Electrical Insulation, vol. 27, no. 3, pp. 848-856, June 2020.

2. L. Loizou, L. Chen, Q. Liu, I. Cotton, M. Waldron and J. Owens, "Technical Viability of Retro-filling C_3F_7CN/CO_2 Gas Mixtures in SF_6-designed Gas Insulated Lines and Busbars at Transmission Voltages," in IEEE Transactions on Power Delivery.

International Conference Papers

3. L. Loizou, R. Fernandez Bautista, L. Chen, M. Seltzer-Grant and Q. Liu, "Evaluation of UHF Partial Discharge Measurements for SF_6 and 20% C_3F_7CN / 80% CO_2 Gas Mixture," 2020 IEEE International Conference on Dielectrics (ICD), Valencia, Spain.

4. L. Loizou, L. Chen and Q. Liu, "A Comparative Study on the Breakdown Characteristics of SF_6 and 20% C_3F_7CN / 80% CO_2 Gas Mixture in a Coaxial Configuration," 2019 IEEE Conference on Electrical Insulation and Dielectric Phenomena (CEIDP), Richland, WA, USA, 2019, pp. 234-237.

5. L. Loizou, L. Chen and Q. Liu, "Breakdown Characteristics of C_3F_7CN/CO_2 Gas Mixtures in Rod-Plane Gaps," 2018 IEEE International Conference on High Voltage Engineering and Application (ICHVE), ATHENS, Greece, 2018, pp. 1-4.